




2016

Cytokine Networks And Immunosurveillance In Cancer

Timothy Chao

University of Pennsylvania, timchao@upenn.edu

Follow this and additional works at: <https://repository.upenn.edu/edissertations>

 Part of the [Allergy and Immunology Commons](#), [Immunology and Infectious Disease Commons](#), [Medical Immunology Commons](#), and the [Oncology Commons](#)

Recommended Citation

Chao, Timothy, "Cytokine Networks And Immunosurveillance In Cancer" (2016). *Publicly Accessible Penn Dissertations*. 2950.
<https://repository.upenn.edu/edissertations/2950>

This paper is posted at ScholarlyCommons. <https://repository.upenn.edu/edissertations/2950>
For more information, please contact repository@pobox.upenn.edu.

Cytokine Networks And Immunosurveillance In Cancer

Abstract

The cytokine milieu in the tumor microenvironment plays a key role in modulating the immune response either in favor of or against tumorigenesis. For many tumors, this complex network of cytokine and immune interactions represent a formidable means of escape from immune surveillance. These cytokine networks are particularly important in pancreatic ductal adenocarcinoma (PDA), where a prominent infiltration of immunosuppressive immune populations could be found. Myeloid-derived suppressor cells (MDSCs) have previously been shown to be potent suppressors of anti-tumor immunity in PDA, but the cytokine networks regulating their recruitment to the tumor microenvironment remain incompletely understood. Here, I found that CXCR2 ligand expression is specifically correlated with enrichment of the granulocytic subset of MDSCs (G-MDSCs) in human PDAs. Using a genetically engineered mouse model of PDA, I showed that CXCR2 is required for G-MDSC trafficking to the tumor microenvironment, but not necessary for their systemic differentiation and expansion. The specific lack of G-MDSCs in the tumor microenvironment led to a T cell-dependent inhibition of tumor growth. Expression of CXCR2 ligands in PDA tumor cells can be potently induced by NF- κ B activation. These findings describe a cytokine network in PDA where inflammatory signals in the tumor microenvironment drive the expression of CXCR2 ligands and the recruitment of immunosuppressive G-MDSCs. To discover other potentially important cytokine networks, I developed a novel analysis pipeline to reconstruct and compare cytokine networks from whole tumor gene expression data. Using expression of cytolytic genes as a gauge for anti-tumor immune activity, I found that PDA patients with high cytolytic activity have a slight survival advantage compared to those with lower activity. While macrophages were the most influential in tumors with low cytolytic activity, tumors with high cytolytic activity were characterized by increased activity of NK cells, recruitment of B cells, and increased importance of CD8 T cells, CD4 T helper cells, and B cells, among others. I further highlighted the cytokines that might be associated with these immune populations. Therefore, my analysis identified potentially important components of the cytokine network associated with high and low cytolytic activity. Collectively, the work in this thesis suggests that cytokine networks are crucial for maintaining an immunosuppressive microenvironment in cancer. Furthermore, disrupting key components of these networks can tip the balance in favor of cancer immunosurveillance.

Degree Type

Dissertation

Degree Name

Doctor of Philosophy (PhD)

Graduate Group

Cell & Molecular Biology

First Advisor

Robert H. Vonderheide

Keywords

CXCR2, Cytokine networks, Cytolytic activity, Immunosurveillance, MDSC, Pancreatic cancer

Subject Categories

Allergy and Immunology | Immunology and Infectious Disease | Medical Immunology | Oncology

CYTOKINE NETWORKS AND IMMUNOSURVEILLANCE IN CANCER

Timothy Chao

A DISSERTATION

in

Cell and Molecular Biology

Presented to the Faculties of the University of Pennsylvania

in

Partial Fulfillment of the Requirements for the

Degree of Doctor of Philosophy

2017

Supervisor of Dissertation

Robert H. Vonderheide, Director, Abramson Cancer Center

John H. Glick, MD Abramson Cancer Center's Director Professor

Graduate Group Chairperson

Daniel S. Kessler

Associate Professor of Cell and Developmental Biology

Dissertation Committee

M. Celeste Simon, Arthur H. Rubenstein, MBBCh Professor

Ellen Pure, Professor and Chair of Biomedical Sciences

Gregory Beatty, Assistant Professor of Medicine

Xiaolu Yang, Professor of Cancer Biology

CYTOKINE NETWORKS AND IMMUNOSURVEILLANCE IN CANCER

COPYRIGHT

2017

Timothy Hue-Fung Chao

This work is licensed under the
Creative Commons Attribution-
NonCommercial-ShareAlike 3.0
License

To view a copy of this license, visit

<https://creativecommons.org/licenses/by-nc-sa/3.0/us/>

ACKNOWLEDGMENTS

First and foremost, I would like to thank my thesis advisor, Dr. Robert Vonderheide for his enthusiasm, support, and guidance throughout the course of my thesis work. Without his encouragement and insight this work would not have been possible. I would also like to acknowledge all my lab members for helping me as I began my study in this field; working with them familiarized me with important approaches and techniques which allowed me to develop the experimental methodology needed to ask the questions I was interested in. I would also like to thank the mouse hospital staff, especially Dr. Cynthia Clendenin, for helping to manage my “special needs” colony. The analysis of primary human pancreatic cancer was carried out in collaboration with Dr. Emma Furth in the department of Pathology.

ABSTRACT

CYTOKINE NETWORKS AND IMMUNOSURVEILLANCE IN CANCER

Timothy Chao

Robert H. Vonderheide

The cytokine milieu in the tumor microenvironment plays a key role in modulating the immune response either in favor of or against tumorigenesis. For many tumors, this complex network of cytokine and immune interactions represent a formidable means of escape from immune surveillance. These cytokine networks are particularly important in pancreatic ductal adenocarcinoma (PDA), where a prominent infiltration of immunosuppressive immune populations could be found. Myeloid-derived suppressor cells (MDSCs) have previously been shown to be potent suppressors of anti-tumor immunity in PDA, but the cytokine networks regulating their recruitment to the tumor microenvironment remain incompletely understood. Here, I found that CXCR2 ligand expression is specifically correlated with enrichment of the granulocytic subset of MDSCs (G-MDSCs) in human PDAs. Using a genetically engineered mouse model of PDA, I showed that CXCR2 is required for G-MDSC trafficking to the tumor microenvironment, but not necessary for their systemic differentiation and expansion. The specific lack of G-MDSCs in the tumor microenvironment led to a T cell-dependent inhibition of tumor growth. Expression of CXCR2 ligands in PDA tumor cells can be potently induced by NF- κ B activation. These findings describe a cytokine network in PDA where inflammatory signals in the tumor microenvironment drive the expression of CXCR2 ligands and the recruitment of immunosuppressive G-MDSCs. To discover other potentially important cytokine networks, I developed a novel analysis pipeline to reconstruct and compare cytokine networks from whole tumor gene expression data. Using expression of cytolytic genes as a gauge for anti-tumor

immune activity, I found that PDA patients with high cytolytic activity have a slight survival advantage compared to those with lower activity. While macrophages were the most influential in tumors with low cytolytic activity, tumors with high cytolytic activity were characterized by increased activity of NK cells, recruitment of B cells, and increased importance of CD8 T cells, CD4 T helper cells, and B cells, among others. I further highlighted the cytokines that might be associated with these immune populations. Therefore, my analysis identified potentially important components of the cytokine network associated with high and low cytolytic activity. Collectively, the work in this thesis suggests that cytokine networks are crucial for maintaining an immunosuppressive microenvironment in cancer. Furthermore, disrupting key components of these networks can tip the balance in favor of cancer immunosurveillance.

MANUSCRIPTS

The following manuscripts are discussed in this thesis:

1. **T. Chao**, E.E. Furth, R.H. Vonderheide. "CXCR2-dependent accumulation of tumor-associated neutrophils regulates T-cell immunity in pancreatic ductal adenocarcinoma." *Cancer Immunol Res.* 2016 Nov;4(11):968-82.
2. **T. Chao** and R.H. Vonderheide. "*In silico* reconstruction and comparison of cytokine networks in pancreatic ductal adenocarcinomas with high and low cytolytic activity." *In preparation.*

Manuscripts not discussed in this thesis:

1. R.A. Evans, M.S. Diamonds, A.J. Rech, **T. Chao**, M.W. Richardson, J.H. Lin, D.L. Bajor, K.T. Byrne, B.Z. Stanger, J.L. Riley, N. Markosyan, R. Winograd, and R.H. Vonderheide. "Lack of immunoediting in murine pancreatic cancer reversed with neo-antigen." *JCI Insight.* 2016; 1(14):e88328.
2. V. Kumar, L. Donthireddy, D. Marvel, T. Condamine, F. Wang, S. Lavilla-Alonso, A. Hashimoto, P. Vonteddu, R. Behera, M.A. Goins, C. Mulligan, B. Nam, N. Hockstein, F. Denstman, S. Shakamuri, **T. Chao**, D.W. Speicher, A.T. Weeraratna, R.H. Vonderheide, L.R. Languino, P. Ordentlich, Q. Liu, X. Xu, A. Lo, E. Puré, C. Zhang, A. Loboda, M.A. Sepulveda, L.A. Snyder, D. Gabrilovich. "Cancer-associated fibroblasts neutralize the anti-tumor effect of CSF-1 receptor blockade by inducing PMN-MDSC infiltration of tumors." *Accepted.*
3. J. Li, K.T. Byrne, Z. Chen, A. Rech, D. Balli, T. Yamazoe, Y. Sela, R. Norgard, C. Hay, **T. Chao**, E.J. Wherry, R.H. Vonderheide, and B.Z. Stanger. "Tumor cell-intrinsic factors underlie immune heterogeneity." *In preparation.*

TABLE OF CONTENTS

ACKNOWLEDGMENT	iii
ABSTRACT	iv
MANUSCRIPTS	vi
LIST OF ILLUSTRATIONS.....	viii
CHAPTER 1: INTRODUCTION.....	1
CHAPTER 2: MATERIALS AND METHODS.....	21
CHAPTER 3: CXCR2-Dependent Accumulation of Tumor-Associated Neutrophils Regulates T-cell Immunity in Pancreatic Ductal Adenocarcinoma	31
CHAPTER 4: Cytokine networks underlying cytolytic activity in pancreatic cancer.....	83
CHAPTER 5: DISCUSSION AND FUTURE DIRECTIONS	133
REFERENCES.....	152

LIST OF ILLUSTRATIONS

Figure 1. Relative expression of the neutrophil gene signature across TCGA.	50
Figure 2. Stratification of human PDA samples by neutrophil signature genes.	51
Figure 3. Immune populations and PDA subtypes enriched in TAN-high samples.	52
Figure 4. Significant neutrophil infiltration in a subset of human pancreatic cancer.	53
Figure 5. Elevated CXCL5 expression in PDA.	54
Figure 6. Clustering of human PDA into CXCR2L-high and CXCR2L-low groups.	55
Figure 7. CXCR2L-high samples have elevated expression of neutrophil-specific genes. .	56
Figure 8. Elevation of genes in pathways related to innate immune response and NF- κ B activation in CXCR2L-high samples.	57
Figure 9. Correlation of immunome populations with all chemokines in PDA.	58
Figure 10. CXCL8 and CXCL5 are the most important chemokines in predicting the neutrophil signature score in PDA.	59
Figure 11. Significant Ly6G ⁺ neutrophil infiltration throughout the pancreatic tumors of KPCY mice.	60
Figure 12. Increased CD11b ⁺ Ly6G ⁺ neutrophils in the pancreas of KPC mice.	61
Figure 13. Increased CD11b ⁺ Ly6G ⁺ neutrophils in the spleens of tumor-bearing KPC mice.	62
Figure 14. Elevated CXCL1 and CXCL5 levels in KPC pancreatic tumors.	63
Figure 15. Differential CXCR2 ligand expression in cancer and stromal cells in KPC tumors.	64
Figure 16. CXCL5 is abundantly secreted by KPC-derived PDA cell lines <i>in vitro</i>	65
Figure 17. CXCR2 ligand expression profile in KCY pancreas is similar to KPCY tumors. .	66
Figure 18. Inhibition of the KRAS/MEK pathway increases CXCL5 expression.	67
Figure 19. CXCL5 level is not affected by inhibition of alternative downstream KRAS pathways.	68

Figure 20. MEK inhibition-induced elevation of CXCL5 expression is dependent on NF-κB activation.	69
Figure 21. Anti-CXCL5 treatment slows PDA tumor growth.....	70
Figure 22. No changes in the tumor immune composition with anti-CXCL5 treatment.	71
Figure 23. No changes in the splenic immune composition with anti-CXCL5 treatment.	72
Figure 24. CXCR2 ablation slows tumor growth and prolongs survival.	73
Figure 25. CXCR2 ablation eliminates the accumulation of tumor-infiltrating neutrophils.	74
Figure 26. Changes in the immune composition of tumors in <i>Cxcr2^{+/+}</i> and <i>Cxcr2^{-/-}</i> mice. ..	75
Figure 27. Changes in the splenic immune composition of tumor-bearing <i>Cxcr2^{+/+}</i> and <i>Cxcr2^{-/-}</i> mice.....	76
Figure 28. Increased density of activated CD4 ⁺ T cells in tumors of <i>Cxcr2^{-/-}</i> mice.	77
Figure 29. Increased ratios of activated T cells to immunosuppressive populations in tumors of <i>Cxcr2^{-/-}</i> mice.	78
Figure 30. Increased IFNγ and IL17 secretion in tumor-infiltrating T cells in <i>Cxcr2^{-/-}</i> mice.	79
Figure 31. Depletion of T cells rescues tumor growth in <i>Cxcr2^{-/-}</i> mice.	80
Figure 32. Additive response to chemo-agonistic CD40 therapy with CXCR2 ablation.....	81
Figure 33. Summary of tumor-neutrophil interactions in PDA.....	82
Figure 34. Stratification of human PDA samples by cytolytic activity and cytotoxic gene expression signatures.	103
Figure 35. Cox multiple regression shows significant reduction in hazard ratio in cytolytically hot vs cold tumors.	104
Figure 36. Immune GSVA scores in human PDA.....	105
Figure 37. Immune populations differentially enriched and correlated with survival in hot and cold PDA.....	106
Figure 38. Immune GSVA scores cluster differently in cytolytically hot and cold tumors.	107
Figure 39. Immune GSVA score correlations with the largest changes between cytolytically hot and cold tumors.....	108

Figure 40. Cytokine differential expression in human PDA.....	109
Figure 41. Cytokines correlation with immune GSEA scores in PDA.	110
Figure 42. Immune-cytokine correlations with the largest changes between cytolytically hot and cold tumors.....	111
Figure 43. The overall cytokine network in PDA.....	112
Figure 44. Community 1 in the overall cytokine network.	113
Figure 45. Community 2 in the overall cytokine network.	114
Figure 46. Communities 3-6 in the overall cytokine network.	115
Figure 47. Cytokine network in cytolytic hot PDAs.....	116
Figure 48. Community 1 in the cytolytically hot cytokine network.....	117
Figure 49. Community 2 in the cytolytically hot cytokine network.....	118
Figure 50. Community 3 in the cytolytically hot cytokine network.....	119
Figure 51. Communities 4 and 5 in the cytolytically hot cytokine network.	120
Figure 52. Cytokine network in cytolytic cold PDAs.....	121
Figure 53. Community 1 in the cytolytically cold cytokine network.....	122
Figure 54. Community 2 in the cytolytically cold cytokine network.....	123
Figure 55. Community 3 in the cytolytically cold cytokine network.....	124
Figure 56. Community 4 in the cytolytically cold cytokine network.....	125
Figure 57. Communities 5-8 in the cytolytically cold cytokine network.....	126
Figure 58. Centrality of immune populations in hot and cold immune-cytokine networks.	127
Figure 59. Immune populations with significantly altered degree centralities.....	128
Figure 60. Immune populations with significantly altered eigenvector centralities.	129
Figure 61. Centrality of cytokines in hot and cold immune-cytokine networks.....	130
Figure 62. Cytokines with significantly altered degree centrality in hot and cold tumors. 131	
Figure 63. Cytokines with altered eigencentality in hot and cold tumors.	132

CHAPTER 1: INTRODUCTION

Pancreatic ductal adenocarcinoma

Pancreatic cancer is currently the fourth leading cause of cancer-related deaths in the United States and responsible for over 200,000 deaths annually worldwide (Siegel et al., 2017). With a 5-year survival rate of only around 8% and rising incidence, pancreatic cancer is projected to become the second leading cause of cancer related deaths in the United States by 2030 (Rahib et al., 2014). The incidence and mortality rates of pancreatic cancer are also increasing worldwide, particularly in European countries (Ilic and Ilic, 2016). The high lethality of this cancer can be primarily attributed to the fact that only 20% of patients are diagnosed at an early enough stage where surgical intervention is possible (Gillen et al., 2010). Even with complete surgical excision, recurrence usually occurs and limits the 5-year survival to about 25-34% (Sohn et al., 2000; Lim et al., 2003; Yamamoto et al., 2015). Unfortunately, the vast majority of patients do not derive substantial benefit from existing chemotherapies. Unlike some other cancers, there are currently no standard population-wide screening guidelines for its early diagnosis. However, a number of factors have been identified that significantly increase the risk of developing pancreatic cancer. A family history of the disease is perhaps the single most significant risk factor (Klein et al., 2004). In fact, about 10% of pancreatic cancer cases are hereditary, only a few of which are accounted for by mutations in common tumor suppressor genes such as *BRCA1*, *CDKN2A*, and *LKB1* (Hruban et al., 2010). In addition, cigarette smoking causes approximately a 75% increased risk that can persist for more than 10 years after cessation (Iodice et al., 2008). Other risk factors for pancreatic cancer include obesity, heavy alcohol use, chronic pancreatitis, and diabetes mellitus (Midha et al., 2016; Hao et al., 2017). Currently, initial suspicion of pancreatic cancer often relies on incidental radiological findings or the development of highly non-specific symptoms such as back pain, lethargy, and new-onset diabetes (Chari, 2007; Keane et al., 2014). A number of tests can then be made to confirm the diagnosis of pancreatic cancer, including multidetector computed topography (MDCT), magnetic resonance cholangiopancreatography (MRCP), and

contrast-enhanced endoscopic ultrasonography (EUS) (Ahn et al., 2009; Gong et al., 2012; Maccioni et al., 2010). However, most patients with pancreatic cancer do not even exhibit any noticeable symptoms until the disease is already at an advanced stage. In fact, 52% of patients present with metastatic disease (Siegel et al., 2017). Therefore, an understanding of the biology underlying pancreatic cancer's tendency to metastasize and resist treatment is urgently needed.

Pancreatic ductal adenocarcinoma (PDA) is by far the most common type of pancreatic cancer and also the most lethal, consisting of over 90% of all cases (Fesinmeyer et al., 2005). PDA usually appears as a firm, white, hypovascular mass that is surrounded by atrophic non-malignant pancreatic tissue. In fact, PDA characteristically presents as a "hypo-enhancing mass" on radiological images because the lack of vasculature prevents infiltration of the contrast agent (Fusaroli et al., 2010). Histologically, PDA is characterized by mucin-producing irregularly-shaped glands, incomplete glandular lumina, luminal necrosis, nuclear pleomorphism, perineural and lymphovascular invasion, and an intense stromal desmoplastic reaction (Kamisawa et al., 2016). Tumors can be histologically graded into three groups: well-, moderately-, or poorly-differentiated. Staging with tumor size (T), number of nodes involved (N), and presence of distant metastases (M) tracks significantly with survival and is used to determine the treatment strategy (La Cruz et al., 2014). Detailed histological analyses of PDA samples showed that microscopic hyperplasia of pancreatic ducts, commonly referred to as pancreatic intraepithelial neoplasias (PanINs), can usually be found in tissues surrounding the tumor (Hruban et al., 2001). Traditionally, PanINs can be classified into three progressive grades based on their morphological and cytological features. PanIN-1 lesions compose of columnar epithelial cells with basally oriented and rounded nuclei. PanIN-2 lesions are characterized by the development of atypical nuclear features, including pleomorphism and hyperchromasia. Finally, PanIN-3 lesions consist of extensive papillae and cribriforms, along with highly atypical nuclei and nucleoli morphologies. More recently, the classification scheme of PanINs was simplified to just two grades: low grade (PanIN-1 and 2) and high grade (PanIN-3) (Basturk et al., 2015). Histological studies have shown that PanIN lesions are more frequent in patients with PDA than normal controls (Kozuka et al., 1979). Furthermore,

patients who underwent partial pancreatectomy for chronic pancreatitis were found to have PanINs years before the development of PDAs (Brat et al., 1998). Another study further showed that high-grade PanINs are more proliferative than low grade lesions (Klein et al., 2002). These observations led to the development of a progressive model where low-grade PanINs evolves to high-grade PanINs, which then progresses to full-blown PDA (Bardeesy and DePinho, 2002). PDA can occasionally arise from macroscopic cystic lesions known as intraductal papillary mucinous neoplasms (IPMNs) (Matthaei et al., 2011). However, unlike PanINs, most IPMNs can usually be appreciated grossly and radiographically. IPMNs can also progress to form intraductal papillary-mucinomas carcinomas (IPMCs) of the pancreas.

Treatment of PDA depends heavily on the stage of disease. Clinically, PDA can be staged as being local or metastatic (La Cruz et al., 2014). Local disease is further subdivided as being resectable, borderline resectable, or locally advanced. Borderline resectable disease is usually defined as having no distant metastases but have some involvement with nearby major vasculatures. However, there is currently no official definition of borderline resectable disease as it is highly dependent on surgical techniques. Surgical removal of resectable or borderline resectable tumors currently offers the best survival benefits for PDA patients as previously discussed. However, these major procedures are also associated with significant morbidities and require close monitoring at specialized centers (Begg et al., 1998). Although laproscopic techniques can potentially reduce some of these complications, such procedures are only available at few select institutions and require highly specialized surgical skills (Shin et al., 2015). After surgical removal of the tumor, patients are then subjected to adjuvant gemcitabine treatment (Oettle et al., 2013). For marginally improved benefit, local unresectable diseases can also be subjected to radiation therapy (Loehrer et al., 2011). On the other hand, first-line treatment for advanced and metastatic PDA usually consists of one of the recently approved combination chemotherapy regimens. In 2011, a phase III randomized trial demonstrated that combination chemotherapy consisting of folic acid, fluorouracil, irinotecan, and oxaliplatin (FOLFIRINOX) significantly extended overall survival (OS) and progression-free survival (PFS) in patients

compared to gemcitabine alone (OS 11.1 vs. 6.8 months and PFS of 6.4 vs. 3.3 months) (Conroy et al., 2011). The objective response rate was also higher in FOLFIRINOX treated compared to gemcitabine treated patients (31.6% vs. 9.4%). However, FOLFIRINOX treatment was associated with significant side effects, including febrile neutropenia, intestinal toxicities, and sensory neuropathies. Furthermore, this study did not include patients older than 75 years old. After showing efficacy in the phase III clinical trial, the combination of gemcitabine and nanoparticle albumin-bound paclitaxel (nab-paclitaxel) was approved by the FDA in 2013 for the treatment of metastatic pancreatic cancer (Hoff et al., 2013). The combination regimen was reported to be superior to gemcitabine monotherapy (OS of 8.5 vs. 6.7 months and PFS of 5.5 vs. 3.7 months). Furthermore, about 23% of patients responded to combination therapy compared to only 7% with gemcitabine alone. Importantly, because the adverse effects of gemcitabine plus nab-paclitaxel were more manageable, more patients can benefit from this combination than FOLFIRINOX. Gemcitabine can also be used alone or in combination with erlotinib for patients who have poor tolerance of the combination therapies (Moore et al., 2007). Although treatment for PDA has seen tremendous progress over the past decades, most patients still do not benefit and long-term curative responses remain the rare exceptions.

Rational design of more effective therapies for PDA will require a deeper understanding of its biology. In an early effort to understand the genetic basis of PDA, Almoguera et al. discovered that over 95% of patients harbor activating mutations in the *KRAS* proto-oncogene, which normally encodes a GTPase that acts as a signal transducer for various growth factors (Almoguera et al., 1988). Activating mutations of *KRAS* usually results in either the direct impairment of *KRAS*-GTPase activity (Q61) or the impairment of *KRAS*-GTP's ability to bind GTPase activating proteins (GAPs), which is required for *KRAS*-GTPase activation (G12 and G13) (Scheffzek et al., 1997; Scheidig et al., 1999). Because of impaired GTPase activity, oncogenic *KRAS* remains constitutively in its activated conformation. Point mutations in codon 12 account for over 98% of oncogenic *KRAS* mutations in PDA, the majority of which is a G to A mutation leading to the substitution of glycine with aspartic acid (G12D) (Bryant et al., 2014).

Other common mutations have since been found, including inactivating mutations in the tumor suppressor genes *CDKN2A* (which encodes both p16 and ARF) (95%), *TP53* (50-75%), and *SMAD4* (55%) (Jaffee et al., 2002). Multiple whole exome sequencing (WES) studies of PDAs have since confirmed the occurrence and frequency of these mutations (Jones et al., 2008; Biankin et al., 2012; Witkiewicz et al., 2015; Bailey et al., 2016). Besides these few common mutations, the prevalence of most other individual mutations is fairly low. However, pathway enrichment analysis showed that most of these low-prevalence mutations actually converge on only a few biological processes, including RAS, TGF- β , DNA repair, and chromatin remodeling pathways. Although they do not show causality, these studies nonetheless suggest that PDA tumorigenesis is likely to be driven by only a handful of aberrant biological processes.

Far from being a homogenous disease, recent integrative studies of the genomic and transcriptomic landscapes of whole tumors have shown that PDAs might actually consist of several subtypes (Bailey et al., 2016; Collisson et al., 2011; Moffitt et al., 2015). Using an unsupervised machine-learning algorithm known as nonnegative matrix factorization (NMF) to cluster whole tumor gene expression data, Collisson et al. identified 62 genes whose differential expressions define three distinct PDA subtypes: classical, quasimesenchymal (QM-PDA), and exocrine-like (EL-PDA) (Collisson et al., 2011). While the QM-PDA subtype was associated with the poorest survival, it was also more sensitive to gemcitabine. On the other hand, the classical PDA subtype was more addicted to oncogenic KRAS and sensitive to EGFR inhibition by erlotinib. Moffitt et al. later extended the use of NMF to deconvolute tumor-, stromal-, and normal tissue-associated genes (Moffitt et al., 2015). Two subtypes emerged from the differential expression of tumor-specific genes: classical and basal-like. Using only stroma-specific genes, tumor-associated stroma were further characterized as either activated or normal. The basal-like PDA and activated stroma subtypes were independently associated with poorer prognosis. While the classical PDA subtypes described in Collisson's and Moffitt's reports were essentially identical, Collisson's QM-PDA signature was shown to be a mixture of Moffitt's basal-like and stromal signatures. In light of this comparison and consistent with Collisson's results, Moffitt et al.

showed that only patients with basal-like PDA subtype benefited from adjuvant gemcitabine chemotherapy. Most recently, Bailey et al. applied NMF to identify four PDA subtypes from whole tumor RNA sequencing data: squamous, pancreatic progenitor (PP), aberrantly differentiated endocrine exocrine (ADEX), and immunogenic (Bailey et al., 2016). The squamous subtype was the most similar to Collisson's QM-PDA and also has the poorest prognosis. By integrating genomic and epigenomic data, Bailey et al. showed that the squamous subtype was enriched in *TP53* mutations, hyper-methylation of pancreas cell-fate genes, and up-regulation of genes related to TGF- β signaling. The ADEX subtype is essentially identical to Collisson's EL-PDA subtype and displays up-regulation of genes associated with KRAS activation. Finally, the PP and immunogenic subtypes together constituted Collisson's classical PDA subtype. While pancreas cell-fate determining transcription factors are upregulated in both of these subtypes, only the immunogenic subtype was associated with significant up-regulation of immune-specific genes. Altogether, these studies have demonstrated the utility of computational approaches to identify candidate genomic characteristics that might be important for PDA tumorigenesis. Importantly, they suggested that PDA could be further divided into several subtypes that are associated with distinct biological processes and possessed different vulnerabilities. Studies such as these have significantly enhanced our understanding of PDA and are paving the way toward the development of targeted therapeutic approaches.

The KPC model of PDA

Although genomic studies have greatly accelerated the discovery of associated mutations and biological processes, they do not provide functional evidence that these aberrations play any role in PDA tumorigenesis. To demonstrate functionality, experimental evidence in pre-clinical models is usually required. While *in vitro* studies and xenograft of human tumors in immunodeficient mice are convenient models, they do not accurately capture the complexities of host-tumor interactions and have very low clinical predictive value (Voskoglou-Nomikos et al., 2003). In contrast, genetically engineered mouse models (GEMMs) of PDA have proven to

faithfully recapitulate key aspects of human disease. By breeding and characterizing the $Pdx1^{Cre/+}; Kras^{G12D/+}$ (KC) mice, Aguirre et al. were the first to functionally confirm that pancreas-specific expression of oncogenic KRAS is sufficient to spontaneously induce PanIN lesions (Aguirre, 2003). Expression of the PDX1 transcription factor is primarily restricted to pancreatic progenitor cells during mouse embryonic day 8.5-12.5 and in adult islet cells (Ahlgren et al., 1996). In these transgenic mice, the endogenous *Pdx1* promoter drives expression of Cre recombinase only in pancreas-lineage cells. Cre recombinase then removes the flanking loxP sites of a silencing sequence (STOP) in the “LSL” cassette and permits transcription of the *Kras-G12D* allele in a pancreas-specific manner (Sauer and Henderson, 1988). Serial histological analyses revealed that these lesions indeed progress from more low-grade to more high-grade PanINs with increasing age. Together with evidence from human PanINs, this result supports the model of PanIN progression from low-grade to high-grade lesions (Rustgi, 2006). In another study using the same KC model, Hingorani et al. not only confirmed that pancreas-restricted expression of oncogenic KRAS is sufficient to induce PanINs, but also reported that some KC mice even developed PDA (Hingorani et al., 2003). Furthermore, these murine PanIN and PDA lesions share essentially the same histological features as their human counterparts. The authors also noted essentially no difference in KC models with Cre recombinase driven by either of the pancreas-specific promoters *Pdx1* or *Ptf1a*. In contrast, *Pdx1*-Cre mediated conditional homozygous deletion of any one of *Cdkn2a*, *Tp53*, *Smad4*, or *Tgfbr2* in the pancreas did not result in the development of any observable PanINs or PDAs even in older mice (Aguirre, 2003; Hingorani et al., 2005; Bardeesy et al., 2006; Ijichi et al., 2006). Together, these results demonstrate that oncogenic KRAS expression is sufficient to drive the formation of PanINs and the development of PDA. More recent GEMMs with pancreas-specific, doxycycline-inducible *Kras-G12D* expression showed that removal of oncogenic KRAS results in the regression of established PanIN lesions to form essentially normal pancreatic tissue within 2 weeks (Collins et al., 2012). Using the same inducible KRAS-G12D model in conjunction with p53 knockout, the authors further demonstrated that even established PDA tumors regress to form residual scar

tissue upon oncogenic KRAS inactivation. Therefore, oncogenic KRAS is required for both the initiation and maintenance of PanINs and PDAs.

Although KC mice develop PanINs within only a few months, these lesions typically do not progress to PDA until more than 12 months of age (Hingorani et al., 2005). This long latency period suggests that other genetic perturbations are likely required for development of full-blown PDA. Indeed, conditional homozygous deletion of *Cdkn2a* and expression of oncogenic KRAS in the *Pdx1^{Cre/+}; Kras^{LSL-G12D/+}; Cdkn2a^{L/L}* (KCC) mice resulted in the rapid development of low-grade PanINs by 3 weeks, full-blown PDA by 6-7 weeks, and 100% mortality by 11 weeks of age (Aguirre, 2003). At the time of death, widespread metastatic lesions could already be found in the adjacent organs. Although this model faithfully recapitulated most histological features of human PDA, the authors also reported that nearly one-third of KCC tumors have a spindle-cell or sarcomatoid histology, which rarely occurs in human disease. Pancreas-specific, homozygous deletion of *Tgfb2*, which encodes a TGF β receptor upstream of SMAD4 signaling, in the *Ptf1a^{Cre/+}; Kras^{LSL-G12D/+}; Tgfb2^{L/L}* (KTC) mouse model similarly resulted in the rapid progression of PanINs at 3 weeks to PDA at 7-10 weeks of age, with complete penetrance (Ijichi et al., 2006). Heterozygous deletion of *Tgfb2* in the same model significantly delayed PDA formation until around 6-7 months of age. PDAs from the KTC model uniformly present with a well-differentiated, ductal histology. Although both KTC models displayed widespread metastases, significantly more metastatic lesions were found in the heterozygous KTC mice at the time of death. Homozygous and heterozygous deletion of *Smad4* in context of oncogenic KRAS resulted in the development of IPMNs and mucinous cystic neoplasms (MCNs), respectively, en route to formation of PDAs with well-differentiated histology (Bardeesy et al., 2006; Izeradjene et al., 2007). Surprisingly, distant metastases could still be found in a substantial percentage of these mice despite having homozygous *Smad4-deficient* tumors (i.e. 18% have metastases in the liver). Although *Cdkn2a*, *Tgfb2*, and *Smad4* deletion in conjunction with oncogenic KRAS all resulted in the development of PDA, none of these models accurately capture the full spectrum of histological features and metastatic pattern found in human disease.

Pancreas-specific, heterozygous dominant-negative p53 mutation in the $Pdx1^{Cre/+}$; $Kras^{LSL-G12D/+}$; $Tp53^{LSL-R172H/+}$ (KPC) mouse model resulted in a relatively slower progression of PanIN to PDA development typically at around 5-6 months (Hingorani et al., 2005). Importantly, these KPC PDA tumors displayed the full spectrum of histology with similar frequencies as seen in human disease. Besides tumor cell morphology, this model also faithfully recapitulated the intense desmoplastic reaction and hypovascular nature of the tumor-associated stroma in human PDA. Again similar to human disease, distant metastases to the liver, lung, and diaphragm were frequently found. Detailed cytogenetic analyses further revealed that KPC tumor cells faithfully recapitulated the high degree of chromosomal instability (CIN) that is pathognomonic of human PDAs. The authors then showed that while all primary and metastatic PDA cell lines harbored silencing mutations in the remaining wild-type p53 allele, all normal and preinvasive PanIN cell lines retained its expression. Given the lack of mutations in any other common tumor suppressor genes, it was reasoned that silencing mutations in the remaining wild-type p53 allele represent the key rate-limiting step in the progression from PanINs to PDAs in the KPC model. This conclusion supported a progressive model of sequential genetic aberrations leading up to PDA, namely: (1) an activating KRAS mutation drives aberrant pancreatic cell growth and PanIN progression, and (2) accumulating mutations in essential tumor suppressor genes (such as p53) ultimately leads to escape from cell cycle regulations and full-blown PDA (Rustgi, 2006). Curiously, spectral karyotyping (SKY) showed that primary and metastatic PDA cell lines derived from the same host have very distinct genomic abnormalities, a result which strongly suggested the early dissemination and independent evolution of metastatic cells. By inserting a lineage marker in the $Pdx1^{Cre/+}$; $Kras^{LSL-G12D/+}$; $Tp53^{LSL-R172H/+}$; $Rosa^{LSL-YFP/+}$ (KPCY) model, Rhim et al. later showed that YFP^+ pancreatic-lineage cells can indeed be found in circulation and in liver micro-metastases prior to any detectable PDA (Rhim et al., 2012). They further reported that cerulein-induced pancreatitis greatly accelerated PanIN progression and also significantly increased the frequency of circulating pancreatic cells (CPCs). Conversely, dexamethasone-mediated suppression of inflammation led to the regression of established PanINs and

undetectable levels of CPCs. If this early and widespread dissemination of CPCs also occur in humans, it can potentially explain the high frequency of metastases seen in PDA patients at presentation. Future comparisons of the genomic features of paired primary and metastatic tumor samples can retrace their evolutionary relationship more precisely and provide additional evidence for the early dissemination of PDA.

Another crucial aspect of the KPC model is its ability to faithfully recapitulate response to existing chemotherapy regimens. To demonstrate the superiority of the KPC model, Olive et al. performed an *in vivo* comparison of the responses to gemcitabine monotherapy in spontaneous KPC tumors, subcutaneously transplanted KPC-derived cancer cells, and xenografts of human PDA cell lines (Olive et al., 2009). While all transplantation models responded at least partially to gemcitabine treatment, the KPC model proved to be highly resistant. In fact, transient reductions in tumor volume occurred in only about 12% of spontaneous KPC tumors. This low response rate was highly reminiscent of human PDAs, where typically about 5-10% of patients have transient responses to gemcitabine (Conroy et al., 2011; Hoff et al., 2013). In contrast to gemcitabine or nab-paclitaxel monotherapy, Frese et al. showed that only the combination of gemcitabine plus nab-paclitaxel significantly slowed tumor growth in the spontaneous KPC model (Frese et al., 2012). About 28% of these tumors even regressed slightly within the 8 days of the study, which is remarkably similar to the 23% response rate observed in the phase III human clinical trial. However, the authors were unable to emulate the repeated doses of nab-paclitaxel in the human regimen and assess long-term survival because of the development of mouse anti-human albumin antibodies. Despite the short duration of this study, KPC mice treated with nab-paclitaxel or combination chemotherapy already have significantly reduced number of metastases. Using the spontaneous KPCY model, Aiello et al. later demonstrated that gemcitabine plus nab-paclitaxel therapy significantly reduced the frequency of liver metastases uniformly regardless of their sizes (Aiello et al., 2016). Indeed, a retrospective study of CT and MRI images in the phase III clinical trial recently confirmed that combination therapy was associated with significantly

greater reductions in both primary and metastatic tumor burden as compared to gemcitabine treatment alone (Kunzmann et al., 2017).

The KPC model has proven to faithfully recapitulate the genomic aberrations, histology, disease progression, and even response to existing chemotherapy. Over the past decade, extensive experimental investigations using this model have resulted in a tremendous increase in our understanding of the biological processes underlying PDAs. Despite this, it is important to keep in mind the difference between the KPC model and human PDA. For instance, human tumors usually develop progressively over many years, which allows enough time for the accumulation of many mutations. In contrast, KPC mice only require a LOH of the wild-type p53 allele in order to progress to detectable PDA at merely 5-6 months of age. This relatively rapid development may also explain the less intense desmoplastic stroma usually seen in KPC tumors as opposed to in human PDA. Because of the relative ease to acquire a LOH mutation, primary tumor in a KPC mouse is usually polyclonal and results from the merging of multifocal precursor lesions (Maddipati and Stanger, 2015). The rapid transformation of KPC tumor cells may also prevent individual clones from accumulating as many passenger mutations as their human counterparts during the course of their evolution. Indeed, KPC-derived cell lines were shown to harbor far fewer mutations than is typically found in human PDAs (Evans et al., 2016; Waddell et al., 2015). Furthermore, it is currently unclear whether KPC tumors accurately reflect the full spectrum and frequency of human PDA subtypes. Because of its reliance on p53 mutations, KPC tumors may disproportionately represent the squamous, quasimesenchymal, and basal-like subtype. As a result of the leakiness of the Pdx1 promoter and having only one wild-type p53 allele, KPC mice are also prone to developing biliary papillomas, sarcomas, and keratoacanthomas of the anal and oral mucosae. Although the KC model may be better than KPC model in regards to some of these issues, its widespread use is severely limited by the long latency period required prior to tumor development. Therefore, KPC mice remain the most widely used pre-clinical model of PDA.

Immunosurveillance and PDA

One essential advantage of using GEMMs with intact immune systems, such as the KPC model, is their ability to model the immune response throughout tumorigenesis. The host immune response is increasingly appreciated as a fundamental aspect of tumor biology. In the early 1900s, Paul Ehrlich was the first to propose that the immune system may be involved in preventing the development of an otherwise “overwhelming frequency” of cancers in larger organisms (Ehrlich, 1909). In the 1950s, Sir Macfarlane Burnet expanded this idea in his proposal of the “immunological surveillance” of cancer (Burnet, 1964; 1970). Here, he postulated that the “evolutionary necessity” of eliminating or inactivating potentially dangerous mutant cells is fulfilled by the immune system. One of the most straightforward strategies to test this hypothesis is to look for increased incidence of cancers in the absence of key components of the immune system. Indeed, interferon-gamma ($IFN\gamma^{-/-}$) and perforin1 ($PRF1^{-/-}$) knockout mice were both more susceptible to developing spontaneous or carcinogen-induced tumors (Street et al., 2001). $Rag2^{-/-}$ mice, which lack B, T, and natural killer T (NKT) cells, were also more prone than wild-type mice to develop tumors spontaneously or in response to carcinogens (Shankaran et al., 2001). Inhibition of other key components of the immune system, such as $\gamma\delta$ -T or NK cells, similarly led to increased susceptibilities of developing certain carcinogen-induced cancers (Smyth et al., 2000; Girardi et al., 2001). Evidence of immunosurveillance also exists in human cancers. For instance, patients who have primary or AIDS-induced immunodeficiencies are at much higher risk of developing certain viral-associated malignancies (Gatti and Good, 1971; Boshoff and Weiss, 2002). In addition, several large long-term studies tracking organ transplant recipients showed that these patients have much higher incidences of kidney, lung, liver, colorectal, ovarian, and head & neck cancers as well as lymphoma and melanoma (Adami et al., 2003; Engels et al., 2011). On the other hand, strong positive correlations between tumor-infiltrating lymphocytes (TILs), especially $CD8^+$ T cells, and patient survival have been noted in a variety of cancers, including in PDA (Pagès et al., 2010; Gentles et al., 2015). Altogether, the immune system plays an important role in restraining tumor formation.

In a landmark study, Shankaran et al. demonstrated that the immune system is capable of “sculpting” or editing tumor immunogenicity (Shankaran et al., 2001). Here, the authors showed that carcinogen-induced tumors from wild-type mice grew equally well when transplanted to syngeneic wild-type or Rag2^{-/-} mice. In contrast, 40% of tumors that developed in Rag2^{-/-} mice failed to grow in wild-type mice. Therefore, tumors that developed in the presence of an intact immune system were less immunogenic and more likely to escape from additional immunosurveillance. On the other hand, tumors that developed in the absence of immunosurveillance remain highly susceptible to regulation by an intact immune system. To explain these results, the authors proposed the theory of “cancer immunoediting” with three sequential phases of tumor-immune interactions: (1) elimination, (2) equilibrium, and (3) escape (Dunn et al., 2002). The elimination phase encompasses the original idea of immunosurveillance, where nascent tumor cells are recognized and killed by the immune system. Tumor cells that survive the elimination phase then enter the equilibrium phase, where the immune system manages to contain the outgrowth of many genetically unstable tumor cells but cannot completely eliminate all of them. Here, selective pressures from the immune system cause the remaining tumor cells to become progressively less immunogenic. Finally in the escape phase, some tumor cells eventually acquire characteristics that allow them to escape immune regulation and proliferate uncontrollably. Together, the “3 E’s” of the cancer immunoediting theory have provided a very useful framework to describe the regulation of tumor growth by the immune system.

The elimination phase can be further broken down into four steps (Dunn et al., 2002). Firstly, pro-inflammatory signals from small growing tumors attract innate immune cells, such as NK, NKT, $\gamma\delta$ -T, macrophages, and dendritic cells (DCs). Dysregulation of surface major histocompatibility complex class I (MHC-I) molecule expression on transformed cells can activate NK cells, which can kill tumor cells in an interferon-gamma (IFN- γ) and tumor necrosis factor-related apoptosis-inducing ligand (TRAIL) dependent manner (Takeda et al., 2001). Similarly, $\gamma\delta$ -T cells can also eliminate tumor cells via an IFN γ -dependent mechanism (Street et al., 2004). In addition, IFN- γ is critical in inducing apoptosis, suppressing proliferation, inhibiting angiogenesis,

and orchestrating the activation of a variety of immune populations (Qin et al., 2003; Wall et al., 2003; Schroder et al., 2004; Gollob et al., 2005). Secondly, tumor cells undergoing immunogenic cell death release tumor-associated antigens (TAAs), which can be ingested and processed by antigen presenting cells (APCs). The presence of “danger-associated molecular patterns” (DAMPs) in the tumor, such as certain species of DNA and RNA, activates APCs and prompts them to migrate to draining lymph nodes (Bianchi, 2007). Thirdly, activated APCs can present TAAs via MHC-II or MHC-I to naïve CD4⁺ and CD8⁺ T cells, respectively. TAA-specific CD4⁺ T cells can then “license” APCs via ligation of CD40, which causes them to up-regulate antigen presentation (signal 1), costimulatory molecules (signal 2), and secrete stimulatory cytokines (signal 3) (Bennett et al., 1998; Schoenberger et al., 1998). While signals 1 and 2 are sufficient to induce cognate CD8⁺ T cell proliferation, development of effector cytolytic function is thought to require the presence of signal 3, such as IL-12 or type 1 interferons (IFN- α/β) (Curtsinger et al., 2003; 2005). Curiously, cognate CD4⁺ T cells ligation of CD40 on cognate CD8⁺ T cells were shown to induce them to become memory T cells (Bourgeois et al., 2002). Finally, activated TAA-specific CD8⁺ T cells expand in number and travel to the tumor to eliminate TAA-expressing cancer cells. After recognition of MHC-I-bound TAAs, effector CD8⁺ T cells can kill tumor cells in a number of ways, including secretion of IFN- γ and the release of granules containing perforins (PRFs) and granzymes (GZMs) (Berke, 1995). Indeed, a “cytolytic index” signature consisting of PRF1 and GZMA expression was recently shown to accurately and specifically represent effector CD8⁺ T cell cytotoxic activity (Rooney et al., 2015). Altogether, successful immune-mediated elimination of tumor cells depends largely on the existence of TAAs and also requires the cooperation of both innate and adaptive immunity.

The equilibrium phase is characterized by continuous production of new tumor variants and their selective elimination by the immune system. One strategy to demonstrate this process is to inhibit components of the immune system after establishment of small, non-progressive tumors and look for their subsequent proliferation. Koebel et al. was the first to demonstrate this process by showing that inhibition of key components of adaptive immunity (CD4/8 T cells and

IFN- γ) after establishment of small, non-progressing tumors resulted in a significantly increased frequency of late outgrowths (Koebel et al., 2007). In contrast, inhibition of components of innate immunity with NK and NKT depletion did not result in any outgrowths. Furthermore, stable tumors in Rag1^{-/-} and Rag2^{-/-} mice rarely exhibit late outgrowths. Therefore, most of the late outgrowths upon inhibition of adaptive immunity in wild-type mice were from the expansion of pre-existing tumors rather than from late *de novo* tumorigenesis in older mice. In human transplant recipients, there are now multiple reports of late outgrowth of donor-derived *de novo* malignancies a few years post-engraftment (Myron Kauffman et al., 2002). Importantly, all of these donors were considered to be either completely healthy or cured of their cancers for decades. Another important aspect of the equilibrium phase is the selective elimination and survival of certain tumor cell variants, a process commonly referred to as “sculpting” or immunoediting. Using an elegant tumor clone mixture model system, Matsushita et al. demonstrated the existence of sculpting by showing the preferential outgrowth of clones lacking expression of a strong TAA (mutant spectrin- β 2) and the simultaneous selective elimination of mutant spectrin- β 2 expressing clones by T cells (Matsushita et al., 2012). Therefore, expression of highly immunogenic TAAs is likely the major factor in deciding which tumor cell variants are eliminated during cancer immunoediting.

A number of factors contribute to tumor escape from immunosurveillance. Loss of tumor antigens, dysfunctional antigen processing and presentation, up-regulation of immune checkpoint molecules such as programmed cell death protein-ligand 1 (PD-L1), and resistance to apoptosis are all major tumor-intrinsic mechanisms that can mediate escape from immune regulation (Hanahan and Weinberg, 2011; Pitt et al., 2016). Accumulation of tumor-extrinsic factors can also promote evasion of immunosurveillance. For instance, tumor-associated factors such as vascular endothelial growth factor (VEGF), interleukin-10 (IL-10), transforming growth factor- β (TGF- β), adenosine, prostaglandin E2 (PGE2), and granulocyte-monocyte colony stimulating factor (GM-CSF) together constitute a complex cytokine network that can directly inhibit effector immune cells and promote the accumulation of immunosuppressive populations, which include fibroblast activation protein-expressing (FAP⁺) stromal cells, tumor-associated macrophages (TAMs),

regulatory T cells (Tregs), and myeloid-derived suppressor cells (MDSCs) (Zou, 2005; Feig et al., 2013; Vonderheide and Bayne, 2013). Secretion of CXCL12 by FAP⁺ stromal cell can mediate the exclusion of effector T cells from the tumor microenvironment (Feig et al., 2013). Rather than promoting adaptive immunity, tumor-infiltrating APCs such as TAMs are often suppressive toward cytotoxic T-helper 1 (Th1)-mediated immunity (type 1 immunity) (Noy and Pollard, 2014). These TAMs typically produce high levels of IL-10, which can simultaneously promote T-helper 2 (Th2) mediated immunity (type 2 immunity) and suppress type 1 immunity (Mantovani et al., 2002). TAMs are also major secretors of cytokines such as TGF- β , IL-10, and CCL2, which promote the differentiation, growth, and recruitment of Tregs (Gajewski et al., 2013). Tregs, in turn, can suppress the expansion of effector T cells by consuming IL-2 in the local environment (Pandiyan et al., 2007). Tregs are also capable of preventing APCs from properly stimulating effector T cells by the trans-endocytosis and sequestration of co-stimulatory molecules CD80/CD86 (Qureshi et al., 2011). Importantly, surface cytotoxic T-lymphocyte-associated protein 4 (CTLA-4) on Tregs can outcompete CD28 for the binding of CD80 and CD86 on APCs, which ultimately leads to development of anergic TAA-specific T cells and tolerance to TAAs (Takahashi et al., 2000). More recently, MDSCs have been characterized as highly immunosuppressive myeloid cells that expand prolifically in context of diseases such as cancer (Gabrilovich and Nagaraj, 2009; Gabrilovich et al., 2012). There are two major subsets of MDSCs: granulocytic (G-MDSC) and monocytic (M-MDSC). The G-MDSC population usually constitutes the major subset and can directly suppresses TAA-specific CD8⁺ T-cells by producing reactive oxygen species (ROS) in an IFN γ -dependent manner (Movahedi et al., 2008; Youn et al., 2008). In addition, the relationship between G-MDSCs and neutrophils is currently unclear, as they share essentially the same lineage markers (Coffelt et al., 2016). M-MDSCs are phenotypically distinct and can suppress CD8⁺ T-cells through inducible nitric oxide synthase (iNOS)-mediated pathways (Movahedi et al., 2008; Youn et al., 2008). While G-MDSCs remain committed to the granulocyte lineage, M-MDSCs were shown to be capable of differentiation into TAMs and DCs *in vivo*, which suggests that at least a subpopulation of them are immature cells (Bronte et al., 2000; Kusmartsev and

Gabrilovich, 2003; Li et al., 2004). MDSCs can also induce Treg differentiation and proliferation through the secretion of cytokines such as IL-10 and TGF- β (Huang et al., 2006). Both subsets of MDSCs express arginase 1 (ARG1), which depletes L-arginine in the local environment and restrains T cell proliferation (Rodriguez et al., 2004; Zea et al., 2005). Furthermore, both MDSCs and TAMs can inhibit effector T cells through surface expression of PD-L1, which engages the PD-1 receptor and directly inhibits T cell receptor (TCR) signaling (Lu et al., 2016; Prima et al., 2017). Therefore, an enormous array of tumor intrinsic and extrinsic factors can cooperate together to promote immune escape.

Many immune escape factors have also been found in PDA. Using the KPC model, our lab has previously reported that TAMs, Tregs, and MDSCs are all prominently present in the tumor microenvironment (Clark et al., 2007). In particular, both TAMs and Tregs were already elevated and negatively correlated with CD8⁺ T cells infiltration in pre-invasive PanIN lesions. This early and increasing accumulation of TAMs and Tregs suggests that suppression of effective T cell priming by APCs is likely a preeminent immune escape mechanism employed throughout PDA development. In support of this hypothesis, effector T cells are essentially absent throughout tumorigenesis in both murine and human PDAs. In contrast to carcinogen-induced models, absence of adaptive immunity by T cell depletion did not affect PDA initiation or growth in the KPC model (Evans et al., 2016). Furthermore, cell lines derived from KPC tumors of T cell-depleted mice grew equally well when transplanted into syngeneic wild-type and T cell-depleted mice, which suggested a lack of T cell-mediated immunoediting in PDA. This dearth of effector T cells at all stages of PDA development may also explain the resistance of both murine and human PDAs to anti-PD1/PDL1 therapy, which works primarily by reinvigorating pre-existing TAA-specific T cells (Brahmer et al., 2012; Winograd et al., 2015). Furthermore, the ineffectiveness of anti-CTLA4 therapy in PDA patients suggests the existence of dysfunctions even more upstream of the provision of signal 2 by APCs to effector T cells (Royal et al., 2010; Winograd et al., 2015). Recently, various tumor vaccine approaches that simultaneously promote the release of TAAs and activate APCs have proven to be particularly efficacious in both murine

and human PDAs. For example, addition of agonistic anti-CD40 antibody, which mimics CD40 ligation to activate APCs, greatly enhanced the efficacy of gemcitabine in patients with advanced and metastatic PDAs (Beatty et al., 2011; 2013). Interestingly, this combination therapy induced a macrophage-dependent tumor regression in the KPC model. However, when circulating macrophages are depleted, the combination of gemcitabine and agonistic anti-CD40 elicited a CD8⁺ T cell-dependent tumor regression (Beatty et al., 2015). Altogether, these findings show that subversion of APC functions constitute a prominent immune escape mechanism in PDA.

Immune suppression mediated by MDSCs represents another important tumor-extrinsic escape mechanism in PDA. In contrast to TAMs and Tregs, systemic expansion and pancreas accumulation of MDSCs occurred only in conjunction with development of full-blown PDAs in the KPC model (Clark et al., 2007). This result suggests that MDSCs might be particularly important in mediating the immune escape of invasive tumors. Although MDSCs have been defined and characterized in other models, their regulation and role in PDA remains unclear. Using the KPC model, our lab has previously shown that tumor-derived GM-CSF is sufficient for inducing the differentiation and expansion of MDSCs *in vitro* (Bayne et al., 2012). In a transplanted model of KPC tumors, inhibition of GM-CSF signaling resulted in reduced MDSC accumulation and a CD8⁺ T cell-dependent tumor regression. Pylayeva-Gupta et al. further showed that oncogenic KRAS promotes GM-CSF expression through the MEK and PI3K signaling pathways (Pylayeva-Gupta et al., 2012). Together, these studies unveiled an immunosuppressive cytokine network where oncogenic KRAS promotes MDSC-dependent tumor immune evasion via the up-regulation of GM-CSF in PDA tumor cells. On the other hand, GM-CSF is the key immune stimulator in the “GVAX” vaccine formulation where tumor cells are transduced to express GM-CSF, irradiated, and then subcutaneously injected into tumor-bearing hosts (Lutz et al., 2014; Le et al., 2015). The contradictory functions of GM-CSF may be largely attributed to differences in the underlying “cytokine networks,” which consist of groups of immune cells and their associated signaling molecules. For instance, abundance of DAMPs in the vaccine formulation may provide additional activating signals to APCs, causing them to polarize toward an immune-stimulatory phenotype

and the secretion of activating cytokines. These cytokines can, in turn, cause other cell types to adopt an effector phenotype and further secrete other stimulatory cytokines, which culminates in a complex cytokine network that promotes anti-tumor immunity. These results demonstrate that the function cytokines and immune populations depend largely on the underlying cytokine networks. Uncovering these underlying cytokine networks is, therefore, paramount to our understanding of the immune response in PDA.

Goals and key findings of this thesis project

In the discussions above, we have shown that: (1) human PDA is a deadly and heterogeneous disease that is likely driven by several biological processes, (2) the KPC model accurately recapitulate most aspects of human PDA, (3) PDA employs multiple mechanisms to evade immunosurveillance, and (4) cytokine networks constitute an important means of immune escape in PDA. Our lab has previously described one such cytokine network whereby tumor-derived GM-CSF promotes the differentiation and expansion of MDSCs, which then suppress anti-tumor T cell responses (Bayne et al., 2012). However, it remains unclear which MDSC subset is important for mediating immunosuppression. Furthermore, the sequential order of MDSC recruitment and subset differentiation is also unclear. Because their immunosuppressive capabilities have not been individually verified, we will at first refer to these potential G-MDSCs and M-MDSCs in the tumor microenvironment as tumor-associated neutrophils (TANs) and monocytic myeloid cells, respectively. For this work, I decided to focus on investigating TANs. The first major goal of this thesis project was to characterize TAN involvement in PDA and discover the cytokine network that regulates them. We first found that subsets of both human and murine PDAs are enriched in TANs and CXCR2 ligand expression, especially CXCL5. We then showed that CXCR2 is specifically required for TAN trafficking to the tumor microenvironment, but not for their differentiation and expansion. Importantly, CXCR2 ablation did not significantly affect accumulation of monocytic myeloid cells in the tumor, which suggests that MDSC subset commitment occurs primarily before their separate recruitment. Furthermore, we demonstrated

that TANs primarily promote tumor growth by suppressing anti-tumor T cell responses. Given their ability to suppress T cells, a subset of TANs can be referred to as G-MDSCs. Finally, we showed that CXCR2 ablation confers additional benefits in conjunction with combination gemcitabine, nab-paclitaxel, plus agonistic anti-CD40 treatment. Therefore, we have uncovered an important immunosuppressive cytokine network in PDA that involves CXCR2 ligands and TAN-mediated inhibition of anti-tumor T cell immunity.

Given the importance of cytokine networks in regulating immunosurveillance, we next sought to discover more of these networks in human PDAs *in silico*. Here, we devised a novel analysis pipeline by combining techniques from tumor immune infiltration profiling, gene co-expression analysis, and network theory to infer cytokine networks and highlight the most important components within them. After demonstrating the survival benefit of high intratumoral cytolytic activity, we further showed that PDA tumors with high and low cytolytic activity are associated with significantly different cytokine networks. The relative strength of correlations between immune populations and cytokines were indicative of their recruitment, activation, or function in the different networks. The most important or distinguishing features of cytokine networks in tumors with high cytolytically activity include CD8 T cells, CD4 T follicular helper cells, CD4 memory cells, B cells, TNFSF14/LIGHT, and IL24. On the other hand, macrophages, CLEC11A/SCGF, and CCL13 are among the most important in the cytokine networks in tumors with low cytolytic activity. To our knowledge, this analysis is the first to use a *de novo* approach to construct and compare the landscape of tumor-associated cytokine networks. Altogether, this thesis highlighted cytokine networks that may be important in regulating immune activity in PDA.

CHAPTER 2: MATERIALS AND METHODS

* The majority of the methods described in this chapter are described in:

(1) T. Chao, E.E. Furth and R.H. Vonderheide. CXCR2-Dependent Accumulation of Tumor-Associated Neutrophils Regulates T-cell Immunity in Pancreatic Ductal Adenocarcinoma. *Cancer Immunology Research*. November 1 2016. 4(11), 968-982.

(2) T. Chao and R.H. Vonderheide. "In silico reconstruction and comparison of cytokine networks in pancreatic ductal adenocarcinomas with high and low cytolytic activity." In preparation.

Analysis of TCGA RNA-seq Data

Normalized RSEM counts from primary tumor samples and their matched controls were downloaded from the TCGA Research Network through the GDAC data portal (<http://gdac.broadinstitute.org/>) and included all available Illumina HiSeq 2000 Level 3 gene-level data as of January 28, 2016. The following 15 cancer types (TCGA project, n = sample size) were included in our analysis: hormone receptor positive breast cancer (BRCA, n = 823), colorectal adenocarcinoma (COADREAD, n = 379), esophageal carcinoma (ESCA, n = 184), glioblastoma (GBM, n = 153), head and neck squamous cell carcinoma (HNSC, n = 520), kidney renal clear cell carcinoma (KIRC, n = 533), kidney renal papillary carcinoma (KIRP, n = 290), liver hepatocellular carcinoma (LIHC, n = 371), lung adenocarcinoma (LUAD, n = 515), lung squamous carcinoma (LUSC, n = 501), pancreatic ductal adenocarcinoma (PAAD, n = 134), prostate adenocarcinoma (PRAD, n = 497), colorectal adenocarcinoma (COADREAD, n = 382), liver hepatocellular carcinoma (LIHC, n = 373), lung adenocarcinoma (LUAD, n = 517), lung squamous cell carcinoma (LUSC, n = 501), skin cutaneous melanoma (SKCM, n = 103), stomach adenocarcinoma (STAD, n = 415), and thyroid carcinoma (THCA, n = 501). Genes with less than 20% of samples have a normalized RSEM count ≥ 1 were filtered out from subsequent analysis. The normalized RSEM values were then log-transformed using the formula: $\log_2(\text{RSEM} + 1)$.

The average log₂ expression of each chemokine was calculated for cancer and normal samples in each of the 15 different tumor types. Unsupervised hierarchical clustering was performed on the difference (log₂ fold change) between the cancer and normal expression using the “heatmap.2” or “heatmap3” packages available in R/Bioconductor. Spearman’s rank based correlations between chemokines were calculated with their respective P values using the “Hmisc” package. The neutrophil gene signature was calculated as the log-average of normalized RSEM expression of 31 genes that constitute a previously defined neutrophil-signature. To compare expression of CXCL5 and neutrophil-signature across the 15 different cancer cohorts, the log₂-normalized RSEM values were transformed to z-scores using the formula: $z\text{-score} = (X - \text{average}(X)) / \text{stdev}(X)$, where X represents the RSEM values. The average and standard deviation were calculated from the expression of X across all samples included in this study.

Unsupervised hierarchical clustering was used to cluster the 134 PDA samples based on the expression of the neutrophil-signature genes or CXCR2 ligands. PDA subtype classifier, immunome gene sets, and canonical pathway gene sets were acquired from the indicated literature and Broad Institute’s Molecular Signature Database (MSigDB) (Bailey et al., 2016; Bindea et al., 2013; Collisson et al., 2011; Moffitt et al., 2015; Subramanian et al., 2005). The “GSVA” package available in R/Bioconductor was used to calculate GSVA signature scores for each gene set (rnaseq=T, mx.diff=T). Differential expression of GSVA signature scores between cluster groups was calculated using the Holm-Sidak multiple comparison test. Adjusted values of ≤ 0.05 were considered significant. Spearman’s rank based correlation was calculated between immunome GSVA signature scores and chemokines as above. To identify chemokines most predictive of the neutrophil GSVA signature score, we built a random forest regression model to predict the signature score based on chemokine expression using the “randomForestSRC” and “ggRandomForests” packages in R/Bioconductor.

Immune Gene Sets and Cytokine Expression Analysis in Human PDA

Gene expression in transcript per million (TPM) of the 134 resected, primary PDA tumor samples available in TCGA were downloaded from UCSC's TOIL RNAseq recompute analysis (Vivian et al., 2017). A total of 55 immune gene sets were acquired from the immunome (IM, $n = 26$), CIBERSORT's LM22 (LM22, $n = 22$), and the FANTOM 5 Consortium (F5, $n = 7$) (Bindea et al., 2013; FANTOM Consortium, 2014; Newman et al., 2015; Rooney et al., 2015). For the LM22 signatures, only genes that were uniquely and significantly overexpressed in each population were included. The cytolytic activity (GZMA and PRF1) and the cytotoxic gene signatures were both defined in previous studies (Rooney et al., 2015). The "GSVA" package available in R/Bioconductor was used to calculate the gene set variation analysis (GSVA) signature scores for each gene set ($rnaseq=T$, $mx.diff=T$). Because genes in three of the signatures were not expressed, only 52 GSVA signatures were calculated. Human genes annotated with cytokine activity (GO:0005125), growth factor activity (GO:0008083), chemokine activity (GO:0008009), or hormone activity (GO:0005179) were defined as cytokines in this study. Only 255 cytokines were expressed in more than 20% of the samples and included in our analysis. Cytokine TPM values were converted to log scale via the formula: $\log_2(TPM+1)$.

Hierarchical clustering was performed using the "heatmap.2" package, where the distance was defined using Spearman's correlation ($1-\rho$) when comparing genes/signatures or Euclidean distance when comparing samples. The complete agglomeration algorithm was used for clustering both genes/signatures and samples. The "cutree" function was used to define cytolytically hot and cold samples ($k=4$). Cox regression analyses and survival plots were performed using the "coxph" and "survfit" functions in the "survival" package, respectively. Differential cytokine or GSVA signature expression was determined using two-tailed Wilcoxon test. FDR-adjusted P -values ≤ 0.05 were considered statistically significant.

Cytokine Network Analysis

To calculate the distribution of correlations and network properties, 1000 bootstrapped populations with sample replacement were created using all ($n = 134$), only the hot ($n = 30$), or

only the cold ($n = 71$) samples. In each bootstrapped population, Spearman's correlation (ρ) was calculated for each pair-wise immune-immune GSVA signature scores and immune-cytokine relationships. Furthermore, all asymptotically significant immune-cytokine correlations ≥ 0.4 were incorporated into a cytokine network using the "igraph" package, where the absolute values of ρ were used as weights of the edges. The normalized degree and eigenvector centrality of each node was calculated for each network, such that all possible values lie between 0-1. Correlations, degrees, and eigenvectors were considered significant if their empirical 95% confidence intervals do not contain zero. Empirical P -values comparing two populations were calculated using the formula: $(1 + r) / (1 + n)$, where n is the number of samples in a population and r is the number of samples in that population that are greater than or equal to the mean value of the second population. Empirical P -values ≤ 0.05 were considered statistically significant.

To select the top correlations or network properties, random forest classifiers separating cytolytically hot populations from cytolytically cold populations were trained using the "randomForestSRC" package with 1000 trees and included only differentially enriched correlations, degrees, or eigenvectors as input variables. Both the mean decrease of accuracy over all out-of-bag cross-validated predictions (VIMP score) and the averaged depth (from the root node) to the first sub-tree involved (minimal depth score) were used to rank the input variables. The "ggRandomForest" package was then used to visualize the results.

Histological Analysis of Human PDA

Hematoxylin and eosin stained slides from the resected tumors of 12 patients with previously untreated, resectable PDA were prepared per routine at the Department of Pathology, Hospital of the University of Pennsylvania. The percent of cancer epithelium, stroma, and lumen that have significant neutrophil involvement for each sample were then recorded. These studies were approved by the University of Pennsylvania Institutional Review Board.

Mouse PDA Models

All mouse protocols were reviewed and approved by the Institutional Animal Care and Use Committee (IACUC) of the University of Pennsylvania. Animals were maintained in a specific pathogen-free facility. $Kras^{LSL-G12D/+};Trp53^{LSL-R172H/+};Rosa^{LSL-YFP};Pdx1-Cre$ (KPCY) and $Kras^{LSL-G12D/+};Trp53^{LSL-R172H/+};Pdx1-Cre$ (KPC) mice were bred in-house and backcrossed for over ten generations with C57BL/6J mice (Hingorani et al., 2005; Rhim et al., 2012; Evans et al., 2016). All of these mice were confirmed on the C57BL/6 background at the DartMouse™ Speed Congenic Core Facility at the Giesel School of Medicine at Dartmouth College as previously described (Byrne and Vonderheide, 2016). Four- to six- months old KPC/KPCY mice with palpable tumors or with tumors $>100\text{mm}^3$ by ultrasound were used in this study, with their age-matched controls. $Cxcr2^{-/-}$ and $Cxcr2^{+/+}$ littermates were bred in-house from backcrossed, syngeneic $Cxcr2^{+/-}$ mice purchased from the Jackson Laboratories. These mice were maintained on acidified water (pH ~ 3-4) to minimize opportunistic infections. Genotypes were determined by Transnetyx. C57BL/6J wild-type mice were purchased from Jackson Laboratories. Six to twelve week old mice were used for tumor implantation studies.

Mouse PDA Cell Lines

All murine PDA cell lines, including 4662, were derived from primary pancreatic tumors of KPC mice. Briefly, dissociated cells from primary tumor were plated in a 6-well dish with serum-free DMEM to select for tumor cells. After two weeks, the cells were expanded in DMEM with 10% Fetal Bovine Serum (FBS). Only cells of ten or fewer passages were used for experiments. The pancreatic-lineage origin of all PDA cell lines were validated by PCR for the presence of rearranged $Kras^{LSL-G12D}$ allele (Evans et al., 2016). Cell lines were tested and authenticated using IMPACT and RADIL. Cell lines used for implantation studies were also tested and confirmed to be Mycoplasma and endotoxin free. All cell lines were maintained at 37°C and 5% CO₂ in complete media (cDMEM), which contains Dulbecco's Modified Eagle Medium (DMEM-GlutaMAX™) (Thermo Scientific) supplemented with 10% fetal bovine serum, 1% L-glutamine, and 50 µg/mL gentamicin (Gibco).

In vitro treatment of 4662 PDA cell line with inhibitors and siRNA

4662 PDA cells were seeded at a density of 1×10^5 cells/mL on 6-well plates in cDMEM for 24 hours in triplicates. After washing with DMEM, cells were incubated for 24 h with DMEM containing DMSO control, 10 ng/mL mTNF α (R&D), 10 μ M U0126 (MEK1/2-i, Cell Signal Technologies), or 20 μ M LY294002 (PI3K inhibitor, Cell Signal Technologies), each with or without 20 μ M Wedelolactone (IKK1/2-i, Sigma-Aldrich). After 24 h, the supernatant was collected and frozen at -20°C until further analysis. Qiagen's RNeasy-Plus Mini Kit was used to isolate total RNA from pelleted cells. RNA quality was assessed using a NanoDrop ND-1000. Only samples with a 260/280 value of ≥ 1.9 were used. First strand cDNA was synthesized using High-Capacity cDNA Reverse Transcription Kit (Applied Biosystems). Primer probes for 18S (Applied Biosystems), Csf2 (GM-CSF), Kras, RelA, RelB, Gsk3 α , Gsk3 β , Tbk1, Yap1, Cxcl1, Cxcl2, Cxcl3, Cxcl5, Cxcl7 (PPBP), and Cxcr2 (IDT) were used for qPCR in a ViiA™ 7 Real-Time PCR System. Relative expression was determined after normalizing to 18S expression.

For siRNA inhibition of Yap1 and Kras, 4662 PDA cells were seeded as described above. After washing with DMEM, the cells were transfected with 10 nM of siRNA against Kras (Life Technologies, S68935), Yap1 (Sigma-Aldrich, NM_009534), RelA (Sigma-Aldrich, NM_009045), RelB (Sigma-Aldrich, NM_009046), Gsk3 α (Sigma-Aldrich, NM_001031667), Gsk3 β (Sigma-Aldrich, NM_178613), Tbk1 (Sigma-Aldrich, NM_019786), and a Td-Tomato fluorescent negative control (Sigma-Aldrich, SIC005) using the Lipofectamine® RNAiMAX Transfection Reagent (Life Technologies). After 48 hours of incubation, the supernatant and RNA were collected and analyzed as described above.

In vivo subcutaneous tumor implantation studies

PDA cells were cultured and harvested at 80-90% confluence. After assessing for > 90% viability via hemocytometer with Trypan blue staining, 5×10^5 cells were injected subcutaneously into the right flank. Tumor volume was monitored using digital calipers and calculated as (l x

$w^2)/2$, where l is the longest dimension and w is the perpendicular dimension. Mice were euthanized if tumor volume reached $> 1 \text{ cm}^3$. For the CXCL5 inhibition study, 100 μg of anti-CXCL5 (R&D Systems, MAB433) or 100 μg of isotype control (R&D Systems, MAB0061) were injected intraperitoneally every 3 days starting on Day 10 for the duration of the study. For T-cell depletion studies, 200 μg of anti-CD4 (BioXCell, GK1.5l) and 200 μg of anti-CD8 (BioXCell, YTS 169.4), or 400 μg of isotype control (BioXCell, LTF-2) were administered intraperitoneally every 3 days for the duration of the study, starting 4 days prior to tumor implantation (Evans et al., 2016).

For the combination chemo- and immune-therapy study, mice were implanted with 5×10^5 KPC-derived 4662 cells subcutaneously into the right flank. This regimen has been previously reported (Winograd et al., 2015; Byrne and Vonderheide, 2016). Briefly, on day 10, mice were injected intraperitoneally with 2.4 mg gemcitabine and 2.4 mg Abraxane or with PBS and 2.4 mg human albumin. On day 12, mice were further injected with 100 μg of anti-CD40 (BioXCell, FGK4.5) or isotype control (BioXCell, 2A3). Tumor growth was monitored using a digital caliper until endpoint was reached.

Processing of plasma, tumor supernatant, and single-cell suspension from tissues

Mice were euthanized in a CO₂ chamber. Whole blood from cardiac puncture was collected in EDTA-containing Eppendorf tubes. The tubes were centrifuged at 12,000 x g for 10 mins. The resulting supernatants were centrifuged at 14,000 x g for 15 mins to remove remaining debris. Plasma samples were stored at -20°C until further use. Pancreata or subcutaneous tumors were dissected and rinsed with RPMI. To prepare samples for flow cytometric analysis or FACS, tissues were minced with fine scissors (≥ 200 cuts) and incubated in collagenase IV solution (1 mg/ml in RPMI) for 30-45 minutes at 37°C. The solution was then placed on ice and a 1:4 dilution with ice cold RPMI + 10%FBS was added to stop the reaction. Dissociated cells were passed through a 70 μm cell strainer and pelleted. The supernatant was collected and frozen until further use. The pelleted cells were washed with FACS Buffer (PBS + 0.5% BSA + 0.5 mM

EDTA). After centrifugation, the cells were resuspended in FACS Buffer, filtered through another 70 µm cell strainer, and kept on ice.

Histopathology and Immunofluorescence of tumors

Fresh pancreatic or subcutaneous tumors were rinsed in PBS and placed in Zinc Formalin Fixative (Sigma-Aldrich) overnight. Then they were dehydrated serially in 70%, 95%, and 100% ethanol. The tissues were then embedded in paraffin, which were processed to generate H&E and unstained sections. To rehydrate for immunofluorescence, unstained sections were serially submerged in Xylene (Sigma), 100% ethanol, 95% ethanol, 70% ethanol, and PBS. Sections were then blocked with 10% donkey serum + 0.1% TritonX-100 in PBS overnight at 4°C; followed by incubation with a goat anti-GFP antibody (Abcam, ab6673; 1:200) and a rat anti-mouse Ly6G antibody (BioXCell, BE0075-1; 1:200) for 1 hour at room temperature. After washing, the sections were incubated with Alexa Fluor 488 donkey anti-goat IgG (Invitrogen, A-11055; 1:200), Alexa Fluor 488 or Alexa Fluor 594 donkey anti-rat IgG (Invitrogen, A-21208 or A-21209; 1:200), and DAPI (Biolegend; 1:1000) for 1 hour at RT in the dark. Sections were then washed and mounted with Aqua-Poly/Mount (Polysciences). A Nikon Eclipse Ti-U fluorescent microscope was used to acquire images at a 64-bit data depth.

Measurement of chemokine concentrations in plasma, tumor and cell culture supernatant

Plasma, tumor and cell culture supernatant CXCL1 and CXCL5 protein levels were measured using the LEGENDplex™ Mouse Proinflammatory Chemokine Panel (13-plex) kit following manufacturer's protocol. Bead identity and intensity were measured with a FACSCanto and subsequently analyzed with FlowJo.

FACS Sorting and Transcriptional analysis

YFP⁺ and YFP⁻ populations from KPCY pancreata were sorted using a FACSAria II Flow Cytometer directly into TRIzol Reagent (Invitrogen). Total RNA was isolated following

recommendations from the manufacturer. Briefly, cells were homogenized in TRIzol reagent. Chloroform (0.2ml per 1ml of TRIzol Reagent) was then added, vigorously mixed, and incubated for 2-3 mins. After centrifugation at 12,000 x g for 15 mins at 4°C, the aqueous phase was isolated. Glycogen was added to the RNA solution to aid subsequent visualization of RNA pellet. Isopropanol was added to precipitate RNA, which was followed by washing with ethanol. The RNA pellet was resuspended in DNase/RNase-free water. RNA quality was assessed using a NanoDrop ND-1000. First strand cDNA was synthesized using High-Capacity cDNA Reverse Transcription Kit (Applied Biosystems). Primer probes for 18S (Applied Biosystems), Cxcl1, Cxcl2, Cxcl3, Cxcl5, Cxcl7, and Cxcr2 (IDT) were used for qPCR in a ViiA™ 7 Real-Time PCR System. Relative expression was determined after normalizing to 18S expression.

Flow Cytometry

Between 5×10^6 and 1×10^7 cells were plated per well in a 96 well plate. For ex vivo stimulation, cells were incubated with the Leukocyte Activation Cocktail, with BD GolgiPlug™ (1:500) in RPMI for 5 hours at 37°C before subsequent staining. Viability was assessed using Live/Dead Fixable Aqua Dead Cell Stain Kit. Cells were then washed and stained with labeled antibodies (1:100) against surface markers at 4°C for 30 minutes in FACS Buffer. For intracellular stains, cells were fixed, permeabilized, and stained with labeled intracellular antibodies using the Transcription Factor Staining Buffer Set (eBioscience). After washing, labeled cells were analyzed using a FACSCanto or a LSR II flow cytometer (BD Biosciences). The FlowJo software was used to perform subsequent gating and quantification of cell populations. The gating strategies from several recent publications were used to define immune cell populations (12,15). Cell labeling was performed with the following fluorescently conjugated mAbs directed against mouse CD31 (MEC 13.3), CD45 (30-F11), CD3E (145-2C11), CD4 (RM4-5), CD8a (53-6.7), CD44 (IM7), CD62L (MEL-14), CD11a (M17/4), CD11c (N418), CD19 (6D5), F4/80 (BM8), CD11b (M1/70), Ly6C (HK1.4), Ly6G (1A8), IFN γ (XMG1.2), TNF α (MP6-XT22), IL10 (JESS-

16E3), IL2 (JES6-5H4), IL17 (eBio17B7), and FOXP3 (FJK-16s) – all acquired from Biolegend, eBiosciences, or BD Biosciences.

Statistical Analysis

Unless otherwise specified, significance in variations between two groups was determined by two-tailed, unpaired t-test. Significance in variations between two groups for many factors was calculated using the Holm-Sidak multiple comparison test. Differences among three (or more) related groups for one factor were analyzed by one-way ANOVA, followed by the Tukey's multiple comparison test. Differences in tumor growth curves and immune populations were analyzed by two-way ANOVA, followed by Dunnett's multiple comparison test. Statistical analyses were performed using GraphPad Prism (GraphPad). A P value ≤ 0.05 was considered statistically significant.

CHAPTER 3: CXCR2-Dependent Accumulation of Tumor-Associated Neutrophils Regulates T-cell Immunity in Pancreatic Ductal Adenocarcinoma

* The majority of the results described in this chapter have been published in:

T. Chao, E.E. Furth and R.H. Vonderheide. CXCR2-Dependent Accumulation of Tumor-Associated Neutrophils Regulates T-cell Immunity in Pancreatic Ductal Adenocarcinoma. *Cancer Immunology Research*. November 1 2016. 4(11), 968-982.

INTRODUCTION

Despite advances using combination chemotherapy, pancreatic adenocarcinoma (PDA) remains one of the most lethal malignancies, with a dismal 5-year survival rate of ~7.7% (Conroy et al., 2011; Hoff et al., 2013; Siegel et al., 2017). Even with surgery and adjuvant therapy in patients with resectable PDA, the 5-year survival rate is just about 20% (Lim et al., 2003; Sohn et al., 2000; Siegel et al., 2017). Alarming, PDA now kills more Americans than breast cancer and is predicted to become the second leading cause of cancer-related deaths in the United States by 2020 (Rahib et al., 2014). Therefore, expanding our knowledge of mechanisms promoting PDA progression and resistance is urgently needed.

Avoiding host immunity is a key feature of tumor progression (Hanahan and Weinberg, 2011), and understanding the mechanisms by which cancer cells evade immune destruction is critical for the development of more effective treatment strategies. To describe the immune-tumor interactions in PDA, our lab previously characterized the immune infiltrate during progressive stages of PDA development using the *Kras*^{LSL-G12D/+}; *Trp53*^{LSL-R172H/+}; *Pdx1-Cre* (KPC) murine model (Clark et al., 2007). We found extensive infiltration of immunosuppressive Treg and myeloid cells in both pancreatic intraepithelial neoplasia (PanINs) and PDA. In contrast, infiltration of effector T cells was scant in the tumor microenvironment. These observations suggested that a highly immunosuppressive environment is established even at the earliest stages of tumor development. Although immune checkpoint blockade with anti-PD-1/PD-L1 or anti-CTLA-4 is

ineffective in stimulating antitumor immunity, depleting or “re-educating” immunosuppressive myeloid populations has proven to be more effective at eliciting antitumor T-cell responses in PDA (Beatty et al., 2011; 2013; Royal et al., 2010; Brahmer et al., 2012; Winograd et al., 2015; Byrne and Vonderheide, 2016).

Tumor-associated neutrophils (TANs) play important roles in cancer development, progression, and resistance to therapy (Fridlender and Albelda, 2012; Coffelt et al., 2016). A meta-analysis of the literature concluded that TANs are typically pro-tumor and are strongly associated with poorer prognosis in the majority of human cancers (Shen et al., 2014). TANs often exhibit protumorigenic functions, including promotion of angiogenesis, metastases, and immunosuppression (Rodriguez et al., 2004; Shojaei et al., 2007; Wculek and Malanchi, 2015; Spiegel et al., 2016). However, TANs also can be antitumor in early-stage cancer or when TGF β is inhibited (Fridlender et al., 2009; Singhal et al., 2016). Thus, whether TANs are pro- or antitumor depends in part on the specific cancer type and the stage of the tumor. In the context of PDA, presence of TANs is strongly associated with poorer prognosis (Reid et al., 2011; Wang et al., 2016). High intratumoral CXCL5, a chemokine for neutrophils, have also been associated with poorer overall survival (Li et al., 2011). In the KPC model, systemic depletion of GR1⁺ myeloid cells, which includes neutrophils, can increase infiltration of effector T cells and inhibit tumor growth (Stromnes et al., 2014). Therefore, targeting neutrophils may be therapeutic in PDA.

CXCR2 ligands are essential for neutrophil egression from the bone marrow and trafficking toward sites of inflammation (Eash et al., 2010; Mei et al., 2012). CXCR2 is also essential for the recruitment of TANs in various cancers (Jamieson et al., 2012; Katoh et al., 2013; Highfill et al., 2014). In the KPC model, CXCR2 blockade by genetic ablation or pharmacologic inhibition reduces the recruitment of MPO⁺ neutrophils to the PDA tumor microenvironment and potently suppresses metastases (Steele et al., 2016). CXCR2 inhibition sensitized PDA tumors that were otherwise highly resistant to anti-PD-1D-1 therapy. Here, using both human and mouse data, we build on the above results by detailing the mechanisms involved in CXCR2-ligand activation in PDA and discerning the impact on T-cell responses in the setting of

CXCR2 disruption. We show that a subset of human PDA have significant elevation of TAN-related genes. Analysis of gene expression in human PDA revealed a correlation between high expression of CXCR2 ligands and enrichment of neutrophils and NF- κ B related pathways. We further showed that the KPC model faithfully recapitulates human disease in the expression profile of CXCR2 ligands, with CXCL5 being the most prominent in both. Using a KPC-derived PDA cell line, we discovered that NF- κ B activation can potently induce CXCL5 expression and secretion. We found that host CXCR2 ablation dramatically inhibited TAN accumulation and resulted in a spontaneous, T cell-dependent suppression of tumor growth. Therefore, our data support the hypothesis that the CXCR2-ligand axis is a promising therapeutic target in PDA.

RESULTS

A subset of human PDA has significant TAN involvement.

To investigate the extent of neutrophil infiltration in human PDA, we compared the normalized expression of a previously defined neutrophil gene signature in 134 resected PDA compared to 14 other primary cancer cohorts using RNA-sequencing data available from The Cancer Genome Atlas (TCGA) (Bindea et al., 2013; Cancer Genome Atlas Research Network et al., 2013). PDA ranked second, on average, among these 15 cancers in the expression of the neutrophil gene signature (Figure 1). Thus, TANs may be relatively abundant in PDA. The PDA cohort naturally clusters into a TAN-high, a TAN-medium, and a TAN-low group (Figure 2). To identify immune populations co-enriched in TAN-high tumors, gene set variation analysis (GSVA) was performed using previously defined “immunome” gene sets that specifically identify immune populations (Bindea et al., 2013). Confirming our cluster definition, the neutrophil-specific gene set was significantly enriched in the TAN-high group (Figure 3A). Of the 16 other immune populations tested, the macrophage and $\gamma\delta$ T-cell gene sets were also significantly enriched in TAN-high compared to TAN-medium and TAN-low tumors.

As described in the previous chapter, four main subsets of PDA were identified by Bailey *et al.*: squamous, aberrantly differentiated endocrine exocrine (ADEX), pancreatic progenitor

(PP), and immunogenic (Immune) (Bailey et al., 2016). Squamous, ADEX, and PP subtypes are most similar to Collisson *et al.*'s quasimesenchymal (QM-PDA), exocrine-linked, and classical subtypes, respectively (Collisson et al., 2011). PDA tumors could be further divided based on whether they have normal or activated stroma using Moffitt *et al.*'s signatures (Moffitt et al., 2015). To explore whether neutrophil infiltration is associated with certain PDA subtypes, we used GSVA to compare the enrichment of previously defined PDA subtype gene sets in TAN-high and TAN-medium/low tumors. Our analysis showed that TAN-high tumors have significant enrichment of genes in the normal stroma subtype and the squamous subtype, which has the poorest prognosis (Figure 3B). However, high TAN involvement was not significantly associated with the immunogenic subtype, which is primarily characterized by infiltration of adaptive immune cells.

To understand the spatial distribution of TANs in human PDA, a cohort of PDA resected tumors from previously untreated patients ($n = 12$) were examined by standard pathologic examination, in which neutrophils are readily identified on H&E staining (Figure 4A). Eight of 12 tumors exhibited a mild to extensive degree of neutrophil infiltration, with a few tumors having significantly more TANs (Figures 4B and 4C). Four tumors were devoid of neutrophils. One tumor had neutrophils only in neoplastic ductal lumens. In the remaining seven samples, neutrophils were also found within the cancer epithelium and stroma (Figure 4B). Because none of the samples in this cohort was of the rare squamous subtype, comparisons of neutrophil infiltration between different PDA subtypes, as suggested by our analysis of TCGA data could not be made on a histological basis.

CXCR2 ligand expression is strongly associated with neutrophil and NF- κ B pathway in human PDA.

To investigate whether CXCR2 ligands are involved in pancreatic cancer, we compared the expression of CXCR2 ligands (CXCR2Ls) in 134 PDA samples from TCGA. The expression of *CXCL5* was not only higher than the other CXCR2Ls, but it was also markedly elevated in PDA compared to the other tumor types (Figures 5A-B). In general, tumors with higher *CXCL5*

expression had higher neutrophil gene signature expression, and vice versa (Figures 1 and 5B). However, even though PDA had the highest *CXCL5* expression, it was not the highest in neutrophil gene expression. This may be explained by the role of other CXCR2Ls besides *CXCL5* in the recruitment of TANs in other cancers. Although *CXCL5* expression was the highest among CXCR2Ls in human PDA, we also noted significant expression of other CXCR2Ls, especially *CXCL8*. Because these chemokines are likely redundant in their function, all CXCR2Ls were included in the subsequent analysis.

Unsupervised hierarchical clustering divided the PDA cohort into a CXCR2L-high group and a CXCR2L-low group (Figure 6). To identify immune populations enriched in CXCR2L-high tumors, GSEA analysis was done using the “immunome” gene sets as above (Bindea et al., 2013). Of the 17 immune populations tested, only the neutrophil gene set showed significant enrichment in CXCR2L-high compared to CXCR2L-low tumors (Figure 7A). This result supported the hypothesis that CXCR2 ligands are specifically and selectively important for the recruitment of tumor-associated neutrophils (TANs), but not for other immune populations. Because CXCR2L-high tumors should in theory overlap with TAN-high tumors, we hypothesized that CXCR2L-high tumors would be relatively more enriched in genes related to the squamous subtype. However, GSEA analysis of PDA subtypes showed that CXCR2L-high tumors are not significantly associated with any PDA subtypes, though there was a trend toward enrichment of the squamous subtype with an adjusted *P* value of 0.13 (Figure 7B). Therefore, the CXCR2-ligand axis probably plays a role in PDA regardless of subtype.

In addition to immune populations and PDA subtypes, we were also interested in signaling pathways and biological processes that may be enriched in CXCR2L-high tumors. Of the 2,838 Hallmark, Canonical Pathways, and Gene Ontology gene sets that were curated by Broad Institute’s Molecular Signature Database, only 17 gene sets (0.6%) were significantly enriched in CXCR2L-high tumors (Figure 8) (Subramanian et al., 2005). Confirming our stratification of the PDA cohort into chemokine-high and low groups, the majority of these significant gene sets (8 of 17) involved leukocyte trafficking and chemokine/cytokine-receptor

signaling. As may be expected of tumors enriched with neutrophils, pathways involved in innate immune functions, such as pattern recognition and glycosaminoglycan (GAG) binding, were also significantly enriched. Gene sets related to IL1R, NOD-like receptor (NLR), and TNF α signaling were also significantly enriched in CXCR2L-high tumors. Importantly, these inflammatory pathways all converged on NF- κ B signaling downstream. These findings suggested that increased NF- κ B signaling may be associated with elevated CXCR2 ligand expression in PDA.

TAN signature score in PDA is best predicted by CXCL8 and CXCL5.

We have shown that PDA samples in TCGA with high CXCR2 ligand expression associated specifically with the neutrophil GSVA signature score (Figure 7A). This implied that CXCR2 ligands may be playing a role in TAN recruitment in PDA. To identify factors that may be regulating TAN accumulation in PDA, we correlated the expression of all chemokines with immunome signature scores 17 immune populations including neutrophils (Figure 9). In concordance with the GSVA analysis above, the TAN signature score is significantly correlated with many CXCR2 ligands, especially with CXCL5 and CXCL8. The TAN signature also clustered most closely with macrophages, again confirming our previous finding. However, because many of the immunome signatures correlated with each other, it is difficult to identify which chemokines are most important for TANs compared to other immune cells.

To find chemokines most predictive of TAN involvement, we built a random forest regression (RF-R) model to predict the TAN signature score based on chemokine gene expressions. The importance of each chemokine in the RF-R model was measured by two methods: the variable importance (VIMP) and minimal depth scores. The VIMP score is based on the difference in predictive ability of the RF-R model with and without a given variable. On the other hand, the minimal depth score is a direct measure of the importance of a given variable in the RF-R model's decision trees. In this case, an important variable would have a minimal depth score that is closer to the root decision node. Interestingly, CXCL8 and CXCL5 were the two most

important chemokines according to both measures (Figure 10). This result supports the hypothesis that CXCR2 ligands may be important for the accumulation of TANs in PDA.

KPC tumors faithfully recapitulate CXCR2 ligand expression of human disease.

To further elucidate the role of TANs and the CXCR2-ligand axis in PDA, we studied their involvement in murine models using *Kras*^{LSL-G12D/+}; *Trp53*^{LSL-R172H/+}; *Pdx1-Cre* (KPC) and KPC with the *Rosa*^{LSL-YFP} allele (KPCY) mice. Hematoxylin and eosin (H&E) staining of the pancreatic tumors of KPCY mice showed remarkable histological similarity with human PDA (Figures 4A and 11). Similar to human disease, immunofluorescent staining of murine neutrophils with an antibody to Ly6G showed extensive infiltration of neutrophils throughout the tumor micro-environment in most KPC tumors (Figure 11). In contrast, almost no staining was observed in the pancreata of age-matched *Pdx1-Cre* (C) control mice. We further used flow cytometric analysis to further delineate the difference in the accumulation of CD19⁺ B cells, F4/80⁺ macrophages, CD4⁺ T cells, CD8⁺ T cells, CD11b⁺Ly6C⁺ monocytes, and CD11b⁺Ly6G⁺ TANs in pancreatic tumors in KPC compared to control pancreas. The results confirmed a significant accumulation of CD11b⁺Ly6G⁺ neutrophils in KPC tumors compared to control pancreas (Figure 12). Similar flow cytometric analysis of the spleens showed a significant increase in the proportion of neutrophils among immune cells systemically (Figure 13). The increase in the proportion of myeloid cells (neutrophils and monocytes) is accompanied by the corresponding decrease in other immune populations, such as CD19⁺ B cells and CD8⁺ T cells. Therefore, the murine KPC and KPCY models faithfully recapitulated TAN involvement observed in human PDA.

To investigate CXCR2 ligands in murine PDA, we first quantified CXCL1 and CXCL5 protein in KPC tumors and normal pancreas using multiplex ELISA. The results showed that both CXCL1 and CXCL5 were significantly elevated in pancreatic tumors compared to control pancreas (Figure 14). However, the plasma concentrations of both of these chemokines did not differ significantly between KPC and control mice. This implied steeper chemokine gradients for CXCL1 and CXCL5 toward the pancreas of tumor-bearing KPC compared to control mice. To

address which cell populations were responsible for CXCR2 ligand expression in PDA, we compared the gene expression of these chemokines in YFP⁺ pancreatic-lineage and YFP⁻ stromal cells in tumor-bearing KPCY mice using RT-PCR. Similar to human disease, *Cxcl5* was the most highly expressed CXCR2 ligand in YFP⁺ pancreatic cancer cells in KPCY mice (Figure 15). However, YFP⁻ stromal cells in the tumor also expressed many CXCR2 ligands, particularly *Cxcl2*. Further confirming our results above, all 9 KPC-derived PDA cell lines highly secreted CXCL5 as measured by multiplex bead assays, with some also secreting CXCL1 (Figure 16). Although not statistically significant, *Cxcr2* was expressed primarily by YFP⁻ stromal cells and not by YFP⁺ pancreatic cancer cells (Figure 15, inset). Thus, both tumor and stromal cells were involved in the expression of CXCR2 ligands. However, CXCR2 receptor itself was primarily found in stromal populations rather than in the cancer cells themselves.

KRAS/MEK inhibition and TNF α induces CXCL5 expression in a NF- κ B dependent manner.

To explore the effects of mutant *Kras* and mutant *Trp53* in regulating CXCR2 ligand expression, we compared the expression of all CXCR2 ligands in YFP⁺ pancreatic-lineage or YFP⁻ stromal cells in 4-6 months old CY, PCY, and KCY mice. Increased expression of *Cxcl5* in YFP⁺ tumor cells and *Cxcl2* in YFP⁻ stromal cells were associated with mutant *Kras* and not mutant *Trp53* expression (Figure 17). This data led us to hypothesize that pathways directly downstream or indirectly induced by oncogenic *Kras* may be responsible for regulating CXCR2 ligand expression in these KPC-derived, murine pancreatic cancer cells. We therefore compared the expression of *Cxcl5* via RT-qPCR in 4662 KPC cells treated with U0126 (MEK1/2 inhibitor) or DMSO. The 4662 cell line is a well-characterized KPC-derived PDA cell line that has been previously described (Byrne and Vonderheide, 2016; Evans et al., 2016; Lo et al., 2015; Winograd et al., 2015). Inhibition of MEK resulted in a significant increase in *Cxcl5* expression compared to control (Figure 18A). In contrast, MEK inhibition led to a significant reduction in *Csf2* (GM-CSF) expression in PDA, which confirmed previously published observations regarding GM-CSF regulation by oncogenic *Kras* (Pylayeva-Gupta et al., 2012). *Cxcl5* expression was also

significantly increased in *Kras* siRNA–treated 4662 cells compared to control (Figure 18B). Thus, KRAS-MEK signaling is not directly responsible for *Cxcl5* expression; rather, *Cxcl5* expression is likely regulated by pathways that activate in response to KRAS-inhibition in the setting of oncogenic *Kras* expression. An elegant study using an inducible oncogenic *Kras* model of PDA has shown that YAP1 activation in PDA cancer cells allows escape from oncogenic *Kras* addiction (Zhang et al., 2014). Recently, the same group showed that YAP1 directly regulates *Cxcl5* expression in a murine model of prostate cancer (Wang et al., 2016). To test the hypothesis that YAP1 directly regulates *Cxcl5* expression in PDA, we compared the expression of *Cxcl5* in *Yap1* siRNA– and control siRNA–treated 4662 cells (Figure 18C). Unlike the observations in prostate cancer, knock down of *Yap1* did not significantly alter *Cxcl5* expression in PDA cells in our model.

Using multiplex bead assays and flow cytometric analysis, we confirmed that MEK inhibition of the 4662 cells not only increased their CXCL5 mRNA expression but also their CXCL5 protein secretion into the media (Figure 19A). In comparison, 4662 cells treated with LY294002 (PI3K inhibitor) did not alter their CXCL5 secretion. To test the involvement of other signaling pathways potentially downstream of oncogenic *Kras*, we treated 4662 cells with siRNA directed against RelA, RelB, Gsk3 α , Gsk3 β , and Tbk1 (Pylayeva-Gupta et al., 2011). However, none of these treatment resulted in significant changes in CXCL5 secretion compared to control (Figure 19B). These results suggested that the baseline CXCL5 expression in 4662 PDA cells is not reliant on any one of these pathways.

From our analysis of TCGA PDA data, we noted that tumors with high CXCR2 ligand expression were significantly enriched in expression of genes associated with inflammatory signaling pathways which all converged on NF- κ B signaling. Therefore, we hypothesize that NF- κ B signaling may be regulating *Cxcl5* expression in PDA cells. To test this hypothesis, we compared the amount of secreted CXCL5 in the supernatant of 4662 PDA cells treated with mouse TNF α , which is a potent inducer of NF- κ B activity, and those treated with DMSO control (Figure 20A). In support of our hypothesis, TNF α treatment significantly increased CXCL5

secretion. The TNF α -induced increase in CXCL5 was abrogated upon co-treatment with wedelolactone (NF- κ B inhibitor), a selective inhibitor of IKK α / β that does not affect p38 MAPK or AKT activities. In congruence with the siRNA result, NF- κ B inhibition alone did not significantly alter baseline CXCL5 secretion. These results showed that NF- κ B activity can potentially induce CXCL5 secretion in PDA cells, but does not seem to affect baseline levels.

We then tested the hypothesis that NF- κ B signaling in the setting of KRAS/MEK inhibition is responsible for the increased CXCL5 level. Indeed, NF- κ B inhibition completely abrogated the increase in CXCL5 in the presence of MEK inhibition (Figure 20A). Using MotifMap's prediction tool, we found that high confidence NF- κ B binding sites are indeed predicted to be in the promoter region immediately upstream of the human *CXCL5* gene (Figure 20B). This showed that CXCL5 expression may be similarly regulated by NF- κ B in humans. Altogether, NF- κ B signaling may be an important pathway induced in response to KRAS/MEK inhibition in PDA cancer cells.

TAN accumulation in KPC tumors is not significantly altered by anti-CXCL5 treatment.

To test the hypothesis that CXCL5 is responsible for the accumulation of TANs in PDA, we used an implantable model of the KPC tumors. The subcutaneous tumor growth of a KPC-derived PDA cell line, 4662, was monitored in syngeneic wildtype mice treated with anti-CXCL5 or isotype control antibodies for three weeks (Figure 21A). Anti-CXCL5 treatment significantly slowed tumor growth compared to control during this duration (Figure 21B). However, flow cytometric analysis of tumors excised on Day 21 did not reveal significant differences in any infiltrating immune populations (Figure 22). Similarly, no differences were observed systemically in the spleens of mice treated with anti-CXCL5 or isotype control (Figure 23). This result indicated that CXCL5 is not absolutely necessary for TAN recruitment in PDA, especially when other CXCR2 ligands are also present in the microenvironment.

CXCR2 ablation specifically prevents TAN accumulation and inhibits tumor growth.

The expression of multiple CXCR2 ligands by different cell populations in the tumor microenvironment suggested significant redundancy in chemotactic signal to recruit TANs in PDA. This complexity made targeting individual CXCR2 ligands difficult and confounded, as demonstrated by inhibition of CXCL5 alone. However, CXCR2 ligands all converged on their binding to CXCR2, which as noted above, was primarily expressed in the non-tumor cells. To study the role of stromal CXCR2 in PDA, we compared the subcutaneous growth of 4662 KPC tumor cells in syngeneic *Cxcr2*^{-/-} or *Cxcr2*^{+/+} hosts. Tumor growth was significantly delayed in the absence of host *Cxcr2* (Figure 24A). A significant survival benefit was also observed in *Cxcr2* knockouts (Figure 24B). Differences in tumor weight between *Cxcr2*^{-/-} and *Cxcr2*^{+/+} hosts only became significant two to three weeks post implantation (Figure 24C). The lack of initial differences in growth kinetics and tumor weights showed that the 4662 PDA cell line was able to seed and establish tumors in both *Cxcr2*^{-/-} and *Cxcr2*^{+/+} hosts, suggesting that late factors were likely responsible for the observed differences in growth kinetics.

To understand if CXCR2 signaling was required for TAN accumulation in this PDA model, we compared the tumor-infiltrating immune populations in *Cxcr2*^{-/-} and *Cxcr2*^{+/+} hosts. Histological analysis with H&E staining showed remarkable similarity between the subcutaneous model and the KPC/KPCY model of PDA (Figures 11 and 25). Immunofluorescent staining with anti-Ly6G on tumor sections showed diffuse tumor infiltration of neutrophils in *Cxcr2*^{+/+} hosts, similar to the pattern seen in human and KPCY PDA tumors. In contrast, TANs were almost completely absent in the tumors of *Cxcr2*^{-/-} hosts. Using flow cytometry to compare tumor-infiltrating immune populations on days 10, 14, and 21 after implantation, we noted a striking reduction in the density of tumor-infiltrating CD11b⁺Ly6G⁺ neutrophils in *Cxcr2*^{-/-} compared to *Cxcr2*^{+/+} hosts, with no difference in the density of F4/80⁺ macrophages and CD11b⁺Ly6C⁺ monocytes (Figure 26). Consistent with a previously published study, CD11b⁺Ly6G⁺ granulocytes were found to be highly abundant in the spleen of *Cxcr2*^{-/-} hosts at the earliest time point, which suggested that CXCR2 signaling primarily affected trafficking and not the differentiation of granulocytes (Figure 27). Importantly, the density of tumor infiltrating CD3⁺ T cells was

significantly elevated in *Cxcr2*^{-/-} compared to *Cxcr2*^{+/+} hosts 21 days post-implantation. Therefore, these data support the hypothesis that CXCR2 signaling is specifically required for the accumulation of TANs, but not for other myeloid populations. Furthermore, lack of TAN accumulation corresponded with increased accumulation of tumor-infiltrating T cells 2-3 weeks post-implantation.

Absence of TANs correlates with increased infiltration and function of activated T cells.

Flow cytometric analysis showed no significant difference in the density of CD45⁻CD31⁺ endothelial cells. In contrast, we found a significant increase in the infiltration of CD3⁺ T cells in *Cxcr2*^{-/-} compared to *Cxcr2*^{+/+} hosts (Figure 26C). Correspondingly, there was also a significant increase in the density of tumor-infiltrating CD4⁺ T cells in *Cxcr2*^{-/-} compared to *Cxcr2*^{+/+} hosts (Figure 28A). More detailed analysis showed that activated CD44^{hi}CD62L⁺ memory and CD44^{hi}CD62L⁻ effector CD4⁺ T cells were both significantly increased in *Cxcr2*^{-/-} hosts (Figure 28B). In contrast, no difference was observed in the density of infiltrating CD4⁺FOXP3⁺ Tregs (Figure 29A). As above, TANs were almost completely absent in this cohort of *Cxcr2*^{-/-} compared to wild-type hosts (Figure 29A). Therefore, the absence of TANs corresponded with significant infiltration of activated T cells in the TME.

To highlight the change in the proportion of effector to suppressive immune populations, ratios of the density of activated CD4⁺CD44^{hi} T cells to the density of Tregs cells and TANs were calculated and found to be increased (Figure 29B). The ratio of the density of tumor infiltrating CD8⁺ T cells to the density of TANs was also significantly elevated. These ratios highlighted the significant increase in the proportion of effector T cells and corresponding decrease in the proportion of suppressive immune cells in the tumors of *Cxcr2*^{-/-} hosts. We further hypothesized that tumor-infiltrating effector T cells are more functional in *Cxcr2*^{-/-} than in *Cxcr2*^{+/+} hosts. Indeed, *ex vivo* PMA/ionomycin stimulation induced higher proportions of IFN γ -expressing cells in both CD4⁺ and CD8⁺ T-cell populations in *Cxcr2*^{-/-} compared to *Cxcr2*^{+/+} hosts (Figure 30A). A higher proportion of CD4⁺ T cells was also induced to express IL17, which indicated more

functional T_h17 cells (Figure 30B). These results supported the hypothesis that T cells were indeed more functional in the absence of TANs.

To test the hypothesis that T cells were responsible for inhibiting tumor growth in *Cxcr2*^{-/-} mice, we compared tumor growth in *Cxcr2*^{-/-} and *Cxcr2*^{+/+} mice treated with dual depleting antibodies against CD4 and CD8 or isotype control (Figure 31A). Tumor growth did not differ between control and CD4/8-depleted *Cxcr2*^{+/+} mice, which suggested that CD4⁺ and CD8⁺ T cells do not naturally impact PDA tumor growth, confirming our recent results (Evans et al., 2016). There was a significant difference in tumor growth comparing *Cxcr2*^{+/+} and *Cxcr2*^{-/-} mice in the control group. In contrast, tumor growth in isotype-treated *Cxcr2*^{+/+} and CD4/CD8-depleted *Cxcr2*^{-/-} mice were not significantly different. Kaplan-Meier survival curves showed similar findings (Figure 31B). Thus, depletion of T cells in *Cxcr2*^{-/-} hosts rescued tumor growth. This result strongly supported the hypothesis that CD4⁺/CD8⁺ T cells were responsible for inhibiting tumor growth in *Cxcr2*^{-/-} mice. Altogether, these data show that the CXCR2-ligand axis is required for recruitment of TANs, which regulates T-cell immunity in PDA.

Our lab has previously reported that the combination of gemcitabine, abraxane (nab-paclitaxel or nP), and agonistic anti-CD40 (Gem/nP/aCD40) treatment resulted in a T-cell dependent anti-tumor response in about 50% of tumors in our KPC pancreatic cancer model (Byrne and Vonderheide, 2016). Because CXCR2 ablation similarly elicited a T-cell dependent anti-tumor response, we hypothesized that it could provide benefits in addition to Gem/nP/aCD40 therapy. Indeed, 4662 tumor growth was significantly slowed in *Cxcr2*^{-/-} mice treated with Gem/nP/aCD40 therapy compared to control *Cxcr2*^{-/-} mice (Figure 32). Therefore, CXCR2 inhibition may provide additional benefit to combination therapy in pancreatic cancer.

DISCUSSION AND CONCLUSIONS

Multiple studies have demonstrated the importance of CXCR2 in the recruitment of tumor-promoting and immunosuppressive myeloid cells in various cancers, including PDA (Highfill et al., 2014; Steele et al., 2016; Wang et al., 2016). It has recently been shown that CD3⁺

T-cell infiltration increases upon CXCR2 inhibition in murine PDA (Steele et al., 2016). Here, we aimed to understand the relevant CXCR2 ligands and mechanisms regulating CXCR2 ligand expression in the TME, as this insight may help advance efforts at clinical translation. Our work adds to previously published studies in several key areas. We report: (1) neutrophils are an important aspect of the human PDA TME particularly in the squamous subtype; (2) human PDA has particularly high *CXCL5* expression and other CXCR2 ligands compared to other cancer types, as confirmed in our murine model; (3) *CXCL5* expression is correlated to NF- κ B signaling pathways in human PDA and, in our mouse model, *CXCL5* is strongly induced by NF- κ B activation; (4) abrogation of CXCR2 signaling slows tumor growth in mice and triggers an influx of activated and functional CD4⁺ T cells into the TME; and (5) depletion of T cells completely reverses the antitumor effects of CXCR2 inhibition. Our data adds to important accumulating evidence that the CXCR2-ligand axis is a promising target for the treatment of PDA (Hertzer et al., 2013).

We have previously shown that the PDA tumor microenvironment has elevated frequency of myeloid cells (Clark et al., 2007; Bayne et al., 2012). Several landmark studies have described novel methods of using predefined gene signatures to derive the relative abundance of immune populations from gene expression data in complex tissues (Bindea et al., 2013; Newman et al., 2015). Here, similar to comparing relative expression of a single gene between samples, we compare the expression of such previously defined gene sets as a surrogate for the relative abundance of immune cells, pathway activation, and PDA subtypes. Our analysis of human TCGA data confirms that at least a subset of human PDA, especially those of the squamous subtype, also has significantly elevated infiltration of TANs. This is in remarkable congruence with the recent work by Steele et al. showing that absence of TAN accumulation in murine KPC PDA tumors is associated with decreased expression of genes in the squamous subtype compared to controls (Steele et al., 2016). We also report here that TAN-high tumors have elevated expression of macrophages and $\gamma\delta$ T-cell related genes. This result supports the recent evidence that $\gamma\delta$ T cells can promote TAN accumulation and may relate to their ability to suppress $\alpha\beta$ T

cells in PDA (Coffelt et al., 2015; Daley et al., 2016). TANs have also been shown to highly express CCL chemokines, which can recruit macrophages (Fridlender et al., 2012; Gabrilovich et al., 2012). Although it remains to be confirmed, our analysis suggests that such interactions between TANs, macrophages, and $\gamma\delta$ T cells may also exist in PDA.

Despite ample evidence of TAN accumulation in PDA, the mechanism leading to increased TAN infiltration is not fully understood and may be due to active recruitment via chemokines or passive response to tissue damage. Recently, Steele et al. demonstrated that *Cxcl2* expression is significantly elevated in the KPC mouse model of PDA and showed that CXCR2 inhibition significantly reduces the infiltration of MPO⁺ neutrophils using IHC (Steele et al., 2016). In another study also using the KPC model, Seifert et al. showed that CXCL1 is elevated in a RIP1/3-dependent manner and that anti-CXCL1 treatment reduces the infiltration of Gr1⁺CD11b⁺ cells, which consist of a heterogeneous population including TANs and monocytes (Seifert et al., 2016). Using an implantable model of KPC PDA, we confirmed that CXCR2 regulates the accumulation of TANs. In addition, our data revealed that CXCR2 ablation specifically inhibited the accumulation of neutrophils, without affecting infiltration of other myeloid populations. A role for CXCR1 was not directly studied in our work and cannot be excluded from our results here. Indeed, CXCR1 and CXCR2 have both been shown to be individually sufficient for chemotaxis of human neutrophils *in vitro* when induced by CXCL8 and CXCL1, respectively (Hammond et al., 1995). However, from the near absence of granulocytes recruited to the tumor *in vivo* using our *Cxcr2* knockout mice, we hypothesize that CXCR2, rather than CXCR1, plays the dominant role in the recruitment of granulocytes in our mouse PDA model. Considering the inherent differences between mouse and human genome, whether this conclusion also applies in human PDA remains unknown and difficult to study *in vivo* using our immune-competent PDA mouse model. It is possible that CXCR1 inhibition may further decrease granulocyte recruitment when in combination with CXCR2 inhibition.

Although previous studies have shown elevation of various CXCR2 ligands in PDA, only a few have attempted to delineate the source of these chemokines within the tumor

microenvironment (Seifert et al., 2016; Steele et al., 2016; Wang et al., 2016). Here, an unbiased analysis of all CXCR2 ligands using TCGA RNA-sequence data revealed that *CXCL5* and *CXCL8* expression were orders of magnitude higher than other CXCR2 ligands in PDA. Furthermore, *CXCL5* expression was much higher in PDA compared to other solid tumors. Analysis of all murine CXCR2 ligands in KPCY tumors revealed an abundance of *Cxcl2* and *Cxcl5* expression, which are primarily expressed by stromal and pancreatic-lineage cells, respectively. Interestingly, Steele et al. also reported an enrichment of *Cxcl2* and *Cxcl5* expression in the tumor epithelium of KPC tumors compared to WT pancreas (Steele et al., 2016). Assigning direct orthologous relationships between human and mouse chemokines can sometimes be difficult (Zlotnik and Yoshie, 2012). For instance, the mouse has no homolog of human *CXCL8*. Immunohistochemistry analysis has shown that *CXCL8* is up-regulated and associated with poorer prognosis in human PDA (Hussain et al., 2010). Indeed, *CXCL8* was the second highest expressed CXCR2 ligand in the PDA samples in TCGA and may also be playing an important role in neutrophil recruitment in human disease. Indeed, the random forest model showed that *CXCL5* and *CXCL8* expression were the most predictive chemokines for the expression of the neutrophil-specific gene signature. Because *CXCL8* is absent in the mouse genome, its role cannot be further explored using our KPC or KPCY mouse models. Furthermore, human *CXCL5* and *CXCL6* are both very similar to *Cxcl5* in the mouse, which also does not have *Cxcl6*. Given the difference between species, we find the congruence of elevated *CXCL5* expression in human and *Cxcl5* expression in mouse PDA even more remarkable. *CXCL5* protein level is strongly associated with reduced overall survival in a cohort of human PDA (Li et al., 2011). Using our implantable model of murine PDA, systemic inhibition of *CXCL5* only resulted in slightly delayed tumor growth. However, this treatment did not significantly affect TAN accumulation. Therefore, *CXCL5* is not likely to be necessary for TAN recruitment. This should be expected as many other CXCR2 ligands are also present in the tumor microenvironment. Future studies will be required to determine the specific function of tumor-derived *CXCL5*. Regardless, our data here highlighted the prominence and uniqueness of *CXCL5* expression in PDA.

Because *CXCL5* was the most highly and universally expressed CXCR2 ligand, we studied the regulation of its expression in more detail. Here, we discovered that NF- κ B activation can potently increase CXCL5 protein level in KPC PDA cells. Again, this was consistent with human TCGA data, in which PDA tumors with high CXCR2 ligand expression are also significantly enriched in the expression of inflammatory pathways involving NF- κ B. Although the populations expressing these pathways could not be determined using TCGA data alone, our results from the mouse model suggested that NF- κ B activity may be enhanced in the cancer cells themselves. Studies in a mouse model of pancreatic intraepithelial neoplasia (PanIN), show that RELA is activated in the presence of oncogenic KRAS and regulates the expression of *Cxcl1* (Lesina et al., 2016). Indeed, RELA/p50 is constitutively activated in almost 70% of pancreatic cancers (Wang et al., 1999). An elegant study by Ling et al. using pancreas-targeted knockout of IKK β in *Pdx1-Cre;Kras^{LSL-G12D/+};Cdkn2a^{L/L}* mice showed that inactivation of NF- κ B signaling completely inhibited PDA development (Ling et al., 2012). They further demonstrated that KRAS^{G12D}-driven AP-1 activation can induce the expression of IL1 α , which in turn acted in an autocrine manner and activated NF- κ B to induce more IL1 α expression in a positive feedforward loop. Contrary to the implications from this study, we found that NF- κ B activity actually increased when KRAS or MEK was inhibited. Although the mechanism of this increased activity remains to be determined, we speculate that it may have resulted from enhanced PI3K/AKT signaling, which is upstream of NF- κ B activation, upon MEK inhibition (Wee et al., 2009). Altogether, our data suggested that NF- κ B activation is important for inducing CXCL5 expression in PDA.

The frequency of tumor-infiltrating T cells were shown to increase significantly in the setting of CXCR2 inhibition (Steele et al., 2016; Wang et al., 2016). This observation was also true in our subcutaneous, implantable murine model of PDA. This subcutaneous model faithfully recapitulated the histology, immune infiltration, and even response to therapy of spontaneous KPC pancreatic tumors (Winograd et al., 2015; Byrne and Vonderheide, 2016; Evans et al., 2016). Another group used the spontaneous, autochthonous KPC model and reported similar conclusions to those presented in this paper (Steele et al., 2016). In this study, pharmacologic

CXCR2 inhibition suppressed metastasis and prolonged survival in KPC mice. Furthermore, in the context of anti-PD-1 therapy, co-treatment with a CXCR2 inhibitor led to increased infiltration of effector CD4⁺ and CD8⁺ T cells. Adding to this study, we observed that the tumor-infiltrating T cells in *Cxcr2*^{-/-} hosts consisted mostly of activated, effector CD4⁺ T cells. Although the density of tumor infiltrating CD8⁺ T cells was not increased in *Cxcr2*^{-/-} mice, the proportion of IFN γ -producing cells increased among both activated CD4⁺ and CD8⁺ T-cell populations. This result supported the hypothesis that TANs are immunosuppressive in PDA.

However, the specific mechanisms of how TANs suppress infiltration of T cells in PDA remain to be elucidated. Possible mechanisms include expression of arginase 1 (ARG1), inducible nitric oxide synthase (iNOS), and reactive oxygen species (ROS) (Gabrilovich and Nagaraj, 2009). Besides the direct suppression of T cells, TANs may also be able to subvert the development of cytotoxic cellular responses by modulating the phenotype of macrophages (Sinha et al., 2007; Filardy et al., 2010). In addition, presentation of antigens via MHC-I on TANs can theoretically sequester antigen-specific CD8⁺ T cells away from antigen presenting cells and tumor cells. Because granulocytic-myeloid derived suppressor cells (G-MDSCs) are defined in mice as CD11b⁺Ly6G⁺Ly6C^{lo} cells that suppresses T-cell proliferation or function, TANs or at least a subset of them in our PDA model, fulfill this definition (Bronte et al., 2016). Future work must be done to further delineate the relationship between TANs and G-MDSCs. Given that PDA is naturally void of effector T cells, the observation that effector T cells could infiltrate in the absence of TANs is particularly exciting. Indeed, CXCR2 inhibition sensitized the otherwise highly resistant KPC PDA to anti-PD-1 therapy, with durable response in a small subset of tumors (Steele et al., 2016). We have shown here that CXCR2 ablation can also confer additional benefits to combination gemcitabine, nab-paclitaxel, and agonistic anti-CD40 therapy. Therefore, our data support the emerging notion that targeting combinations of components of the pancreatic tumor microenvironment may be needed in order to sensitize tumors to combination chemotherapy and immune checkpoint inhibitors (Feig et al., 2013; Lo et al., 2015; Winograd et al., 2015; Byrne and Vonderheide, 2016; Jiang et al., 2016; Nywening et al., 2016).

Besides their immunosuppressive function, TANs can also promote angiogenesis (Shojaei et al., 2007). In fact, reduced blood vessel density was observed in xenografts of a CXCL8 knockdown human PDA cell line compared to controls (Sparmann and Bar-Sagi, 2004). However, in our model with syngeneic immunocompetent mice, depletion of CD4⁺ and CD8⁺ T cells was sufficient to rescue tumor growth in *Cxcr2*^{-/-} hosts. Furthermore, the density of endothelial cells did not differ significantly between the tumors of *Cxcr2*^{+/+} and *Cxcr2*^{-/-} hosts. These results argued that TANs primarily promote tumor growth via immunosuppressive mechanisms in our model rather than through reduction in angiogenesis.

In summary, we conclude that CXCR2 is required for the recruitment of TANs, which in turn can suppress antitumor T-cell responses. We showed that CXCR2 ligands, particularly CXCL5, are elevated in both human and mouse PDA. Furthermore, expression and secretion of CXCL5 in our mouse model is potently induced by NF-κB activation. Finally, we showed that PDA tumor growth can be inhibited in a T cell–dependent manner in the context of CXCR2 inhibition. Therefore, the CXCR2-ligand axis is emerging as a potential target for the treatment of PDA.

Neutrophil gene signature

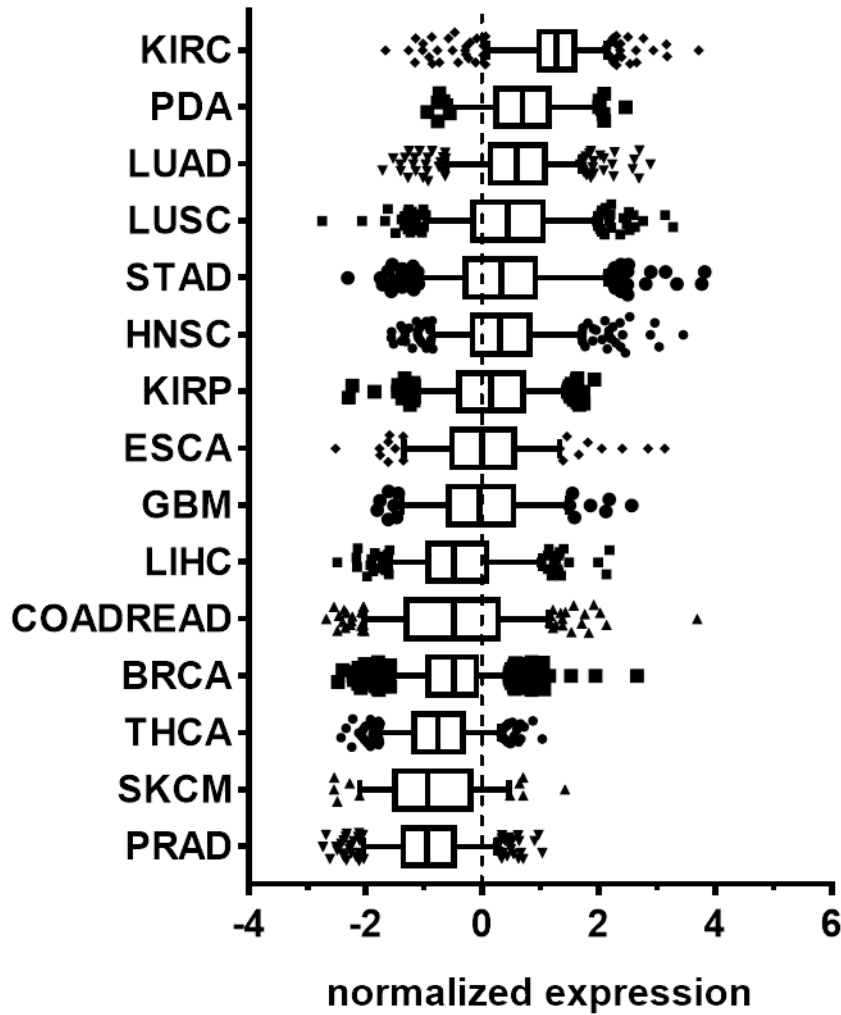


Figure 1. Relative expression of the neutrophil gene signature across TCGA.

Normalized expression (z-scores) of the neutrophil gene signature in primary tumors across 15 TCGA cancer cohorts. Boxplot whiskers at 5-95th percentile. Dashed line represents the average expression value.

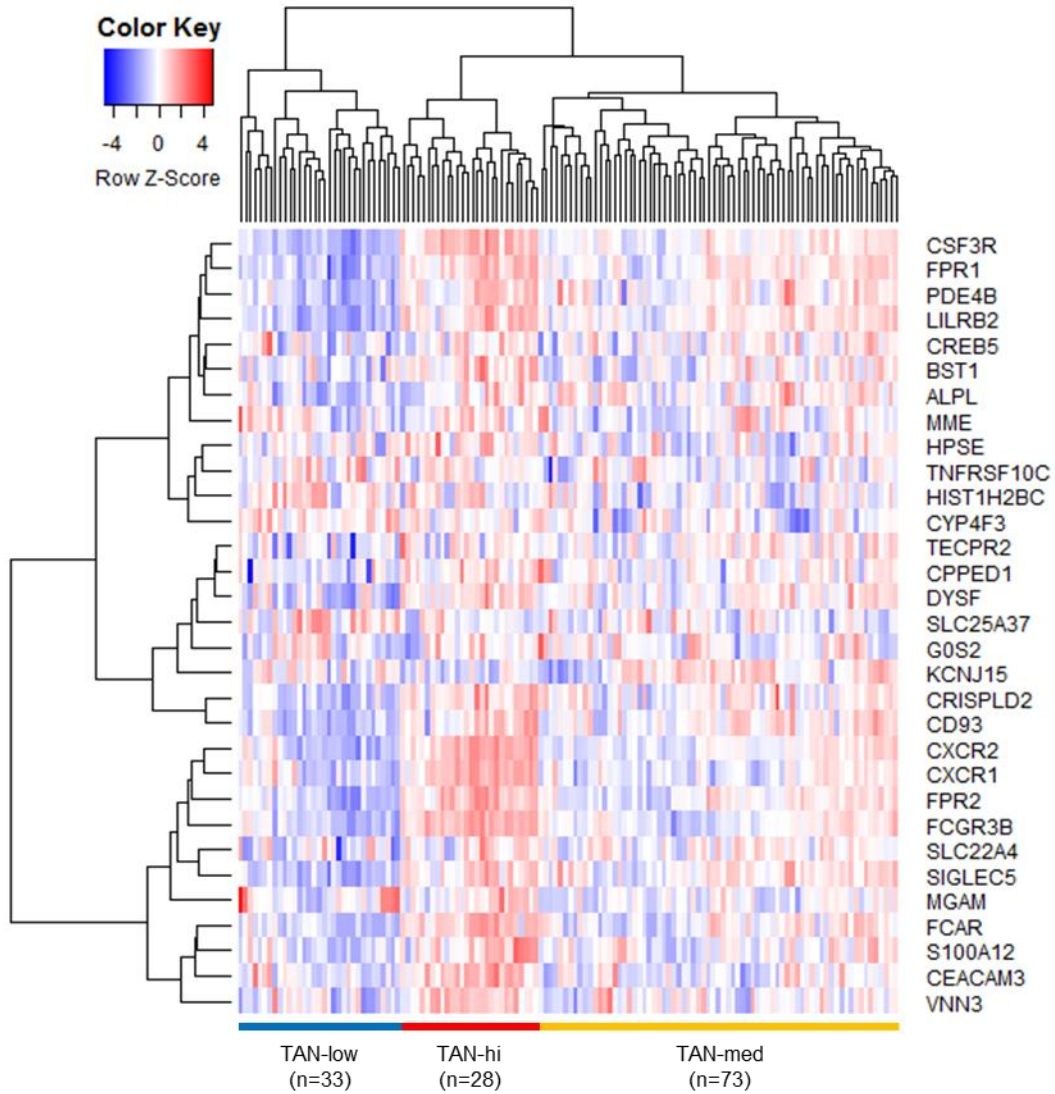


Figure 2. Stratification of human PDA samples by neutrophil signature genes.

Clustering of 134 human TCGA PDA samples using 31 genes in the neutrophil signature into TAN-high, TAN-med, and TAN-low groups.

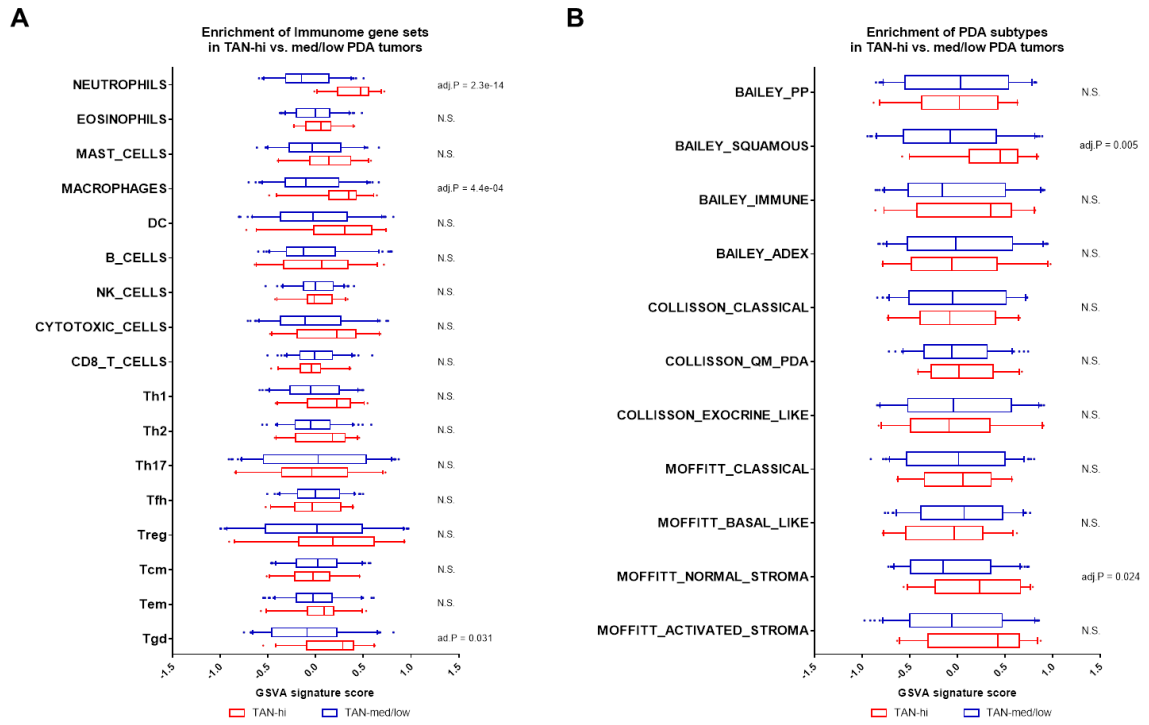


Figure 3. Immune populations and PDA subtypes enriched in TAN-high samples.

(A) Comparison of GSVAsignature scores for 17 different immune cell types between TAN-high and TAN-med/low groups. Holm-Sidak multiple comparison test; N.S. = Not Significant. **(B)** Comparison of GSVAsignature scores for PDA subtypes between TAN-high and TAN-med/low groups. Holm-Sidak multiple comparison test; N.S. = Not Significant.

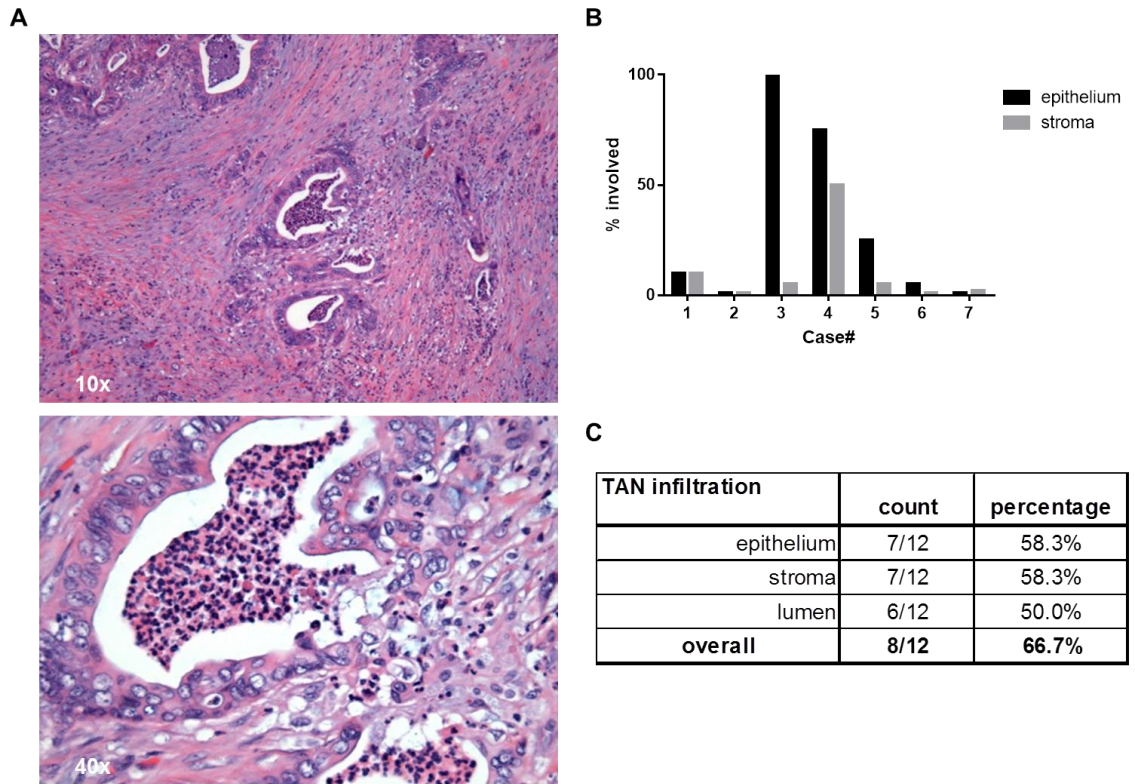


Figure 4. Significant neutrophil infiltration in a subset of human pancreatic cancer.

(A) H&E stain of a representative, resected human PDA sample (n = 12) showing TAN involvement in the cancer epithelium, stroma, and lumen. **(B)** Bar graph of the percentage of cancer epithelium or stroma involved in each of the 7 PDA cases with TAN infiltration. **(C)** Percentage of cancer epithelium, stroma, and lumen with TAN involvement as scored a pathologist.

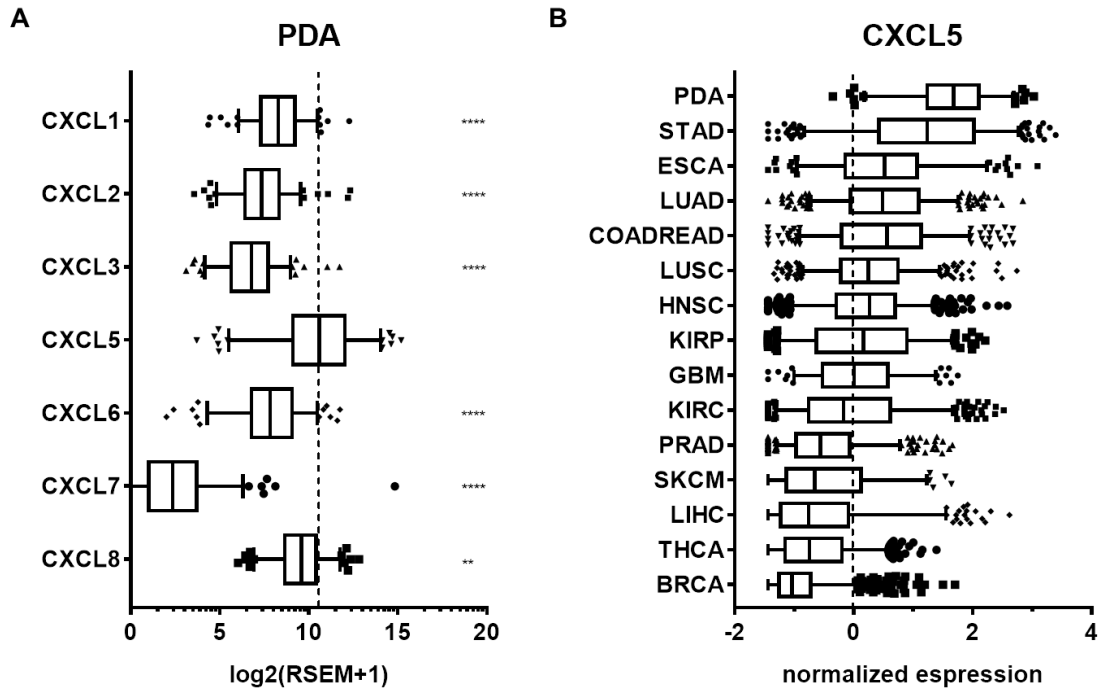


Figure 5. Elevated CXCL5 expression in PDA.

(A) Distribution of RSEM expression for all CXCR2 ligands in 134 human TCGA PDA tumors.

Boxplot whiskers at 5-95th percentile. Dashed line represents the average expression value of

CXCL5. **, $P \leq 0.01$; ****, $P \leq 0.001$ (1-way ANOVA, Dunnett's multiple comparison test against

CXCL5). **(B)** Normalized expression (z-scores) of CXCL5 in primary tumors across 15 TCGA

cancer cohorts. Boxplot whiskers at 5-95th percentile. Dashed line represents the average

expression value.

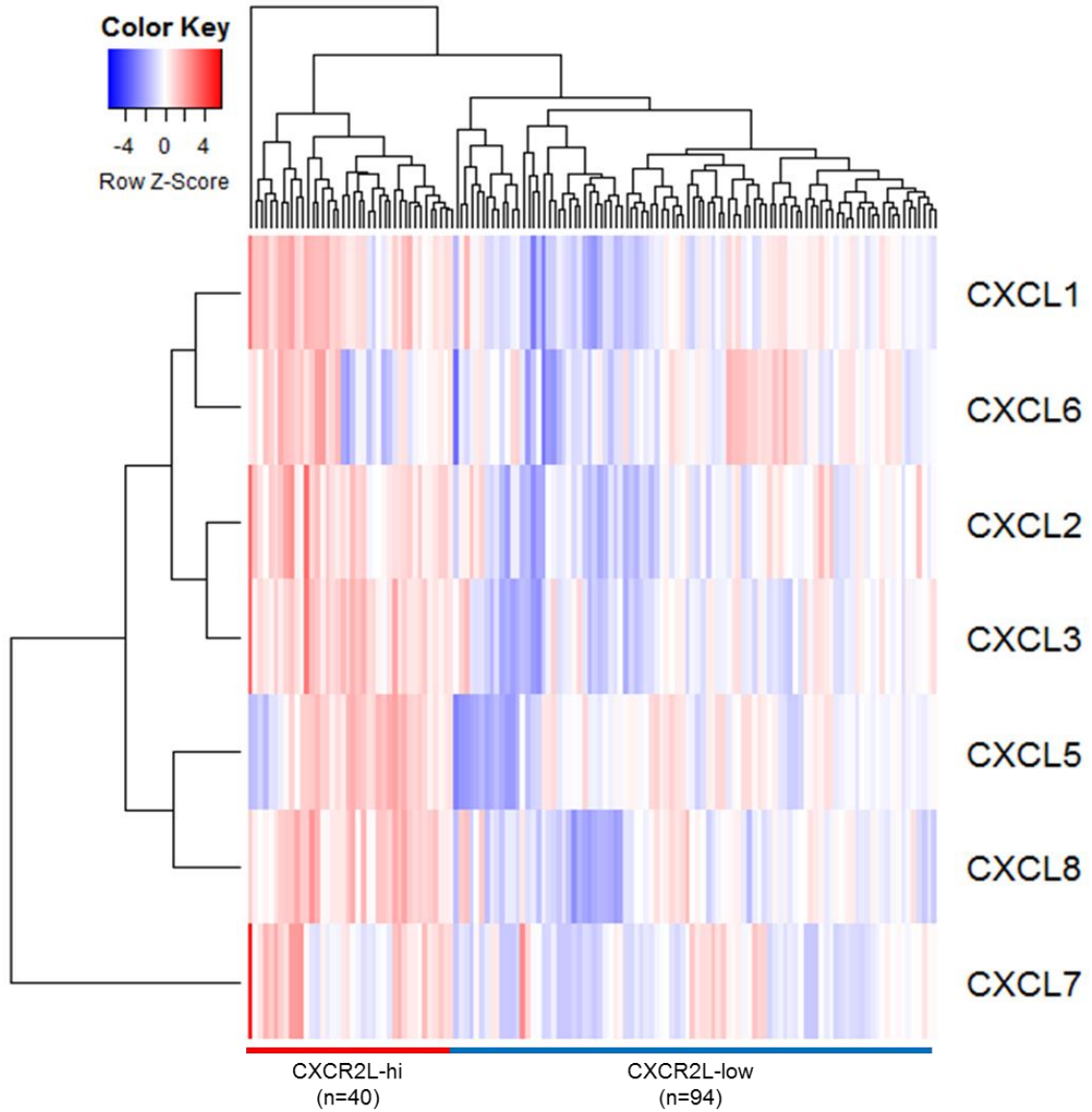


Figure 6. Clustering of human PDA into CXCR2L-high and CXCR2L-low groups.

Unsupervised hierarchal clustering of the 134 human TCGA PDA sampes into CXCR2L-high and CXCR2-low groups by their log normalized RSEM CXCR2 ligand expression.

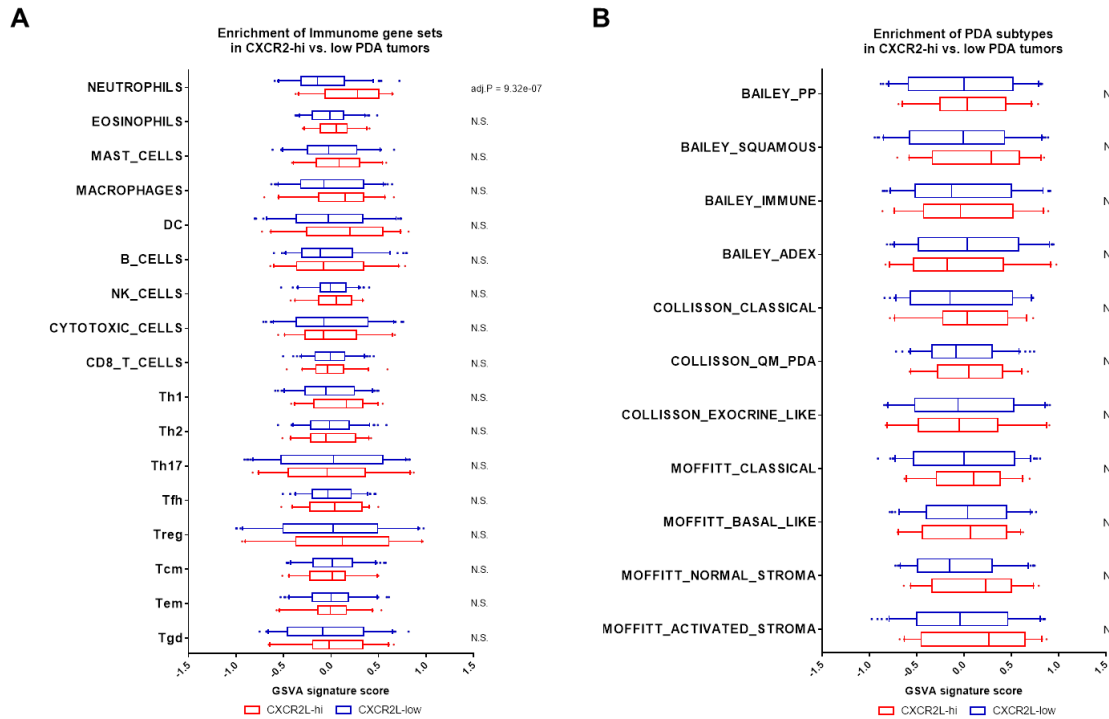


Figure 7. CXCR2L-high samples have elevated expression of neutrophil-specific genes.

(A) Comparison of GSVA signature scores for 17 different immune cell types between CXCR2L-high and CXCR2L-low groups. Holm-Sidak multiple comparison test; N.S. = Not Significant. **(B)** Comparison of GSVA signature scores for PDA subtypes between CXCR2L-high and CXCR2L-low groups. Holm-Sidak multiple comparison test; N.S. = Not Significant.

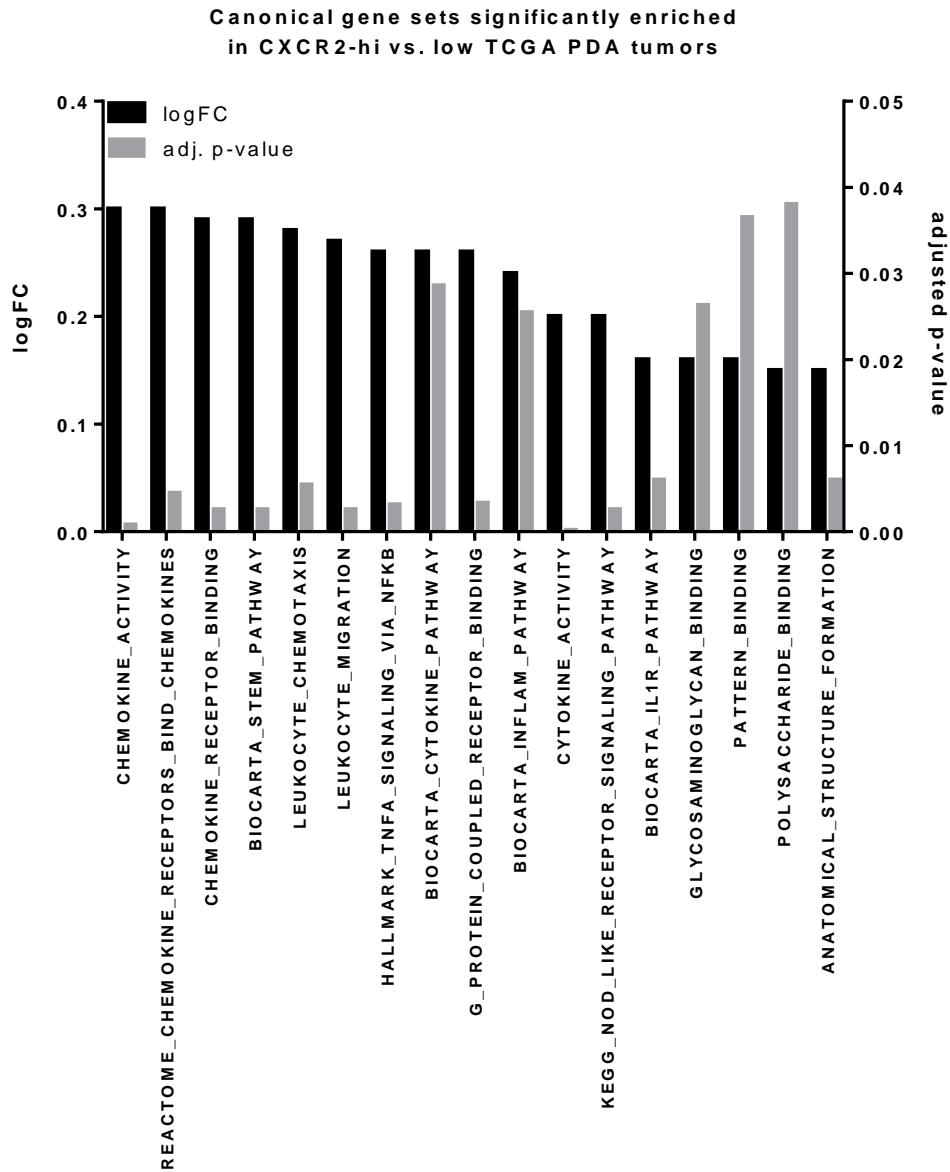


Figure 8. Elevation of genes in pathways related to innate immune response and NF- κ B activation in CXCR2L-high samples.

Log fold-change of GSVA signature scores and the adjusted p-values of canonical gene sets that are significantly elevated in CXCR2L-high compared to CXCR2L-low groups.

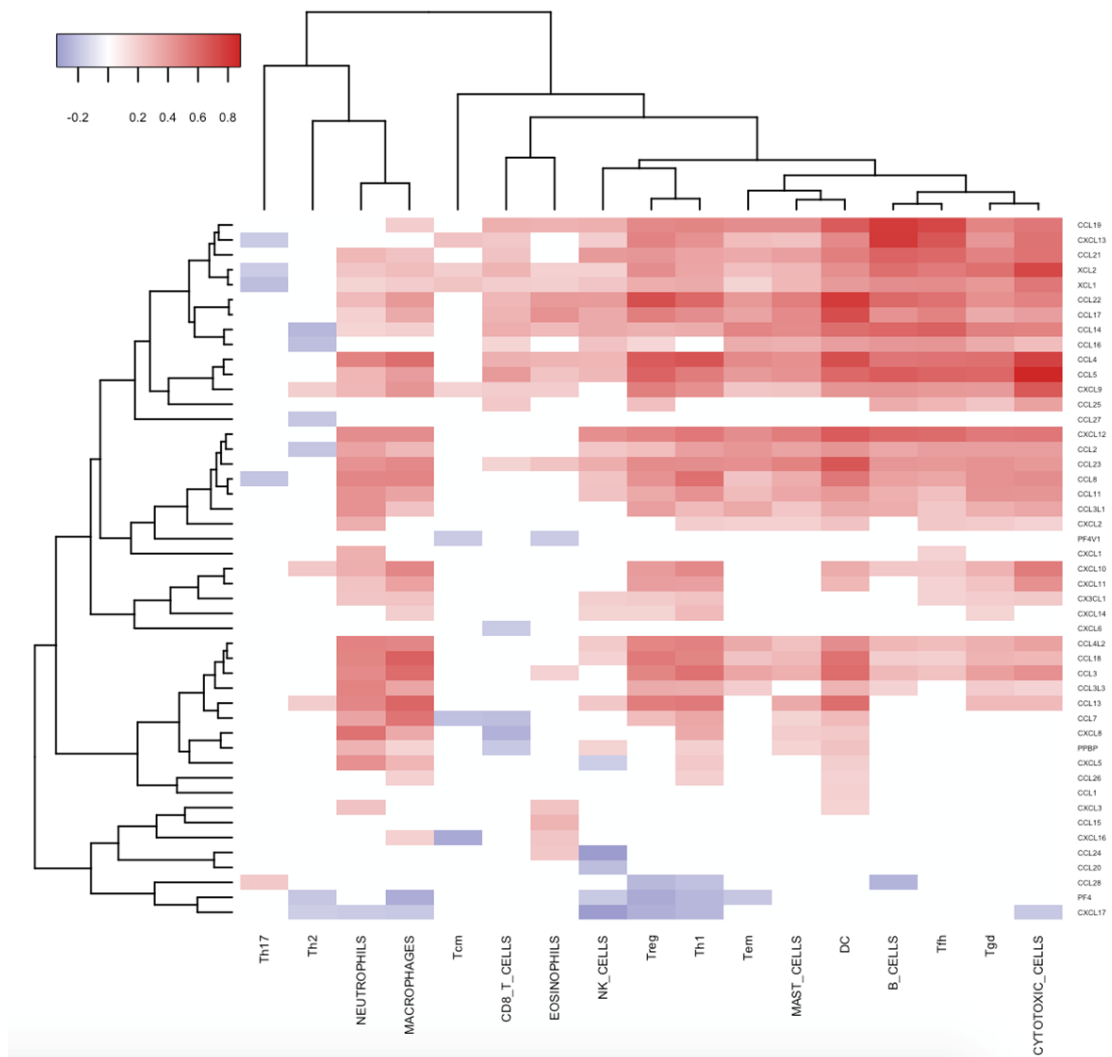


Figure 9. Correlation of immunome populations with all chemokines in PDA.

Clustering of the Spearman's rank correlation of immunome signature scores with all expressed chemokines in the 134 human PDA samples in TCGA (Red = positive; Blue = negative correlations). Only those correlations with asymptotic p-value ≤ 0.05 are colored.

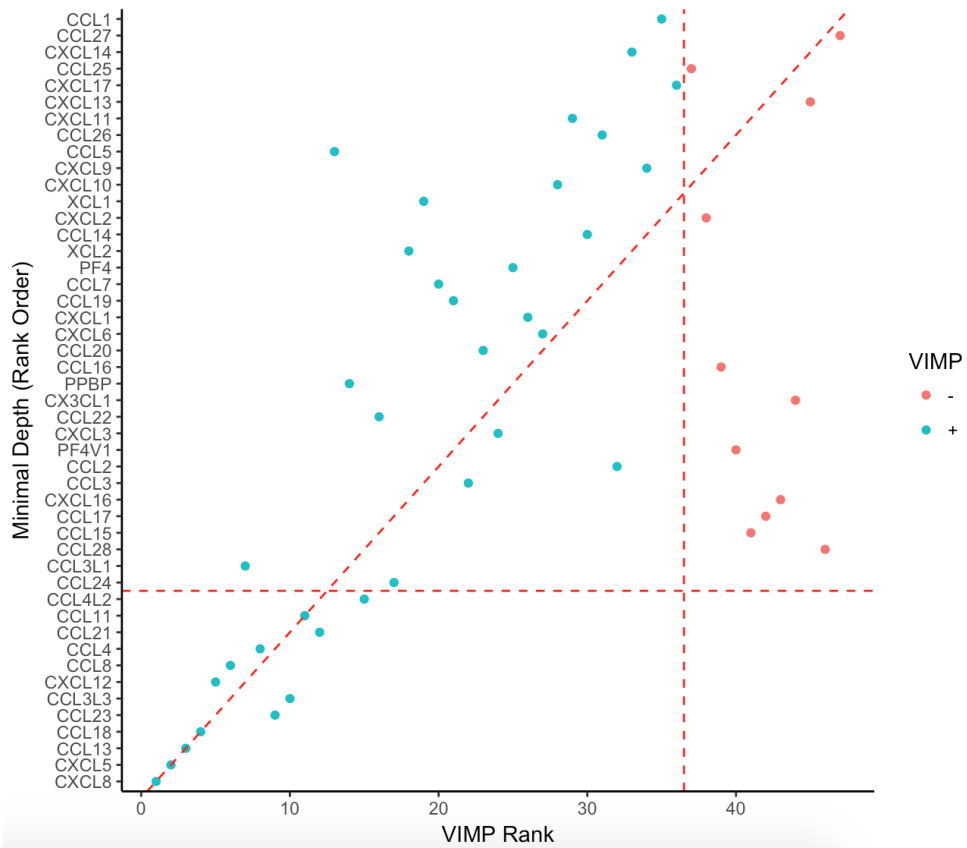


Figure 10. CXCL8 and CXCL5 are the most important chemokines in predicting the neutrophil signature score in PDA.

Comparison of the variable importance (VIMP) and the minimal depth rankings of all chemokines in a random forest regression model of the neutrophil signature score in 134 human PDA samples. The diagonal dashed line indicates perfect match between the VIMP and minimal depth rankings. The vertical dashed line divides the chemokines with positive predictive values (light-blue dots) and those with detrimental predictive values (red dots) in the model. The horizontal dashed line indicates the mean minimal depth of the chemokines, where those chemokines below the line are considered as important in the model. Chemokines where the VIMP and minimal depth rankings fall in the lower left quadrant are considered as important in the model using both measures.

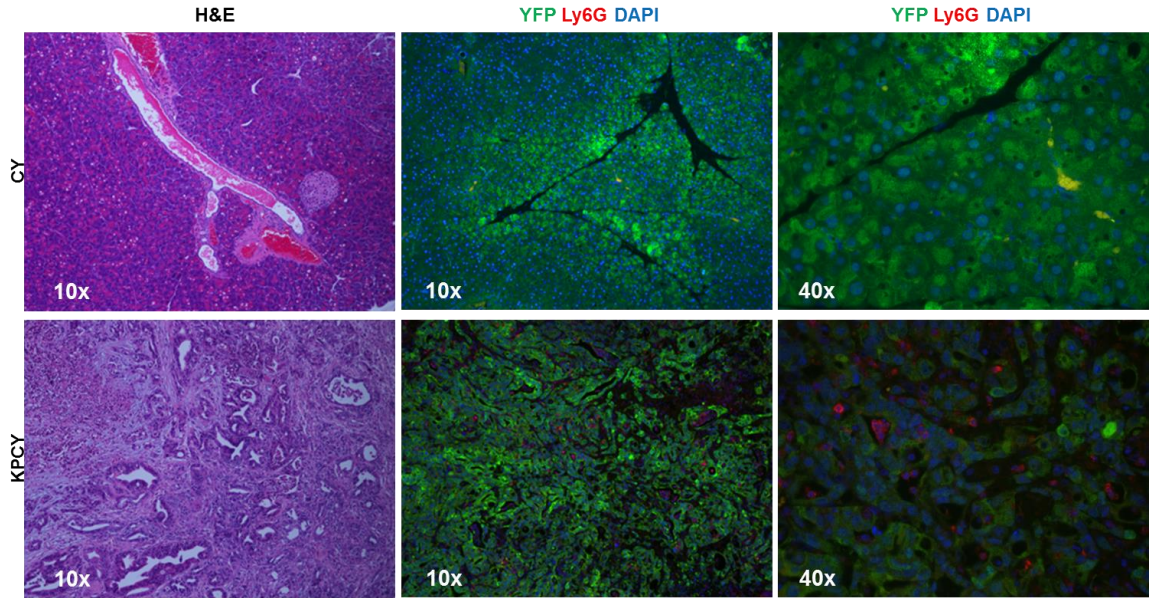


Figure 11. Significant Ly6G⁺ neutrophil infiltration throughout the pancreatic tumors of KPCY mice.

Representative H&E (10x) and YFP-Ly6G-DAPI (10x and 40x) stains of slides from the pancreas of 4-6 months old tumor-bearing KPCY mice and their age-matched CY controls ($n = 4$ per group).

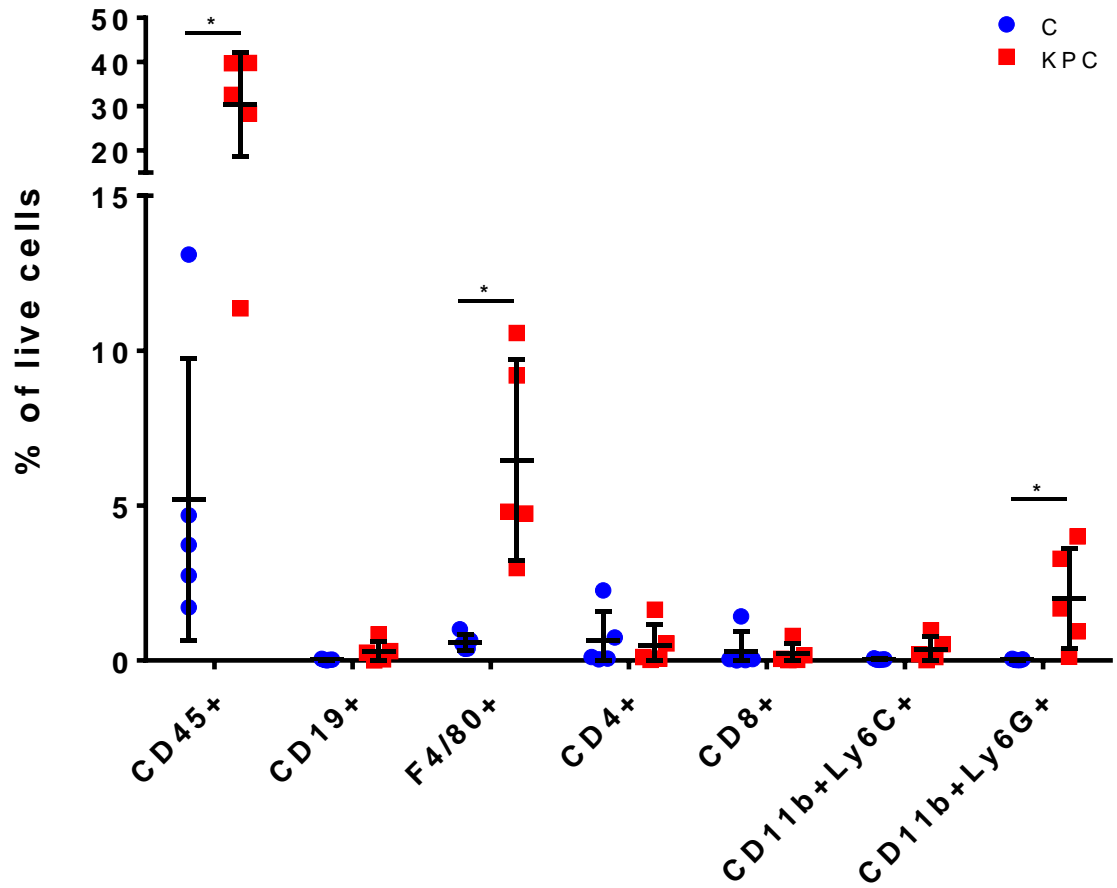


Figure 12. Increased CD11b⁺Ly6G⁺ neutrophils in the pancreas of KPC mice.

Flow cytometric analysis of immune cells as a percentage of total live cells in the pancreas of tumor-bearing KPC mice ($n = 5$) compared to age-matched controls ($n = 5$). Graphs show mean \pm s.d. *, P value ≤ 0.05 (unpaired t -test).

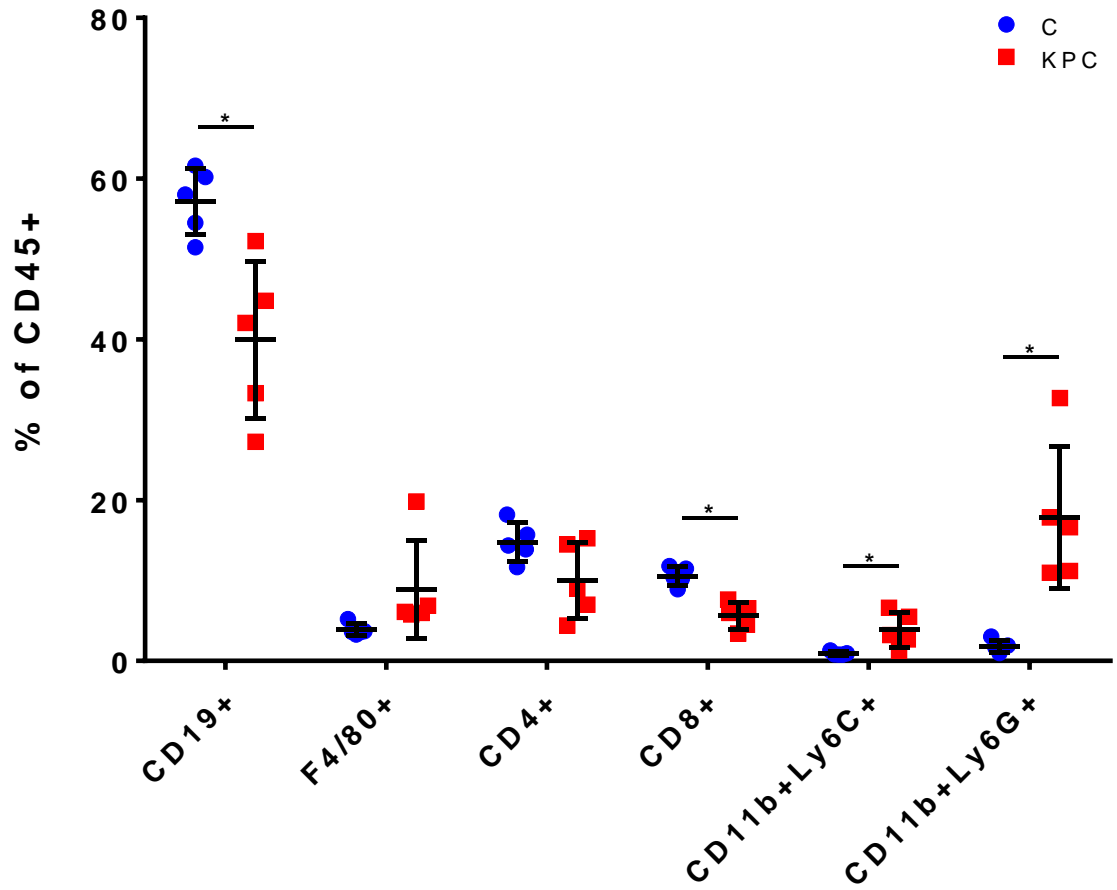


Figure 13. Increased CD11b⁺Ly6G⁺ neutrophils in the spleens of tumor-bearing KPC mice.

Flow cytometric analysis of immune cells as a percentage of live CD45⁺ cells in the spleens of tumor-bearing KPC mice ($n = 5$) compared to age-matched controls ($n = 5$). Graphs show mean \pm s.d. *, P value ≤ 0.05 (unpaired t -test).

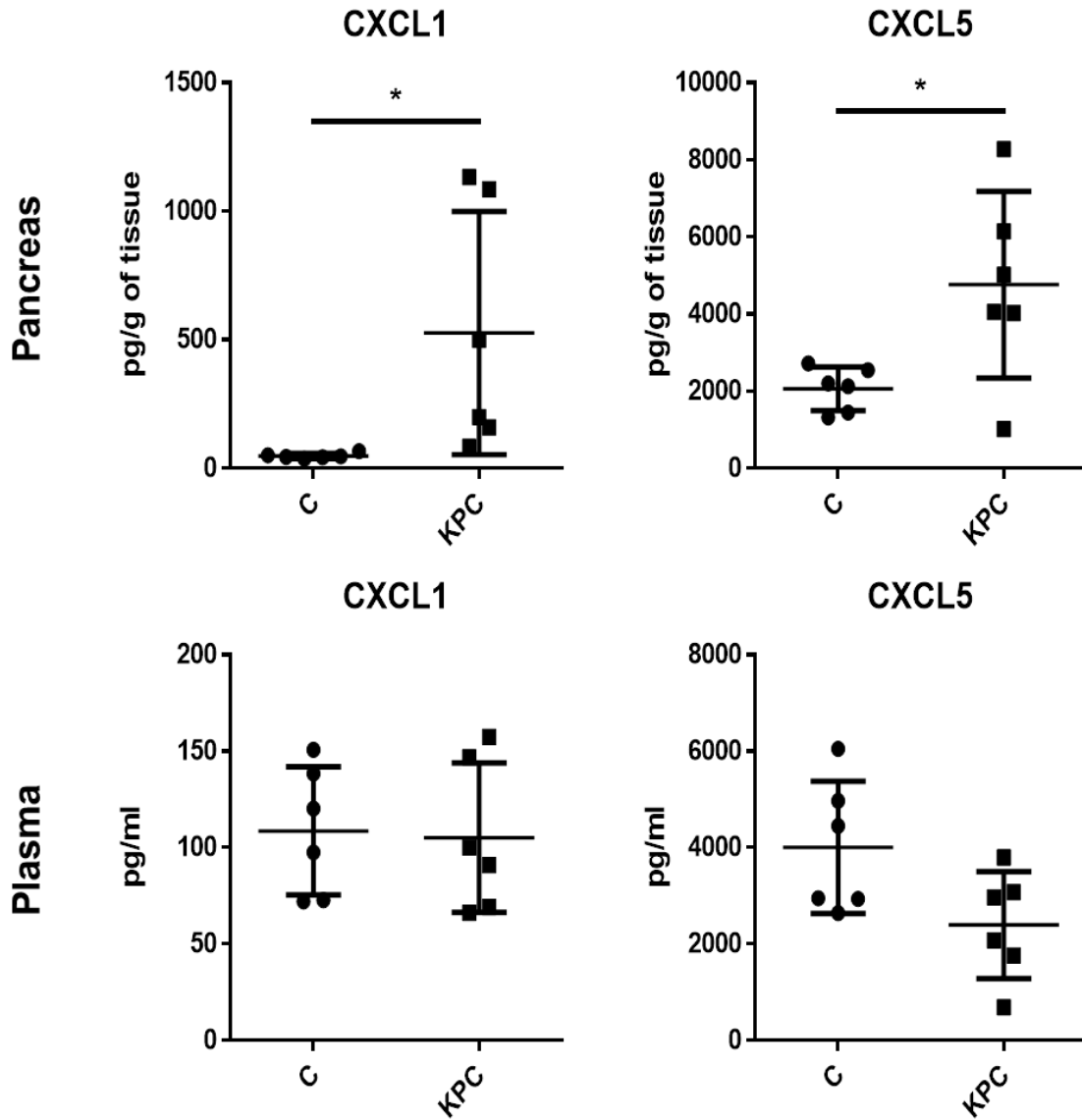


Figure 14. Elevated CXCL1 and CXCL5 levels in KPC pancreatic tumors.

Protein quantification of CXCL1 and CXCL5 in the pancreas and plasma of KPC ($n=6$) compared to controls ($n=6$) mice. Graphs show mean \pm s.d. of one experiment. *, P value ≤ 0.05 ; (unpaired t -test).

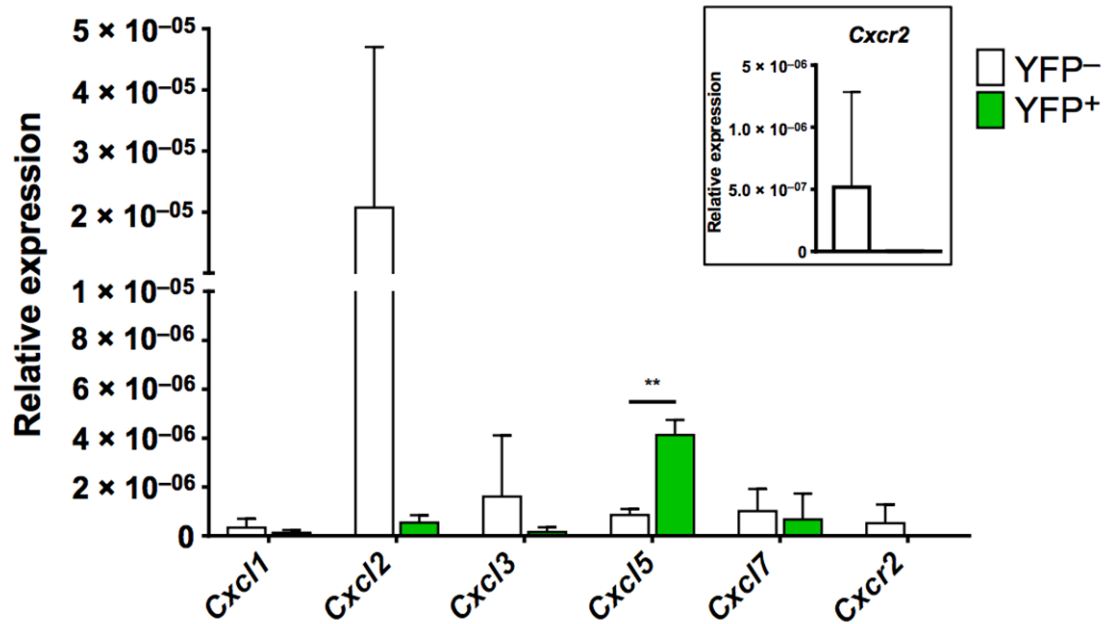


Figure 15. Differential CXCR2 ligand expression in cancer and stromal cells in KPC tumors.

CXCR2 ligand expression in YFP⁺ cancer cells compared to YFP⁻ stromal cells in KPCY pancreatic tumors ($n = 3$). Inset shows *Cxcr2* expression on a different scale. Gene expressions were normalized to *18S*. Graphs show mean \pm s.d. of one experiment. *, P value ≤ 0.05 ; **, P value ≤ 0.01 (unpaired t -test).

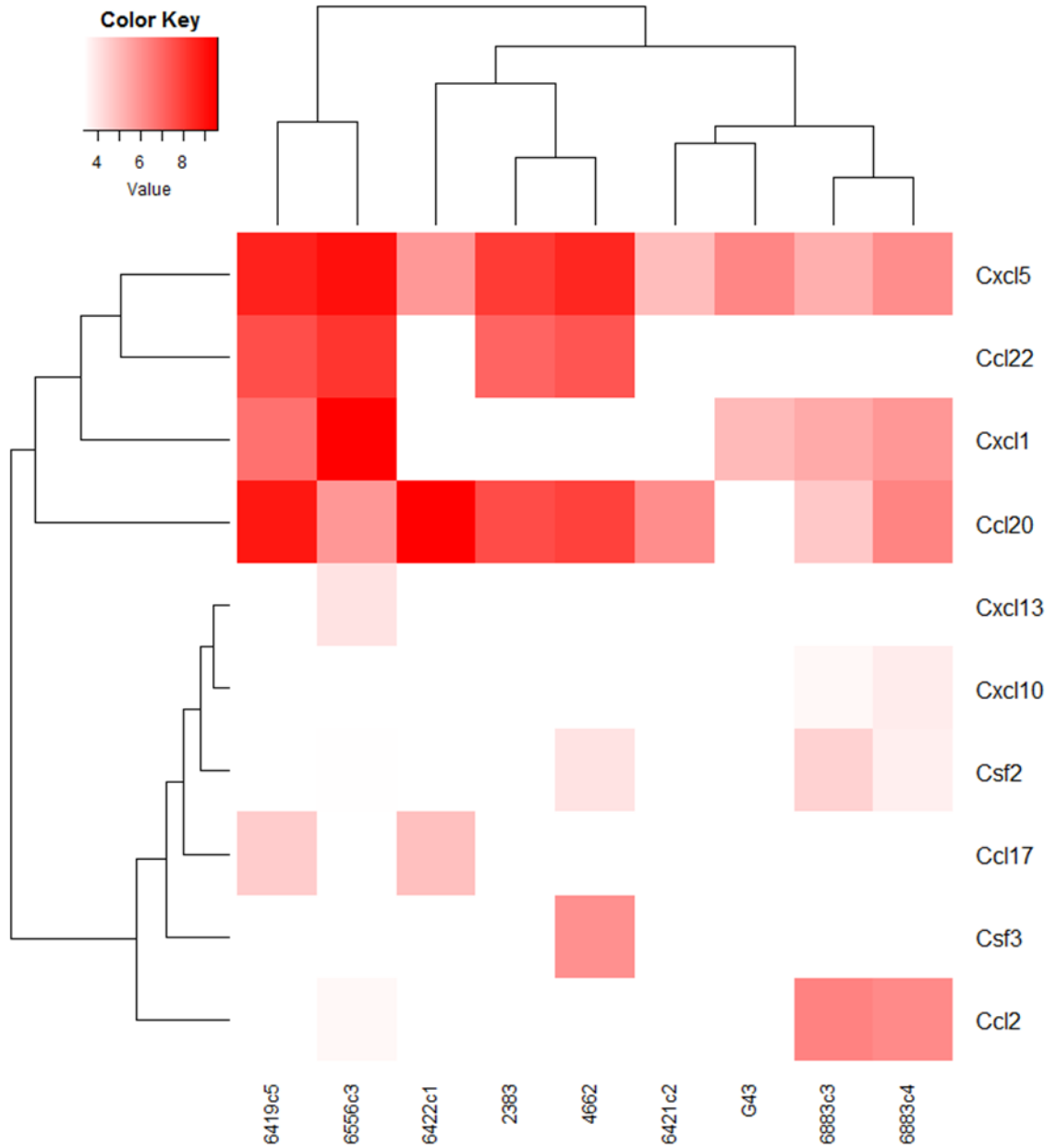


Figure 16. CXCL5 is abundantly secreted by KPC-derived PDA cell lines *in vitro*.

KPC-derived PDA cell lines were seeded at 1×10^6 cells/ml in triplicate and the supernatants were collected at 24 hrs. Figure shows heatmap of the log₂ concentration (pg/ml/ 1×10^6 cells) of the secreted cytokines and chemokines.

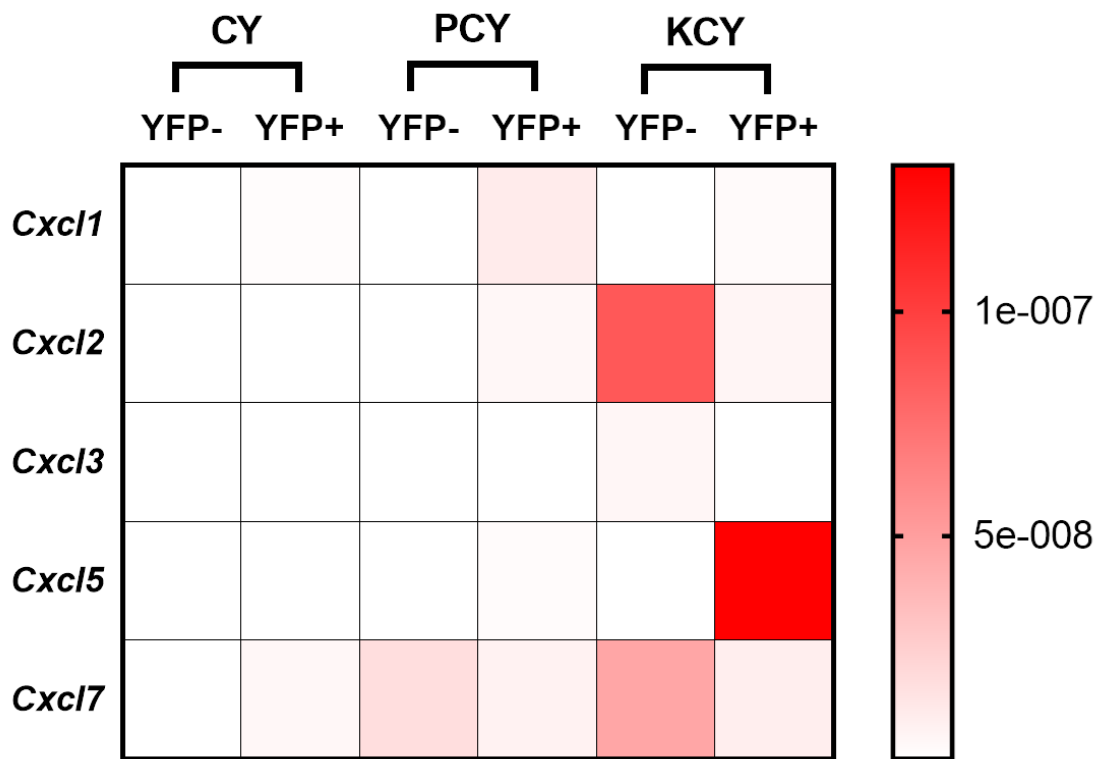


Figure 17. CXCR2 ligand expression profile in KCY pancreas is similar to KPCY tumors.

Heatmap of average CXCR2 ligand expression by YFP+ pancreatic and YFP- stromal cells in 4-6 months old CY, PCY, and KCY mice (n = 3 per group). Gene expressions were measured by RT-PCR and normalized to 18S.

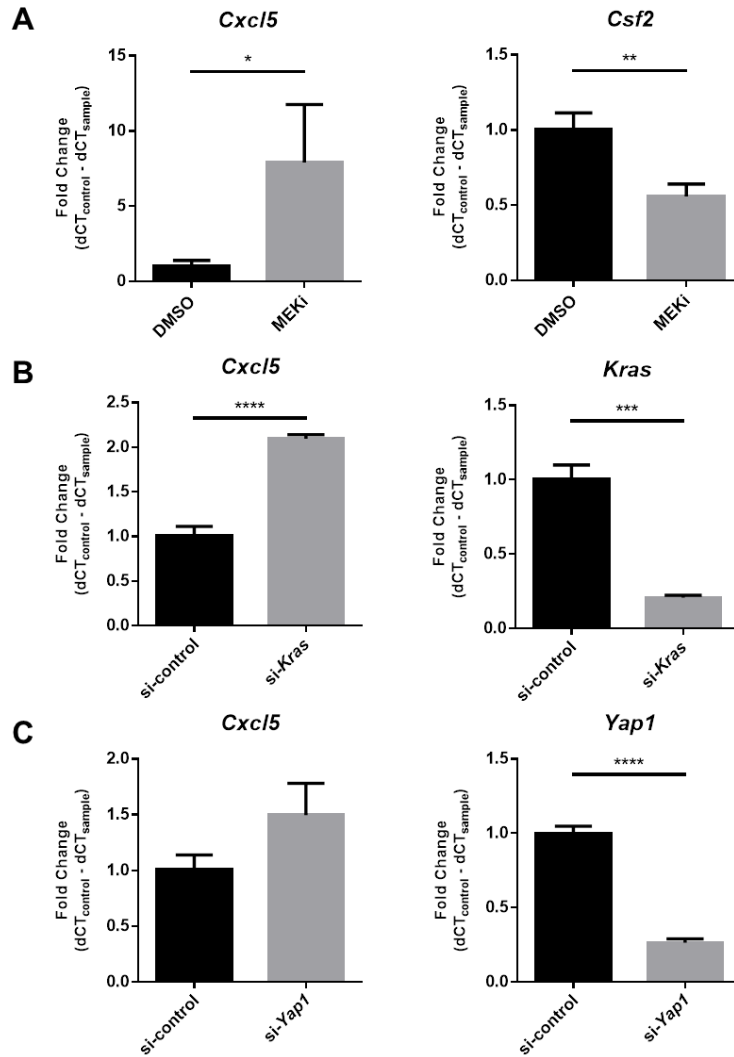


Figure 18. Inhibition of the KRAS/MEK pathway increases CXCL5 expression.

(A) Fold change of *Cxcl5* and *Csf2* (GM-CSF) expression in 4662 PDA cells treated with 10 μ M U0126 (MEK inhibitor) compared to DMSO. Graphs show mean \pm s.d. of 3 independent experiments. *, $P \leq 0.05$; **, $P \leq 0.01$ (unpaired t -test). **(B)** Fold change of *Cxcl5* and *Kras* expression in *Kras* siRNA-treated compared to control siRNA-treated 4662 PDA cells. Graph

shows mean \pm s.d. of 3 independent experiments. ***, $P \leq 0.001$; ****, $P \leq 0.0001$ (unpaired t -test). **(C)** Fold change of *Cxcl5* and *Yap1* expression in si-*Yap1* treated compared to si-control

treated 4662 PDA cells. Graph shows mean \pm s.d. of 3 independent experiments. ****, $P \leq 0.0001$ (unpaired t -test).

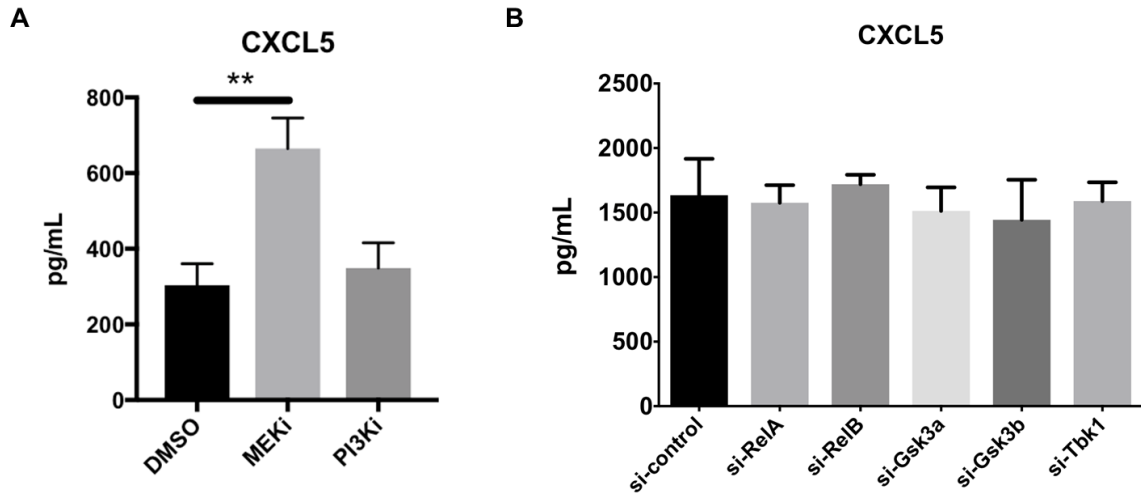


Figure 19. CXCL5 level is not affected by inhibition of alternative downstream KRAS pathways.

(A) CXCL5 protein level in the supernatant of 4662 PDA cells treated with DMSO control, 10 μ M U0126 (MEK inhibitor), or 20 μ M LY294002 (PI3K inhibitor) for 24 hours. Graph shows mean \pm s.d. of 3 independent experiments. **, $P \leq 0.01$ (unpaired t -test). **(B)** CXCL5 protein level in the supernatant of 4662 PDA cells collected 72 hours after treatment with control siRNA compared to siRNA targeting *RelA*, *RelB*, *Gsk3a*, *Gsk3b*, and *Tbk1*. Graphs show mean \pm s.d. of 3 independent experiments.

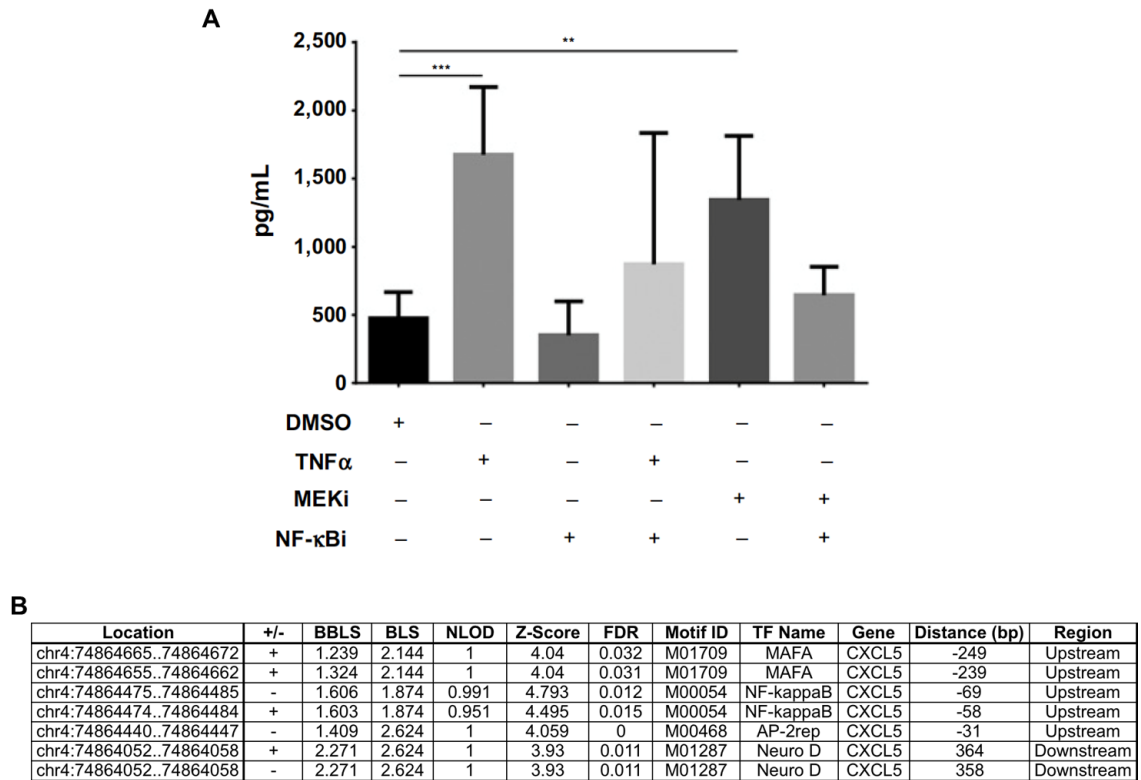


Figure 20. MEK inhibition-induced elevation of CXCL5 expression is dependent on NF- κ B activation.

(A) CXCL5 protein level in the supernatant of 4662 PDA cells treated with the indicated combinations of DMSO control, 10ng/mL TNF α , 10 μ M U0126 (MEK inhibitor), or 20 μ M wedeloactone (NF- κ B inhibitor). Graph shows mean \pm s.d. of 3 independent experiments. *, $P \leq 0.05$; **, $P \leq 0.01$ (1-way ANOVA, Holm-Sidak's multiple comparison test). **(B)** MotifMap prediction of transcription factor binding sites 1000bp upstream and downstream of the human CXCL5 gene (FDR ≤ 0.05).

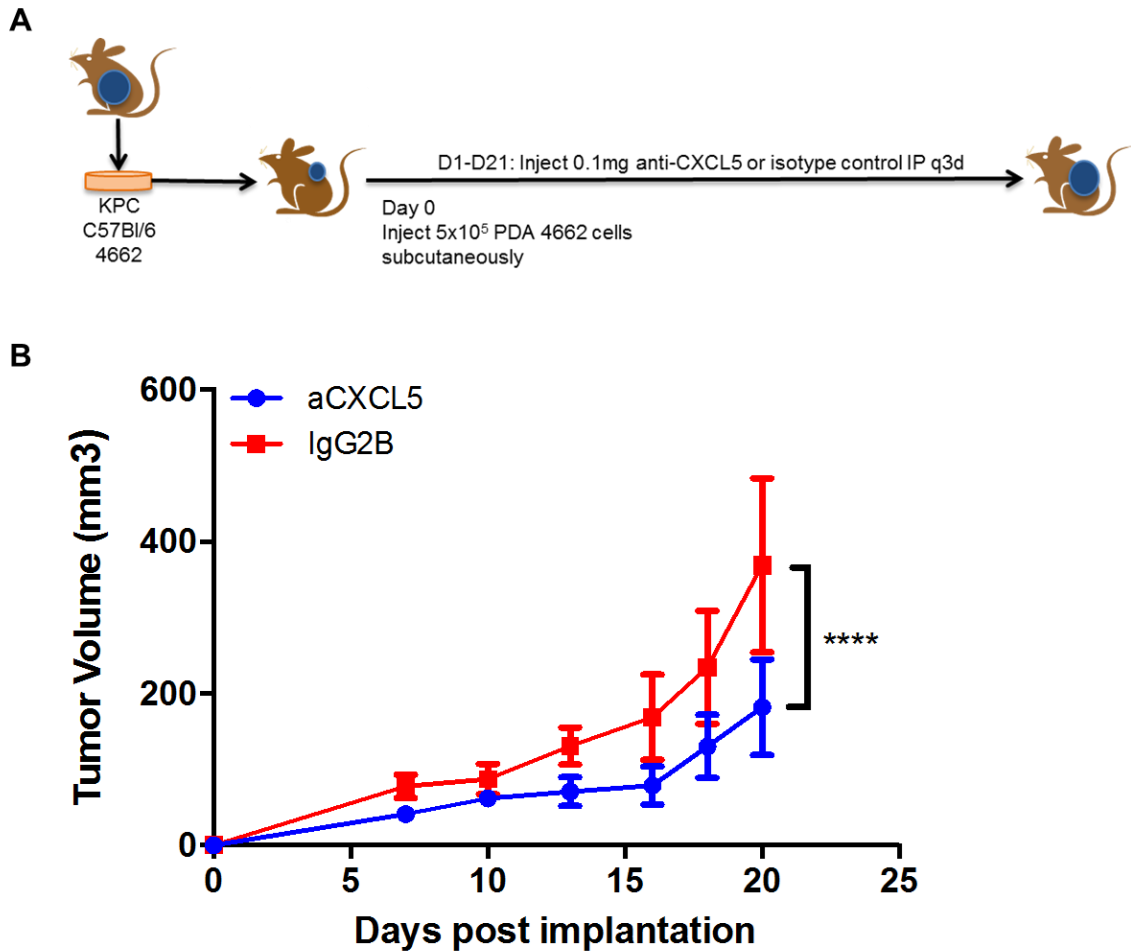


Figure 21. Anti-CXCL5 treatment slows PDA tumor growth.

(A) The KPC-derived PDA cell line 4662 was implanted subcutaneously in syngeneic WT mice. Mice were injected intraperitoneally with either 0.1mg anti-CXCL5 or 0.1mg isotype control every 3 days for the duration of the experiment starting one day post implantation. Tumor growth was monitored with digital calipers. **(B)** 4662 PDA tumor growth in mice treated with isotype control (n=8) or anti-CXCL5 (n=10). Graph shows mean \pm s.d. ****, $P \leq 0.0001$ on day 21 (2-way ANOVA with column factor P value = 0.0007, Sidak's multiple comparison test).

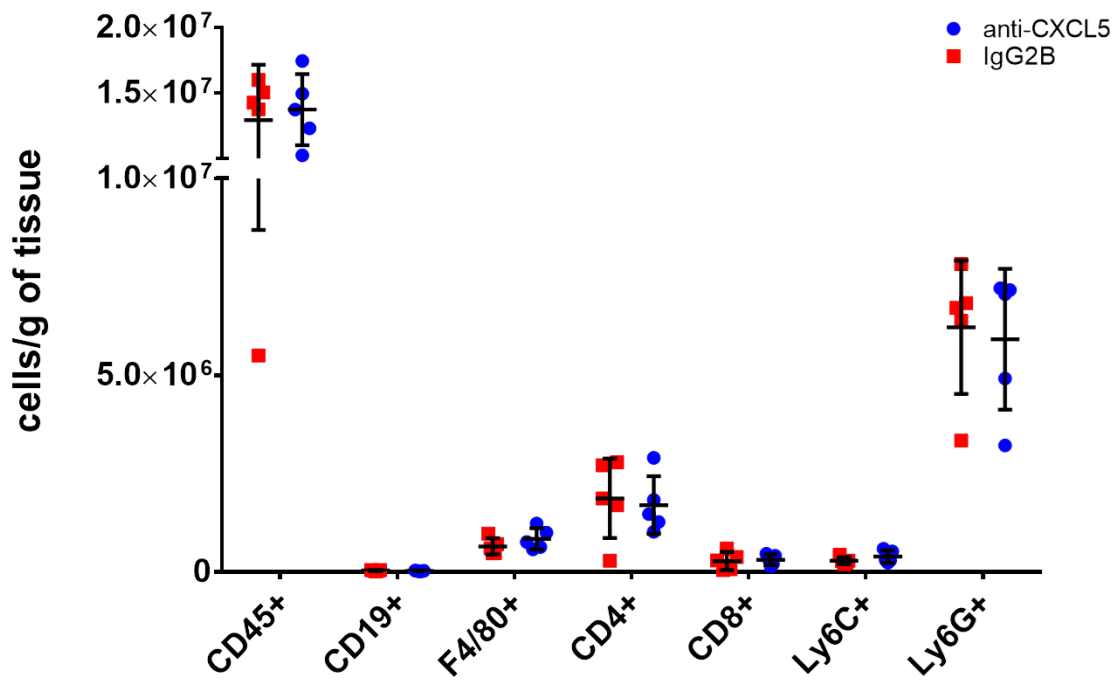


Figure 22. No changes in the tumor immune composition with anti-CXCL5 treatment.

Flow cytometric measurement of the density of different immune populations in the tumors of isotype control or anti-CXCL5 treated mice (n=5/group). Graph shows mean ± s.d.

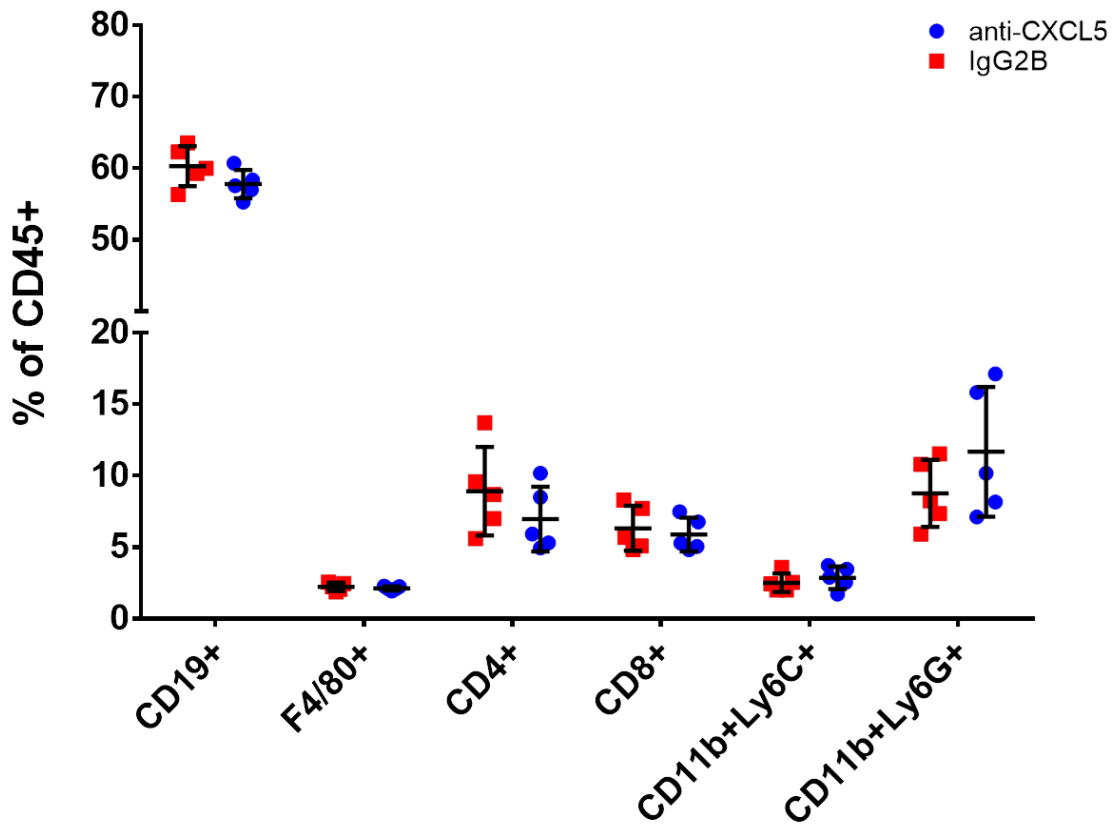


Figure 23. No changes in the splenic immune composition with anti-CXCL5 treatment.

Flow cytometric measurement of the density of different immune populations in the spleens of isotype control or anti-CXCL5 treated mice (n=5/group). Graph shows mean \pm s.d.

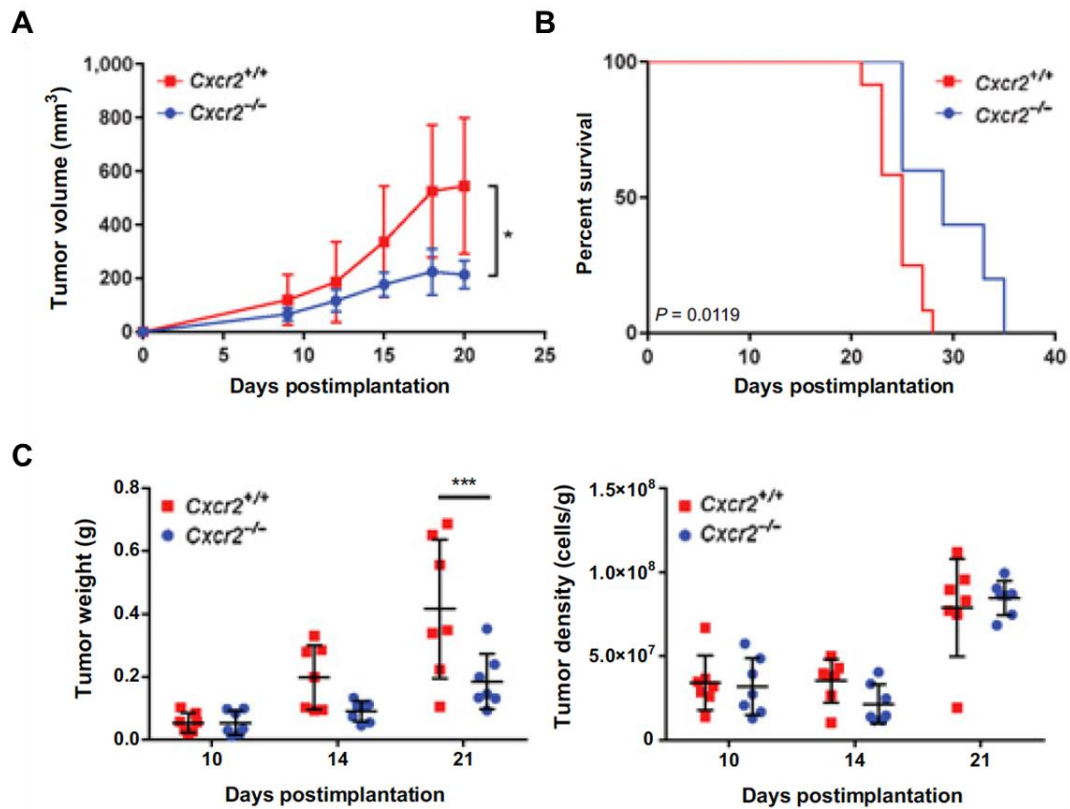


Figure 24. CXCR2 ablation slows tumor growth and prolongs survival.

(A) 4662 PDA tumor growth in *Cxcr2*^{-/-} compared to *Cxcr2*^{+/+} littermates after subcutaneous implantation ($n = 7$ per group). Graph shows mean \pm s.d. *, $P \leq 0.05$ on day 21 (2-way ANOVA, Sidak's multiple comparison test). **(B)** Kaplan-Meier survival analysis of *Cxcr2*^{-/-} ($n = 6$) compared to *Cxcr2*^{+/+} ($n = 10$) littermates subcutaneously implanted with 4662 PDA tumors. (P value = 0.0119, log rank test). **(C)** Comparison of tumor weights and cell-density in *Cxcr2*^{-/-} compared to *Cxcr2*^{+/+} hosts on Day 10, 14, and 21 ($n = 7$ per group/day). Graph shows mean \pm s.d. ***, $P \leq 0.001$ (2-way ANOVA, Sidak's multiple comparison test).

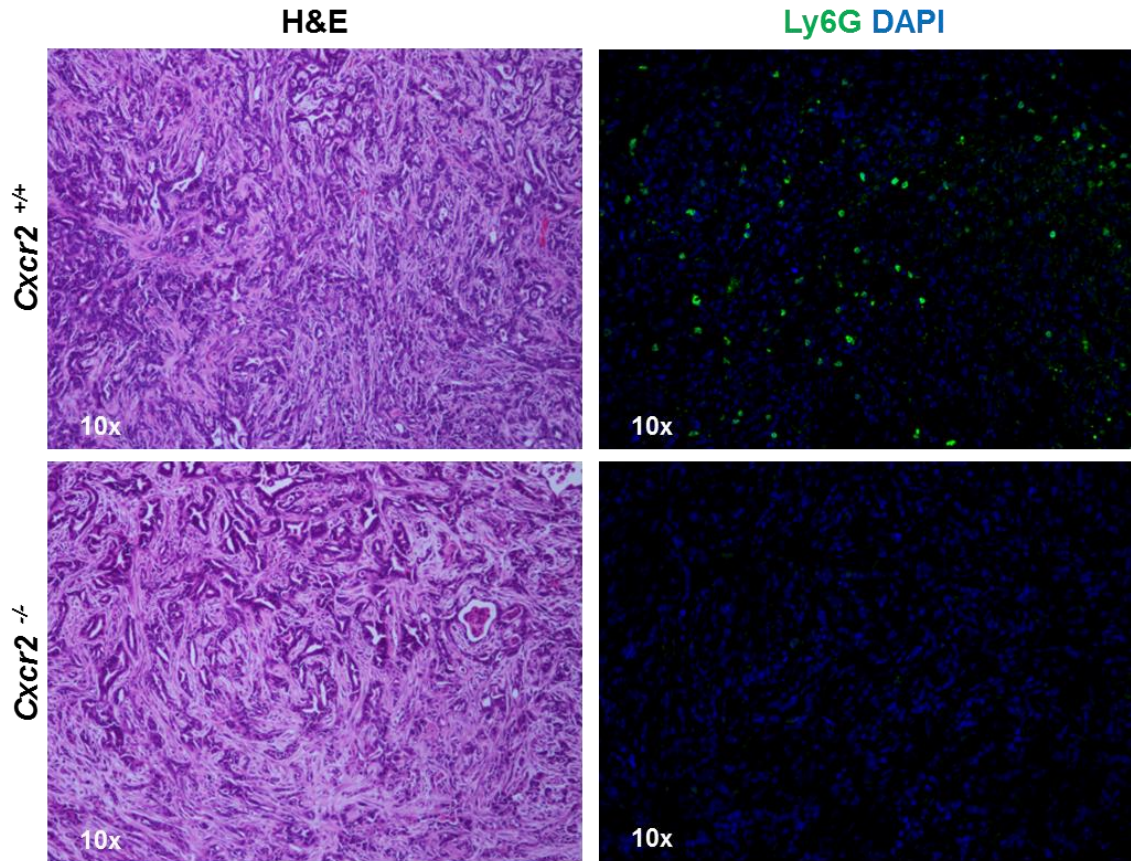


Figure 25. CXCR2 ablation eliminates the accumulation of tumor-infiltrating neutrophils. Representative H&E (10x) and Ly6G-DAPI (10x) stain in *Cxcr2*^{-/-} compared to *Cxcr2*^{+/+} controls (n=8 per group).

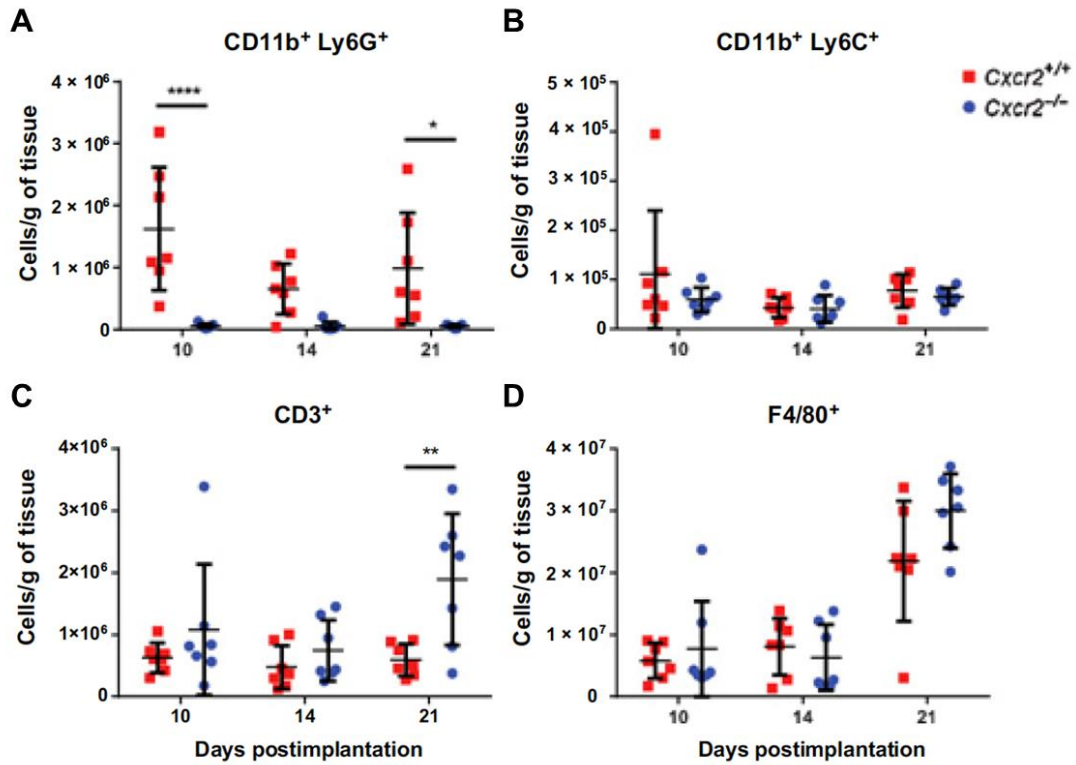


Figure 26. Changes in the immune composition of tumors in *Cxcr2*^{+/+} and *Cxcr2*^{-/-} mice.

Flow cytometric measurement of the density of CD11b⁺Ly6G⁺ TANs (**A**), CD11b⁺Ly6C⁺ monocytes (**B**), CD3⁺ T cells (**C**), and F4/80⁺ macrophages (**D**) in the tumors of *Cxcr2*^{-/-} and *Cxcr2*^{+/+} littermates on Day 10, 14, and 21 (n=7/day/group). Graph shows mean ± s.d. *, $P \leq 0.05$; **, $P \leq 0.01$; ***, $P < 0.001$ (2-way ANOVA, Sidak's multiple comparison test).

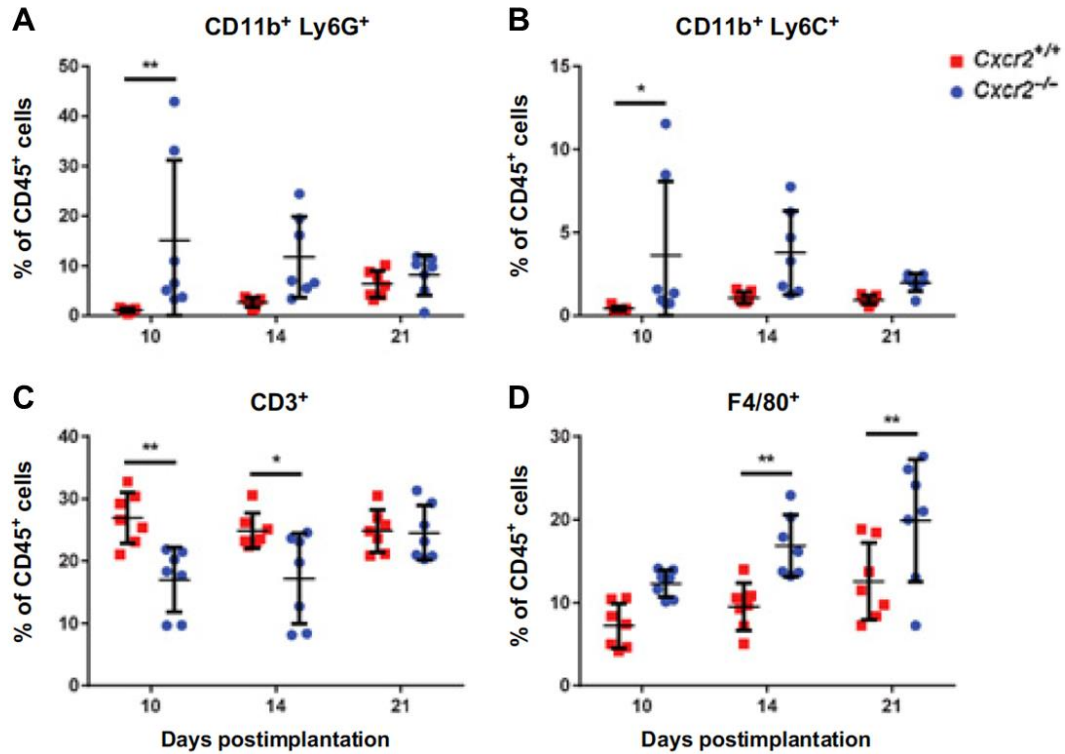


Figure 27. Changes in the splenic immune composition of tumor-bearing *Cxcr2*^{+/+} and *Cxcr2*^{-/-} mice.

The percentage of CD11b⁺Ly6G⁺ TANs (**A**), CD11b⁺Ly6C⁺ monocytes (**B**), CD3⁺ T cells (**C**), and F4/80⁺ macrophages (**D**) in the spleens of *Cxcr2*^{-/-} and *Cxcr2*^{+/+} littermates on Day 10, 14, and 21 post tumor implantation (n=7/day/group). Graph shows mean ± s.d. *, $P \leq 0.05$; **, $P \leq 0.01$ (2-way ANOVA, Sidak's multiple comparison test).

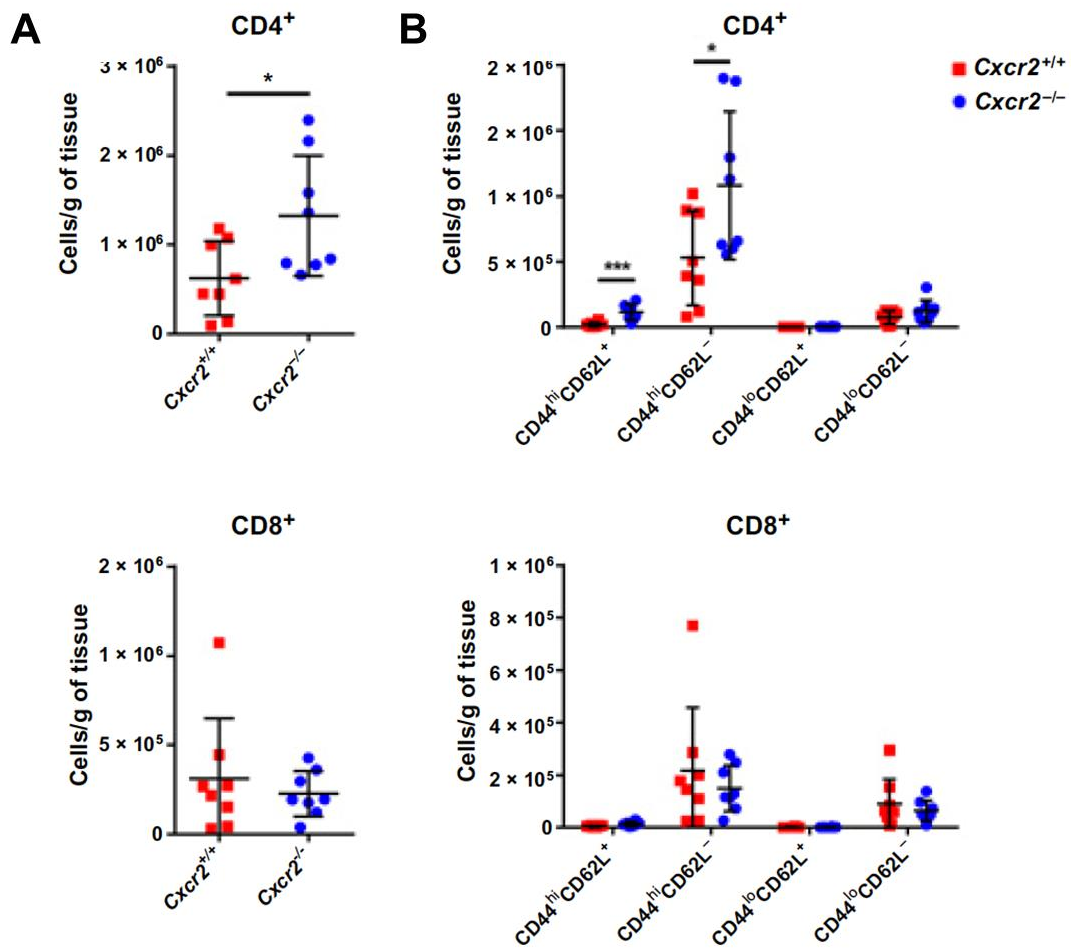


Figure 28. Increased density of activated CD4⁺ T cells in tumors of *Cxcr2*^{-/-} mice.

Cxcr2^{-/-} and *Cxcr2*^{+/+} mice were subcutaneously implanted with the 4662 cell line and sacrificed at 4 weeks (n=8 per group). **(A)** Densities of tumor-infiltration CD4⁺ and CD8⁺ T cells. **(B)** Densities of CD44^{hi}CD62L⁺ memory, CD44^{hi}CD62L⁻ effector, and CD44^{lo}CD62L⁺ or CD44^{lo}CD62L⁻ naïve CD4⁺ or CD8⁺ T cells. Graphs show mean ± s.d. *, *P* < 0.05; ***, *P* < 0.001 (unpaired *t*-test).

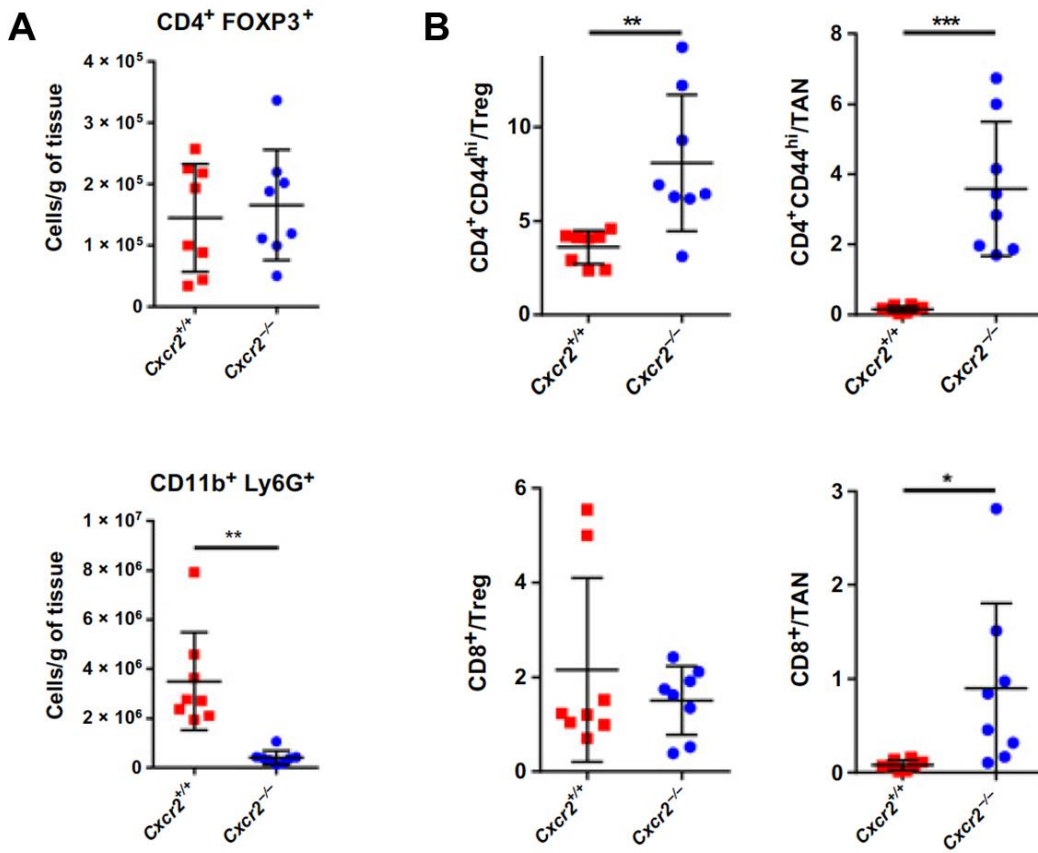


Figure 29. Increased ratios of activated T cells to immunosuppressive populations in tumors of *Cxcr2*^{-/-} mice.

Cxcr2^{-/-} and *Cxcr2*^{+/+} mice were subcutaneously implanted with the 4662 cell line and sacrificed at 4 weeks (n=8 per group). **(A)** Densities of CD4⁺FOXP3⁺ Tregs and CD11b⁺Ly6G⁺ tumor-associated neutrophils. **(B)** Ratios of the densities of CD4⁺CD44^{hi} or CD8⁺ effector T cells to the densities of CD4⁺FOXP3⁺ Tregs or CD11b⁺Ly6G⁺ TANs. Graphs show mean ± s.d. *, *P* < 0.05; **, *P* < 0.01; ***, *P* < 0.001 (unpaired *t*-test).

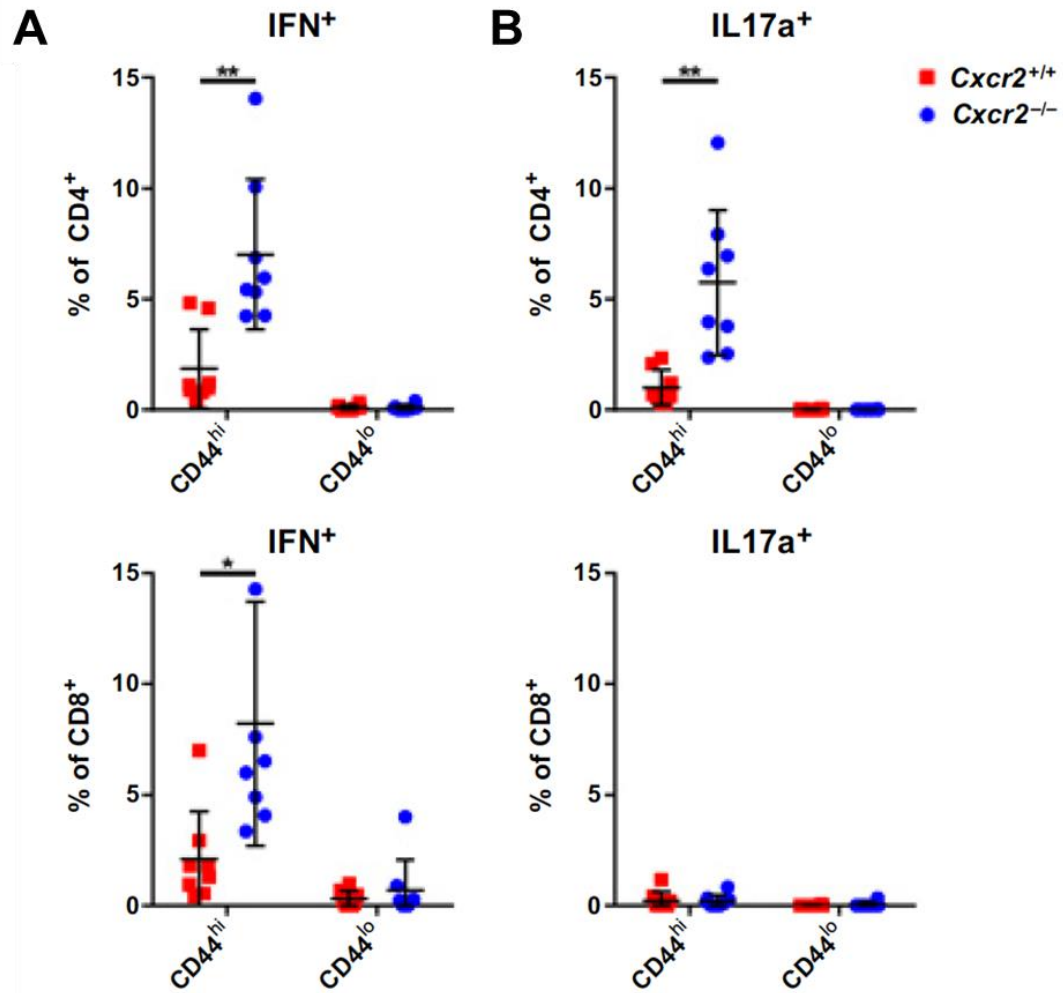


Figure 30. Increased IFN γ and IL17 secretion in tumor-infiltrating T cells in *Cxcr2*^{-/-} mice.

Cxcr2^{-/-} and *Cxcr2*^{+/+} mice were subcutaneously implanted with the 4662 cell line and sacrificed at 4 weeks (n=8 per group). The percentage of CD44^{hi} activated or CD44^{lo} naïve CD4⁺ or CD8⁺ T cells that expresses IFN γ (A) or IL17 (B) after *ex vivo* stimulation with PMA/ionomycin for 5 hours at 37°C. Graphs show mean \pm s.d. *, $P < 0.05$; **, $P < 0.01$; ***, $P < 0.001$ (unpaired *t*-test).

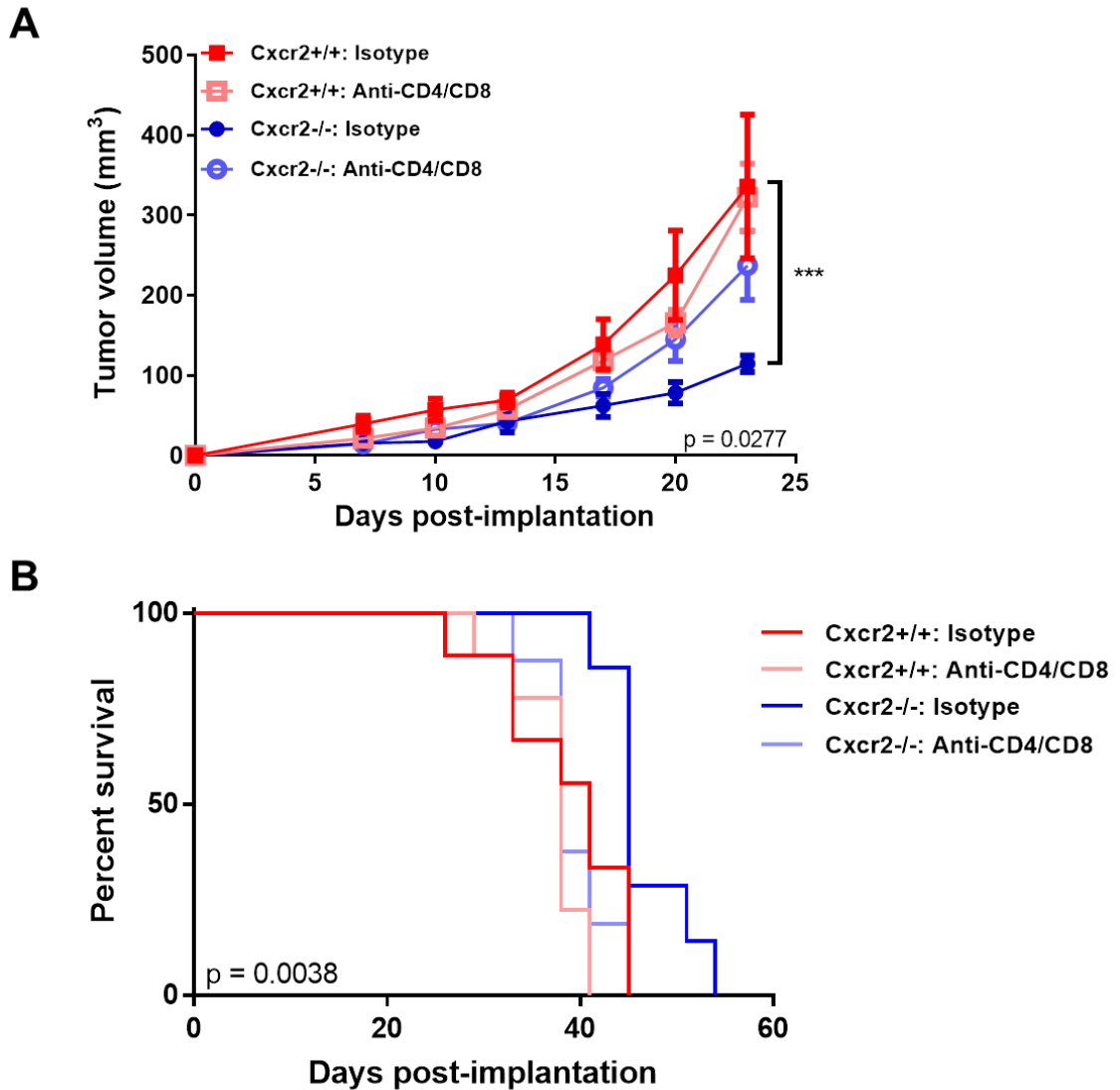


Figure 31. Depletion of T cells rescues tumor growth in *Cxcr2*^{-/-} mice.

(A) 4662 PDA tumor growth in *Cxcr2*^{-/-} and *Cxcr2*^{+/+} mice treated with 0.2mg anti-CD4/anti-CD8 depleting antibodies or 0.2mg isotype every three days intraperitoneally ($n \geq 7$ per group). Graph shows mean \pm s.e.m. ***, $P \leq 0.001$ on Day 23 (2-way ANOVA with column factor P value = 0.0277, Sidak's multiple comparison test). **(B)** Kaplan-Meier survival analysis of *Cxcr2*^{-/-} ($n = 6$) compared to *Cxcr2*^{+/+} ($n = 10$) littermates subcutaneously implanted with 4662 PDA tumors and treated with anti-CD4/anti-CD8 antibodies or isotype controls. (P value = 0.0038, log rank test).

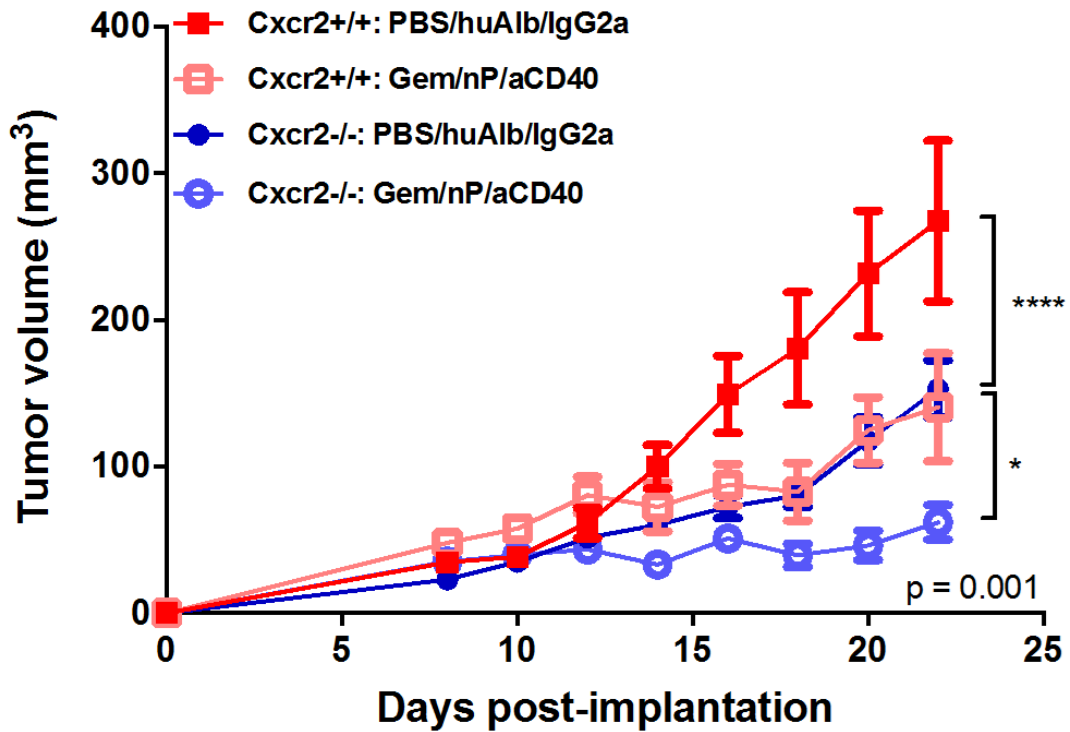


Figure 32. Additive response to chemo-agonistic CD40 therapy with CXCR2 ablation.

4662 PDA tumor growth in *Cxcr2*^{-/-} and *Cxcr2*^{+/+} mice treated with gemcitabine/nab-paclitaxol/anti-CD40 or PBS/human-albumin/isotype IgG2a intraperitoneally ($n \geq 7$ per group).

Graph shows mean \pm s.e.m. *, $P \leq 0.05$; ****, $P \leq 0.0001$ (2-way ANOVA with column factor P value = 0.001, Sidak's multiple comparison test).

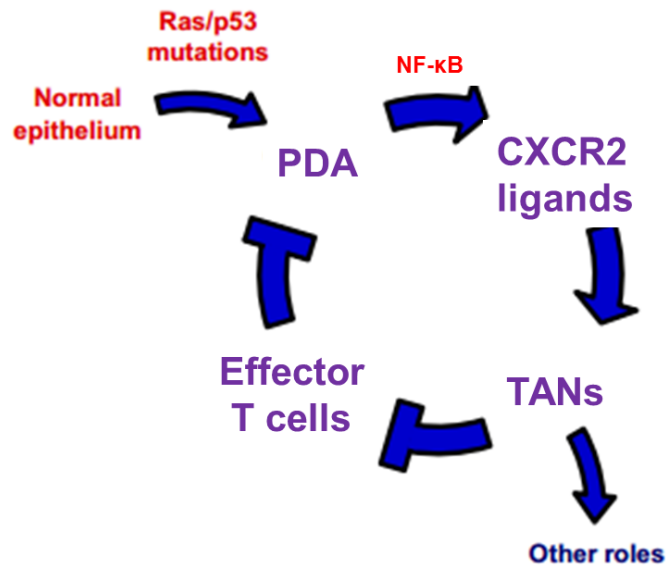


Figure 33. Summary of tumor-neutrophil interactions in PDA.

$Kras^{G12D}$ expressing PDA tumor cells with activated NF- κ B secrete CXCR2 ligands, especially CXCL5, which recruit neutrophils to the tumor microenvironment. These tumor-associated neutrophils are then responsible for suppressing effector T cells, thus preventing an anti-tumor response.

CHAPTER 4: Cytokine networks underlying cytolytic activity in pancreatic cancer.

* The results described in this chapter are described in a manuscript currently in preparation:

T. Chao and R.H. Vonderheide. "In silico reconstruction and comparison of cytokine networks in pancreatic ductal adenocarcinomas with high and low cytolytic activity." In preparation.

INTRODUCTION

Treatment for pancreatic ductal adenocarcinoma (PDA) has displayed some progress in the past two decades, nearly doubling the 5-year overall survival rate from merely 4.4% in 1998 to 8.5% in 2016 (Siegel et al., 2017). Despite these advances, PDA remains one of the most lethal malignancies and is projected to become the second leading cause of cancer-related mortality in the United States by 2030 (Rahib et al., 2014). Immune checkpoint blockade has recently been demonstrated to be efficacious in a variety of solid tumors (Pardoll, 2012). However, very few PDA patients seemed to benefit from checkpoint blockade alone (Royal et al., 2010; Brahmer et al., 2012). The highly desmoplastic and immunosuppressive microenvironment of PDA is thought to contribute to its high rate of resistance. In fact, multiple studies have now demonstrated that targeting specific components of the microenvironment can sensitize PDA to existing therapies (Beatty et al., 2013; Feig et al., 2013; Winograd et al., 2015; Byrne and Vonderheide, 2016; Jiang et al., 2016; Nywening et al., 2016). Therefore, efforts to accelerate target selection in the PDA tumor microenvironment are urgently needed.

One major determinant of survival and response to therapy is the presence of cytotoxic immune cells in the tumor microenvironment (Pagès et al., 2010). The anti-tumor effect of these cytotoxic cells is largely attributed to their potent cytolytic activity. Total mutation and neoepitope burdens have been shown to correlate with both infiltration of cytotoxic CD8⁺ T cells and cytolytic activity in various cancers (Rooney et al., 2015). However, we have previously found that mutational burden did not correlate with cytolytic activity in human PDA (Balli et al., 2016). This suggests that other factors in the microenvironment are also important in regulating the activity of

cytotoxic cells. Several immune cell types, especially the myeloid populations, have already been shown to be immunosuppressive in PDA (Bayne et al., 2012; Beatty et al., 2013; Chao et al., 2016; Nywening et al., 2016; Steele et al., 2016). Although the individual effects of some components have been demonstrated, how the complex network of immune and cytokine interactions result in microenvironments that are permissive or suppressive to cytotoxic cells remains poorly understood. We propose that such a network-based approach is necessary to understand the complexities of the tumor immune responses. Furthermore, analysis of these cytokine networks can help highlight target candidates that most effectively disrupt the immunosuppressive microenvironment.

Recent analyses of whole tumor RNA expression data using gene signatures have led to characterizations of tumor immune infiltrates with high resolution (Bindea et al., 2013; Gentles et al., 2015; Newman et al., 2015; Rooney et al., 2015; Charoentong et al., 2017). In these studies, cytotoxic immune infiltration is often associated with enhanced survival, mutations associated with loss of antigen presentation or resistance to apoptosis, and up-regulation of immune-checkpoint molecules. Furthermore, gene correlation networks have proven to be useful in providing *de novo* insights to the underlying pathways in various diseases, including cancer (Miller et al., 2008; Yang et al., 2014; Bailey et al., 2016; Iyer et al., 2017). Here, we applied these techniques to infer and characterize cytokine networks in human PDA using RNA sequencing data available in The Cancer Genome Atlas (TCGA) (Cancer Genome Atlas Research Network et al., 2013). In addition, we demonstrate that concepts from social network theory could be applied to cytokine networks to aid in the discovery of the most influenced or influential players (Marsden, 2002; Friedkin, 2015). We found that cytolytic activity corresponds with increased cytotoxic immune infiltration and survival in PDA. We further discovered that different immune populations and cytokines are enriched in tumors with high and low cytolytic activity. Differential correlation analysis provided evidence that immune cell recruitment, activation, and function vary according to the level of cytolytic activity. Finally, correlation network analysis showed that the most the most influential immune populations and cytokines are also different in tumors with high and low

cytolytic activity. By comparing immune-cytokine networks of cytolytically high and low tumors, our study provided novel targets, such as CLEC11A and TNFSF14/LIGHT, that may effectively disrupt the immunosuppressive network or promote anti-tumor cytolytic activity in PDA.

RESULTS

Cytolytic activity correlates with increased survival in PDA.

The cytolytic activity of effector immune cells is critical for their ability to suppress tumor growth and prolong survival (Shankaran et al., 2001). To explore the relative expression of cytolytic activity in the 134 primary PDA tumors available in TCGA, gene set variation analysis (GSVA) was performed using two previously defined signatures consisting of genes that define the cytolytic activity of effector CD8+ T cells or genes shared between all cytotoxic immune cells (Bindea et al., 2013; Rooney et al., 2015). Hierarchical clustering of the PDA samples using these two signatures resulted in a group that has relatively high scores in both signatures (cytolytically “hot” tumors) and a group that has low scores in both signatures (cytolytically “cold” tumors) (Figure 34A). More precisely, groups were defined using K-means clustering of all samples into 4 groups. The group associated with the highest expression of the cytolytic and cytotoxic signatures was labeled as cytolytically “hot” tumors. Because their expression levels were highly similar, the two groups associated with the lowest expression were combined into one larger group and labeled as cytolytically “cold” tumors.

Given that increased cytolytic activity in tumors was correlated with survival in many other cancers, we hypothesized that this is also the case in PDA (Rooney et al., 2015). In support of our hypothesis, PDA patients with cytolytically hot tumors have significantly enhanced, though modest, survival benefit compared to those with cold tumors (Figure 34B). Given that patients with cytolytically hot and cold tumors have slightly different clinical characteristics, the observed survival benefit may have been confounded by these clinical factors (Figure 35A). Using Cox multiple regression, we analyzed the survival benefit of grouping by cytolytic activity, stage, age, and sex (Figure 35B). Patients with cytolytically hot tumors retained their survival advantage even

when taking into account these clinical factors. Therefore, our results highlight the clinical significance of cytolytic activity in PDA.

Immune populations enriched and correlated with survival.

The interactions of immune populations in the tumor microenvironment play an important role in regulating the development and activity of cytotoxic effector cells. To estimate the relative abundance of immune populations in cytolytically hot and cold PDA, we performed GSVA using 52 previously defined gene signatures that uniquely identify immune populations from three different databases (Bindea et al., 2013; Newman et al., 2015; Rooney et al., 2015). Hierarchical clustering showed that gene signatures of the same immune population but acquired from different databases tend to cluster together (Figure 36). For example, the macrophage signature derived from the immunonome (IM-Macrophages), CIBERSORT leukocyte matrix (LM22-M0), and FANTOM Consortium (F5-Macrophages) were all directly adjacent with each other. Therefore, gene signatures of the same immune population are generally consistent with each other. Clustering the 134 samples by the 52 gene signatures resulted in a near complete separation of cytolytically hot and cold tumors (Figure 36). Indeed, 46 of the 52 immune gene signatures were significantly altered between hot and cold tumors (Figure 37A). With the exception of two immune populations, the vast majority of the differentially expressed gene signatures (44 of 46) were enriched in cytolytically hot tumors. Consistent with the fact that the cytolytic signatures were derived in part from activated CD8⁺ T cells, the most significantly enriched populations in cytolytically hot tumors were the two CD8⁺ T cell signatures. Increase in CD8⁺ T cells was accompanied by the enrichment of a variety of other immune populations, including professional antigen-presenting cells (APCs) and regulatory CD4⁺ T cells (Treg). This result suggested that enrichment of CD8⁺ T cells and cytolytic activity did not occur in isolation, but rather occurred as part of a larger immune response.

To discover which immune populations may have an effect on overall survival, Cox regression analysis was performed for each immune signature using samples from all, hot, or

cold tumors (Figure 37B). Using all the samples, we found that 16 immune signatures have significant positive protective ratios, including CD8⁺ T cells. The cell types with the highest protective ratios are effector memory (Tem) and follicular-helper (Tfh) CD4⁺ T cells. Consistent with the co-enrichment of these populations in hot tumors, some classically immunosuppressive populations, such as Treg, were also found to have positive protective ratios in cytolytically hot tumors. Rather than being beneficial, the presence of these cell types might indicate increased counter-measures in response to enhanced cytolytic activity. Therefore, it is possible that the presence of immunosuppressive populations could serve as a gauge for the intensity of cytolytic activity in the tumor, depending on their mechanism of immunosuppression.

In contrast, activated memory (CD4m-act) and type 2 helper CD4⁺ T cells (Th2) were both negatively correlated with survival in at least 2 of the populations (Figure 37B). In addition, an activated NK (NK-act) population and CD56-bright NK (NK-CD56bright) cells were also negatively correlated with survival, in cold and hot tumors respectively. CD4m-act and NK-CD56bright cells were both significantly enriched in cytolytically cold tumors (Figure 37A). These results suggested that specific subsets of CD4⁺ T cells and NK cells might be antagonistic to cytotoxic immune responses and adversely affecting survival.

Immune networks in hot and cold tumors.

From the analyses above, 47 immune signatures were either differentially enriched or impacted survival in PDA. To investigate potential relationships among these relevant populations, correlations between all possible pairs of immune cell types were calculated in each of 1000 bootstrapped populations using all, only hot, or only cold samples. Hierarchical clustering of the averaged correlations showed that signatures belonging to the same immune population grouped together even though they were derived from different sources (Figures 38A-C). This demonstrated that signatures of the same immune cell type are not only consistent with each other as mentioned before, but they also relate with other immune signatures in a similar manner. The vast majority of immune populations were positively correlated with each other (Figure 38A).

Also consistent with the results above, NK-CD56^{bright} and CD4^{m-act} signatures were both broadly and negatively correlated with many other immune populations, which included at least one of the CD8⁺ T cell signatures. Therefore, these two cell types might be antagonistic to the presence of cytotoxic CD8⁺ T cells in the tumor microenvironment.

In support of the hypothesis that immune populations behave differently between the two groups, we found that immune populations formed different clusters in hot and cold tumors (Figures 38B-C). For instance, CD8⁺ T cells, CD4⁺ Tem cells, Tfh cells, B cells, and plasmacytoid dendritic cells (pDCs) clustered together only in cytolytically hot tumors. The CD4^{m-act} signature was positively correlated with the Th2 population only in cytolytically cold tumors. These clustering differences may be indicative of changes in the behavior of immune populations between these two groups. Of the 1081 possible pair-wise immune-immune correlations, we found that 287 (27%) correlations were significantly altered. This result suggested that a portion of immune populations relate to others in a significantly different way in cytolytically hot compared to cold tumors. To further select the most altered relationships, we found that only 10 of these 287 correlations changed by an absolute value of over 0.7 between the averaged correlation of hot and cold tumors (Figure 39A). Using only these 10 correlations as input variables, a random forest model was built to classify the cytolytic status of each bootstrapped population. The importance of each correlation was quantified using both variable importance (vimp) and minimal depth scores (Figures 39B-C). Although not significantly more important than the other input variables, the correlation between NK and Tfh cells was ranked first in both measures (Figures 39B-C). In fact, six of the ten most altered correlations involved this NK cell signature switching from being generally negatively correlated in cold tumors to being positively correlated with various immune populations in hot tumors (Figure 39A). This result suggested that that NK cells might have different functions or activation status in hot and cold tumors.

The correlation between a B cell signature and a memory B cell (B_m) signature ranked as the second most important variable in the random forest model (Figures 39B-C). Furthermore, we observed that the same B cell signature changed from being more correlated with the naïve B

cells (Bn) in cold tumors to being strongly correlated with the Bm cells in hot tumors, which is suggestive of B cell activation (Figures 38B-C). The co-enrichment of Tfh signatures and increase in their positive correlations with the Bm signature in hot tumors lend further support to this hypothesis. Altogether, our results suggested that certain immune populations, especially Bm and NK cells, might behave differently in cytolytically hot compared to cold tumors.

Cytokines correlation with immune populations in hot and cold tumors.

Cytokines constitute a major avenue of communication among immune cells, regulating a large variety of their biological processes including proliferation, differentiation, and function. Clustering the 134 PDA samples by 255 expressed cytokines showed that cytolytically hot tumors tend to group together, suggesting that these tumors have a similar cytokine milieu (Figure 40A). Further analyses showed that 40 cytokines were differentially expressed with over 2-fold difference between the mean expressions in cytolytically hot and cold tumors (Figure 40B). The top three most differentially elevated cytokines in hot tumors, CXCL13, CCL19, and CCL21, which are all important for B cell recruitment (Okada et al., 2002). In addition, CCL19 and CCL21 are both known for their role in recruiting CCR7⁺ T cells and dendritic cells to lymphoid structures (Andrian and Mempel, 2003). The enrichment of these cytokines is, therefore, consistent with the enrichment of Bm cells, T cells, and dendritic cells in cytolytically hot tumors.

To identify relationships between immune populations and cytokines, immune signature scores were correlated with cytokine expression in each of the 1,000 bootstrapped populations using all, hot, or cold tumor samples (Figure 41). Many of these connections, such as the correlations between neutrophils and CXCR2 ligands, B cells and CXCL13, and Treg and CCL22, have already been documented in the context of various cancers (Curiel et al., 2004; Chao et al., 2016; Lee et al., 2016; Steele et al., 2016; Gu-Trantien et al., 2017). Other correlations, such as those between CD40LG and CD8⁺ T cells, reflected indirect relationships that have also been shown in the context of PDA (Byrne and Vonderheide, 2016). However, there were many other correlations suggestive of relationships yet to be explored, such as between CLEC11A and NK

cells and macrophages. In addition, four cytokines, TFF1, GDF15, ADM (adrenomedullin), and MIF, were both significantly enriched in cytolytically cold tumors and negatively correlated with many immune cell types, including CD8⁺ T cells (Figures 40B, 41A-C).

Hierarchical clustering of these immune-cytokine correlations revealed groups of immune populations very similar to those groups observed when immune signatures were correlated amongst themselves (Figures 38 and 41). The groups of immune populations further clustered with different cytokines, which is reflective of the specificity of immune-cytokine relations. Instead of being immunologically silent, cold tumors actually have an extensive cytokine network (Figures 41B-C). Because cytokine expression is reflective of the status of immune cell activation and function, we hypothesize that the strength of immune-cytokine correlations will change significantly depending on their activation. For instance, we would expect enhanced correlations of T cells or NK cells with certain cytokines, such as IFN γ , to reflect their activation in cytolytically hot tumors. To test these hypotheses, we compared immune-cytokine correlations in cytolytically hot and cold bootstrapped populations. Of the 11,985 possible pair-wise immune-cytokine correlations, we found that 2103 (17%) were significantly altered in hot and cold tumors. Only 26 of these correlations changed by an absolute value of over 0.7 between the averaged correlations of hot and cold tumors (Figure 42A). In congruence with our observations above, many of these top correlations that were increased in hot tumors involved NK cells and Bm cells. The increased correlations between TNFSF14/LIGHT and two CD4⁺ T cell types (T helper and Tcm) further suggest that these T cell populations are more activated in hot tumors. Therefore, changes in the strength of immune-cytokine correlations could indeed reflect with the activation and functional status of immune populations.

A random forest model using the top 26 correlations as input variables was constructed to classify the cytolytic status of each bootstrapped population. The top 2 variables in the model involved two cytokines, IL24 and IL33, and their correlations with Bm cells (Figures 42B and 42C). In addition, the correlation between CCL5 and NK cells ranked third, suggesting that this cytokine might be important for NK cells in hot tumors. Therefore, our results highlighted the

activation of Bm and NK cells in cytolytically hot as compared to cold tumors. Altogether, these results were highly congruent with our findings above.

Cytokine and immune communities in hot and cold tumors.

To visualize all immune-cytokine connections simultaneously, network graphs were made using only significant (FDR-adjusted, empirical P-value ≤ 0.05) and moderately strong ($\rho \geq 0.4$) immune-cytokine correlations as edges between nodes in all, hot, and cold tumor samples (Figures 43, 47, and 52). Here we define a “cytokine network” as the network of all immune-cytokine connections in a population. Nodes, which could be either immune populations or cytokines, were arranged such that those with more frequent and stronger connections clustered closer together. The thickness and color of each edge was directly proportional to the absolute value of the correlation and to the sign of the correlation (positive is red and negative is blue), respectively. A fast-greedy algorithm was used to detect communities, which are defined as groups of nodes that share more connections within the group than with those outside the group (Figures 44-46, 48-51, and 53-57). The color of each node corresponded to the community it belonged to in the overall network, which was carried through to the hot and cold network graphs (Figures 44-46). This coloring scheme provided a convenient method to compare the connectivity of the same node in the different networks.

There were two major communities, colored with orange and light blue nodes, observed in the overall network (Figures 44 and 45). The orange community consisted primarily of myeloid lineage cells, such as macrophages, neutrophils, immature DCs, and subsets of NK cells (Figure 44). The second, light blue community consisted of a variety of cells types, including those that are often found in lymphoid structures such as Tfh cells, B cells, and pDCs (Figure 45). While the orange community was present in both hot and cold tumors (Figures 48, 53-55), the light blue community was much more prominent in the cytolytically hot network (Figures 49 and 54). Indeed, the IM-CD8⁺ T cell population, which belonged to the orange community, even became part of the light blue community in cytolytically hot tumors (Figure 49). In this community, CD8⁺ T

cells were connected to pDCs through their mutual positive correlations with XCL2, which is highly reminiscent of a recently described cytokine network in the context of viral infections (Brewitz et al., 2017). In contrast, this same CD8⁺ T cell population was grouped in a community with CD56^{bright} NK cells and Th2 CD4⁺ T cells in the cold network (Figure 55). These results suggested that the at least a part of the orange community may be associated with the maintenance of an immunosuppressive environment, while part of the light blue community may be more involved with the presence of cytolytic immune response. More detailed examination of these communities may yield additional insights to the specific immune-cytokine relationships governing these cytokine networks.

Influential immune populations differ in hot and cold cytokine networks.

To quantify the relative influence of each immune population in a network, the normalized degree and eigenvector centrality for each node was calculated in the overall, hot, and cold networks of each bootstrapped population (Csardi and Nepusz, 2006; Perra and Fortunato, 2008). Degree centrality measures the influence of each immune population by the number of cytokines it is correlated to and the strength of those correlations. On the other hand, the eigenvector centrality measures influence based on the concept that connections with well-connected nodes should weigh more than connections with less connected nodes. Therefore, a connection with a well-connected cytokine would increase the eigenvector centrality of a node more than a connection with a less connected cytokine. Because these inferred cytokine networks are non-directional, high centrality values may imply that a node is either highly influential or influenced. For the sake of brevity, we will use the terms “influence” or “influential” to refer to both of these possibilities. Hierarchical clustering of immune cells by their degree and eigenvector centrality revealed groups of immune populations that have similar patterns of influence in hot and cold tumors (Figures 58A-B). For instance, the influence of M0 macrophages decreased significantly from cold to hot tumors according to both centrality measures. On the

other hand, the influence of CD8⁺ T cells, Tfh cells, and B cells increased dramatically from cold to hot tumors.

To find immune cell types with significantly altered influence, we compared the degree and eigenvector centralities of each immune population in hot and cold networks. Considering only degree centrality, we found that 14 (30%) of the 47 immune populations have significantly altered influence in hot compared to cold tumors (Figure 59A). Variable selection using random forest analyses showed that the decrease in macrophage degree centrality from cold to hot tumors was the most distinguishing between hot and cold cytokine networks (Figures 59B-C). M0 macrophages also have the highest degree and eigenvector centrality in the cold cytokine network (Figures 58A-B). The other top variables consisted of increases in the centralities of B cells, CD8⁺ T cells, and memory CD4⁺ T cells (CD4m-act and CD4m-rest) in hot networks. Importantly, these five immune populations were significantly more important than the others in the random forest model in distinguishing hot from cold networks.

Similar analyses considering only eigenvector centrality showed that 24 (51%) immune populations have significantly altered influence in hot and cold tumors (Figure 60A). Random forest analysis of these 24 immune populations selected the increases in the eigenvector centralities of CD4m-rest, generic B cells, Bm cells, and Tfh cells as the top variables (Figures 60B-C). M0 macrophages were again selected as the only population among the top variables with decreased centrality from cold to hot tumors. Altogether, this analysis showed a significant decrease in the influence of M0 macrophages and increase in the influence of CD8⁺ T cells, Tfh cells, memory CD4 cells, and B cells in hot compared to cold cytokine networks.

Cytokine influence differs in hot and cold cytokine networks.

The degree and eigenvector centralities were also calculated for each cytokine in the overall, hot, and cold cytokine network. The degree and eigenvector centralities of cytokines quantified the influence of cytokines by their connections with immune populations as described above. Similar to immune populations, hierarchical clustering of cytokines by their degree and

eigenvector centralities showed that groups of cytokines with similar changes between hot and cold networks (Figures 61A-B). Different groups of cytokines were important in hot and cold tumors, which suggested again that these tumors have very different cytokine milieu.

To determine which of the cytokines were most significantly altered in their influence, we compared the distribution of the degree and eigenvector centralities of each cytokine in hot and cold networks. We found that 53 of 255 (21%) cytokines were significantly altered in degree centrality and 89 (35%) cytokines in eigenvector centrality (Figures 62A and 63A). The majority of them, 48 cytokines, were significantly changed by both measures. The cytokines with the most increased centrality in hot tumors included CCL21, CCL19, CXCL13, and LTB, which again suggested the presence of lymphoid structures (Rennert et al., 1998; Andrian and Mempel, 2003). In addition, the increase in the centralities of TNFSF14 (LIGHT) and CD40LG were indicative of T cell activation (Bennett et al., 1998; Tamada et al., 2002a). To identify the most distinguishing features of hot and cold networks, two random forest models were constructed to classify hot and cold networks based on significantly changed degree and eigenvector centralities respectively (Figures 62B-C and 63B-C). The top two variables in the model were the centralities of CLEC11A and CCL13, both of which had higher centralities in the cold cytokine network. Furthermore, both of these cytokines were found in the likely immunosuppressive orange community. The next two variables were the centralities of IL24 and TNFSF14/LIGHT, both of which had higher centralities in the hot cytokine network and belong to the lymphoid structure-like, light blue community.

DISCUSSION AND CONCLUSIONS

Infiltration of cytotoxic immune cells, particularly of CD8⁺ T cells, has been associated with improved survival in many cancers, including PDA (Pagès et al., 2010; Gentles et al., 2015; Wang et al., 2016; Carstens et al., 2017). Using gene expression data from TCGA, we have previously shown that a subset of PDA has increased infiltration of CD8⁺ T cells and cytolytic activity (Balli et al., 2016). Unlike melanoma, high cytolytic activity did not correlate with increased

mutational burden in PDA (Rooney et al., 2015; Balli et al., 2016). This result suggested that other factors in the tumor microenvironment are likely involved. The immune infiltration and cytokine milieu are important aspects of the tumor microenvironment that could regulate the development and activity of effector immune cells. Here we aimed to characterize the cytokine networks underlying high and low cytolytic activity in PDA. We report: (1) PDA patients with cytolytically hot tumors have a survival advantage; (2) The CD4⁺ Tem and Tfh signatures have the highest protective ratios, while Th2 and CD4m-act signatures have the most negative; (3) Expression of CD4m-act signature, NK-CD56bright signature, TFF1, GDF15/MIC-1, ADM, and MIF were significantly higher in cold tumors and also negatively correlated with many immune signatures, including CD8⁺ T cells; (4) Strong correlations between NK cells-CCL5, Bm-CCL21, and Bm-CXCL13 in hot tumors were among the most distinguishing relationships of hot and cold tumors; (5) Macrophages constitute the most influential population in the cytokine network of cold tumors, while CD8, memory CD4, Tfh, and B cells were among the most influential populations in hot tumors; (6) TNFSF14/LIGHT and IL24 were the most influential cytokines in hot tumors, while CLEC11A was the most influential in cold tumors. Altogether, our analysis confirmed many previous reports, a reassuring “positive control” for our methodology, and simultaneously revealed a number of novel targets that may be regulating cytolytic activity in PDA.

Expression of cytolytic genes in the tumor has been largely attributed to effector CD8⁺ T cells (Rooney et al., 2015). Using a combination of IHC and flow cytometry, Carstens et al. showed that infiltration of CD8⁺ T cells and effector CD4⁺ T cells were both significant indicators of prolonged survival in PDA (Carstens et al., 2017). An independent analysis of TCGA data by Charoentong et al. demonstrated that infiltration of activated CD8⁺ T cells and CD4⁺ Tem cells were both independently linked to lower hazard ratios in PDA (Charoentong et al., 2017). Similar to these reports, our results showed that PDA tumors with increased expression of cytolytic activity also have improved survival, along with enrichment of CD8⁺ T cell and CD4⁺ Tem cells. In fact, CD4⁺ Tem cells have the highest protective ratio among all the immune signatures. However, very little is known about CD4⁺ Tem cells in the context of cancer. Compared to primary

effector cells, memory effector CD4⁺ cells respond to lower levels of antigens, express stimulatory cytokines without need for APCs, and are highly resistant to tolerance induction (London et al., 2000). Furthermore, an early study showed that a persistent CD4⁺ T cell population (likely consisting of CD4⁺ Tem cells) was required for the maintenance of cytotoxic CD8⁺ T cell-mediated control of chronic lymphocytic choriomeningitis virus (LCMV) infection in mice (Matloubian et al., 1994). While much focus has been laid on CD8⁺ T cells, the potential roles of CD4⁺ Tem populations in cancer remain unclear. Our results support the hypothesis that CD4⁺ Tem cells may be an important population in promoting cytolytic activity and survival in PDA.

The Th2 and CD4m-act signatures were both associated with negative protective ratios. In fact, the CD4m-act signature was negatively associated with survival in all three PDA cohorts, significantly enriched in cytolytically cold PDA tumors, and negatively correlated with CD8⁺ cells. This was in congruence with results from the study by Charoentong et al. where higher expression of Th2, activated CD4, and central memory CD4 signatures were associated with positive hazard ratios (Charoentong et al., 2017). While the identity of the CD4m-act population remained uncertain, we note that it was positively correlated with the Th2 signature in the overall and in the cold groups, and negatively correlated with many other T cell signatures including Tregs in the same groups. Therefore, the CD4m-act and Th2 populations may represent similar, if not the same, populations. Cytokines, such as IL-4, that can induce and then be secreted by CD4⁺ Th2 cells can antagonize the polarization of Th1 cells and the development of cellular immunity (Parronchi et al., 1992). In fact, the selective inhibition of Th2 CD4⁺ T cells (via IL-4 neutralization) was recently shown to improve responses to radiotherapy in a model of mammary cancer (Shaio et al., 2015). Polarization of Th2 CD4⁺ cells has been shown to depend on a combination of various factors: the source and processing of the antigen, TLR4 activation, cytokines (TSLP, IL25, and IL33), and relatively weak TCR stimulation (Oliphant et al., 2011). In support of the hypothesis that Th2 cells may be present, our results showed that IL33 was highly expressed in all PDA tumors. Whether Th2 polarization is favored in the context of PDA remains

to be determined. Altogether, these results suggest that at least a subset of CD4⁺ T cells, likely of Th2 polarization, in the tumor microenvironment was detrimental to survival.

Similar to CD4m-act cells, NK-CD56bright cells was also enriched in cytolytically cold tumors, negatively correlated with survival in hot tumors, and also negatively correlated with many other immune populations including CD8⁺ T cells. Although they constitute only a minority in circulation, CD56-bright NK cells constitute a major component of NK cells found in tissues and lymphoid organs (Cooper et al., 2001a). Upon activation, these cells become potent secretors of a variety of cytokines, particularly of type I interferons (IFN- α/β) (Cooper et al., 2001b). In the context of autoimmune diseases and chronic viral infections, activated CD56-bright NK cells were shown to be suppressive or even cytotoxic toward proliferating CD4⁺ T cells, which served to protect tissues against excessive T cell-mediated damage (Nielsen et al., 2012; Morandi et al., 2015). In fact, CD56-bright NK cells were the primary mediators of the therapeutic effect of daclizumab (anti-IL2R) in multiple sclerosis (Bielekova et al., 2006). In the context of cancer, however, the regulatory function of these NK cells could be detrimental to the development of anti-tumor T cells. Therefore, a subset of NK cells could be contributing to the immunosuppressive environment in human PDA.

Multiple studies have now detailed the different genomic landscapes and molecular pathways associated with PDA tumors with high and low CD8⁺ T cells infiltration (Bailey et al., 2016; Balli et al., 2016; Charoentong et al., 2017). Here our analysis showed that there are also substantial differences in the cytokine networks underlying cytolytically hot and cold tumors. Most immune cell populations, particularly CD8⁺ T cells and various populations of DCs, were significantly enriched in cytolytically hot tumors. This was accompanied by the enrichment of many cytokines, including those associated with activated DC such as CXCL9, CXCL10, and XCL2 (Padovan et al., 2002; Brewitz et al., 2017). The three most significantly enriched cytokines in hot tumors, CXCL13, CCL19, and CCL21, are known for their ability to recruit either B cells or CCR7⁺ T cells and APCs to lymphoid structures (Okada et al., 2002; Andrian and Mempel, 2003). This suggested that intratumoral or peritumoral lymphoid structures are more likely to be found in

cytolytically hot tumors and may be important in orchestrating the development of anti-tumor immunity. In support of this hypothesis, presence of intratumoral tertiary lymphoid structures (TLS) have been associated with increased infiltration of effector lymphocytes and improved survival in an independent cohort of human PDA patients (Hiraoka et al., 2015). In addition, intratumoral or peritumoral TLSs were significantly enriched in patients who responded to vaccine-based immunotherapies in PDA (Lutz et al., 2014; Le et al., 2015; Byrne and Vonderheide, 2016). Accumulating evidence such as these have led to the hypothesis that TLSs are important for orchestrating anti-tumor immunity (Dieu-Nosjean et al., 2014). Although tumor samples could be contaminated by lymph nodes, this would imply that cytolytically hot tumors were preferentially contaminated or overlooked in quality checks by TCGA pathologists. Future histological studies are required to confirm the enrichment of TLSs and distinguish them from lymph node contamination. In contrast, only four cytokines, TFF1, GDF15/MIC-1, MIF, and ADM, were significantly enriched in cold tumors by more than two fold. Interestingly, all four of these cytokines have been reported to be either a prognostic marker or directly pro-tumorigenic in pancreatic cancer (Ramachandran et al., 2007; Arumugam et al., 2011; Aggarwal et al., 2012; Funamizu et al., 2013; Wang et al., 2014; Yang et al., 2016a). In fact, anti- MIF therapy even displayed anti-tumor activity in an early phase clinical trial (Mahalingam et al., 2016). However, rather less is known about their role in regulating tumor-associated immune cells.

Given their vastly different immune infiltration, we next hypothesized that the immune-immune and immune-cytokine relationships should also be significantly altered in cytolytically hot and cold tumors. Using correlations to quantify the strength of relationships among immune populations and cytokines, we found that a substantial percentage of correlations (~20-30%) were indeed significantly altered between the two groups. Increased correlations of a NK cell signature with other immune populations and cytokines in hot tumors emerged as the most altered relationships. In particular, the increased strength of correlations between NK cells-CCL5 and NK cells-CCL4 suggested that some NK cells have augmented cytotoxic activity in cytolytically hot tumors (Robertson, 2002). NK cells are increasingly recognized as important

mediators of anti-tumor cytotoxicity (Guillerey et al., 2016). A recent study even showed that NK cells and antigen-specific CD4⁺ T cells were critical for mediating TLR7/8 agonist-induced *in vivo* regression of MHC-I^{low} melanomas, while CD8⁺ T cells were dispensable (Doorduijn et al., 2017). Given the paucity of neoepitopes and dysfunctional antigen presentation typical of certain cancers, augmenting NK-mediated immunity may be a promising therapeutic approach. Besides NK-related correlations, the next most significantly increased correlations were that of the Bm signature with CCL21 and CXCL13, both of which are known to recruit B cells (Okada et al., 2002). Based on these examples and many others found in the correlation matrices, we propose that such correlations could be useful for identifying potential immune-cytokine relationships. In addition, differential correlation analyses could even provide evidence for altered recruitment or activation of specific immune populations.

Although useful in revealing potential changes in pair-wise relationships, differential correlation analysis could not account for simultaneous, multiple relationships. Indeed, most immune cells secrete multiple cytokines, which in turn could have pleiotropic effects on multiple cell types. Therefore, significant enrichment of immune populations and cytokines may not be the most appropriate measures of importance. Here, we first showed that cytokine networks could be extracted from pair-wise immune cytokine correlations. Social network theory then provides quantitative measures of importance for each node in a network. Using this approach, we found that macrophages consisted of the most influential/influenced immune population in the cold network. Indeed, depleting or altering the function of macrophages have proven to be particularly effective in inducing anti-tumor immunity and suppressing tumor growth (Clark et al., 2007; Zhu et al., 2014; Beatty et al., 2015; Nywening et al., 2016). Therefore, our findings support the growing consensus that tumor-associated macrophages (TAMs) represent a promising target to effectively disrupt immunosuppressive networks in PDA.

Among cytokines with significantly higher influence in the cytolytically cold network, CLEC11A and CCL13 were consistently ranked as the top two cytokines with the most distinguishing differences in their influence between hot and cold networks in the random forest

models. CLEC11A, also known as stem cell growth factor (SCGF), encodes a secreted glycoprotein that functions as a potent growth factor for erythroid and myeloid progenitors (Hiraoka et al., 2001). CLEC11A has recently been shown to be required for multiple myeloma growth (Laganà et al., 2017). CCL13, which has no mouse counterpart, is a chemokine that can attract CCR2⁺ or CCR3⁺ monocytes, eosinophils, and basophils (Godiska et al., 1997; Uguccioni et al., 1997). A number of other cytokines also have significantly higher influence in the cytolytically cold network, some of which, such as CTGF and GDF15/MIC-1, are already known targets in pancreatic cancer (Dornhöfer et al., 2006; Neesse et al., 2013; Wang et al., 2014). However, whether any of these cytokines play a role in promoting immunosuppressive networks in PDA remains to be demonstrated.

As expected, several T cell populations, including memory CD4⁺ and CD8⁺ T cells, have significantly higher influence in cytolytically hot cytokine network, which reflected their enhanced recruitment and activation. The increased influence of Tfh and B cells also ranked among the most distinguishing features of hot compared to cold networks. Because they are typically found inside lymphoid structures, our analysis led us to conclude again that TLS may be enriched in cytolytically hot tumors. Among all DC populations, only the centrality of plasmacytoid DCs (pDCs) increased significantly in cytolytically hot tumors. Unlike immature pDCs which are poor APCs and can even induce Tregs, TLR-stimulated pDCs are capable of cross-priming and inducing both antigen-specific effector CD4⁺ and CD8⁺ T cells (Di Pucchio et al., 2008; Goubier et al., 2008; Mouriès et al., 2008). Upon activation, pDCs also become potent secretors of Th1, CD8⁺ T cell, and NK cell-activating cytokines such as type 1 IFNs, CXCL10, CCL4, and IL12 (Swiecki and Colonna, 2015). Expression of CCR7 further allows pDCs to traffic toward CCL19 and CCL20 high regions typical of lymphoid structures (Umemoto et al., 2012). Type I IFNs production by recruited pDCs were recently shown to be critical for optimizing the maturation of and cross-presentation by local XCR1⁺ classical DCs in response to viral infections (Brewitz et al., 2017). In another study, pDCs were reported to be part of the systemic immune activation required for immunotherapy-induced tumor regressions (Spitzer et al., 2017). Altogether, our

analysis suggested that mature pDCs could be linked to TLS within the tumor and associated with the development of cytotoxic immune response. Furthermore, Tfh cells have the second highest protective ratio, which indirectly links the presence of lymphoid structures with survival. Whether these immune populations or the presence of TLSs contribute to the development of anti-tumor cytolytic activity remains to be determined.

Among cytokines with significantly increased influence in hot networks, only IL24 and TNFSF14/LIGHT consistently ranked among cytokines with most distinguishing differences between hot and cold networks. Both cytokines were also significantly enriched in cytolytically hot tumors. Furthermore, the increased positive correlations between LIGHT and T-helper and Tcm CD4⁺ cells ranked among the most altered relationships comparing hot and cold tumors. IL24, an IL-10 family protein also known as melanoma differentiation-associated 7 (MDA-7), can potentially induce cancer cell apoptosis (Sauane et al., 2003). In fact, intratumoral administration of an adenoviral construct expressing the IL24 transgene transiently increased systemic Th1 cytokine production, increased intratumoral CD8⁺ T cell infiltration, and showed some efficacy in a Phase I trial (Cunningham et al., 2005; Tong et al., 2005). On the other hand, LIGHT is a member of the TNF family that could bind both lymphotoxin- β receptor (LT β R) on stromal cells and TNFRSF14/HVEM on immune cells (del Rio et al., 2010). Upon binding to TNFRSF14, LIGHT acts as a co-stimulatory cytokine that can enhance T cell, NK cell, and DC activation (Tamada et al., 2000; 2002a; 2002b; Morel et al., 2001; Fan et al., 2006). LIGHT-activated NK cells could further facilitate anti-tumor CD8⁺ T cell activation via IFN- γ secretion (Fan et al., 2006). Several other studies have shown that tumor cells transduced to express LIGHT potentially promote T cell recruitment and their anti-tumor activity (Yu et al., 2004; Qiao et al., 2017). Therefore, enhancing IL24 and LIGHT signaling might be promising directions for the treatment of PDA.

Altogether, we showed that cytolytically cold tumors have significantly enrichment of CD4m-act cells, CD56bright-NK cells, TFF1, GDF15/MIC-1, ADM, and MIF. Meanwhile, cytolytically hot tumors were most significantly enriched in CD8⁺ T cells, DCs, CXCL13, CCL19, and CCL21. Differential network analysis offered a slightly different perspective. In cytolytically

cold tumors, the most influenced/influential players were macrophages, CLEC11A, and CCL13. On the other hand, cytolytically hot tumors were characterized by NK cell activation, B cell recruitment, and the increased influence of memory CD4⁺ T cells, CD8⁺ T cells, Tfh, B cells, pDCs, IL24, and LIGHT. This pattern is highly suggestive of the enriched presence of TLSs in cytolytically hot tumors.

In summary, we devised a novel network-level computational methodology to reconstruct and compare tumor-associated cytokine networks from gene expression data. We conclude that cytolytic activity correlates with survival in PDA. We then showed that cytolytically hot and cold tumors are enriched with different immune populations and cytokines. Furthermore, a substantial portion of immune-cytokine correlations is altered in hot and cold tumors, reflecting the differential recruitment, activation, and function of specific immune populations. Finally, we showed that the most influential immune populations and cytokines differ between hot and cold tumors. Therefore, our analysis identified many existing targets and also highlighted novel candidates that may effectively disrupt immunosuppressive networks and promote cytolytic activity in PDA.

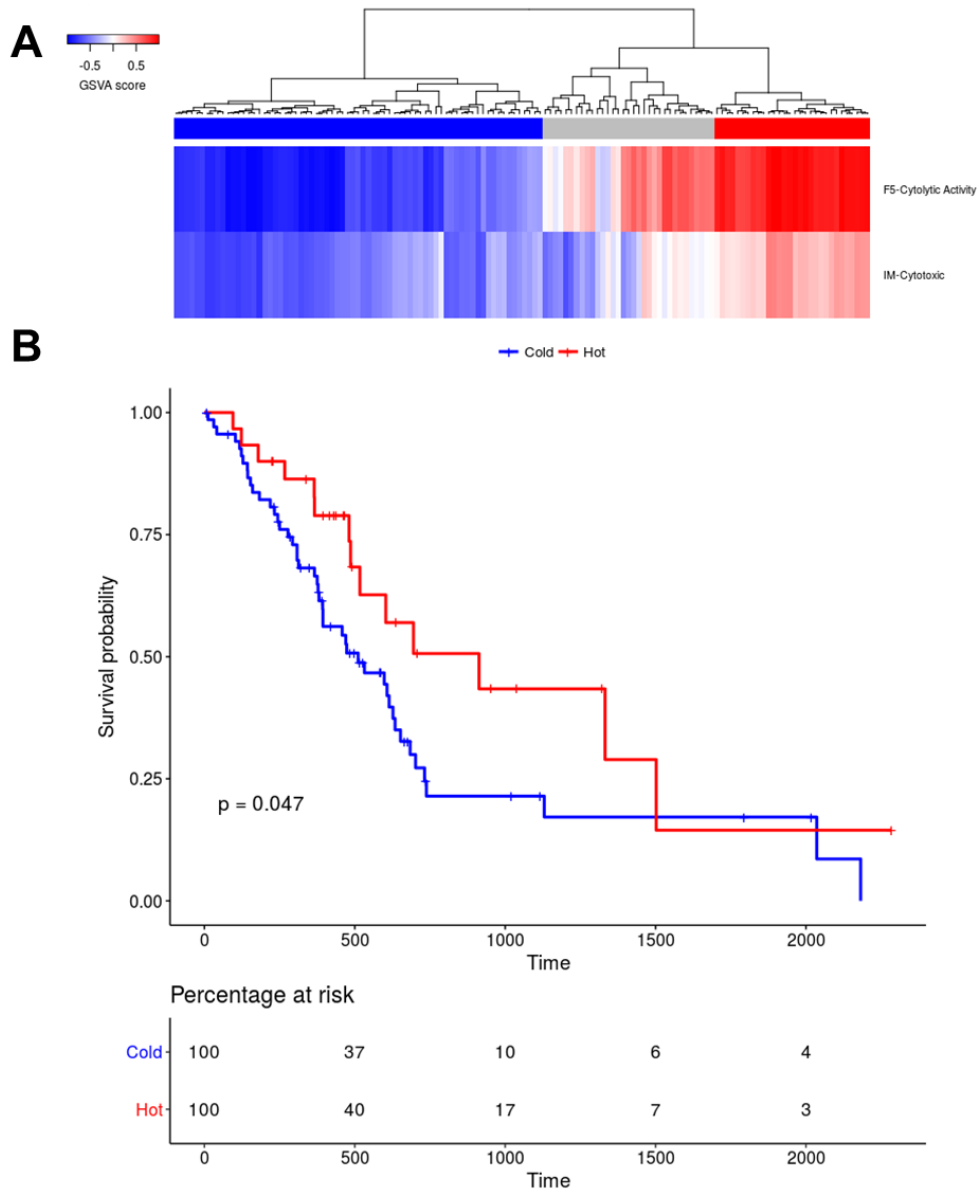


Figure 34. Stratification of human PDA samples by cytolytic activity and cytotoxic gene expression signatures.

(A) Hierarchical clustering of 134 human PDA samples by the log-average of the cytolytic activity (PRF1 and GZMA) and cytotoxic gene signatures into cytolytically “hot” ($n = 30$) and “cold” ($n = 71$) groups. **(B)** Kaplan Meier plot and the corresponding risk table of hot and cold samples. Log-rank p -value is shown. Marks indicate censored data points.

A

Characteristics	All (n=134)	Hot (n=30)	Cold (n=71)
Age	64.6 (11.0)	65.8 (11.3)	64.3 (10.9)
Sex			
Male	70 (52%)	13 (43%)	38 (54%)
Female	64 (48%)	17 (57%)	33 (46%)
Stage			
IA	3 (2%)	1 (3.3%)	2 (3%)
IB	7 (5%)	1 (3.3%)	4 (6%)
IIA	21 (16%)	4 (13.3%)	14 (20%)
IIB	96 (72%)	22 (73%)	47 (66%)
III	3 (2%)	2 (7%)	1 (1%)
IV	3 (2%)	.	2 (3%)
unknown	1 (1%)	.	1 (1%)

B

variable	beta	HR (95%)	p.value
Group	-0.62	0.53 (0.29-0.98)	0.0444
Age	0.015	1.01 (0.99-1.04)	0.2833
Sex	0.042	1.04 (0.62-1.75)	0.8728
Stage	0.026	1.02 (0.46-2.30)	0.9495

Figure 35. Cox multiple regression shows significant reduction in hazard ratio in cytolytically hot vs cold tumors.

(A) Patient sample characteristics grouped by cytolytically hot or cold designations. **(B)** Cox multiple regression survival analysis for all the variables and their respective hazard ratios and p-values. Cytolytically hot or cold classification is represented by the variable “group”.

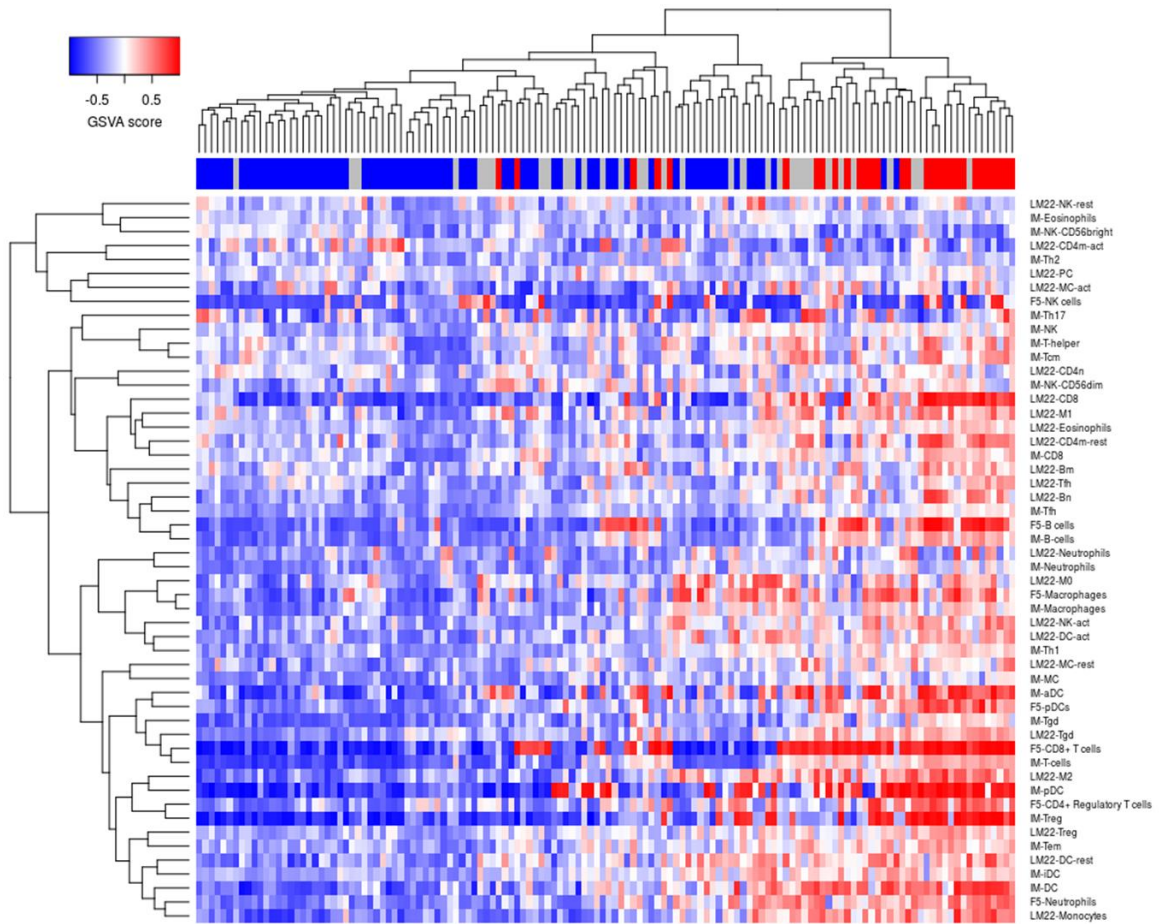


Figure 36. Immune GSVAs in human PDA.

Hierarchical clustering of 134 PDA samples (x-axis) by 52 immune GSVAs (y-axis).

Cytolytically hot and cold samples are marked with red and blue columns respectively.

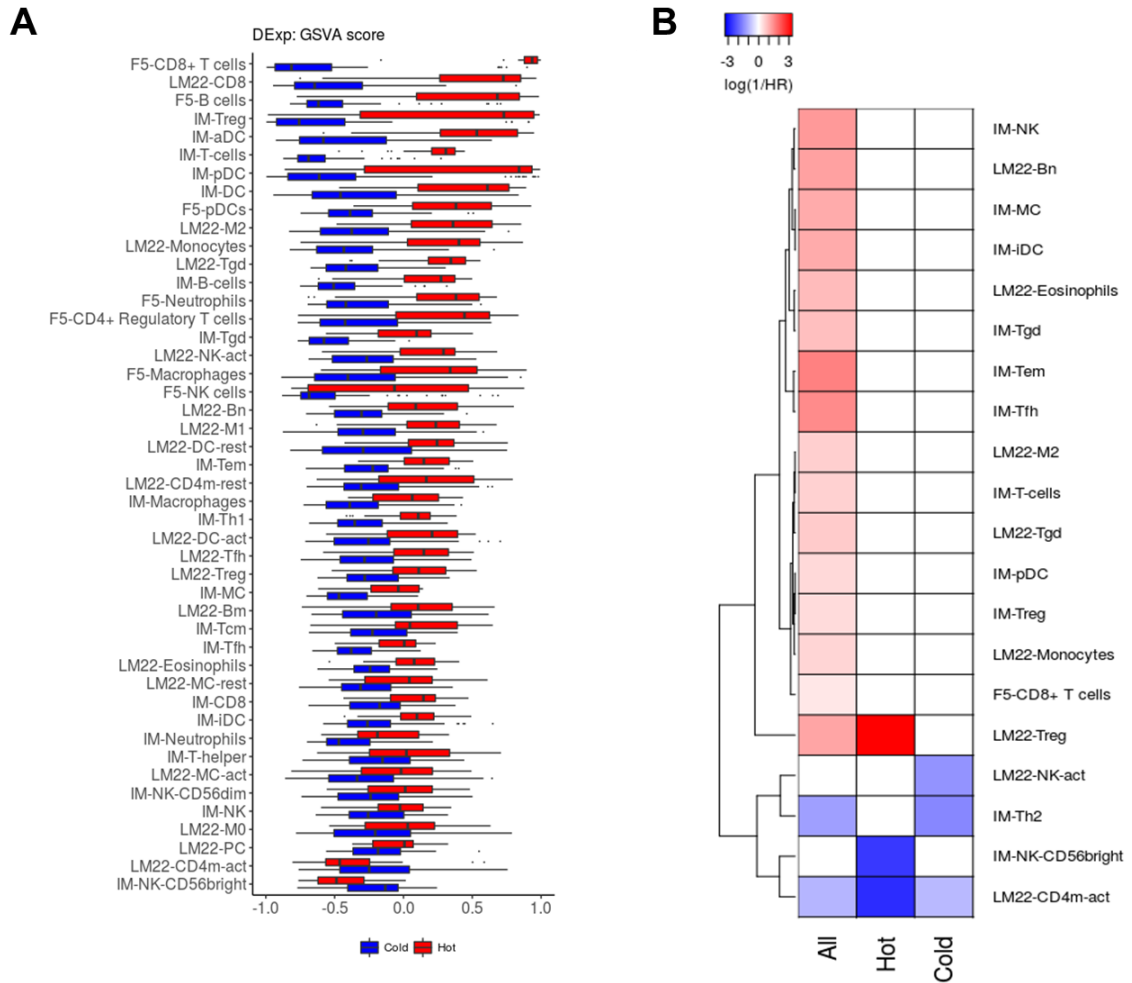


Figure 37. Immune populations differentially enriched and correlated with survival in hot and cold PDA.

(A) Boxplots of 46 immune GSVAs scores with significant differences between hot and cold samples (FDR-adjusted p-value ≤ 0.05 , Wilcox test). Immune scores are ordered by decreasing difference in the mean GSVAs scores of hot and cold samples. **(B)** Heatmap showing the log of the protective ratio (1/HR) from univariate Cox regression of individual immune GSVAs scores in all, hot, or cold tumors. Only the 20 immune GSVAs scores with significant Cox regressions are shown (Wald test, p-value ≤ 0.05).

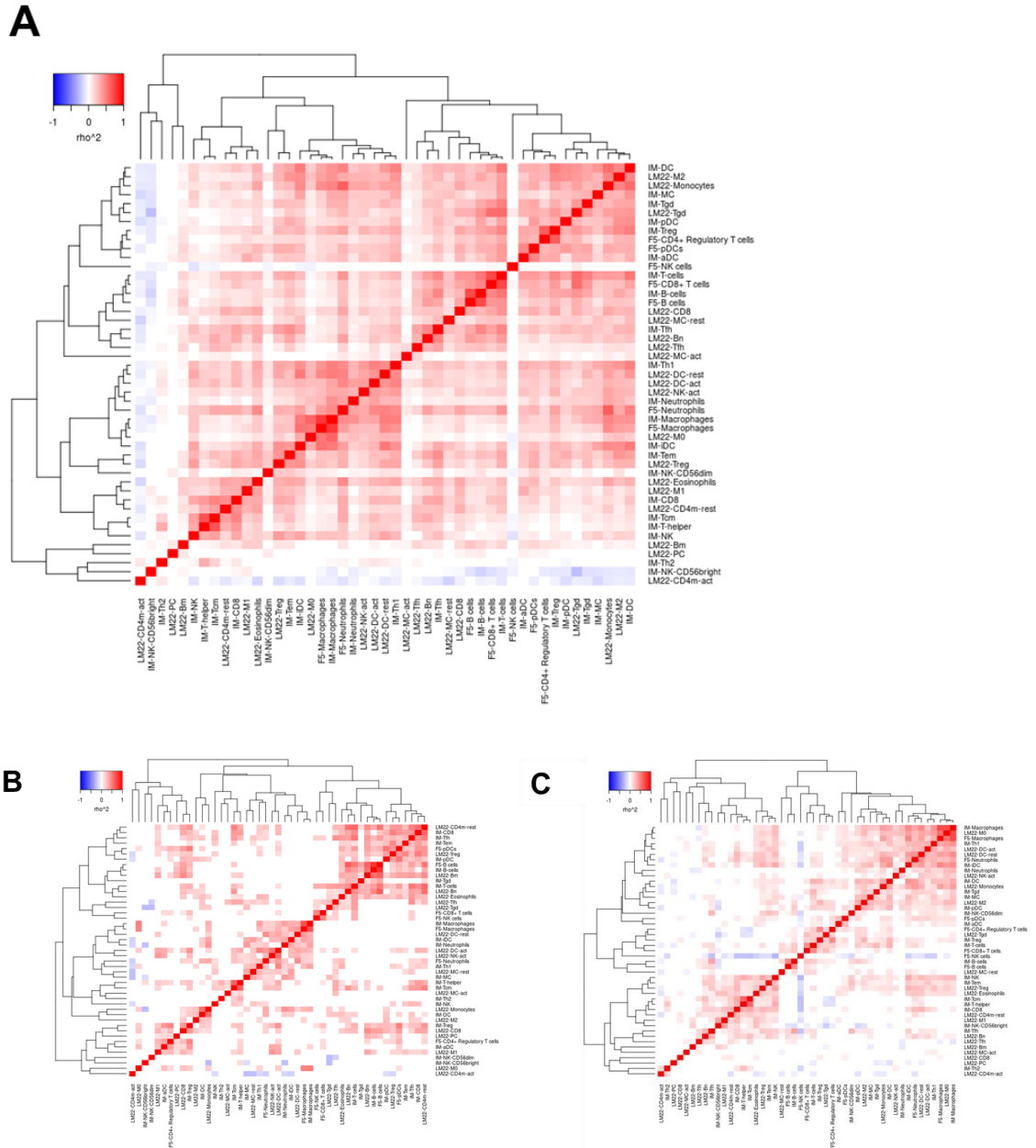


Figure 38. Immune GSVA scores cluster differently in cytolytically hot and cold tumors.

Correlograms of the immune GSVA scores with each other in all **(A)**, hot **(B)**, and cold **(C)** PDA tumors. Graph shows averaged Spearman's rho from 1000 bootstrapped populations (empirical p-value ≤ 0.05).

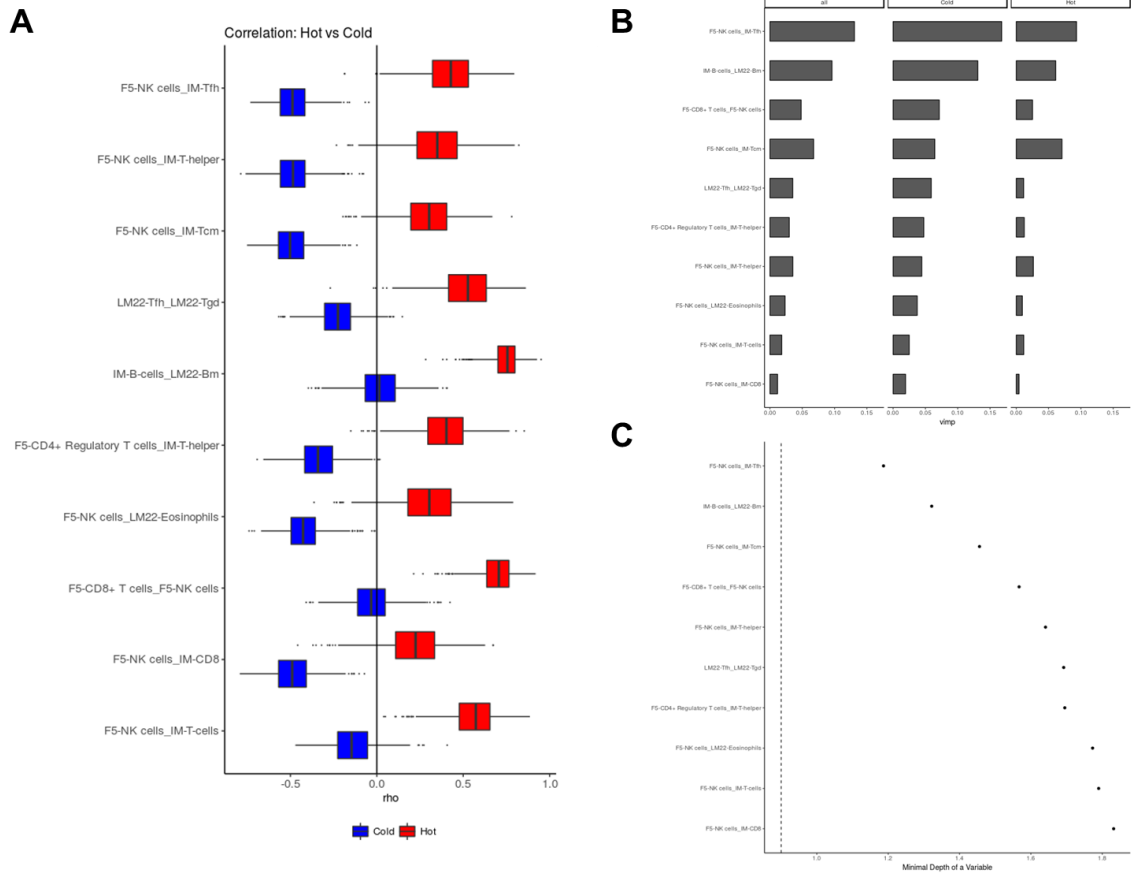


Figure 39. Immune GSVA score correlations with the largest changes between cytolytically hot and cold tumors.

(A) Boxplot of the indicated immune-immune correlations with significant differences in hot and cold tumors (delta Spearman’s rho ≥ 0.7 and FDR-adjusted empirical p-value ≤ 0.05). Graph shows the distribution of Spearman’s rho in 1000 bootstrapped sample populations grouped by hot or cold tumors. **(B)** Barplot of the variable importance (vimp) scores in hot, cold, and all samples using only the top correlations in a random forest model (ntree = 1000) to classify the cytolytic status of each tumor. **(C)** Plot of the minimal depth of the top correlations in a random forest model (ntree = 1000) to classify the cytolytic status of each tumor. The dotted line shows the “high” conservative cutoff for a variable to be considered more significantly important than others in the model.

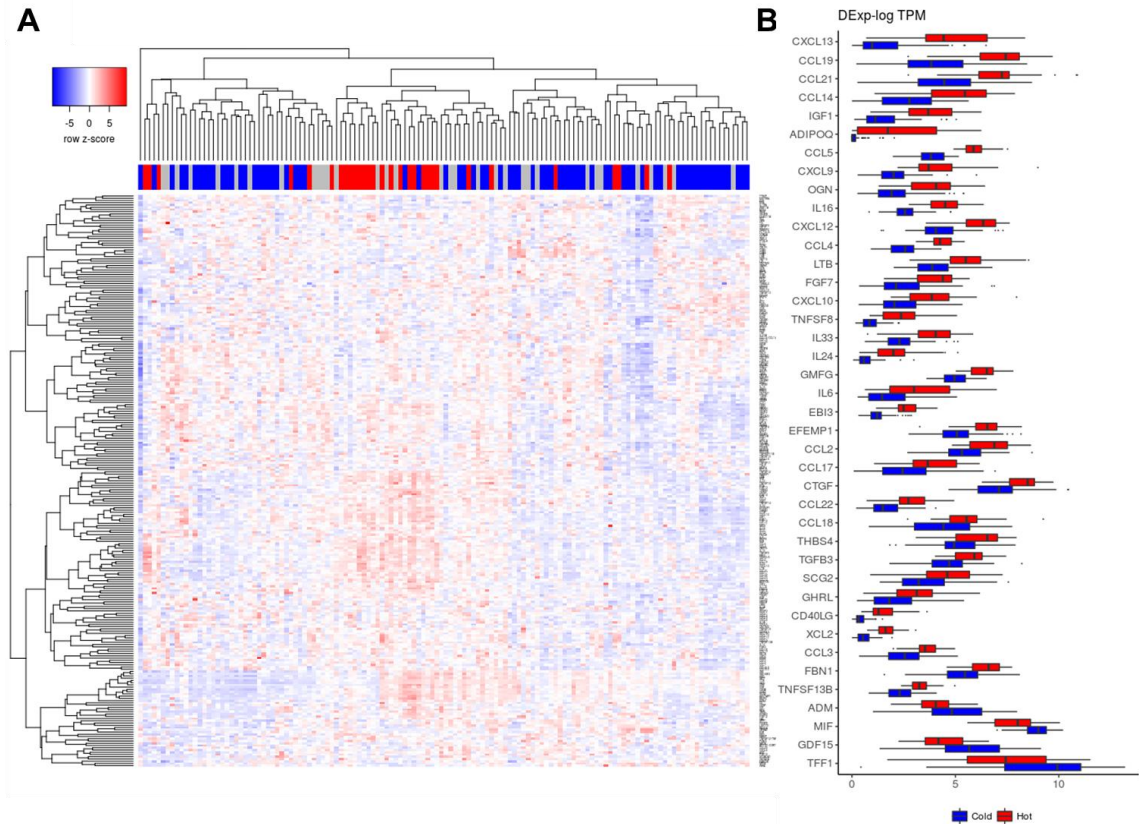


Figure 40. Cytokine differential expression in human PDA.

(A) Hierarchical clustering of 134 PDA tumors (x-axis) by the expression of 255 cytokines (y-axis) that are expressed in over 20% of the samples (row z-score of log TPM). Cytolytically hot and cold samples are marked with red and blue columns respectively. **(B)** Boxplots of 40 cytokines with more than 2 fold gene expression difference between hot and cold tumors (FDR-adjusted p-value ≤ 0.05 , Wilcox test). Cytokines are ordered by decreasing difference in mean expression.

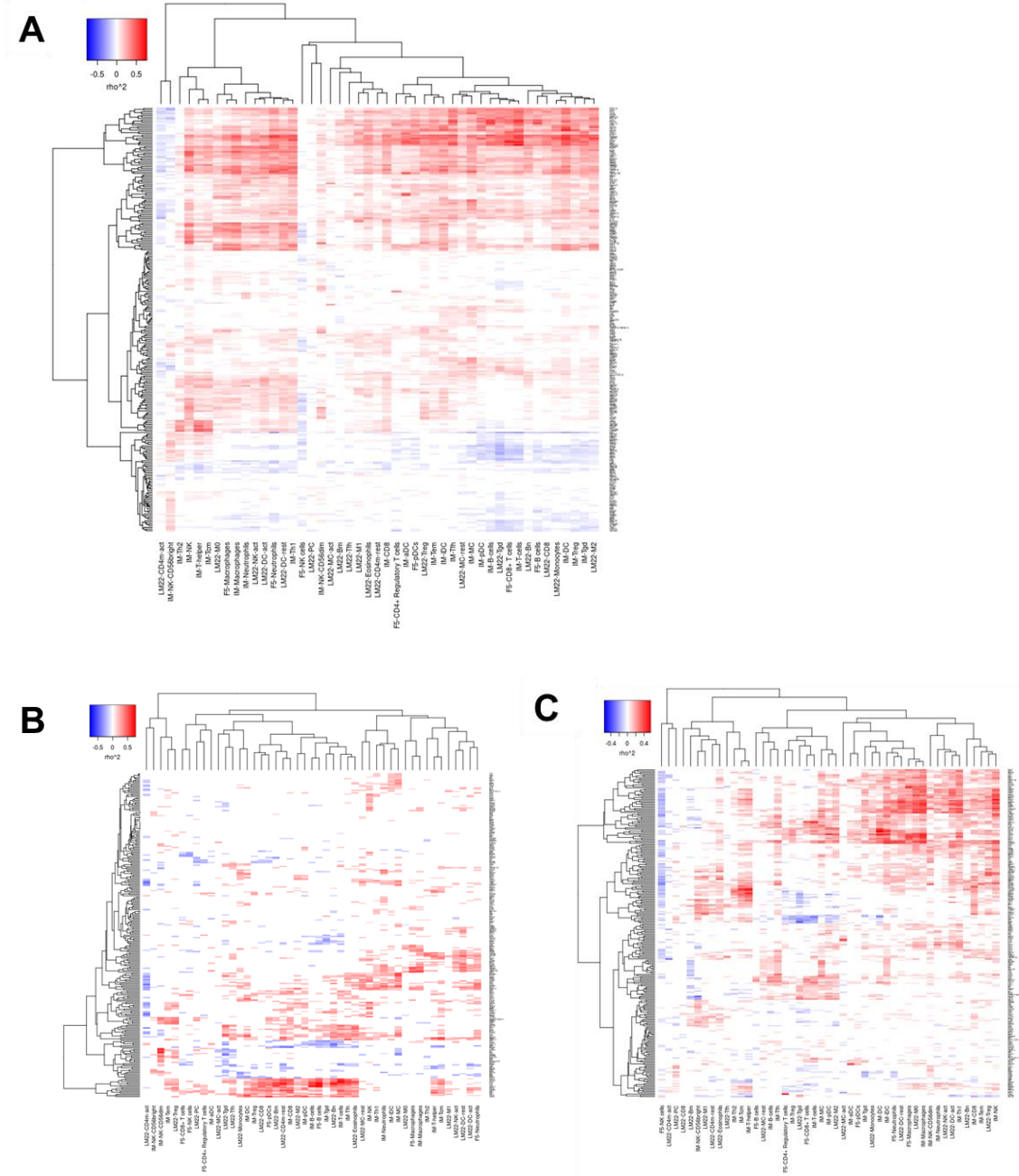


Figure 41. Cytokines correlation with immune GSEA scores in PDA.

Correlations of the 255 expressed cytokines (y-axis) and selected immune populations (x-axis, $n = 47$) in all (A), hot (B), and cold (C) PDA tumors. Graph shows averaged Spearman's rho from 1000 bootstrapped populations (empirical p -value ≤ 0.05).

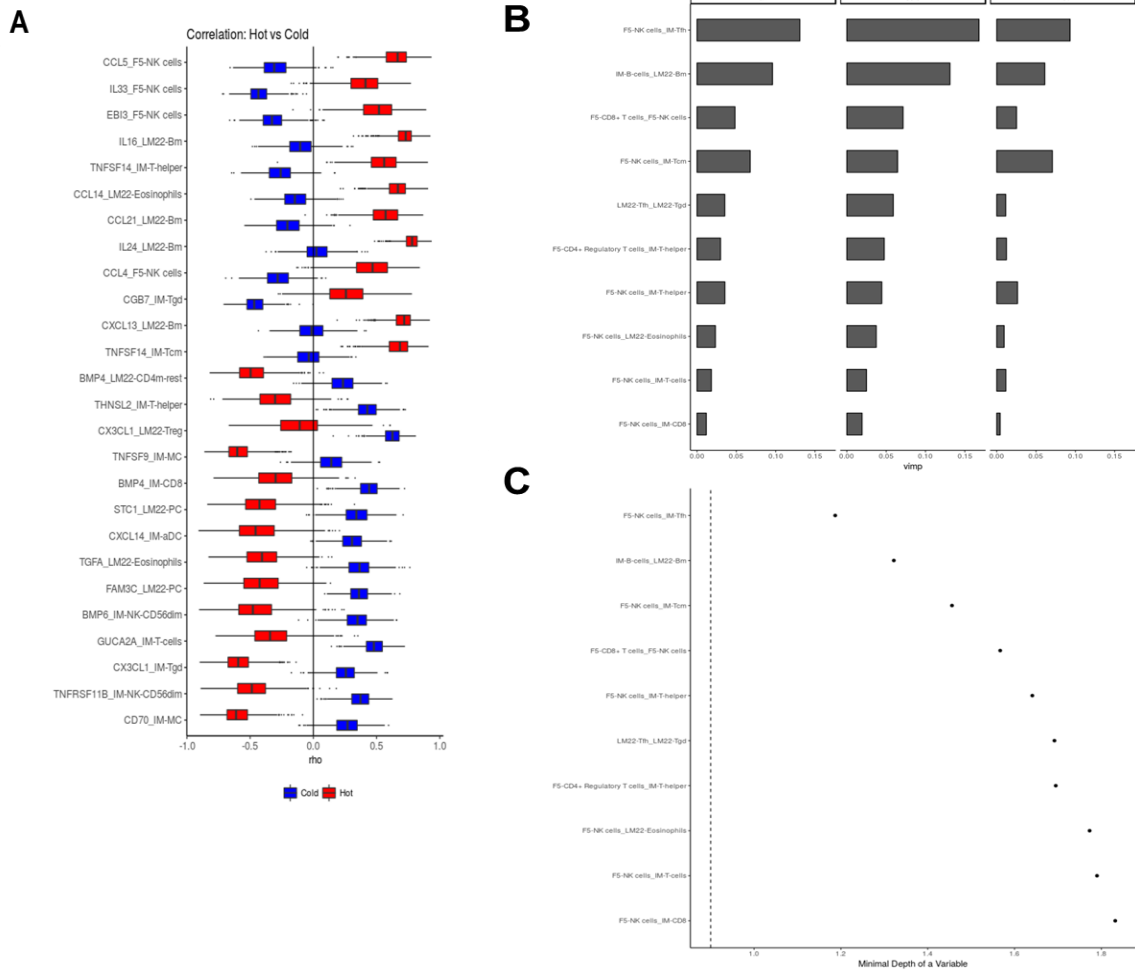


Figure 42. Significantly altered immune-cytokine correlations in hot and cold tumors.

(A) Boxplot of the 26 indicated immune-cytokine correlations with significant differences in hot and cold tumors (delta Spearman's rho ≥ 0.7 and FDR-adjusted empirical p-value ≤ 0.05). Graph shows the distribution of Spearman's rho in 1000 bootstrapped sample populations grouped by hot or cold tumors. **(B)** Barplot of the variable importance (vimp) scores in hot, cold, and all samples using only the top immune-cytokine correlations in a random forest model (ntree = 1000) to classify the cytolytic status of each tumor. **(C)** Plot of the minimal depth of the top immune-cytokine correlations in a random forest model (ntree = 1000) to classify the cytolytic status of each tumor. The dotted line shows the conservative cutoff for a variable to be considered significantly more important than others in the model.

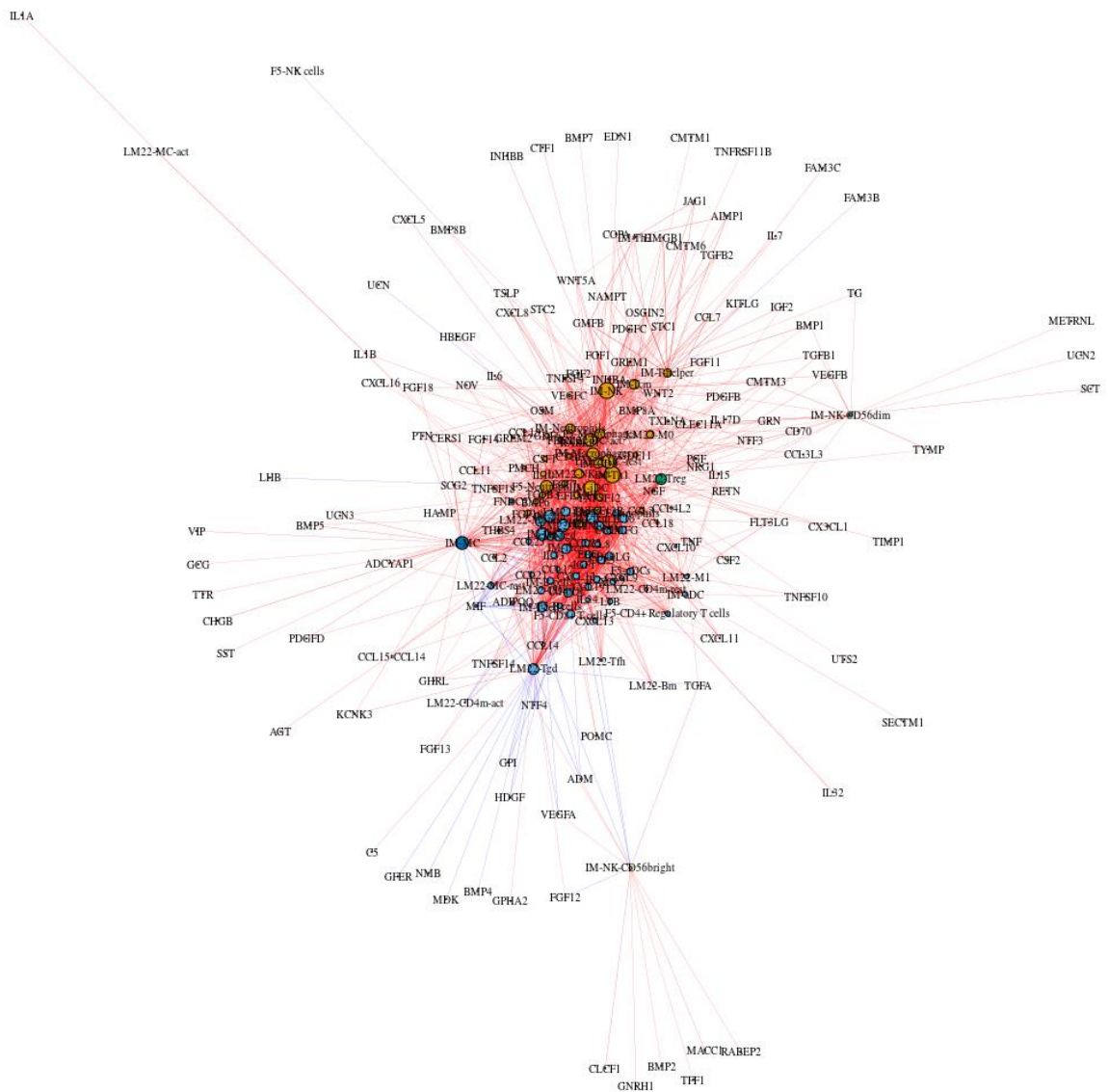


Figure 43. The overall cytokine network in PDA.

Immune GSVA score-cytokine correlation network using all 134 PDA samples depicting only significant Spearman's $\rho \geq 0.4$ as edges (FDR-adjusted empirical p -value ≤ 0.05). Positive and negative correlations are represented by red and blue edges respectively. Edge thickness is proportional to ρ . The size of each node is proportional its degree centrality. Nodes are clustered into 6 non-overlapping communities using the fast-greedy algorithm and colored accordingly (shown in Figures 44-46).

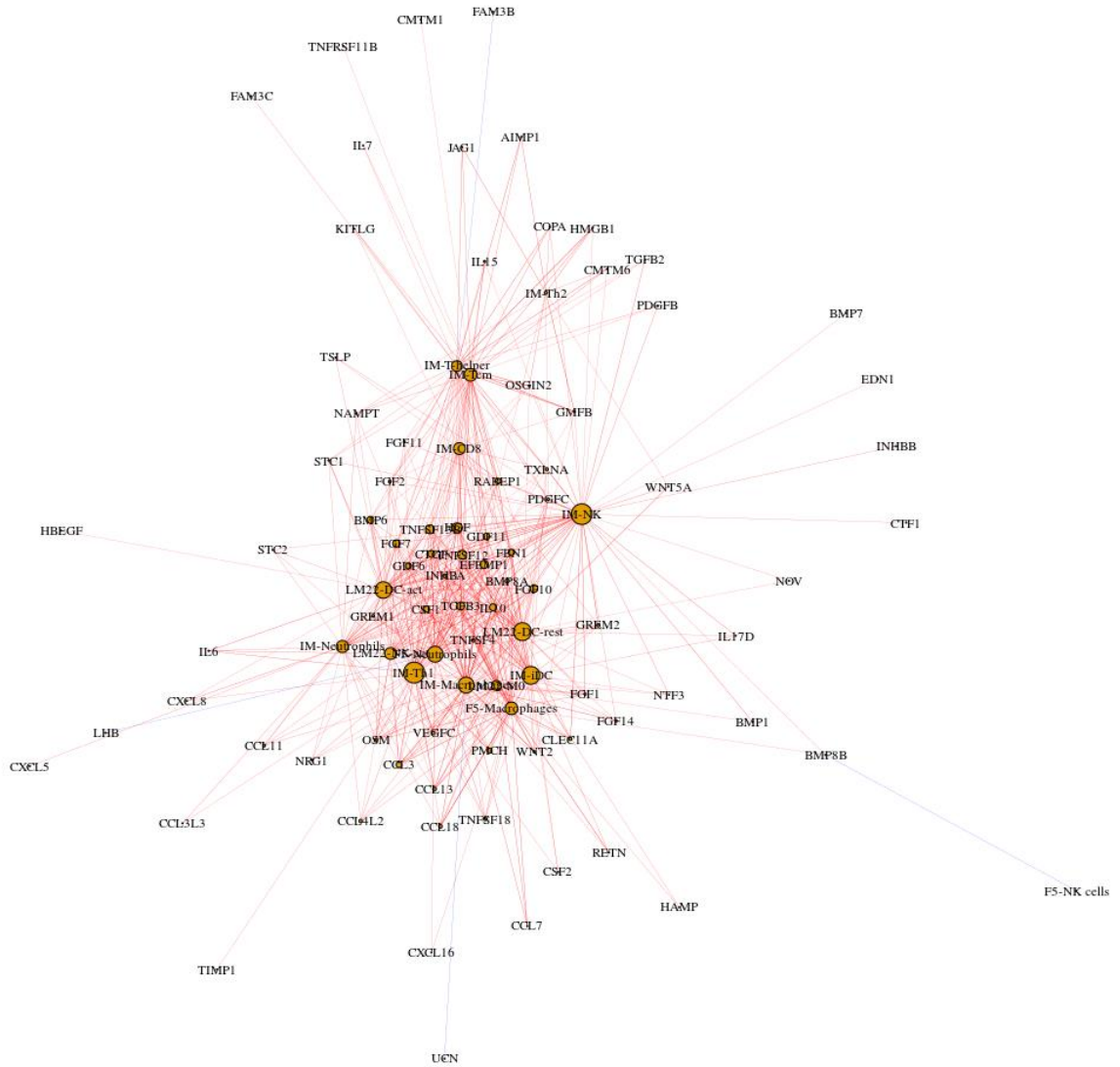


Figure 44. Community 1 in the overall cytokine network.

Community 1 (orange community) in the immune-cytokine correlation network (most complex community) using all 134 PDA samples in Figure 43 as detected by the fast-greedy algorithm.

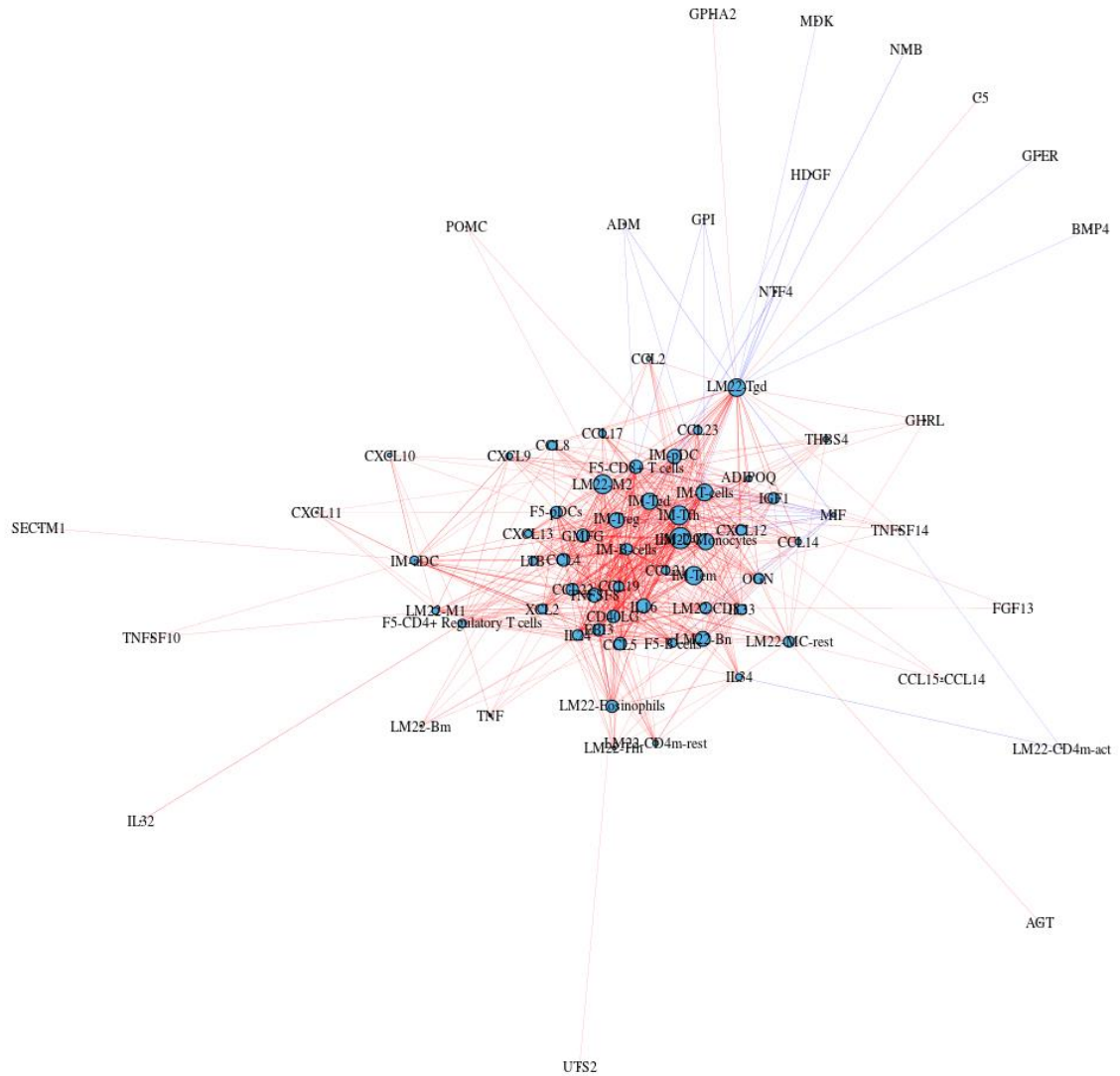


Figure 45. Community 2 in the overall cytokine network.

Community 2 (light blue community) in the immune-cytokine correlation network (2^{nd} most complex community) using all 134 PDA samples in Figure 43 as detected by the fast-greedy algorithm.

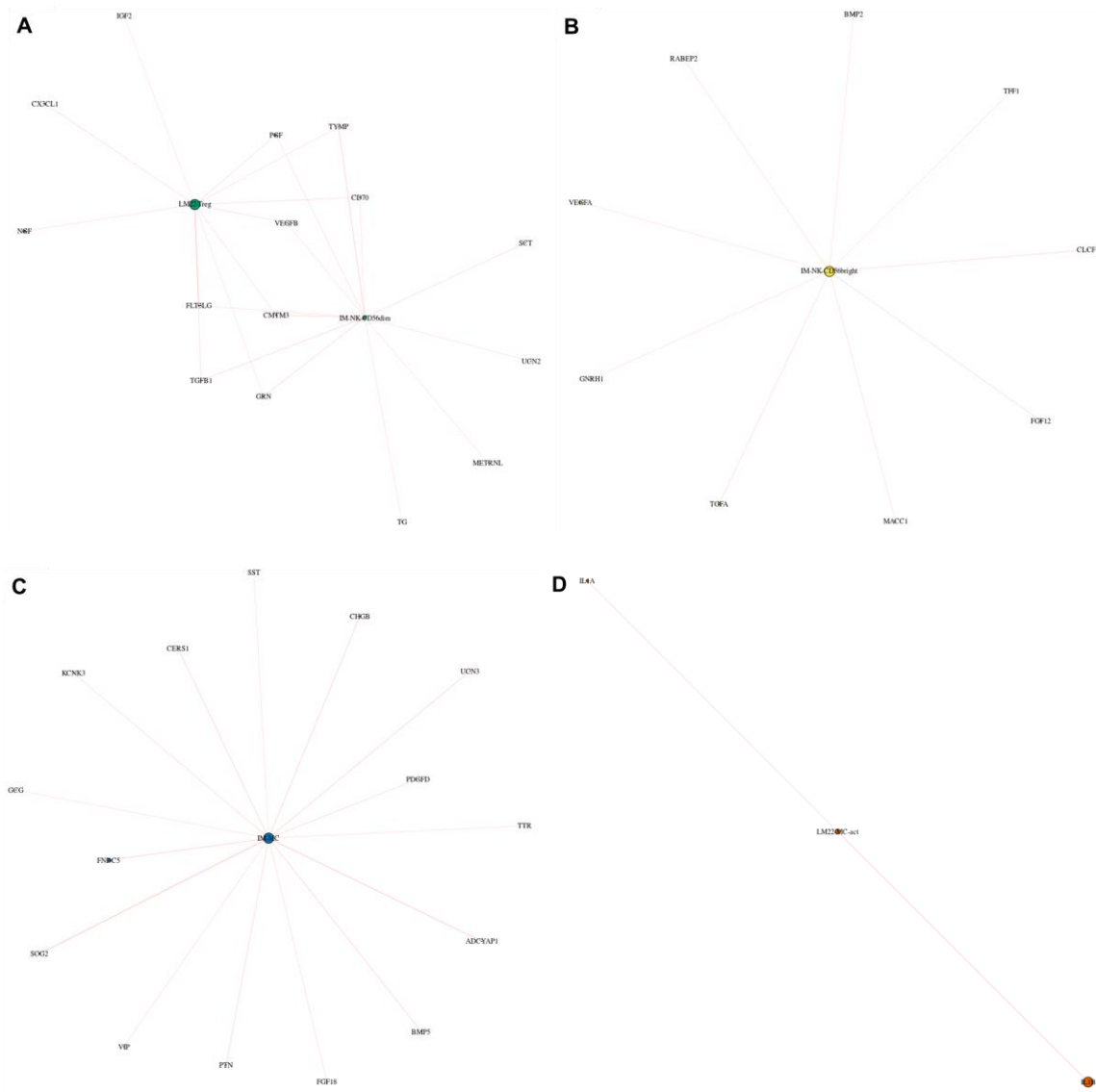


Figure 46. Communities 3-6 in the overall cytokine network.

Communities 3-6 (A-D, respectively) in the immune-cytokine correlation network using all 134 PDA samples in Figure 43 as detected by the fast-greedy algorithm.

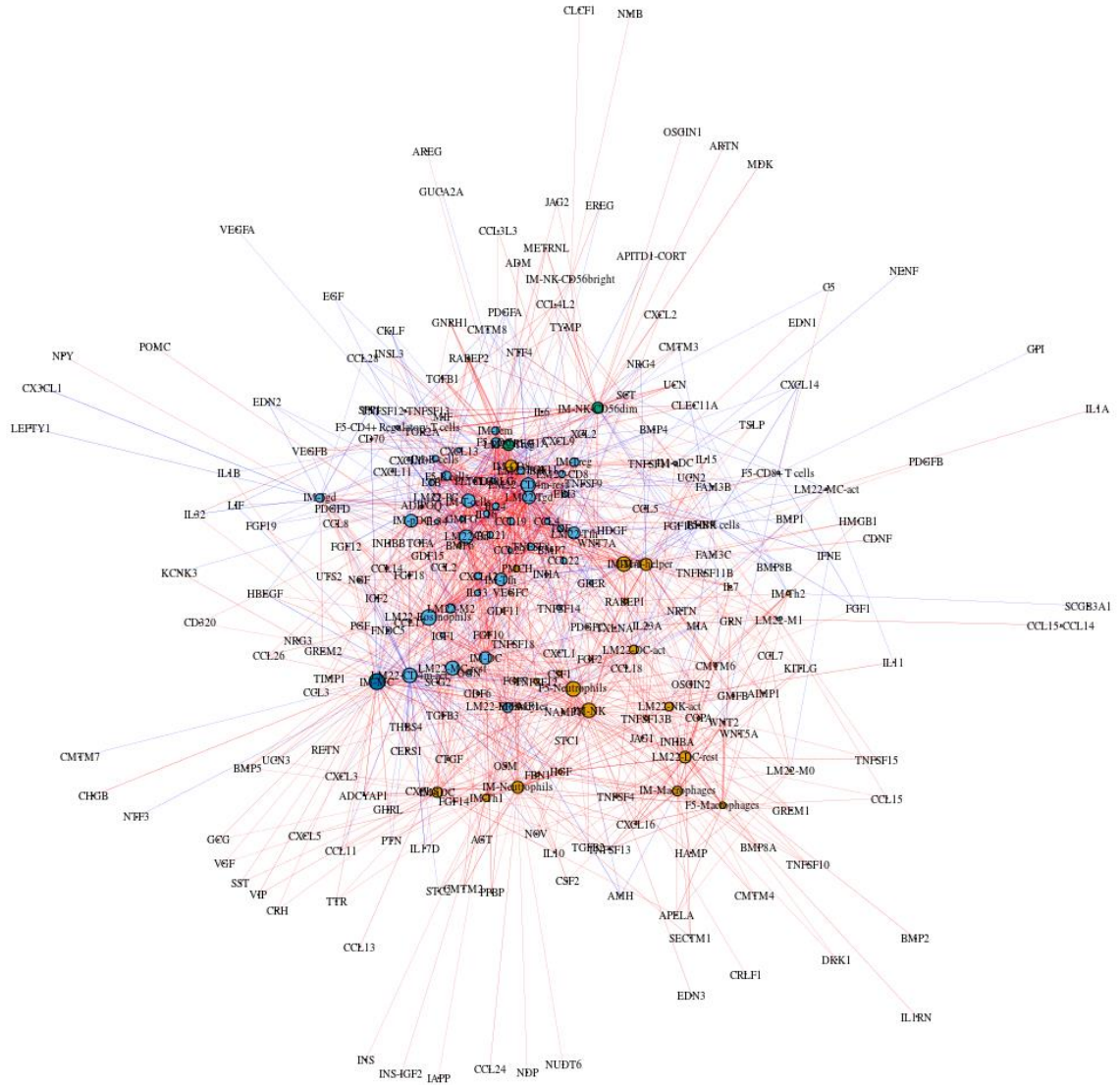


Figure 47. Cytokine network in cytolytic hot PDAs.

Immune GSVA score-cytokine correlation network in the 30 cytolytically hot PDA samples depicting only significant Spearman's $\rho \geq 0.4$ as edges (FDR-adjusted empirical p-value ≤ 0.05). Positive and negative correlations are represented by red and blue edges respectively. Edge thickness is proportional to ρ . The size of each node is proportional its degree centrality. Each node is colored by the community it belonged to in Figure 43. Fast-greedy algorithm detected 5 communities within this network (shown in Figures 48-51).

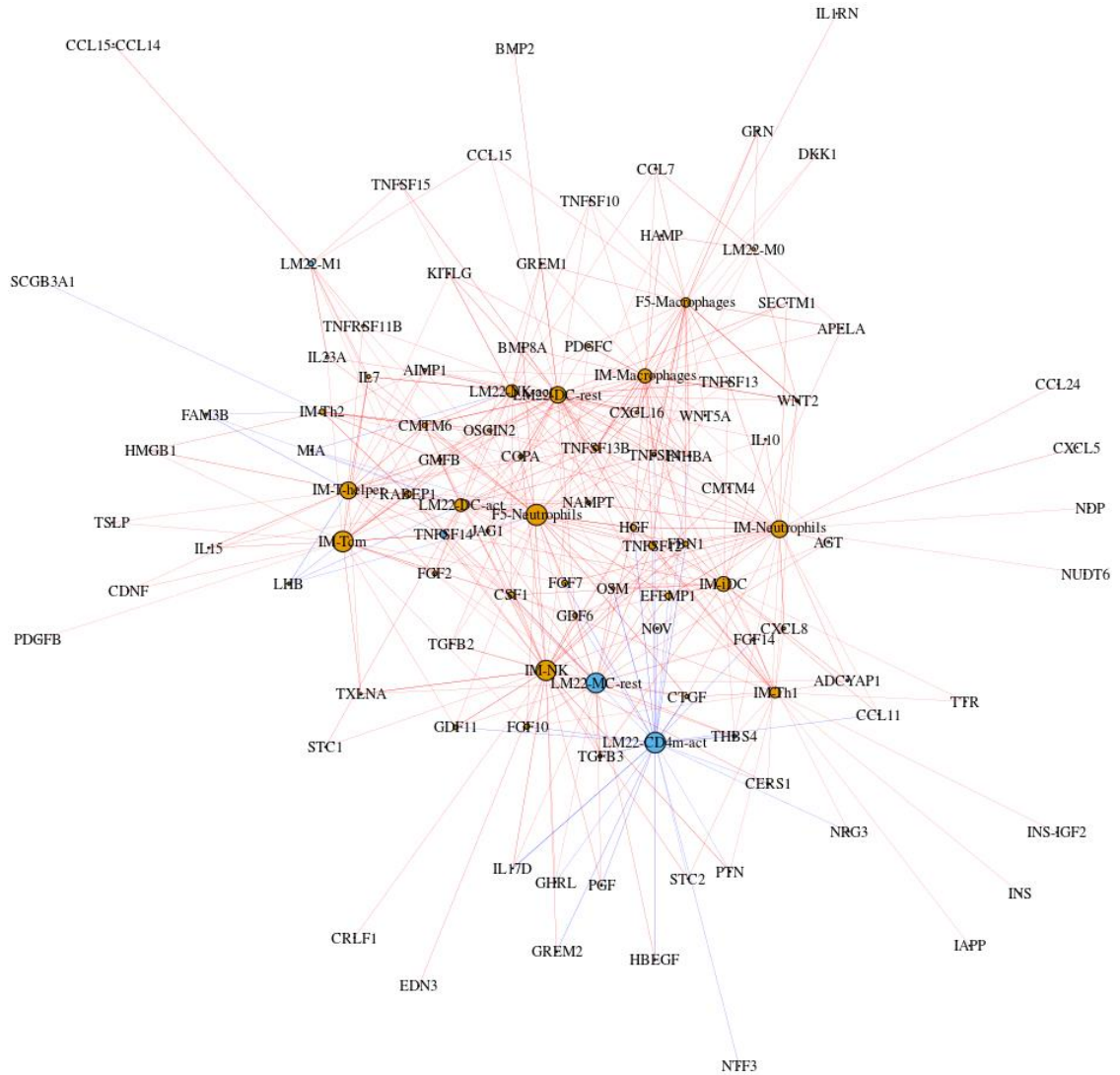


Figure 48. Community 1 in the cytolytically hot cytokine network.

Community 1 in the cytolytically hot network (most complex community) in Figure 47 as detected by the fast-greedy algorithm. Each node is colored by the community in the overall network that it belonged to in Figure 43.

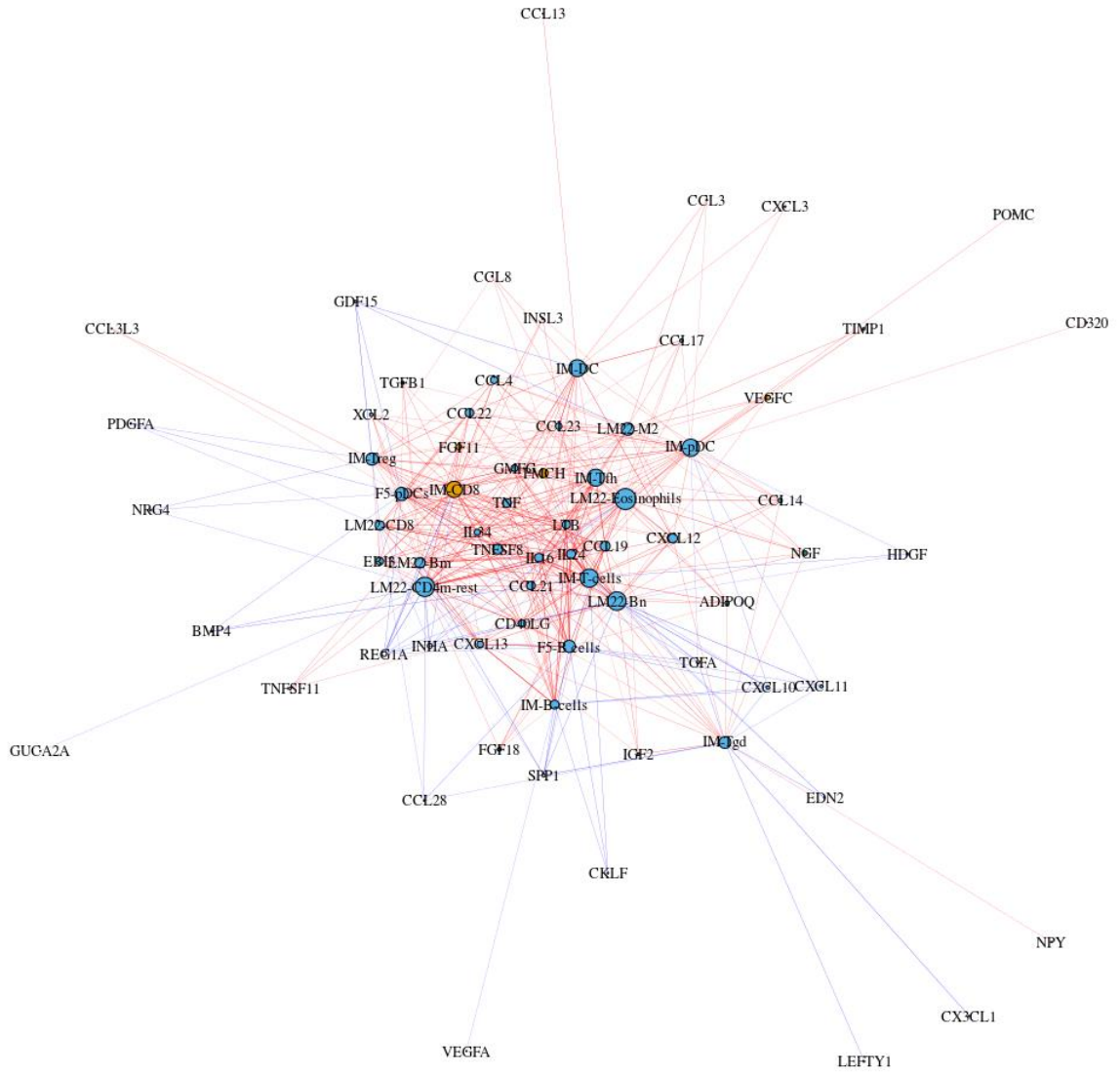


Figure 49. Community 2 in the cytolytically hot cytokine network.

Community 2 in the cytolytically hot network (2nd most complex community) in Figure 47 as detected by the fast-greedy algorithm. Each node is colored by the community in the overall network that it belonged to in Figure 43.

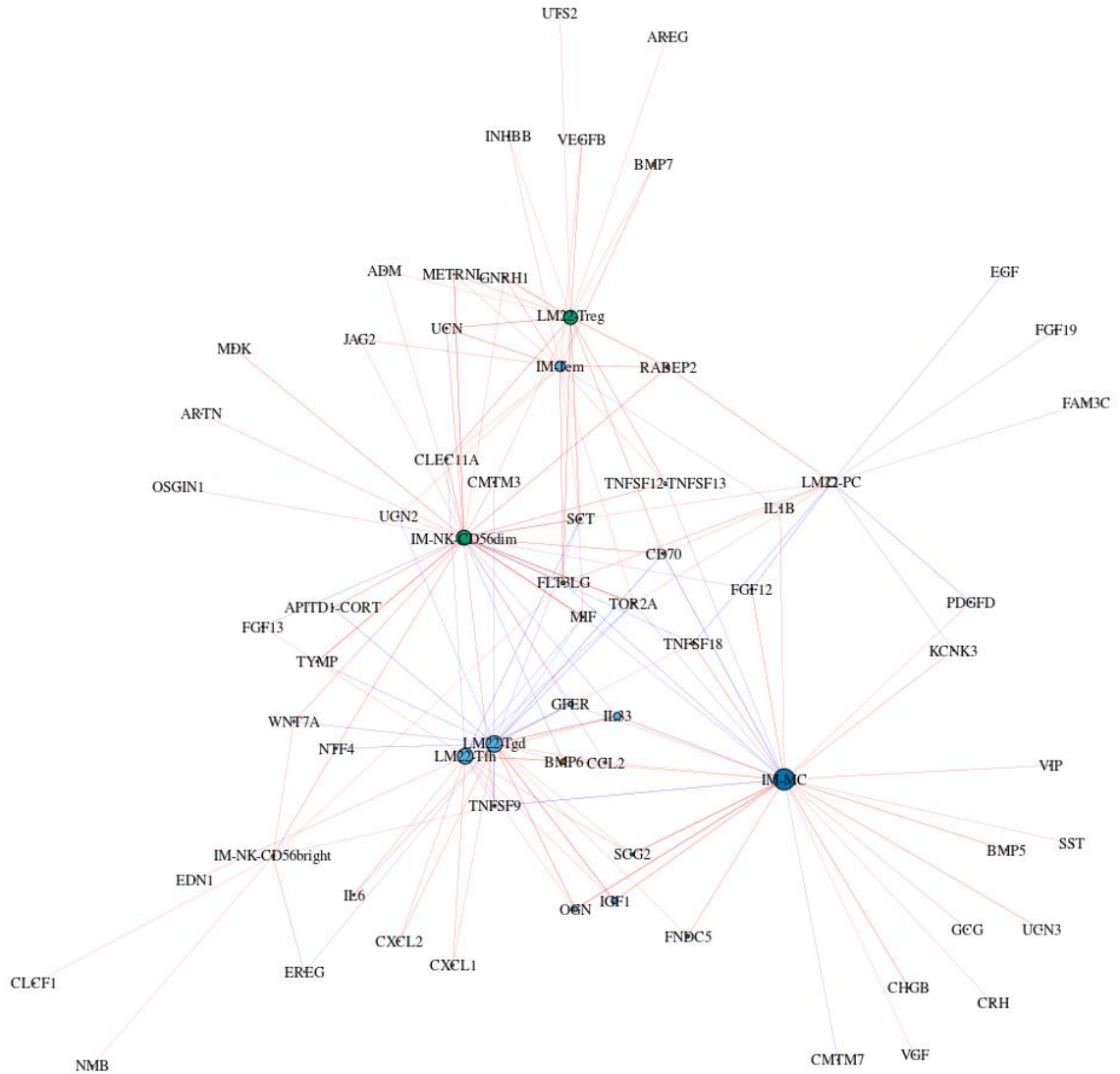


Figure 50. Community 3 in the cytolytically hot cytokine network.

Community 3 in the cytolytically hot network (3rd most complex community) in Figure 47 as detected by the fast-greedy algorithm. Each node is colored by the community in the overall network that it belonged to in Figure 43.

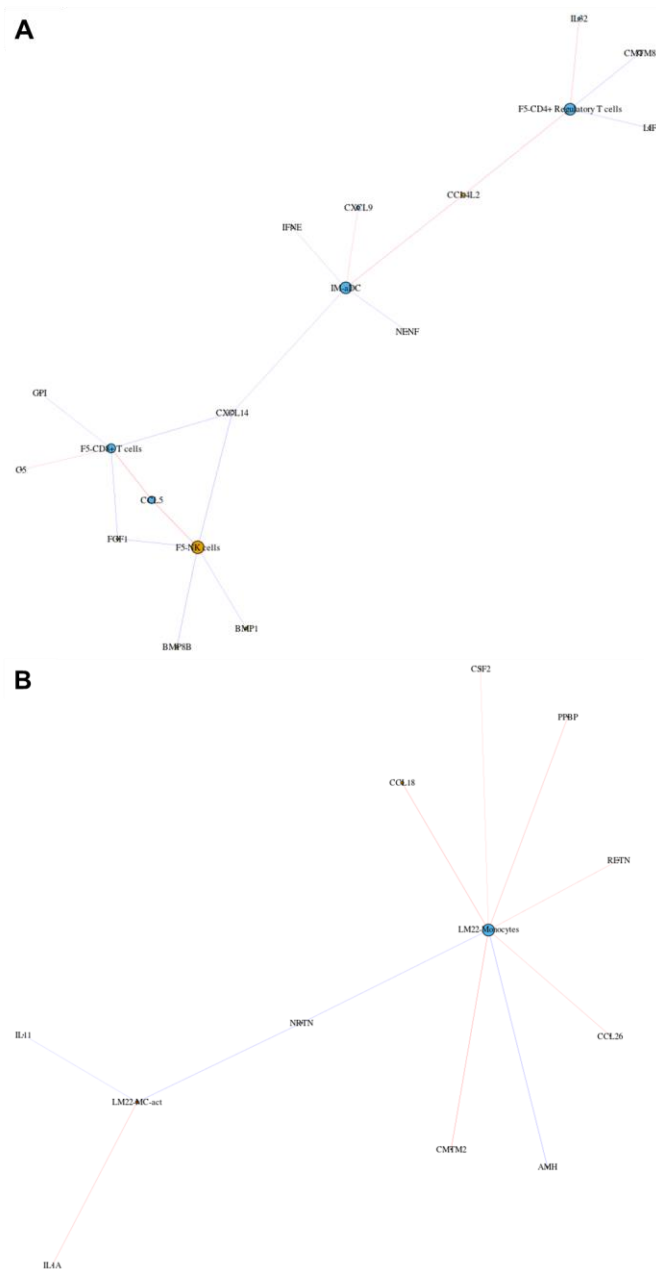


Figure 51. Communities 4 and 5 in the cytolytically hot cytokine network.

Communities 4 and 5 (A and B, respectively) in the cytolytically hot network in Figure 47 as detected by the fast-greedy algorithm. Each node is colored by the community in the overall network that it belonged to in Figure 43.

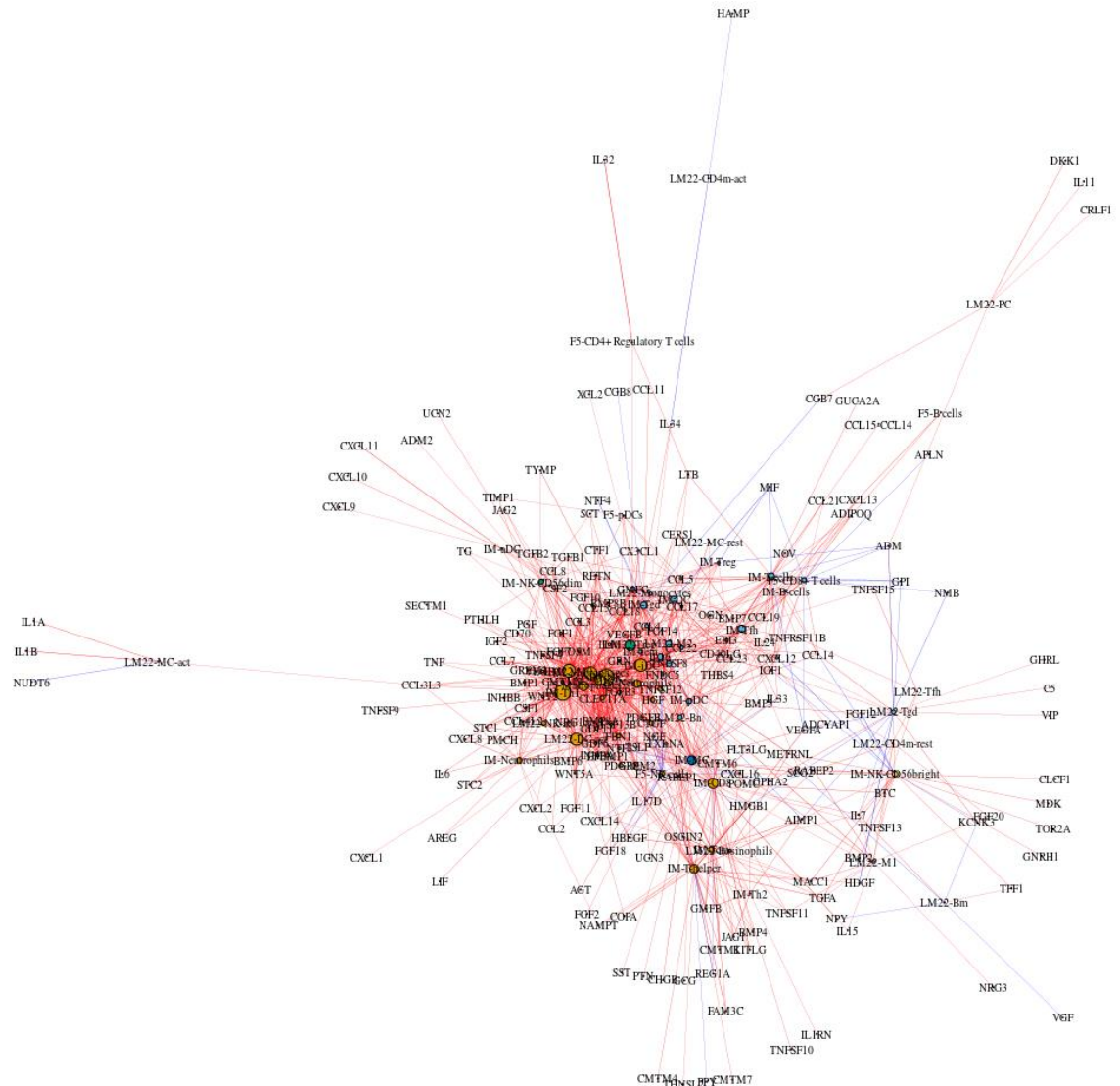


Figure 52. Cytokine network in cytolytic cold PDAs.

Immune GSVA score-cytokine correlation network in the 71 cytolytically cold PDA samples depicting only significant Spearman's rho ≥ 0.4 as edges (FDR-adjusted empirical p-value ≤ 0.05). Positive and negative correlations are represented by red and blue edges respectively. Edge thickness is proportional to rho. The size of each node is proportional its degree centrality. Each node is colored by the community it belonged to in Figure 43. Eight immune-cytokine non-overlapping communities in the cold immune-cytokine network as detected by the fast-greedy algorithm (shown in Figures 53-57).

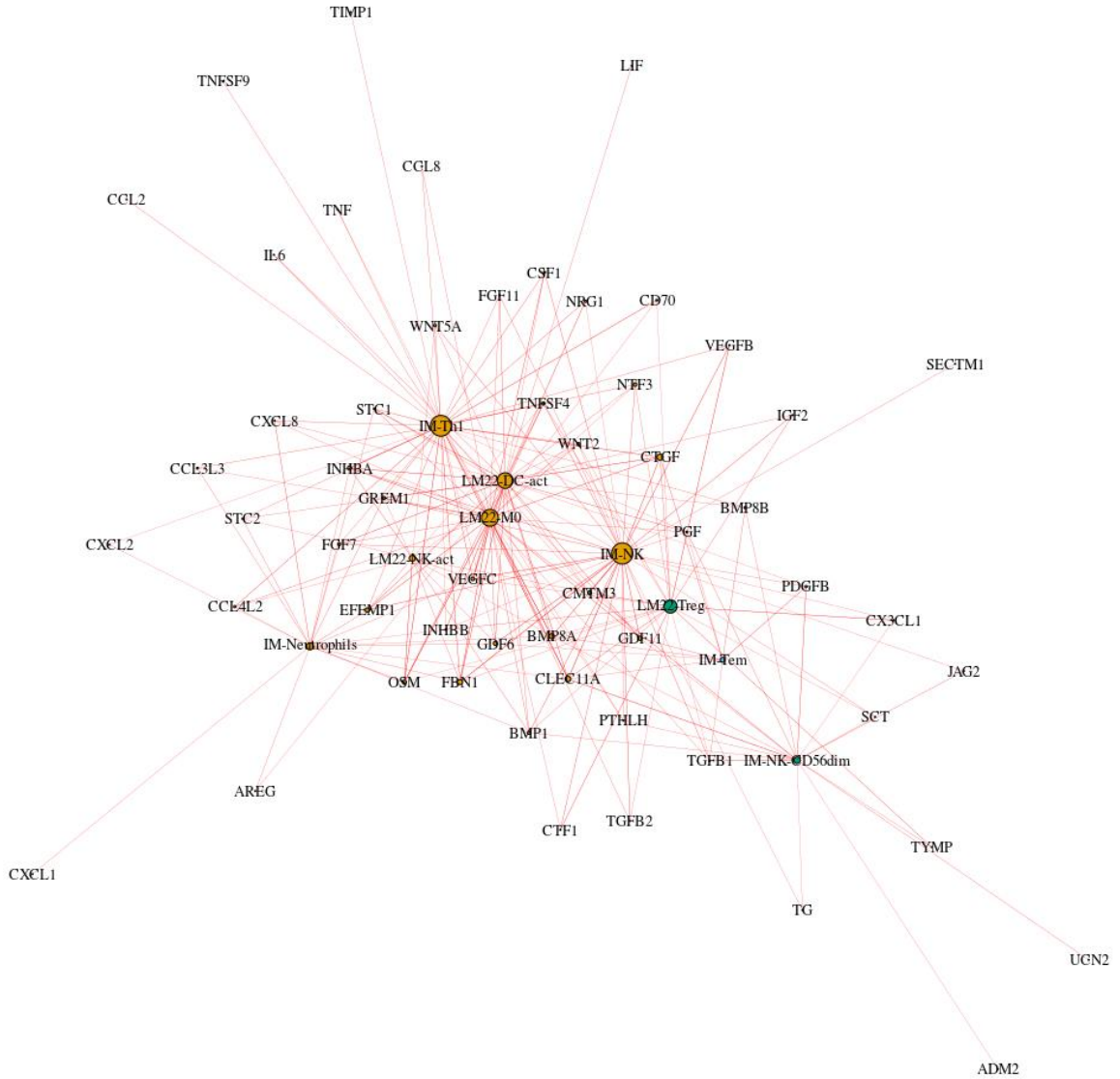


Figure 53. Community 1 in the cytolytically cold cytokine network.

Community 1 in the cytolytically cold network (most complex community) in Figure 52 as detected by the fast-greedy algorithm. Each node is colored by the community in the overall network that it belonged to in Figure 43.

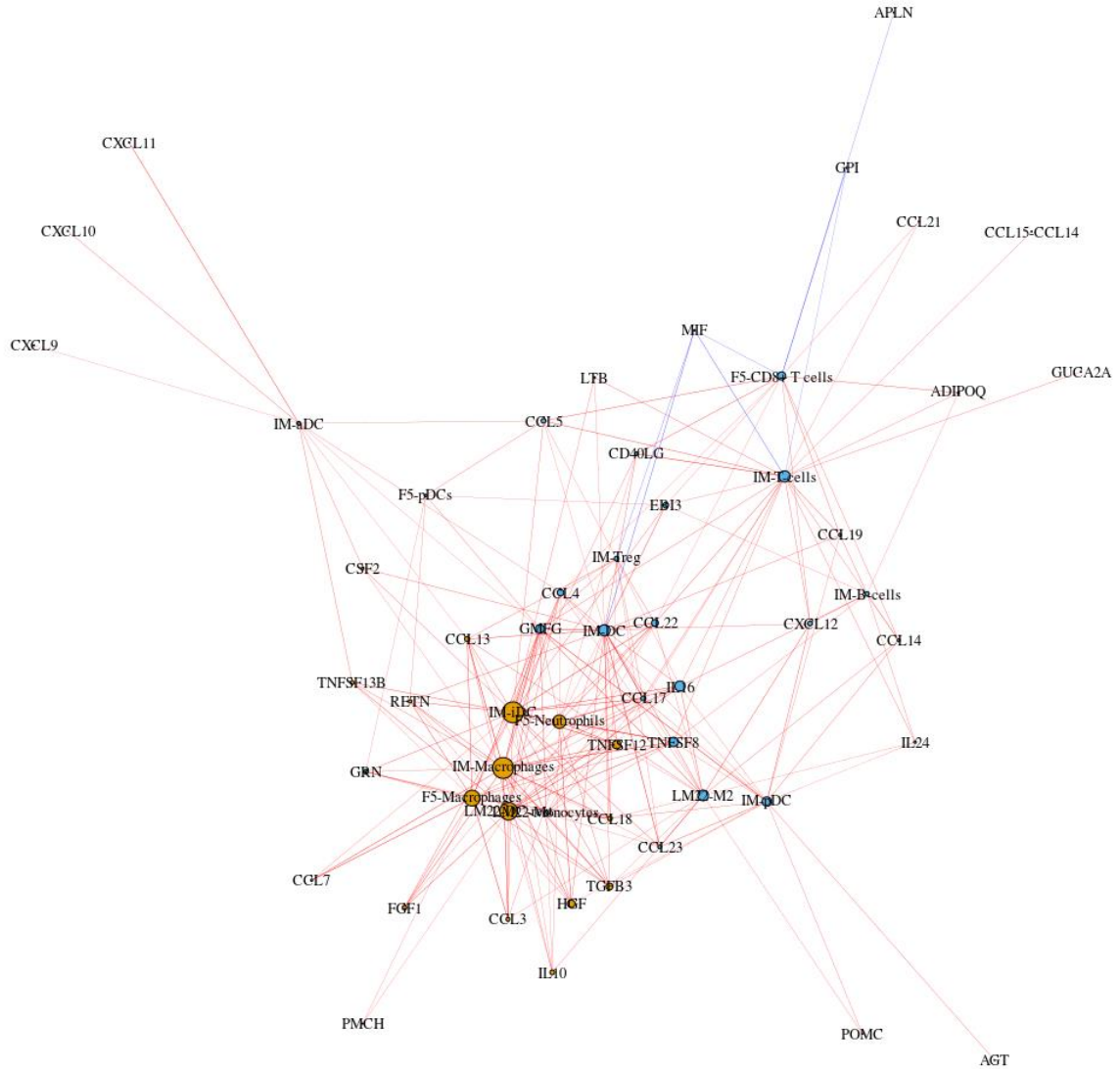


Figure 54. Community 2 in the cytolytically cold cytokine network.

Community 2 in the cytolytically cold network (2nd most complex community) in Figure 52 as detected by the fast-greedy algorithm. Each node is colored by the community in the overall network that it belonged to in Figure 43.

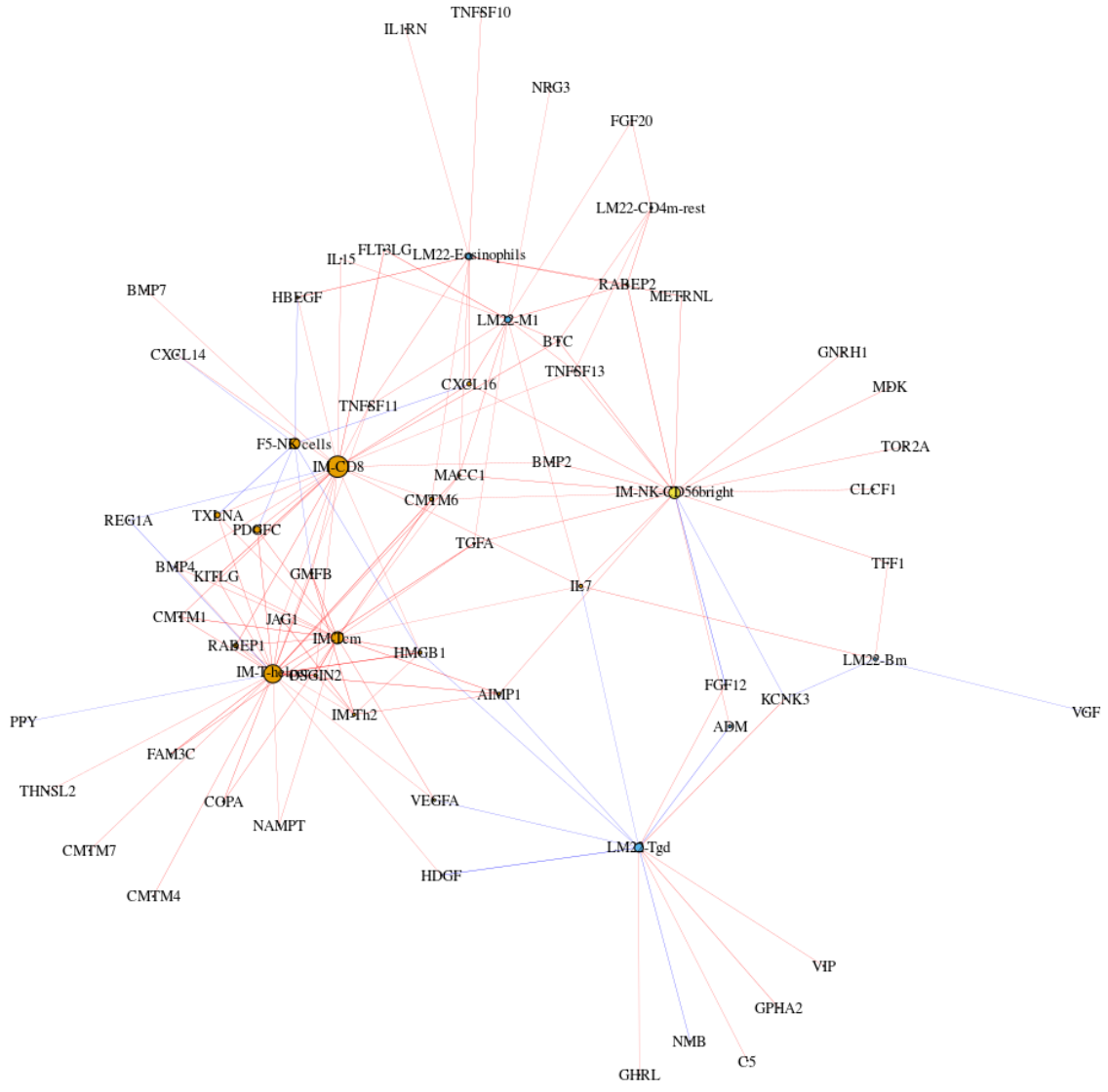


Figure 55. Community 3 in the cytotokically cold cytokine network.

Community 3 in the cytotokically cold network (3rd most complex community) in Figure 52 as detected by the fast-greedy algorithm. Each node is colored by the community in the overall network that it belonged to in Figure 43.

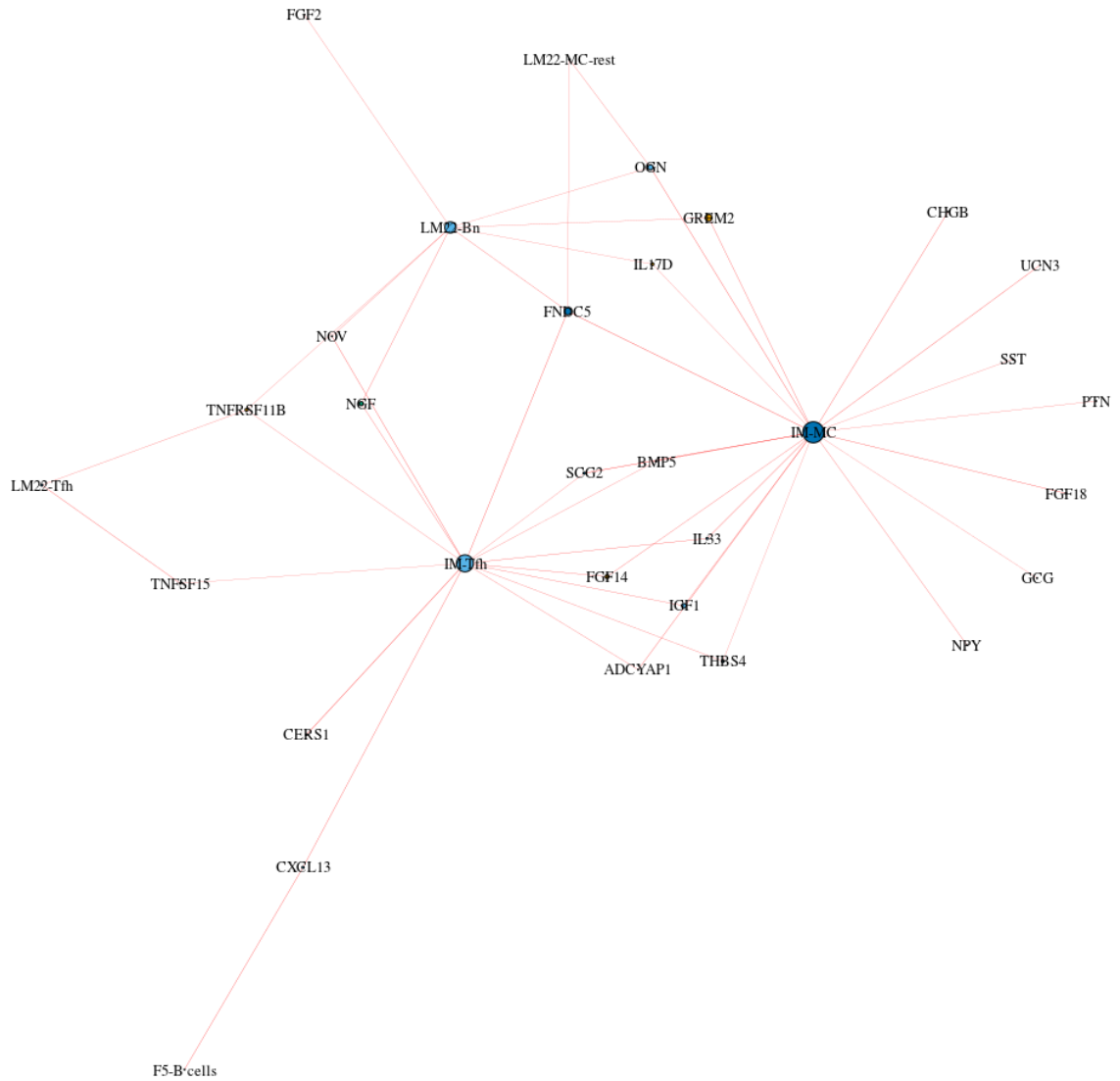


Figure 56. Community 4 in the cytolytically cold cytokine network.

Community 4 in the cytolytically cold network (4th most complex community) in Figure 52 as detected by the fast-greedy algorithm. Each node is colored by the community in the overall network that it belonged to in Figure 43.

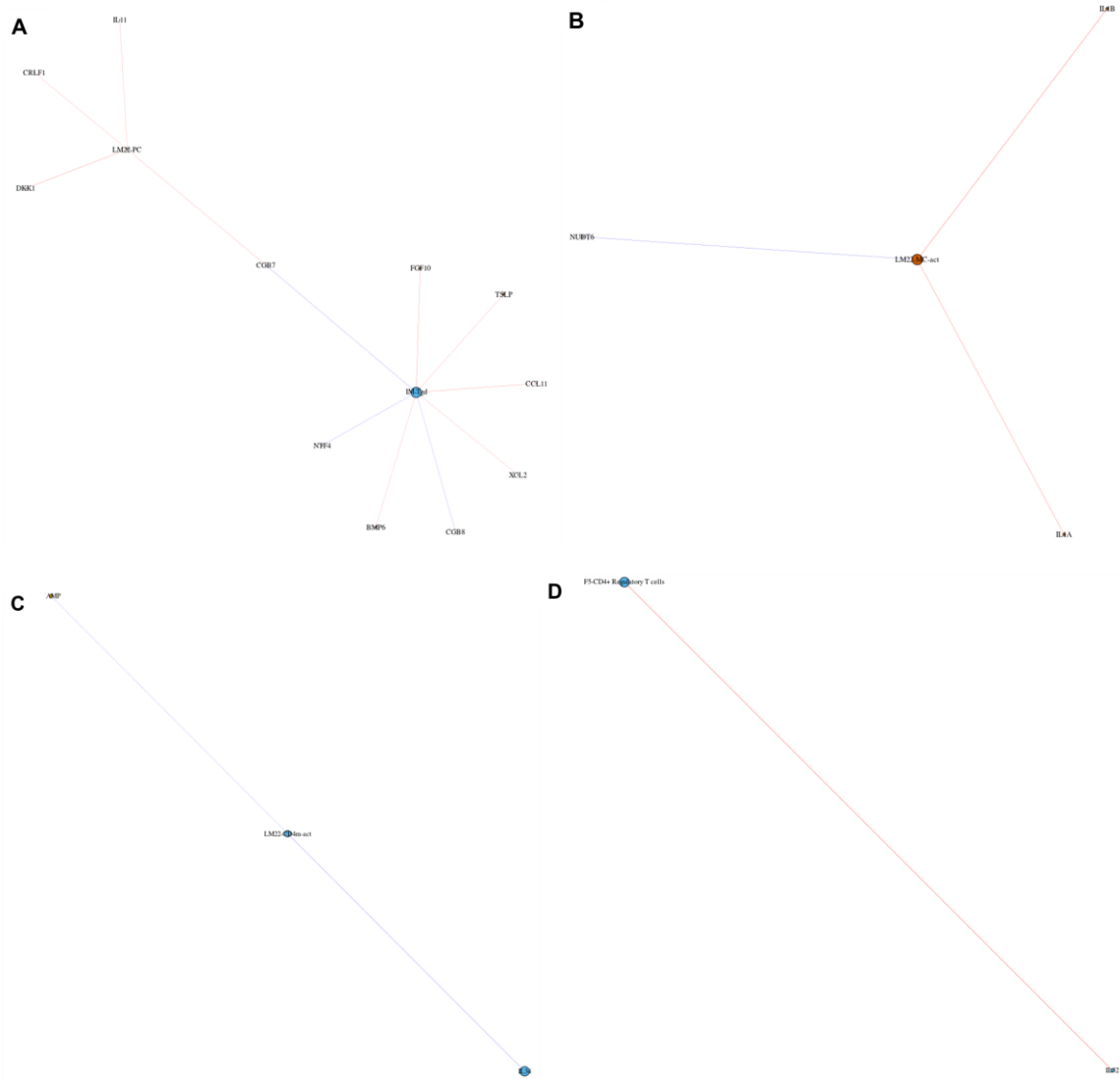


Figure 57. Communities 5-8 in the cytolytically cold cytokine network.

Communities 5-8 (A-D, respectively) in the cytolytically hot network in Figure 52 as detected by the fast-greedy algorithm. Each node is colored by the community in the overall network that it belonged to in Figure 43.

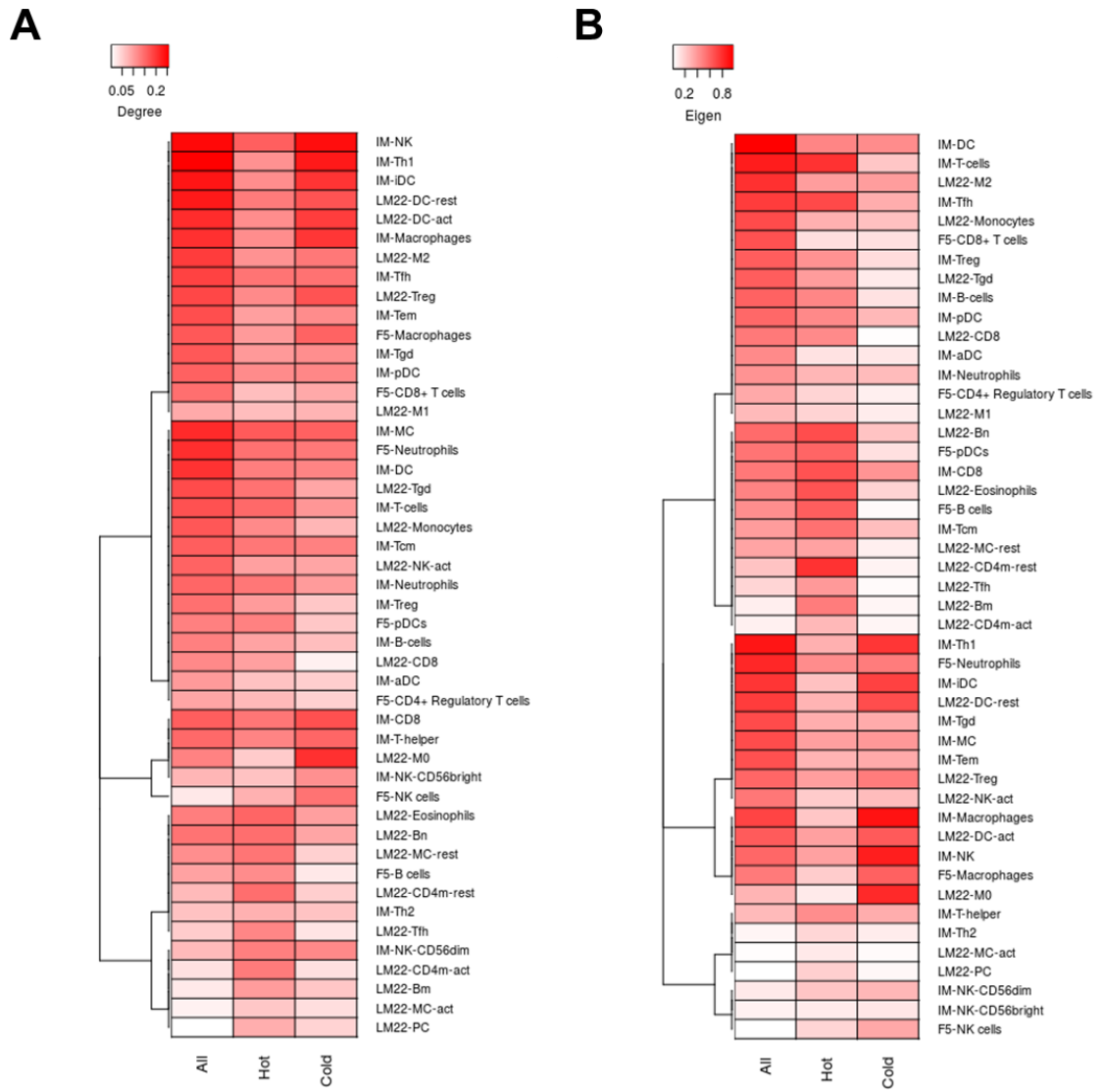


Figure 58. Centrality of immune populations in hot and cold immune-cytokine networks.

Heatmap of the normalized degree centrality **(A)** and eigencentality **(B)** of immune populations in the immune-cytokine networks constructed using all, hot, or cold PDA samples.

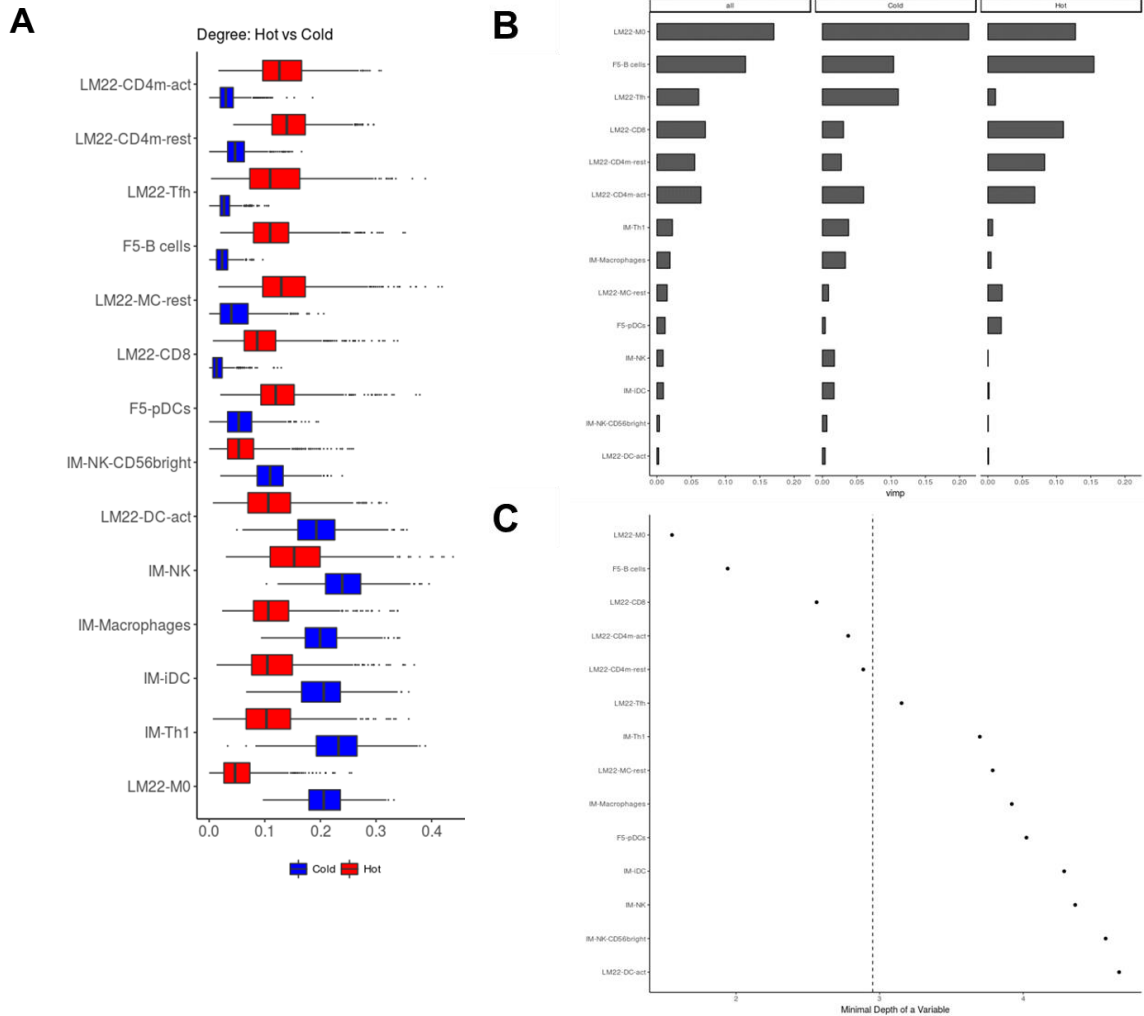


Figure 59. Immune populations with significantly altered degree centralities.

(A) Boxplot of the immune populations with significant differences in their degree centrality in hot and cold tumors (empirical p-value ≤ 0.05). Graph shows the distribution of degree centrality in 1000 bootstrapped sample populations grouped by hot or cold tumors. **(B)** Barplot of the variable importance (vimp) scores in hot, cold, and all samples using the degree centralities of only the top immune populations in a random forest model (ntree = 1000) to classify the cytolytic status of each tumor. **(C)** Plot of the minimal depth of the top immune populations in a random forest model using the degree centralities (ntree = 1000) to classify the cytolytic status of each tumor. The dotted line shows the “high” conservative cutoff for a variable to be considered more significantly important than others in the model.

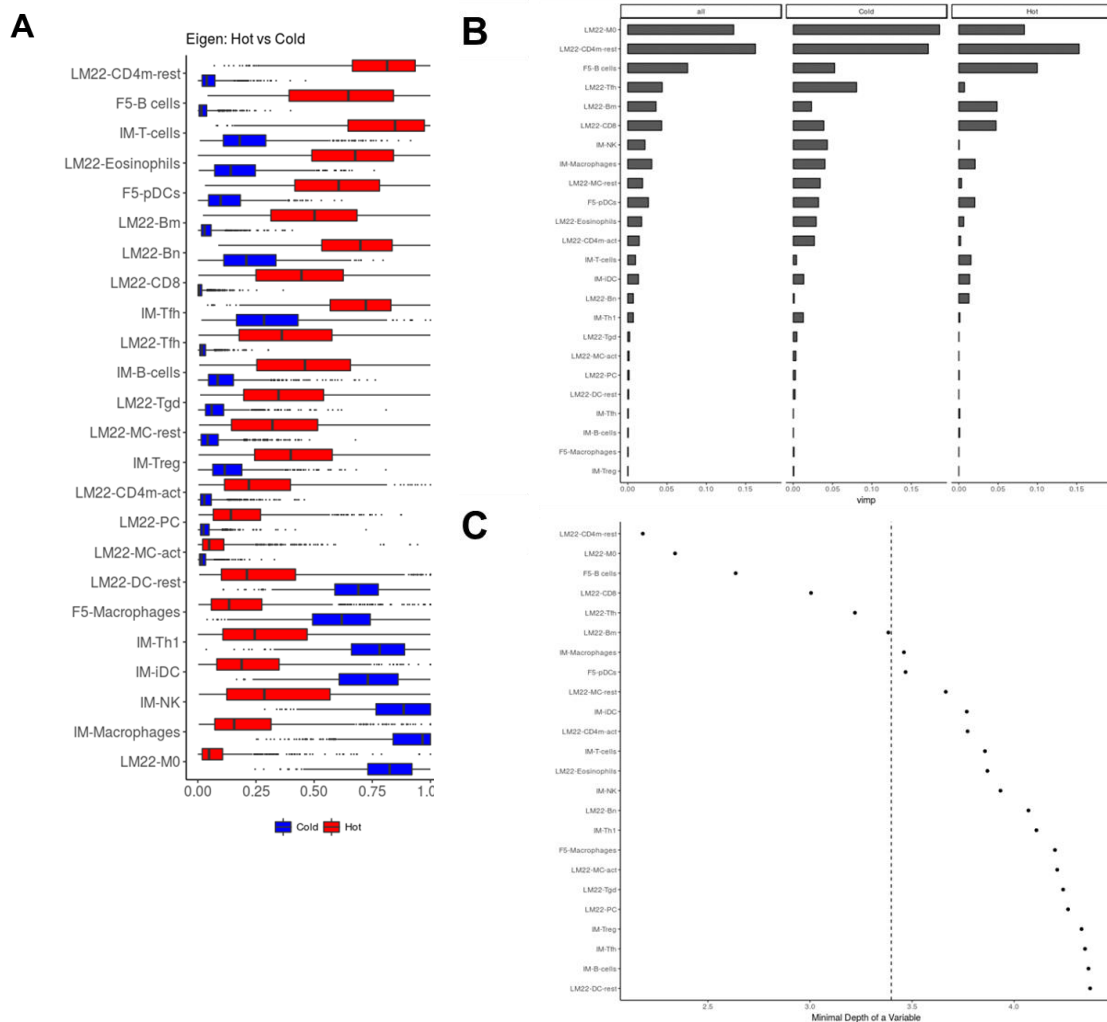


Figure 60. Immune populations with significantly altered eigenvector centralities.

(A) Boxplot of the immune populations with significant differences in their eigencentrality in hot and cold tumors (empirical p-value ≤ 0.05). Graph shows the distribution of eigencentrality in 1000 bootstrapped sample populations grouped by hot or cold tumors. **(B)** Barplot of the variable importance (vimp) scores in hot, cold, and all samples using the eigencentrality of only the top immune populations in a random forest model (ntree = 1000) to classify the cytolytic status of each tumor. **(C)** Plot of the minimal depth of the top immune populations in a random forest model using eigenvector centrality (ntree = 1000) to classify the cytolytic status of each tumor. The dotted line shows the conservative cutoff for a variable to be considered significantly more important than the others in the model.

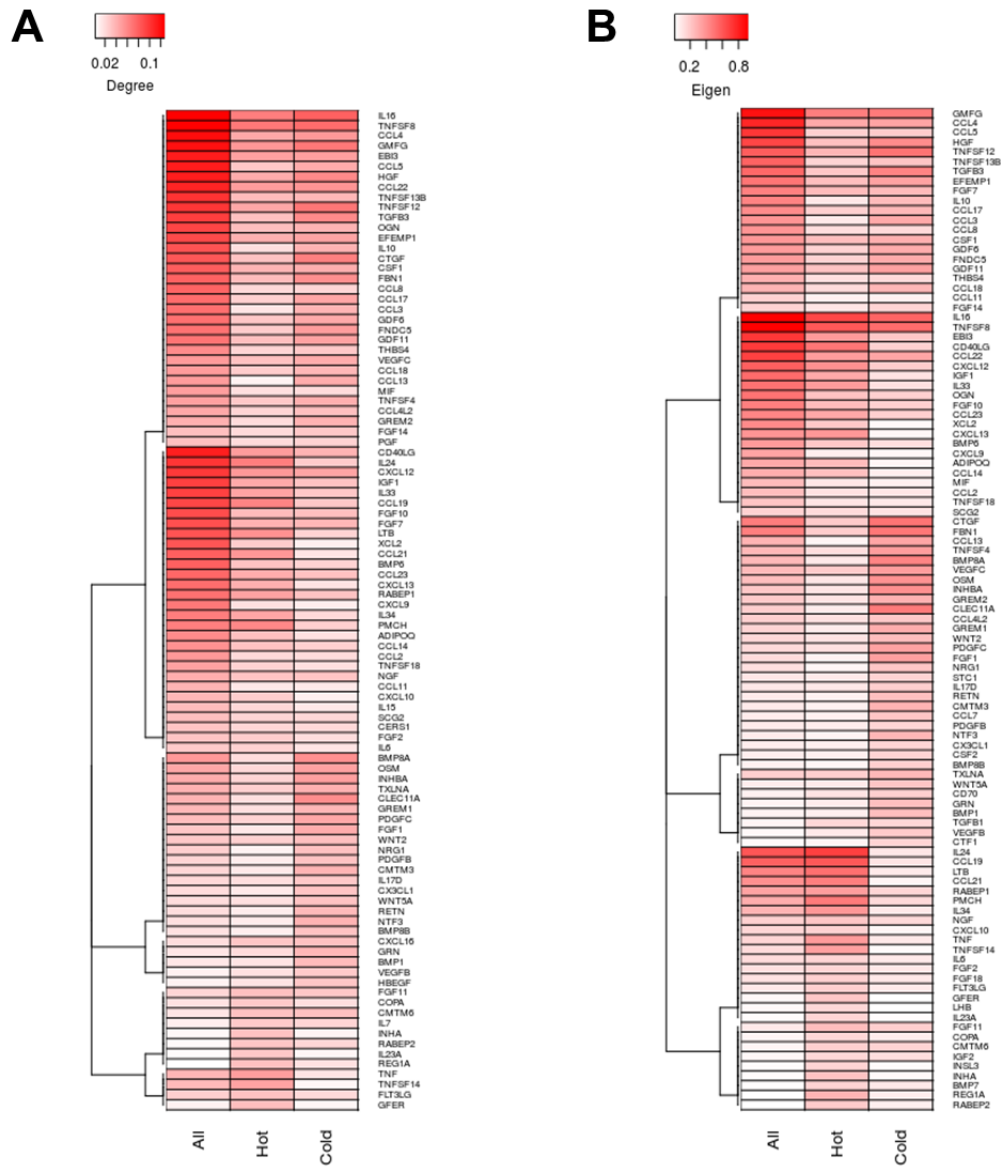


Figure 61. Centrality of cytokines in hot and cold immune-cytokine networks.

Heatmap of the normalized degree centrality **(A)** and eigencentality **(B)** of cytokines in the immune-cytokine networks constructed using all, hot, or cold PDA tumors. Cytokines are only included if their centrality value is in the top quartile in at least one of the sample populations.

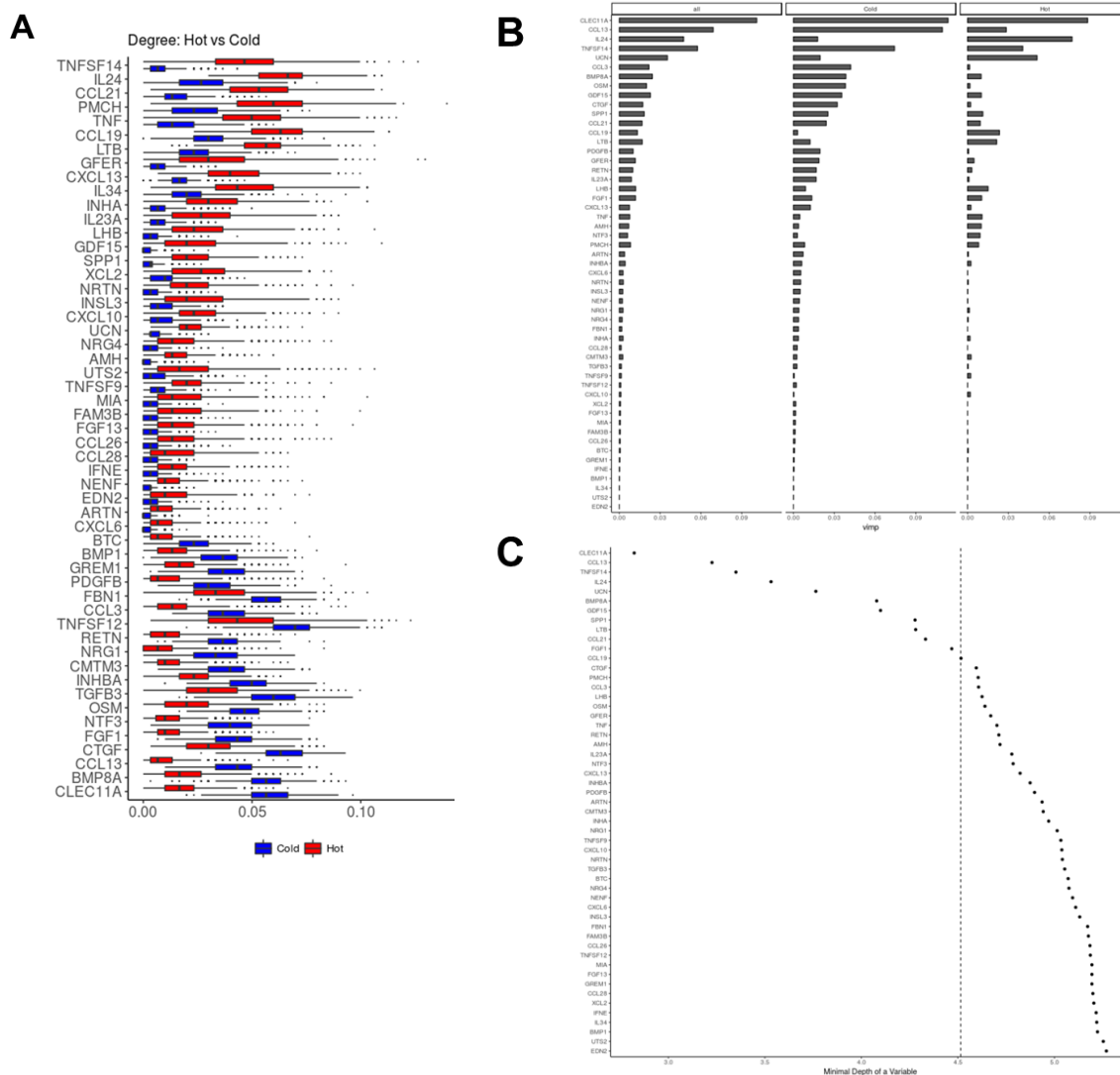


Figure 62. Cytokines with significantly altered degree centrality in hot and cold tumors.

(A) Boxplot of the cytokines with significant differences in their degree centrality in hot and cold tumors (empirical p -value ≤ 0.05). Graph shows the distribution of degree centrality in 1000 bootstrapped sample populations grouped by hot or cold tumors. **(B)** Barplot of the variable importance (vimp) scores in hot, cold, and all samples using the degree centralities of only the top cytokines in a random forest model (ntree = 1000) to classify the cytolytic status of each tumor. **(C)** Plot of the minimal depth of the top cytokines in a random forest model using the degree centralities (ntree = 1000) to classify the cytolytic status of each tumor. The dotted line shows the conservative cutoff for a variable to be considered significantly more important than the others.

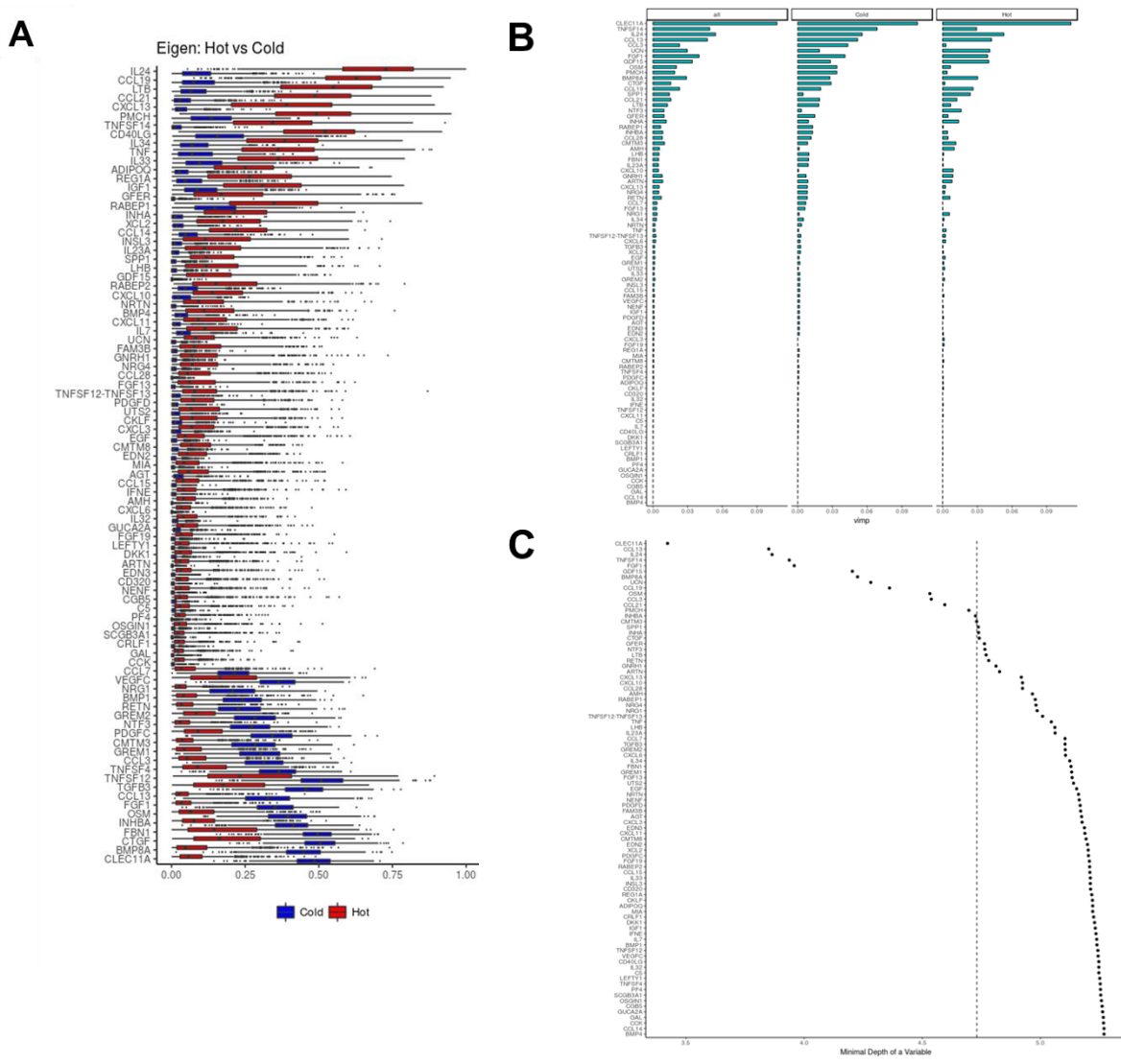


Figure 63. Cytokines with altered eigencentality in hot and cold tumors.

(A) Boxplot of the cytokines with significant differences in their eigencentality in hot and cold tumors (empirical p-value ≤ 0.05). Graph shows the distribution of eigencentality in 1000 bootstrapped sample populations grouped by hot or cold tumors. **(B)** Barplot of the variable importance (vimp) scores in hot, cold, and all samples using the eigencentality of only the top cytokines in a random forest model (ntree = 1000) to classify the cytolytic status of each tumor. **(C)** Plot of the minimal depth of the top cytokines in a random forest model using eigencentality (ntree = 1000) to classify the cytolytic status of each tumor. The dotted line shows the conservative cutoff for a variable to be considered significantly more important than the others.

CHAPTER 5: DISCUSSION AND FUTURE DIRECTIONS

The immune response is critical in regulating tumor development, progression, and response to therapy (Chen and Mellman, 2013). This response is determined in a large part by a complex network of immune and cytokine interactions in the tumor microenvironment. Understanding these “cytokine networks” is crucial for the development of effective strategies to promote anti-tumor immune responses, particularly in tumors naturally void of adaptive immunity such as pancreatic cancer. The findings of this thesis project highlight components of the cytokine network that may be important in regulating anti-tumor immunity in PDA. In Chapter 3, we used gene expression data from human PDA to infer the existence of the CXCR2 ligand-CXCR2-neutrophil network and demonstrated that inhibiting this axis leads to anti-tumor T cell activity in the KPC model (Figure 33). Expression of CXCR2 ligands, particularly CXCL5, by cancer cells themselves show that they are active contributors to the cytokine network and can therefore modulate the immune response. This work adds to the mounting evidence showing that inhibition of the CXCR2 ligand-CXCR2-neutrophil network can unveil anti-tumor T cell immunity. However, inhibition of this axis only resulted in a modest increase in effector T cell infiltration and survival. Therefore, other components are likely to also play substantial roles.

In Chapter 4, we devised a novel analysis pipeline to infer and discover other potentially important cytokine networks using gene expression data from human PDA samples. Our analysis confirmed many already known cytokine networks in PDA, including the CXCL5/CXCL8-neutrophil network. Furthermore, we showed that it is possible to infer the recruitment, activation, or functional status of immune populations using the relative strength of their correlations with specific cytokines. Finally, we demonstrated the utility of network-based approach to complement traditional differential expression analysis to discover biologically relevant targets. Our results showed that cytokine networks involving CD8⁺ T cells, NK cells, memory CD4 T cells, T follicular helper cells, and memory B cells are particularly important in tumors with high cytolytic activity. In contrast, macrophages are the most important in tumors with low cytolytic activity. Our analysis

further highlights the cytokines most likely to be involved in these networks, some of which are already under active clinical investigation for their therapeutic potential. By using expression data to characterize the cytokine networks underlying cytolytic activity in PDA, we aim to use a data-driven approach to accelerate the process of candidate discovery and validation.

The CXCR2-CXCR2 ligand axis in cancer

CXCR2 is a G-protein-coupled receptor (GPCR) that binds to human CXCL1, CXCL2, CXCL3, CXCL5, CXCL6, CXCL7, and CXCL8 (Zlotnik and Yoshie, 2012). In addition, CXCR2 can also bind to two non-traditional ligands: N-acetyl Pro-Gly-Pro (acPGP), which is a neutrophil protease-mediated degradation product of extracellular matrix, and macrophage migration inhibitory factor (MIF). In neutrophils, ligand binding to CXCR2 triggers its coupling to a G-protein of the Gi family (Stadtman and Zarbock, 2012). Coupling of CXCR2 triggers the G α i subunit to exchange a guanosine diphosphate (GDP) for a guanosine triphosphate (GTP). GTP binding induces a conformational change that ultimately results in the dissociation of the G α i and G β γ subunits. The dissociated G β γ subunit can directly activate phosphatidylinositol 3-kinase γ (PI3K- γ), an isoform of PI3K that is preferentially found in immune cells (Hirsch et al., 2000; Xu et al., 2015). Activated PI3K- γ catalyzes the formation of phosphatidylinositol 3,4,5-trisphosphate (PIP3), which leads to protein kinase B (PKB/AKT) and mechanistic target of rapamycin complex (mTOR) phosphorylation. In neutrophils, activated mTOR phosphorylates PKC β II, which in turn activates type 9 adenylyl cyclase (AC9) and the accumulation of cyclic adenosine monophosphate (cAMP) (Liu et al., 2014). G β γ can also activate the phospholipase C (PLC) and mitogen-activated protein kinase (MAPK) pathways (Nasser et al., 2007). All these signaling cascades cumulate in actin polarization and the formation of leading edges in neutrophils. In contrast, relatively little is known about the function of the G α i-GTP subunit. Recently, Surve et al. demonstrated that G α i-GTP inhibition of AC9 is required to counteract excessive adhesion to maintain neutrophil polarity and motility (Surve et al., 2016). Therefore, CXCR2 is an important receptor for the regulation of neutrophil chemotaxis.

CXCR2 signaling is crucial for normal neutrophil egression, extravasation, and migration into inflamed tissues (Sadik et al., 2011). Our work in Chapter 3 and others have now demonstrated that CXCR2 is also required for trafficking of granulocytic myeloid cells into the tumor microenvironment (Jamieson et al., 2012; Highfill et al., 2014; Chao et al., 2016; Steele et al., 2016). Expansion of systemic granulocytes in tumor-bearing CXCR2^{-/-} mice suggests that CXCR2 signaling is specifically required for neutrophil extravasation and infiltration into the tumor microenvironment, but not for their differentiation and proliferation. Consistent with recent reports, we showed that CXCR2 inhibition did not significantly affect the accumulation of other immune populations, including monocytes (Highfill et al., 2014; Steele et al., 2016). The absolute requirement of CXCR2 specifically for the trafficking of neutrophils is important because CXCR2 have occasionally been found on endothelial cells, monocytes, mast cells, and some NK cells (Griffith et al., 2014). For instance, CXCR2 inhibition has been shown to impede angiogenesis and delay growth of breast cancer cells in immune-compromised mice (Sparmann and Bar-Sagi, 2004). However, CXCR2 is not absolutely necessary for angiogenesis because other, more potent angiogenic factors, such as VEGFA, are often found in the tumor microenvironment. On the other hand, the CCL2-CCR2 axis has been shown to be important for monocyte trafficking to the tumor microenvironment, without affecting granulocyte accumulation (Chang et al., 2016). Together, these results support a model where monocytic and granulocytic myeloid cells have committed to their lineage prior to trafficking to the tumor. In contrast, Youn et al. have shown that monocytes isolated from the spleen or bone marrow of tumor-bearing mice or humans are capable of acquiring granulocytic phenotypes via epigenetic silencing of the retinoblastoma (Rb) gene when cultured *in vitro* in the presence of GM-CSF alone (Youn et al., 2013). Whether this phenomenon also occurs within the tumor microenvironment *in vivo* remains unclear. Regardless, potential differentiation of monocytic cells failed to appreciably reconstitute the tumor-infiltrating granulocyte population in our study. Therefore, our work adds to the mounting evidence that tumor-associated neutrophils (TANs) consisted of mostly granulocyte lineage-committed cells that then trafficked into the tumor microenvironment in a CXCR2-dependent manner.

Although not observed in our cell lines, CXCR2 can sometimes be found on the surface of tumor cells themselves (Hussain et al., 2010; Jamieson et al., 2012; Pinnacle et al., 2013; Lesina et al., 2016). The precise intracellular signaling cascades triggered by CXCR2 activation remain to be explored in tumor cells. Despite incomplete knowledge of the signaling pathways involved, the general function of CXCR2 has nonetheless been demonstrated in tumor cells. Forced oncogene expression can up-regulate surface CXCR2 in normal fibroblasts, where it mediates oncogene-induced senescence (OIS) in a p53-dependent manner (Acosta et al., 2008; Guo et al., 2013). Expression of CXCR2 in these cells was further shown to be dependent on the activation of the transcription factors NF- κ B and C/EBP β . A role for CXCR2 in mediating OIS has recently been demonstrated *in vivo* in the LSL-Kras^{G12D}; Ptf1a-Cre (KC) mouse model of pancreatic cancer (Lesina et al., 2016). Here, constitutive activation of NF- κ B/RelA in KRAS^{G12D} expressing pancreatic cells drives the expression of CXCL1, which activates CXCR2 in an autocrine manner and induces senescence. Pancreas specific inhibition of either RelA or CXCR2 is sufficient to completely eliminate OIS and accelerate carcinogenesis. In contrast, pancreas-specific inhibition of RelA in the absence of either p53 or p16 actually slowed tumor growth and prolonged survival. In an independent study, CXCR2 expression in fully transformed human pancreatic cancer cells also associated with increased proliferation and invasive potential (Hussain et al., 2010; Maeda et al., 2017). Therefore, CXCR2 expression in transformed cells plays contrasting roles at different stages of disease. Early in carcinogenesis, CXCR2 activation can drive p53-dependent OIS and delay disease progression. However, after cells have evolved to bypass p53-dependent senescence, CXCR2 activation in tumor cells now serves to promote their growth and invasiveness.

CXCR2 ligands, especially CXCL8, are almost universally elevated in cancer patients (MD and Lippitz, 2013). Although they are generally considered to be redundant, recent evidence suggests that CXCR2 ligands can have different functions depending on the context. For instance, infection-induced pathological elevation of serum CXCL5 competitively displaces CXCL1 and CXCL2 from the erythrocyte Duffy antigen receptor for chemokines (DARC), which

acts as a natural chemokine sink (Mei et al., 2010). The resulting systemic elevation of CXCL1 and CXCL2 destroys the sensitivity of neutrophils toward chemokine gradients at the site of infection, which ultimately serves to prolong the infection. This raises the intriguing possibility that CXCR2 ligands can have different functions and even regulate each other. The source of CXCR2 ligands in the tumor microenvironment is largely attributed to cancer cells themselves. Our results show that CXCL5 is the most highly expressed CXCR2 ligand in PDA, which is followed closely by CXCL8 in humans and CXCL1 in mice. CXCR2 ligand expression, especially CXCL1 and CXCL8, is part of the senescence-associated secretory phenotype (SASP) induced by oncogene expression (Chien et al., 2011). Furthermore, our work and others have demonstrated that activation of the classical NF- κ B pathway can prominently increase CXCR2 ligand expression in tumor cells (Acharyya et al., 2012; Chao et al., 2016; Lesina et al., 2016). Constitutive NF- κ B signaling is often presumed to be the cause of elevated baseline CXCR2 ligand expression in tumor cells. However, simultaneous pharmacological inhibition of both classical and alternative NF- κ B pathways failed to suppress baseline CXCR2 ligand expression in our KPC cell lines. This suggests that other mechanisms may be involved. In a study using 52 human lung cancer cell lines, baseline CXCL1 and CXCL5 expression were inversely correlated with promoter methylation (Pinnacle et al., 2013). Another group reported that TGF β 1-treated mouse breast cancer cells have reduced CXCL1 and CXCL5 expression compared to controls (Novitskiy et al., 2014). More recently, Seifert et al. showed that baseline CXCL1 expression in mouse pancreatic cancer cells was suppressed by inhibition of RIP3, a component of the necrosome (Seifert et al., 2016). Ongoing work in our lab has found that baseline expression of CXCL1 differs significantly among different KPC-derived clonal cell lines. Investigation of their epigenome, chromatin structure, and activated signaling pathways will hopefully reveal the mechanisms regulating baseline CXCR2 ligand expression in cancer cells.

Because cancer cells often secrete copious amounts of them, CXCR2 ligand expression by non-cancer cells is often not reported or ignored. However, stromal and immune populations can express CXCR2 ligands upon activation. In the bone marrow, G-CSF-induced CXCL2

expression in endothelial cells is responsible for neutrophil egression (Eash et al., 2010). Furthermore, successful neutrophil extravasation and infiltration into inflamed tissues is regulated by CXCL2 secretion from activated tissue-resident sentinel macrophages (Schiwon et al., 2014). Once activated inside inflamed tissues, neutrophils secrete IL-1 which further stimulates tissue resident cells to release CXCL1 and CXCL2 to attract even more neutrophils (Chou et al., 2010). Using our unique PDA model with lineage tracing, we showed that CXCL2 is primarily expressed by non-tumor cells in the tumor microenvironment. This result suggests that similar mechanisms to attract neutrophils may be at play in infected tissues and tumors. Importantly, the findings in this thesis show that tumor and stromal cells cooperate together to recruit TANs. Future studies must be done to determine the precise cellular sources of CXCR2 ligands and their individual function in the tumor microenvironment.

Tumor-associated neutrophils

Because of their relatively short lifespan, neutrophils are long presumed to have negligible roles in the tumor microenvironment. However, the findings in this thesis and other recent studies demonstrate that TANs can be potent regulators of tumor initiation, growth, metastasis, and response to therapy. Neutrophils are the most abundant immune population in humans, consisting of 50-70% of all peripheral leukocytes (Coffelt et al., 2016). In various mouse models, a rapid rise in systemic myeloid cells, consisting of mostly neutrophils, usually accompanies tumor development (Clark et al., 2007; Bayne et al., 2012; Pylayeva-Gupta et al., 2012; Casbon et al., 2015; Coffelt et al., 2015; Chao et al., 2016; Steele et al., 2016). To support their rapid rise and turnover in the context of cancer, neutrophils can be produced in extramedullary organs such as the spleen as well as in the bone marrow in a process akin to emergency granulopoiesis observed in acute infections (Manz and Boettcher, 2014). Tumor-induced systemic elevation of cytokines such as granulocyte-colony stimulating factor (G-CSF), granulocyte macrophage-colony stimulating factor (GM-CSF), and interleukin 17 (IL-17) have been shown to cause this overactive granulopoiesis (Bayne et al., 2012; Pylayeva-Gupta et al.,

2012; Casbon et al., 2015; Coffelt et al., 2015). Indeed, G-CSF and IL-17 were both elevated in the serum of our tumor-bearing KPC mouse model of PDA. Although not absolutely required, G-CSF is the dominant regulator of neutrophil generation, proliferation, and differentiation under homeostasis. In fact, compensation with the other factors can only produce about a quarter of the normal number of neutrophils in the absence of G-CSF receptor (Liu et al., 1996). Neutrophils without G-CSFR were also more prone to apoptosis. Binding of G-CSF to the G-CSF receptor (G-CSFR) induces signal-transducer and activator of transcription 3 (STAT3) signaling and RAR-related orphan receptor γ 1 (RORC1)-dependent translation of granulocyte-lineage genes, including CXCR2 (Panopoulos et al., 2006; Strauss et al., 2015). As neutrophils mature, the expression of CXCR2 increases, while expression of CXCR4 decreases. Egression of neutrophils is tightly regulated under homeostatic conditions by a balance of CXCR4-mediated retention and CXCR2-mediated egression (Eash et al., 2010). Under physiological conditions, only mature neutrophils egress from the bone marrow. However in the context of cancer, crowding in the bone marrow niche and elevated systemic factors can encourage the egression of both mature and immature granulocytes (Manz and Boettcher, 2014). The half-life of circulating neutrophils in healthy humans is around 7 hours (Tak et al., 2013). However, half-life of circulating neutrophils is dramatically increased to approximately 17 hours in cancer patients. In addition, non-circulating neutrophils in tissues and in the tumor microenvironment can survive for several days. On the other hand, recent evidence suggests that TANs are more prone to TNF-related apoptosis-induced ligand receptor (TRAIL-R)-mediated apoptosis than normal neutrophils because of their upregulated endoplasmic reticulum (ER) stress response (Condamine et al., 2014). Therefore, contrary to the assumption that TANs are limited to only their acute functions, emerging evidence suggests that they survive long enough to synthesize new proteins and acquire additional effector functions. Indeed, transcriptomic analyses of TANs, splenic neutrophils, and bone marrow granulocytes showed significant differences in the gene expression profile of TANs compared to splenic and circulating granulocytes (Fridlender et al., 2012; Youn et al., 2012).

Studies using spontaneous mouse models of various cancers have led to the conclusion that neutrophils generally promote tumor initiation. The pro-tumorigenic effect of neutrophils is generally attributed to their “normal” pro-inflammatory effector functions, such as degranulation, production of reactive oxygen species (ROS), and secretion of pro-inflammatory cytokines (Coffelt et al., 2016). Furthermore, G-CSF-induced expression of prokineticin (Bv8) in neutrophils has been shown to promote angiogenesis (Shojaei et al., 2007; 2008). Neutrophil-derived elastase (ELANE) can even directly promote the growth of transformed cells through degrading their intracellular insulin receptor substrate-1 (IRS1) and unleashing PI3K signaling (Houghton et al., 2010). The pro-tumorigenic effect of neutrophils is particularly evident in inflammation-induced spontaneous cancer models such as the chemically-induced skin cancer and colitis-associated colon cancer (Jamieson et al., 2012; Katoh et al., 2013). Neutrophils also promote tumor formation in several genetically engineered mouse models (GEMMs), including colon and KRAS-driven lung cancer (Jamieson et al., 2012; Chang et al., 2014). In contrast, global CXCR2 knockout in the KPC pancreatic cancer model impeded TAN accumulation, but it did not slow tumor formation (Steele et al., 2016). However, this may be the result of a balancing act between elimination of CXCR2-induced OIS in transformed cells and inhibition of the infiltration of neutrophils. Future studies with lineage-specific CXCR2 knockdown or targeted depletion of neutrophils in KPC mice during tumorigenesis will be required to resolve these conflicting effects.

The role of TANs during tumor progression is currently a subject of much debate in the field. Experiments in the early 1990's first demonstrated the anti-tumor potential of neutrophils by showing that they can eliminate implanted G-CSF producing colon cancer cells (Stoppacciaro et al., 1993). More recently, TANs isolated from early stage human and murine lung cancers have been shown to be capable of stimulating the proliferation and activation of anti-tumor T cells (Eruslanov et al., 2014). A subset of TANs isolated from stage I-II human non-small cell lung cancers (NSCLCs) was even demonstrated to be capable of cross-presentation in an IFN- γ and GM-CSF dependent manner (Singhal et al., 2016). In contrast, depletion of neutrophils starting 2 weeks in an implantable murine lung cancer model resulted in significantly reduced tumor growth

(Mishalian et al., 2013). This suggested that TANs found in more established tumors tend to have pro-tumor phenotypes. Acquisition of pro-tumor phenotypes in neutrophils depends largely on the cytokine milieu. Prolonged exposure to elevated levels of cytokines such as TGF- β , GM-CSF, and G-CSF can induce pro-tumor phenotypes in TANs (Fridlender et al., 2009; Bayne et al., 2012; Pylayeva-Gupta et al., 2012; Casbon et al., 2015). Inhibition of TGF- β was further shown to be able to convert TANs from a pro-tumor to an anti-tumor phenotype in an implantable mouse NSCLC model (Fridlender et al., 2009). These results suggest that TANs could evolve from being anti-tumor to being pro-tumor as disease progresses.

A much larger number of studies, however, have now unequivocally demonstrated that TANs tend to promote tumor progression. The presence of TANs in many human cancers was found to be associated with worst prognosis (Gentles et al., 2015). Besides their pro-tumorigenic inflammatory functions, TANs can also be highly immunosuppressive. Multiple studies have reported that inhibition of TANs can unleash anti-tumor T cell immunity and sensitize tumors to immunotherapy (Highfill et al., 2014; Steele et al., 2016). The findings in this thesis and the results in Steele et al.'s study both show that this is the case in our KPC model of PDA (Chao et al., 2016; Steele et al., 2016). In addition, we concluded in Chapter 3 that suppression of anti-tumor T cell activity is the predominant pro-tumor function of TANs in our model of PDA. The development of an immunosuppressive phenotype in TANs can be induced by cytokines such as TGF- β and GM-CSF in the tumor microenvironment (Fridlender et al., 2009; Bayne et al., 2012; Pylayeva-Gupta et al., 2012). TANs can directly suppress T cells through their elevated production of reactive oxygen species (ROS) and expression of arginase 1 (ARG1) (Rodriguez et al., 2004; Zea et al., 2005; Movahedi et al., 2008; Youn et al., 2008). TANs can also cause the nitration of CD8 or T cell receptor (TCR), which may disrupt the ability for T cells to bind to their cognate antigens on MHC-I (Nagaraj et al., 2007). TANs could further recruit immunosuppressive macrophages and T regulatory cells to the tumor microenvironment via secretion of CCL2 and CCL17 respectively (Zhou et al., 2016). In addition, phagocytosis of apoptotic neutrophils at sites of infections is known to induce a type-2 phenotype in macrophages, which suggests that TANs

may be able to modulate polarity of macrophages (Filardy et al., 2010). TANs could also present to CD8⁺ T cells and sequester them away from antigen presenting cells or cancer cells. Given that a subset of them could potentially even cross-present antigens, whether TANs could also affect the development of antigen-specific T cells remains to be determined (Singhal et al., 2016). To highlight their ability to suppress T cells, these immunosuppressive neutrophils are commonly labeled as granulocytic myeloid-derived suppressor cells (G-MDSCs) (Bronte et al., 2016). It is likely that G-MDSCs represent a major subset of neutrophils in tumor-bearing hosts. Because they share the same surface markers and functionalities, however, it has been very difficult to decipher the relationship between G-MDSCs and neutrophils. Using Ficoll gradients, Sagiv et al. have recently showed in a murine breast cancer model that low-density neutrophils (LDNs) could suppress T cells whereas high-density neutrophils (HDNs) could not (Sagiv et al., 2015). They further demonstrated that LDNs consist of a heterogeneous mixture of immature neutrophils and HDNs that have converted to LDNs in a TGFβ-dependent manner. However, more work must be done to confirm these findings in other models and in human cancers. Understanding the difference between G-MDSCs and other TANs will potentially allow us to target these cells specifically without affecting the crucial function of normal, mature neutrophils.

TANs also play an important role in tumor metastases. One major mechanism by which TANs promote metastasis is their ability to suppress cytotoxic T cells as discussed above. As in the primary tumor, neutrophils in the metastatic niche can also secrete pro-invasion, pro-angiogenic, and pro-survival factors. For example, expression of alarmins S100A8 and S100A9 by TANs can promote metastatic breast cancer growth and resistance to chemotherapy (Acharyya et al., 2012). Neutrophils can also act as a bridge between circulating tumor cells (CTCs) and tissue-resident cells, effectively trapping and allowing them to colonize distal organs (Spicer et al., 2012; Cools-Lartigue et al., 2013). TANs have recently been shown to be required for the formation of liver and lung metastases in the KPC pancreatic cancer model (Steele et al., 2016). The reasons why TANs are required for the formation of the pre-metastatic niche remain an active area of investigation. Furthermore, whether TANs play a role in metastases to other

distal organs is unclear. Altogether, emerging evidence shows that TANs play important roles during tumor initiation, progression, and metastasis. Understanding the regulation of their expansion, trafficking, and activation is, therefore, necessary to effectively target TANs.

***In silico* profiling of tumor immune infiltration**

Investigation of tumor immune infiltration has traditionally relied on variations of flow cytometry and immunohistochemistry (IHC). Although their capabilities are increasing, high-dimensional resolution of immune populations remains difficult to achieve using these techniques. In contrast, advances in next-generation sequencing (NGS) and computational methods have recently supported the investigation of tumor infiltrating leukocytes (TILs) with increasingly high dimensionality *in silico*. Such approaches will undoubtedly allow even more detailed resolution of TILs as computational power and techniques continue to develop at an exponential pace. Large coordinated efforts such as The Cancer Genome Analysis (TCGA) and the International Cancer Genome Consortium (ICGC) further provide biologically relevant data for the application of such analytical pipelines. Integrative analyses with genomic, epigenomic, transcriptomic, and clinical metadata have already resulted in unprecedented characterizations of many human cancers, including in pancreatic cancer (Bailey et al., 2016). Therefore, *in silico* dissection of immune infiltration using gene expression data may similarly provide us with novel, data-driven insights into tumor immunobiology.

In silico techniques to profile TILs usually employ either the enrichment of immune population-specific gene sets or the direct deconvolution of whole tumor transcriptomes. Both of these techniques are based on gene expression profiles of individual immune population. Early efforts to profile TILs often relied on the enrichment of known immune cell type-specific genes in a list of differentially expressed genes to infer differential immune infiltration. In these studies, a list of genes of interest is acquired before applying techniques such as gene set enrichment analysis (GSEA) to find pre-defined immune-related gene signatures that are preferentially enriched (Subramanian et al., 2005). A gene signature can either be derived from prior biological

knowledge or from differentially expressed genes in purified immune subsets. For instance, Choi et al. used this technique to find that the “immune infiltration” gene signature is enriched in the list of up-regulated, differentially expressed genes in chemo-sensitive compared to chemo-resistant muscle-invasive bladder cancers (MIBC) (Choi et al., 2014). Results such as this can easily provide a basis for additional studies, i.e. investigating the role of immune infiltrates in enhancing the response to chemotherapy. Although straightforward to implement, this analysis pipeline is highly sensitive to data platforms and noise in gene-expression levels. Furthermore, it can neither resolve individual immune population nor provide a sample-by-sample measure of TILs.

To resolve individual immune populations in gene expression data, Bindea et al. used microarray transcriptomic data of 28 purified immune populations to define immune cell-type specific gene signatures after filtering out genes that are also expressed by cancer and stromal cell lines – the “immunome” (Bindea et al., 2013). After clustering colorectal cancer (CRC) samples into two groups based on differentially expressed genes, the authors then proceeded to find that Th1, T $\gamma\delta$, CD8⁺ T cells, macrophages, and mast cells were all significantly enriched in the group with prolonged survival. To compare TILs between individual samples, Rooney et al. used gene set variation analysis (GSVA) to calculate single sample GSEA (ssGSEA) enrichment scores for several immune signatures derived from the FANTOM 5 Consortium in samples across 18 cancer types (Rooney et al., 2015). Because this sample-by-sample, rank-based method is robust against biological and technical noise, it can be used to compare the relative abundance of immune populations across different samples and data types. However, the authors noted that ssGSEA or GSVA enrichment scores should not be used for determining the relative proportion of immune cells within the same sample. Furthermore, this method may have difficulty distinguishing similar cell types with significant overlap of marker genes. Despite these important caveats, our lab has previously found this method to be particularly useful in inferring the relative abundance of immune populations and their associations with cytolytic activity in PDA samples available in TCGA (Balli et al., 2016). Using the same technique in Chapter 3, we found that only neutrophils associated significantly with CXCR2 ligand expression out of the 28 immunome populations

(Chao et al., 2016). In Chapter 4, we expanded our ssGSEA pipeline to incorporate 52 previously defined immune signatures and characterized their interactions with each other and with cytokines in human PDA (Bindea et al., 2013; Newman et al., 2015; Rooney et al., 2015). To help distinguish similar immune populations, the signatures were pre-filtered to contain only genes that are uniquely expressed. Although derived from different sources and usually containing different combinations of marker genes, our analysis showed that signatures of the same immune population tend to cluster together and correlate with others in a similar fashion. The similarity of these signatures validates not only that they are representative of the indicated immune population, but also that ssGSEA is robust to noise of individual gene expression across samples.

Taking advantage of its robustness, Yoshihara et al. employed ssGSEA in their “Estimation of STromal and Immune cells in MAlignant Tumour tissues using Expression data” (ESTIMATE) analysis pipeline to infer relative stromal, immune, and tumor cellularity in all the samples available in TCGA (Yoshihara et al., 2013). More recently, Charoentong et al. incorporated the 28 immunome ssGSEA enrichment scores for 20 solid TCGA tumor types in their web-accessible database The Cancer Immunome Atlas (TCIA) (Charoentong et al., 2017). The authors then used a random forest approach to identify important determinants of intratumoral cytolytic activity based on TIL composition, tumor genetic characteristics, and other immune-related gene expression. These determinants, when aggregated together in an “immunophenoscore,” were significantly correlated with responsiveness to checkpoint blockade therapy in a cohort of melanoma patients. Therefore, despite its limitations, enrichment of immune gene sets has proven to be effective at profiling TILs and highly robust to platform-specific or sample-specific noise. However, this method has yet to be validated with high-dimensional flow cytometry or IHC. Because human samples are often difficult to analyze with these techniques retrospectively, future studies should consider allotting human samples or using animal models to confirm the accuracy of this method.

Emerging computational techniques have allowed the deconvolution of whole tumor expression data to directly infer TIL proportions within a sample. Fundamentally, the expression

profile of a biological mixture (**M**) can be modeled by the set of linear equations $\mathbf{M} = \mathbf{F} \times \mathbf{B}$, where **B** denotes a matrix of the expression profile of purified immune cells and **F** is a vector containing the fraction of each immune population found in **M** (Shen-Orr and Gaujoux, 2013). The gene expression profile of purified immune populations (**B**) can be found in publically available datasets or derived from isolated populations. Similarly, the expression profile of whole tumors (**M**) can be acquired from public databases such as TCGA or from new experiments. Given **M** and **B**, solving for **F** then becomes the goal of these deconvolution techniques. Unlike enrichment methods, deconvolution techniques do not rely heavily on the uniqueness of the genes in an immune population, a trait that would theoretically allow them to better distinguish closely related cell types. In addition, deconvolution methods have the potential to identify novel markers of immune populations by comparing the relative contribution of genes in **B** to solving for **F**. The earliest application of deconvolution techniques focused on calculating the immune fractions from gene expression data of peripheral blood samples, which mainly consists of immune populations found in **B**. For instance, Abbas et al. used an iterative linear least square algorithm to solve for the relative proportions of 18 different immune cell types in the blood of systemic lupus erythematosus (SLE) patients and normal controls (Abbas et al., 2009). Importantly, the predicted immune proportions are essentially identical to the results obtained by flow cytometry. However, general linear models cannot account for unknown cellular populations in a mixture typical of complex tissues. Furthermore, distinguishing immune cell types with highly similar expression profiles is also problematic.

To address these issues, Newman et al. introduced the “Cell-type Identification By Estimating Relative Subsets of RNA Transcripts” (CIBERSORT) analysis pipeline (Newman et al., 2015). Here, the authors derived **B**, which they termed the LM22 matrix, from the gene expression profile of 22 immune populations found in the HGU133A platform and then filtering out genes that are highly expressed by non-hematopoietic cells. CIBERSORT then employs a variation of support vector regression (SVR), a machine learning algorithm that is robust to unknown mixture contents and highly correlated reference profiles, to solve for **F**. Comparison

with flow cytometric results confirmed the accuracy of CIBERSORT-predicted immune fractions even in complex tissues like solid tumors. CIBERSORT has since been used to deconvolute the TIL profiles of thousands of tumor samples across 25 different cancer types (Gentles et al., 2015). The predicted immune fractions in colorectal and lung adenocarcinomas were further demonstrated to be similar to the results obtained from IHC and flow cytometry respectively. However, because the LM22 matrix is based on microarray expression data, direct applicability of CIBERSORT to RNA sequencing data is currently unclear. Despite this, CIBERSORT has already been used to estimate immune proportions from RNA sequencing data in multiple tumors, including in pancreatic cancer (Sivakumar et al., 2017).

Deconvolution of expression data to profile TILs will undoubtedly achieve even higher levels of accuracy as computational techniques become increasingly sophisticated and capable of handling larger datasets. However, this method is reliant on the reference gene expression profile matrix (**B**), most of which are currently derived from normal peripheral immune cells or cultured bone marrow-derived cells. Unlike enrichment methods where gene signatures could be defined from existing biological knowledge, deconvolution methods require high dimensional expression data to be available from purified immune cell types. In addition, immune cell types often have differential activation or polarization status, which makes them even more difficult to isolate or culture. Therefore, future work must also focus on the generation of relevant reference expression profiles in order to expand the utility of deconvolution techniques. Altogether, *in silico* profiling of TILs has become a powerful technique to investigate tumor immunobiology.

***In silico* reconstruction and analysis of tumor cytokine networks**

The proliferation, differentiation, function, and survival of TILs are all regulated by the cytokine milieu in the tumor microenvironment. TILs, in turn, contribute significantly to the tumor cytokine milieu in response to various stimuli. This complicated network of immune-cytokine interactions plays an important role in regulating the tumor immune response. To investigate this complex network, a reductionist approach is traditionally used to study a few of its components at

a time using *in vitro* and *in vivo* experimental models. For instance, our work in Chapter 3 used the KPC and CXCR2^{-/-} models to study the CXCR2-ligand axis in PDA (Chao et al., 2016). Currently, our knowledge of the overall tumor cytokine network relies on manually aggregating the conclusions of these reductionist studies in the occasional reviews on the topic (Balkwill, 2004; MD and Lippitz, 2013; Schett et al., 2013; Vonderheide and Bayne, 2013; West et al., 2015). While they remain the gold standard to verify the function of specific components, these reductionist approaches cannot characterize and compare entire networks. Furthermore, it is difficult to compare the relative influence of individual components in a network or across multiple networks. Finally, there is often little evidence *a priori* to suggest that the candidate component is important to the system. Therefore, a more complete understanding of the complex interactions between cytokines and TILs will require a network-level understanding to complement reductionist experiments. Inspired by the recent success of *in silico* gene network analyses to detect disease-associated pathways, we devised a novel analysis pipeline in Chapter 4 to construct and analyze PDA-associated cytokine networks using immune GSEA enrichment scores and cytokine expression data.

Gene network models typically consist of genes as nodes and their interactions as edges in a graph. The earliest and most common method to computationally infer edges relies on the “guilt by association” concept, which assumes that genes with highly similar expression profiles are more likely to be co-regulated or functionally related (Wolfe et al., 2005). Commonly used methods to infer gene relatedness include correlation coefficients, regression models, and, more recently, mutual information (Butte and Kohane, 2000; Stuart et al., 2003; van Someren et al., 2006). A major study comparing these inference methods found that no one method is generally superior and that their performance varied depending on the context (Marbach et al., 2012). Although they can only capture the strength of linear relationships, correlation coefficients are more readily interpretable in terms of their biological relevance. Furthermore, correlation coefficients are invariant to the linear normalization required of most expression data. Unlike Pearson’s correlations, rank-based correlations such as Spearman’s are nonparametric, more

general, and highly robust to strong outliers (Mukaka, 2012). A comparison of correlation methods further showed that Spearman's significantly outperformed Pearson's correlation to correctly identify real co-expressed pathways and genes (Kumari et al., 2012). In this work, we showed that the relative strength of specific Spearman's immune-cytokine correlations could be used to indicate the functional status of immune populations. Once the correlations are calculated, they are usually either filtered using "hard" thresholding or modified using "soft" thresholding techniques (Zhang and Horvath, 2005). Hard thresholding simply involves removing all correlations that are less than a specific acceptable value. The remaining correlations are then interpreted as equal, resulting in a binary network where nodes are either related or not. However, this method ignores the relative strength of correlation coefficients. To address this issue, Zhang et al. introduced the soft thresholding method to generate a weighted network (Zhang and Horvath, 2005). Here, correlation coefficients are raised to a positive power in order to approximate a scale-free topology. This method simultaneously preserves the value of all correlation coefficients and exaggerates the importance of strong correlations at the expense of weaker correlations. Multiple studies have now successfully implemented this soft thresholding method to explore cancer-associated genes and pathways (Zhao et al., 2010; Jia et al., 2014; Yang et al., 2014; Bailey et al., 2016). However, it is still unclear whether all biological networks should be modeled as having scale-free topologies (Barabási, 2009). Furthermore, highly unlikely and weak correlations are retained in the network, which may negatively impact subsequent analyses. In Chapter 4, we introduced a hybrid method using a modified form of hard thresholding that only retains edges that are both empirically significant and have moderately strong correlation values. This hybrid method preserves the information from correlation coefficients and also eliminates highly unlikely interactions from subsequent analyses. In addition, empirical significance bypasses the poorly asymptotic behavior of correlations and allows for more accurate statistical comparisons. Despite these advantages, more work must be done to compare this hybrid method with traditional hard or soft thresholding methods in their abilities to detect real biological interactions.

Once a gene network is constructed, identification of groups of genes with similar behaviors usually relies on pattern recognition techniques. Clustering, either through K-means or hierarchal clustering, is the most widely used technique to detect patterns in gene correlation networks (Jain, 2010). K-means clustering assigns each gene to exactly one module, while hierarchal clustering allows for more flexibility. However, derivation of gene clusters from these techniques is an ambiguous process requiring the specification of a number of parameters, such as the number of desired clusters or the choice of clustering algorithms. Another approach utilizes community detection techniques from network theory to automatically detect and assign clusters (Dyer and Nason, 2004; Garroway et al., 2008). These techniques generally detect communities by finding groups of nodes where the intra-connectedness is greater than connectedness with outside nodes. In an early effort, Ben-Dor et al. developed an algorithm that constructs one community at a time by iteratively adding or dropping a gene (Ben-Dor et al., 1999). Numerous algorithms have since been developed to detect communities, including using probabilistic models and neural networks (Fortunato, 2010). However, many of these algorithms are often computationally intensive and have limited utility in larger networks. To improve community detection in large networks, Clauset et al. developed the “fast-greedy” community detection algorithm that iteratively maximizes local modularity, which is the ratio of observed intra-connectedness over the expected connectedness in a random network (Clauset et al., 2004). Using artificially generated networks, Yang et al. have recently demonstrated that a variation of this algorithm produced highly accurate results while being orders of magnitude faster than many other methods (Yang et al., 2016b). In Chapter 4, we showed that both hierarchal clustering and the fast greedy community detection algorithm yielded similar immune-cytokine clusters. We further discussed that many of these clusters reflect known interactions among immune cells and cytokines. However, the biological relevance of these inferred communities in PDA-associated cytokine networks remains unclear.

Nearly every study to date ends their bioinformatics analysis pipelines at the detection and functional assignment of gene modules. For example, Bailey et al. identified 26 coordinately

expressed gene clusters representing different biological processes and associated them with four distinct human pancreatic cancer subtypes (Bailey et al., 2016). Although such analyses qualitatively compare the importance of gene clusters to certain groups, they neither quantitatively measure importance nor provide a means to compare the importance of individual genes. To quantitatively measure the importance of gene clusters, Zhang et al. have previously introduced the use of “gene module importance scores,” which are derived from correlating the principal component of a gene cluster with a biological characteristic of interest (Zhang and Horvath, 2005). In the study by Bailey et al., this technique was used to quantify the relative importance of the 26 gene clusters in regards to survival (Bailey et al., 2016). However, this method does not quantify importance in terms of the influence of a node within a network. Instead, network-intrinsic importance of a node can be measured by its “centrality,” a concept from social network theory (Garroway et al., 2008; Friedkin, 2015). Two commonly used measures of node importance are degree and eigenvector centralities. Degree centrality measures importance in terms of the number of direct connections to a node. Meanwhile, eigenvector centrality measures importance of a node by its connectedness with other well-connected nodes. Importantly, the gene centralities in expression networks have been shown to reflect the importance of driver genes in various cancers, including retinoblastoma and breast cancer (Wang et al., 2011; 2015).

In Chapter 4, we used degree and eigenvector centralities to measure the importance of immune populations and cytokines in PDA-associated cytokine networks. In this context, degree centrality reflects the number of cytokines that are strongly associated with an immune population. Given that activated immune cells generally express or are receptive to more cytokines than when they are at rest, the degree centrality of an immune population could act as a rough indication of its activation status. On the other hand, the eigenvector centrality gives an indication of the number of influential cytokines that are associated with a certain immune population. Therefore, eigenvector centrality measures how influential or influenced an immune population is in the network. Here, we demonstrated that both measures of importance could

reveal immune populations and cytokines that are known to play key roles in PDA. Furthermore, we showed that it is possible to compare the relative importance of components in different networks. Given these observations, we propose that these measures could provide quantitative indications of a candidate's potential importance *a priori* to experimental validation.

To our knowledge, our work in Chapter 4 is the first to describe an analytical pipeline to infer and compare cytokine networks from whole tumor expression data. Here, we combined techniques from gene co-expression network and network graph analyses not only to infer immune-cytokine interactions, but also to compare these interactions across different networks. Furthermore, this pipeline provides a statistical measure of the importance of components in the cytokine network, which might guide candidate selection for experimental validation. However, much work remains in order to demonstrate the accuracy of these predictions. It may also be interesting to compare and contrast these cytokine networks across different cancers and databases. As large-scale genomic datasets become more and more common, analyses such as this can be used to complement reductionist approaches and accelerate our understanding of the cytokine networks underlying tumor immune responses.

Summary and closing statements

In summary, this thesis aims to highlight that cytokine networks can play an important role in regulating the tumor immune responses. Using mouse models of pancreatic cancer, I demonstrated the importance of the CXCR2-CXCR2 ligand axis in recruiting immunosuppressive tumor-associated neutrophils to the PDA microenvironment. Both tumor and stromal cells secrete CXCR2 ligands to recruit TANs to the microenvironment, where they primarily promote tumor growth by suppressing T cell immunity. Therefore, this work adds to the mounting evidence that cytokine networks represent a major mechanism by which tumors evade immunosurveillance. To accelerate their discovery, I devised a novel analysis pipeline to identify other potentially important cytokine networks from whole tumor gene expression data. I showed that this pipeline could highlight cytokine networks that are statistically important in cytolytically hot and cold PDA

tumors. Future investigations of the relevance of these candidate cytokine networks will hopefully reveal novel targets to effectively disrupt immunosuppressive networks and enhance immunosurveillance in PDA.

REFERENCES

- Abbas, A.R., Wolslegel, K., Seshasayee, D., Modrusan, Z., and Clark, H.F. (2009). Deconvolution of blood microarray data identifies cellular activation patterns in systemic lupus erythematosus. *PLoS ONE* 4, e6098.
- Acharyya, S., Oskarsson, T., Vanharanta, S., Malladi, S., Kim, J., Morris, P., Manova-Todorova, K., Leversha, M., Hogg, N., Seshan, V., et al. (2012). A CXCL1 Paracrine Network Links Cancer Chemoresistance and Metastasis. *Cell* 150, 165–178.
- Acosta, J.C., O'Loghlen, A., Banito, A., Guijarro, M.V., Augert, A., Raguz, S., Fumagalli, M., Da Costa, M., Brown, C., Popov, N., et al. (2008). Chemokine Signaling via the CXCR2 Receptor Reinforces Senescence. *Cell* 133, 1006–1018.
- Adami, J., Gäbel, H., Lindelöf, B., Ekström, K., Rydh, B., Glimelius, B., Ekblom, A., Adami, H.-O., and Granath, F. (2003). Cancer risk following organ transplantation: a nationwide cohort study in Sweden. *Br. J. Cancer* 89, 1221–1227.
- Aggarwal, G., Ramachandran, V., Javeed, N., Arumugam, T., Dutta, S., Klee, G.G., Klee, E.W., Smyrk, T.C., Bamlet, W., Han, J.J., et al. (2012). Adrenomedullin is up-regulated in patients with pancreatic cancer and causes insulin resistance in β cells and mice. *Gastroenterology* 143, 1510–1517.e1511.
- Aguirre, A.J. (2003). Activated Kras and Ink4a/Arf deficiency cooperate to produce metastatic pancreatic ductal adenocarcinoma. *Genes & Development* 17, 3112–3126.
- Ahlgren, U., Jonsson, J., and Edlund, H. (1996). The morphogenesis of the pancreatic mesenchyme is uncoupled from that of the pancreatic epithelium in IPF1/PDX1-deficient mice. *Development* 122, 1409–1416.
- Ahn, S.S., Kim, M.-J., Choi, J.-Y., Hong, H.-S., Chung, Y.E., and Lim, J.S. (2009). Indicative findings of pancreatic cancer in prediagnostic CT. *Eur Radiol* 19, 2448–2455.
- Aiello, N.M., Bajor, D.L., Norgard, R.J., Sahnoud, A., Bhagwat, N., Pham, M.N., Cornish, T.C., Iacobuzio-Donahue, C.A., Vonderheide, R.H., and Stanger, B.Z. (2016). Metastatic progression is associated with dynamic changes in the local microenvironment. *Nat Commun* 7, 12819.
- Almoguera, C., Shibata, D., Forrester, K., Martin, J., Arnheim, N., and Perucho, M. (1988). Most human carcinomas of the exocrine pancreas contain mutant c-K-ras genes. *Cell* 53, 549–554.
- Andrian, von, U.H., and Mempel, T.R. (2003). Homing and cellular traffic in lymph nodes. *Nature Reviews Immunology* 3, 867–878.
- Arumugam, T., Brandt, W., Ramachandran, V., Moore, T.T., Wang, H., May, F.E., Westley, B.R., Hwang, R.F., and Logsdon, C.D. (2011). Trefoil factor 1 stimulates both pancreatic cancer and stellate cells and increases metastasis. *Pancreas* 40, 815–822.
- Bailey, P., Chang, D.K., Nones, K., Johns, A.L., Patch, A.-M., Gingras, M.-C., Miller, D.K., Christ, A.N., Bruxner, T.J.C., Quinn, M.C., et al. (2016). Genomic analyses identify molecular subtypes of pancreatic cancer. *Nature* 531, 47–52.
- Balkwill, F. (2004). Cancer and the chemokine network. *Nature Reviews Cancer* 4, 540–550.

- Balli, D., Rech, A.J., Stanger, B.Z., and Vonderheide, R.H. (2016). Immune Cytolytic Activity Stratifies Molecular Subsets of Human Pancreatic Cancer. *Clin. Cancer Res.*
- Barabási, A.-L. (2009). Scale-free networks: a decade and beyond. *Science* 325, 412–413.
- Bardeesy, N., and DePinho, R.A. (2002). Pancreatic cancer biology and genetics. *Nature Reviews Cancer* 2, 897–909.
- Bardeesy, N., Cheng, K.-H., Berger, J.H., Chu, G.C., Pahler, J., Olson, P., Hezel, A.F., Horner, J., Lauwers, G.Y., Hanahan, D., et al. (2006). Smad4 is dispensable for normal pancreas development yet critical in progression and tumor biology of pancreas cancer. *Genes & Development* 20, 3130–3146.
- Basturk, O., Hong, S.-M., Wood, L.D., Adsay, N.V., Albores-Saavedra, J., Biankin, A.V., Brosens, L.A.A., Fukushima, N., Goggins, M., Hruban, R.H., et al. (2015). A Revised Classification System and Recommendations From the Baltimore Consensus Meeting for Neoplastic Precursor Lesions in the Pancreas. pp. 1730–1741.
- Bayne, L., Beatty, G., Jhala, N., Clark, C., Rhim, A., Stanger, B., and Vonderheide, R. (2012). Tumor-Derived Granulocyte-Macrophage Colony-Stimulating Factor Regulates Myeloid Inflammation and T Cell Immunity in Pancreatic Cancer. *Cancer Cell* 21, 822–835.
- Beatty, G., Chiorean, E., Fishman, M., and Saboury, B. (2011). CD40 agonists alter tumor stroma and show efficacy against pancreatic carcinoma in mice and humans. *Science* –.
- Beatty, G.L., Torigian, D.A., Chiorean, E.G., Saboury, B., Brothers, A., Alavi, A., Troxel, A.B., Sun, W., Teitelbaum, U.R., Vonderheide, R.H., et al. (2013). A Phase I Study of an Agonist CD40 Monoclonal Antibody (CP-870,893) in Combination with Gemcitabine in Patients with Advanced Pancreatic Ductal Adenocarcinoma. *Clin. Cancer Res.* 19, 6286–6295.
- Beatty, G.L., Winograd, R., Evans, R.A., Long, K.B., Luque, S.L., Lee, J.W., Clendenin, C., Gladney, W.L., Knoblock, D.M., Guirnalda, P.D., et al. (2015). Exclusion of T Cells From Pancreatic Carcinomas in Mice Is Regulated by Ly6C(low) F4/80(+) Extratumoral Macrophages. *Gastroenterology* 149, 201–210.
- Begg, C.B., Cramer, L.D., Hoskins, W.J., and Brennan, M.F. (1998). Impact of hospital volume on operative mortality for major cancer surgery. *Jama* 280, 1747–1751.
- Ben-Dor, A., Shamir, R., and Yakhini, Z. (1999). Clustering gene expression patterns. *J. Comput. Biol.* 6, 281–297.
- Bennett, S.R., Carbone, F.R., Karamalis, F., Flavell, R.A., Miller, J.F., and Heath, W.R. (1998). Help for cytotoxic-T-cell responses is mediated by CD40 signalling. *Nature* 393, 478–480.
- Berke, G. (1995). The CTL's kiss of death. *Cell* 81, 9–12.
- Bianchi, M.E. (2007). DAMPs, PAMPs and alarmins: all we need to know about danger. *J Leukoc Biol* 81, 1–5.
- Biankin, A.V., Waddell, N., Kassahn, K.S., Gingras, M.-C., Muthuswamy, L.B., Johns, A.L., Miller, D.K., Wilson, P.J., Patch, A.-M., Wu, J., et al. (2012). Pancreatic cancer genomes reveal aberrations in axon guidance pathway genes. *Nature* 491, 399–405.

- Bielekova, B., Catalfamo, M., Reichert-Scriver, S., Packer, A., Cerna, M., Waldmann, T.A., McFarland, H., Henkart, P.A., and Martin, R. (2006). Regulatory CD56(bright) natural killer cells mediate immunomodulatory effects of IL-2/alpha-targeted therapy (daclizumab) in multiple sclerosis. *Proc. Natl. Acad. Sci. U.S.A.* 103, 5941–5946.
- Bindea, G., Mlecnik, B., Tosolini, M., Kirilovsky, A., Waldner, M., Obenaus, A.C., Angell, H., Fredriksen, T., Lafontaine, L., Berger, A., et al. (2013). Spatiotemporal dynamics of intratumoral immune cells reveal the immune landscape in human cancer. *Immunity* 39, 782–795.
- Boshoff, C., and Weiss, R. (2002). AIDS-related malignancies. *Nature Reviews Cancer* 2, 373–382.
- Bourgeois, C., Rocha, B., and Tanchot, C. (2002). A role for CD40 expression on CD8+ T cells in the generation of CD8+ T cell memory. *Science* 297, 2060–2063.
- Brahmer, J.R., Tykodi, S.S., Chow, L.Q.M., Hwu, W.-J., Topalian, S.L., Hwu, P., Drake, C.G., Camacho, L.H., Kauh, J., Odunsi, K., et al. (2012). Safety and activity of anti-PD-L1 antibody in patients with advanced cancer. *N. Engl. J. Med.* 366, 2455–2465.
- Brat, D.J., Lillemo, K.D., Yeo, C.J., Warfield, P.B., and Hruban, R.H. (1998). Progression of pancreatic intraductal neoplasias to infiltrating adenocarcinoma of the pancreas. *Am. J. Surg. Pathol.* 22, 163–169.
- Brewitz, A., Eickhoff, S., Dähling, S., Quast, T., Bedoui, S., Kroczeck, R.A., Kurts, C., Garbi, N., Barchet, W., Iannacone, M., et al. (2017). CD8(+) T Cells Orchestrate pDC-XCR1(+) Dendritic Cell Spatial and Functional Cooperativity to Optimize Priming. *Immunity* 46, 205–219.
- Bronte, V., Apolloni, E., Cabrelle, A., Ronca, R., Serafini, P., Zamboni, P., Restifo, N.P., and Zanovello, P. (2000). Identification of a CD11b(+)/Gr-1(+)/CD31(+) myeloid progenitor capable of activating or suppressing CD8(+) T cells. *Blood* 96, 3838–3846.
- Bronte, V., Brandau, S., Chen, S.-H., Colombo, M.P., Frey, A.B., Greten, T.F., Mandruzzato, S., Murray, P.J., Ochoa, A., Ostrand-Rosenberg, S., et al. (2016). Recommendations for myeloid-derived suppressor cell nomenclature and characterization standards. *Nat Commun* 7, 12150.
- Bryant, K.L., Mancias, J.D., Kimmelman, A.C., Der, C.J., and Channing, C. (2014). KRAS: feeding pancreatic cancer proliferation. *Trends in Biochemical Sciences* 39, 91–100.
- Burnet, F.M. (1970). The concept of immunological surveillance. *Prog Exp Tumor Res* 13, 1–27.
- Burnet, F.M. (1964). Immunological factors in the process of carcinogenesis. *Br. Med. Bull.* 20, 154–158.
- Butte, A.J., and Kohane, I.S. (2000). Mutual information relevance networks: functional genomic clustering using pairwise entropy measurements. *Pac Symp Biocomput* 418–429.
- Byrne, K.T., and Vonderheide, R.H. (2016). CD40 Stimulation Obviates Innate Sensors and Drives T Cell Immunity in Cancer. *Cell Rep* 15, 2719–2732.
- Cancer Genome Atlas Research Network, Weinstein, J.N., Collisson, E.A., Mills, G.B., Shaw, K.R.M., Ozenberger, B.A., Ellrott, K., Shmulevich, I., Sander, C., and Stuart, J.M. (2013). The Cancer Genome Atlas Pan-Cancer analysis project. *Nat. Genet.* 45, 1113–1120.

- Carstens, J.L., Correa de Sampaio, P., Yang, D., Barua, S., Wang, H., Rao, A., Allison, J.P., LeBleu, V.S., and Kalluri, R. (2017). Spatial computation of intratumoral T cells correlates with survival of patients with pancreatic cancer. *Nat Commun* 8, 15095.
- Casbon, A.-J., Reynaud, D., Park, C., Khuc, E., Gan, D.D., Schepers, K., Passegué, E., and Werb, Z. (2015). Invasive breast cancer reprograms early myeloid differentiation in the bone marrow to generate immunosuppressive neutrophils. *Proc. Natl. Acad. Sci. U.S.a.* 112, E566–E575.
- Chang, A.L., Miska, J., Wainwright, D.A., Dey, M., Rivetta, C.V., Yu, D., Kanojia, D., Pituch, K.C., Qiao, J., Pytel, P., et al. (2016). CCL2 Produced by the Glioma Microenvironment Is Essential for the Recruitment of Regulatory T Cells and Myeloid-Derived Suppressor Cells. *Cancer Res.* 76, 5671–5682.
- Chang, S.H., Mirabolfathinejad, S.G., Katta, H., Cumpian, A.M., Gong, L., Caetano, M.S., Moghaddam, S.J., and Dong, C. (2014). T helper 17 cells play a critical pathogenic role in lung cancer. *Proc. Natl. Acad. Sci. U.S.a.* 111, 5664–5669.
- Chao, T., Furth, E.E., and Vonderheide, R.H. (2016). CXCR2-Dependent Accumulation of Tumor-Associated Neutrophils Regulates T-cell Immunity in Pancreatic Ductal Adenocarcinoma. *Cancer Immunol Res* 4, 968–982.
- Chari, S.T. (2007). Detecting early pancreatic cancer: problems and prospects. *Semin. Oncol.* 34, 284–294.
- Charoentong, P., Finotello, F., Angelova, M., Mayer, C., Efremova, M., Rieder, D., Hackl, H., and Trajanoski, Z. (2017). Pan-cancer Immunogenomic Analyses Reveal Genotype-Immunophenotype Relationships and Predictors of Response to Checkpoint Blockade. *Cell Rep* 18, 248–262.
- Chen, D.S., and Mellman, I. (2013). Oncology meets immunology: the cancer-immunity cycle. *Immunity* 39, 1–10.
- Chen, M.M., Lam, A., Abraham, J.A., Schreiner, G.F., and Joly, A.H. (2000). CTGF expression is induced by TGF- β in cardiac fibroblasts and cardiac myocytes: a potential role in heart fibrosis. *J. Mol. Cell. Cardiol.* 32, 1805–1819.
- Chien, Y., Scuoppo, C., Wang, X., Fang, X., Balgley, B., Bolden, J.E., Premssirrut, P., Luo, W., Chicas, A., Lee, C.S., et al. (2011). Control of the senescence-associated secretory phenotype by NF- κ B promotes senescence and enhances chemosensitivity. *Genes & Development* 25, 2125–2136.
- Choi, W., Porten, S., Kim, S., Willis, D., Plimack, E.R., Hoffman-Censits, J., Roth, B., Cheng, T., Tran, M., Lee, I.-L., et al. (2014). Identification of Distinct Basal and Luminal Subtypes of Muscle-Invasive Bladder Cancer with Different Sensitivities to Frontline Chemotherapy. *Cancer Cell* 25, 152–165.
- Chou, R.C., Kim, N.D., Sadik, C.D., Seung, E., Lan, Y., Byrne, M.H., Haribabu, B., Iwakura, Y., and Luster, A.D. (2010). Lipid-cytokine-chemokine cascade drives neutrophil recruitment in a murine model of inflammatory arthritis. *Immunity* 33, 266–278.
- Clark, C.E., Hingorani, S.R., Mick, R., Combs, C., Tuveson, D.A., and Vonderheide, R.H. (2007). Dynamics of the immune reaction to pancreatic cancer from inception to invasion. *Cancer Res.*

67, 9518–9527.

Clauset, A., Newman, M.E.J., and Moore, C. (2004). Finding community structure in very large networks. *Phys Rev E Stat Nonlin Soft Matter Phys* 70, 066111.

Coffelt, S.B., Kersten, K., Doornebal, C.W., Weiden, J., Vrijland, K., Hau, C.-S., Verstegen, N.J.M., Ciampricotti, M., Hawinkels, L.J.A.C., Jonkers, J., et al. (2015). IL-17-producing $\gamma\delta$ T cells and neutrophils conspire to promote breast cancer metastasis. *Nature* 522, 345–348.

Coffelt, S.B., Wellenstein, M.D., and de Visser, K.E. (2016). Neutrophils in cancer: neutral no more. *Nature Reviews Cancer* 16, 431–446.

Collins, M.A., Bednar, F., Zhang, Y., Brisset, J.-C., Galbán, S., Galbán, C.J., Rakshit, S., Flannagan, K.S., Adsay, N.V., and Di Magliano, M.P. (2012). Oncogenic Kras is required for both the initiation and maintenance of pancreatic cancer in mice. *Journal of Clinical Investigation* 122, 639–653.

Collisson, E.A., Sadan, A., am, Olson, P., Gibb, W.J., Truitt, M., Gu, S., Cooc, J., Weinkle, J., Kim, G.E., et al. (2011). Subtypes of pancreatic ductal adenocarcinoma and their differing responses to therapy. *Nature Medicine* 17, 500–503.

Condamine, T., Kumar, V., Ramach, I.R., Ramachandran, I.R., ran, Youn, J.-I., Celis, E., Finnberg, N., El-Deiry, W.S., Winograd, R., et al. (2014). ER stress regulates myeloid-derived suppressor cell fate through TRAIL-R-mediated apoptosis. *The Journal of Clinical Investigation* 124, –.

Conroy, T., Desseigne, F., Ychou, M., Bouché, O., Guimbaud, R., Bécouarn, Y., Adenis, A., Raoul, J.-L., Gourgou-Bourgade, S., la Fouchardière, de, C., et al. (2011). FOLFIRINOX versus gemcitabine for metastatic pancreatic cancer. *N. Engl. J. Med.* 364, 1817–1825.

Cools-Lartigue, J., Spicer, J., McDonald, B., Gowing, S., Chow, S., Giannias, B., Bourdeau, F., Kubes, P., and Ferri, L. (2013). Neutrophil extracellular traps sequester circulating tumor cells and promote metastasis. *J. Clin. Invest.* 123, 3446–3458.

Cooper, M.A., Fehniger, T.A., and Caligiuri, M.A. (2001a). The biology of human natural killer-cell subsets. *Trends Immunol.* 22, 633–640.

Cooper, M.A., Fehniger, T.A., Turner, S.C., Chen, K.S., Ghaehri, B.A., Ghayur, T., Carson, W.E., and Caligiuri, M.A. (2001b). Human natural killer cells: a unique innate immunoregulatory role for the CD56(bright) subset. *Blood* 97, 3146–3151.

Csardi, G., and Nepusz, T. (2006). The igraph software package for complex network research. *InterJournal*.

Cunningham, C.C., Chada, S., Merritt, J.A., Tong, A., Senzer, N., Zhang, Y., Mhashilkar, A., Parker, K., Vukelja, S., Richards, D., et al. (2005). Clinical and local biological effects of an intratumoral injection of mda-7 (IL24; INGN 241) in patients with advanced carcinoma: a phase I study. *Mol. Ther.* 11, 149–159.

Curiel, T.J., Coukos, G., Zou, L., Alvarez, X., Cheng, P., Mottram, P., Evdemon-Hogan, M., Conejo-Garcia, J.R., Zhang, L., Burow, M., et al. (2004). Specific recruitment of regulatory T cells in ovarian carcinoma fosters immune privilege and predicts reduced survival. *Nat. Med.* 10, 942–949.

- Curtsinger, J.M., Lins, D.C., and Mescher, M.F. (2003). Signal 3 determines tolerance versus full activation of naive CD8 T cells: dissociating proliferation and development of effector function. *J. Exp. Med.* 197, 1141–1151.
- Curtsinger, J.M., Valenzuela, J.O., Agarwal, P., Lins, D., and Mescher, M.F. (2005). Type I IFNs provide a third signal to CD8 T cells to stimulate clonal expansion and differentiation. *J. Immunol.* 174, 4465–4469.
- Daley, D., Zambirinis, C.P., Seifert, L., Akkad, N., Mohan, N., Werba, G., Barilla, R., Torres-Hernandez, A., Hundeyin, M., Mani, V.R.K., et al. (2016). $\gamma\delta$ T Cells Support Pancreatic Oncogenesis by Restraining $\alpha\beta$ T Cell Activation. *Cell* 166, 1485–1499.e15.
- del Rio, M.L., Lucas, C.L., Buhler, L., Rayat, G., and Rodriguez-Barbosa, J.I. (2010). HVEM/LIGHT/BTLA/CD160 cosignaling pathways as targets for immune regulation. *J Leukoc Biol* 87, 223–235.
- Di Pucchio, T., Chatterjee, B., Smed-Sørensen, A., Clayton, S., Palazzo, A., Montes, M., Xue, Y., Mellman, I., Banchereau, J., and Connolly, J.E. (2008). Direct proteasome-independent cross-presentation of viral antigen by plasmacytoid dendritic cells on major histocompatibility complex class I. *Nat. Immunol.* 9, 551–557.
- Dieu-Nosjean, M.-C., Goc, J., Giraldo, N.A., Sautès-Fridman, C., and Fridman, W.H. (2014). Tertiary lymphoid structures in cancer and beyond. *Trends Immunol.* 35, 571–580.
- Doorduijn, E.M., Sluijter, M., Salvatori, D.C., Silvestri, S., Maas, S., Arens, R., Ossendorp, F., van der Burg, S.H., and van Hall, T. (2017). CD4+ T cell and NK cell interplay key to regression of MHC class II low tumors upon TLR7/8 agonist therapy. *Cancer Immunol Res* 5, canimm.0334.2016–canimm.0334.2653.
- Dornhöfer, N., Spong, S., Bennewith, K., Salim, A., Klaus, S., Kambham, N., Wong, C., Kaper, F., Sutphin, P., Nacamuli, R., et al. (2006). Connective tissue growth factor-specific monoclonal antibody therapy inhibits pancreatic tumor growth and metastasis. *Cancer Res.* 66, 5816–5827.
- Dunn, G.P., Bruce, A.T., Ikeda, H., Old, L.J., and Schreiber, R.D. (2002). Cancer immunoediting: from immunosurveillance to tumor escape. *Nat. Immunol.* 3, 991–998.
- Dyer, R.J., and Nason, J.D. (2004). Population Graphs: the graph theoretic shape of genetic structure. *Mol. Ecol.* 13, 1713–1727.
- Eash, K.J., Greenbaum, A.M., Gopalan, P.K., and Link, D.C. (2010). CXCR2 and CXCR4 antagonistically regulate neutrophil trafficking from murine bone marrow. *Journal of Clinical Investigation* 120, 2423–2431.
- Ehrlich, P. (1909). Über den jetzigen Stand der Karzinomforschung. *Beiträge Zur Experimentellen Pathologie Und Chemotherapie* 117–164.
- Engels, E.A., Pfeiffer, R.M., Fraumeni, J.F., Kasiske, B.L., Israni, A.K., Snyder, J.J., Wolfe, R.A., Goodrich, N.P., Bayakly, A.R., Clarke, C.A., et al. (2011). Spectrum of cancer risk among US solid organ transplant recipients. *Jama* 306, 1891–1901.
- Eruslanov, E.B., Bhojnagarwala, P.S., Quatromoni, J.G., Stephen, T.L., Ranganathan, A., Deshpande, C., Akimova, T., Vachani, A., Litzky, L., Hancock, W.W., et al. (2014). Tumor-associated neutrophils stimulate T cell responses in early-stage human lung cancer. *J. Clin.*

Invest. 124, 5466–5480.

Evans, R.A., Diamond, M.S., Rech, A.J., Chao, T., Richardson, M.W., Lin, J.H., Bajor, D.L., Byrne, K.T., Stanger, B.Z., Riley, J.L., et al. (2016). Lack of immunoediting in murine pancreatic cancer reversed with neoantigen. *JCI Insight* 1.

Fan, Z., Yu, P., Wang, Y., Wang, Y., Fu, M.L., Liu, W., Sun, Y., and Fu, Y.-X. (2006). NK-cell activation by LIGHT triggers tumor-specific CD8+ T-cell immunity to reject established tumors. *Blood* 107, 1342–1351.

FANTOM Consortium, Forrest, A.R.R., Kawaji, H., Rehli, M., Baillie, J.K., de Hoon, M.J.L., Haberle, V., Lassmann, T., Kulakovskiy, I.V., Lizio, M., et al. (2014). A promoter-level mammalian expression atlas. *Nature* 507, 462–470.

Feig, C., Jones, J.O., Kraman, M., Wells, R.J.B., Deonarine, A., Chan, D.S., Connell, C.M., Roberts, E.W., Zhao, Q., Caballero, O.L., et al. (2013). Targeting CXCL12 from FAP-expressing carcinoma-associated fibroblasts synergizes with anti-PD-L1 immunotherapy in pancreatic cancer. *Proc. Natl. Acad. Sci. U.S.A.* 110, 20212–20217.

Fesinmeyer, M.D., Austin, M.A., Li, C.I., De Roos, A.J., and Bowen, D.J. (2005). Differences in survival by histologic type of pancreatic cancer. *Cancer Epidemiol. Biomarkers Prev.* 14, 1766–1773.

Filardy, A.A., Pires, D.R., Nunes, M.P., Takiya, C.M., Freire-de-Lima, C.G., Ribeiro-Gomes, F.L., and DosReis, G.A. (2010). Proinflammatory clearance of apoptotic neutrophils induces an IL-12(low)IL-10(high) regulatory phenotype in macrophages. *J. Immunol.* 185, 2044–2050.

Fortunato, S. (2010). Community detection in graphs. *Physics Reports* 486, 75–174.

Frese, K.K., Neesse, A., Cook, N., Bapiro, T.E., Lolkema, M.P., Jodrell, D.I., and Tuveson, D.A. (2012). nab-Paclitaxel potentiates gemcitabine activity by reducing cytidine deaminase levels in a mouse model of pancreatic cancer. *Cancer Discov* 2, 260–269.

Fridlender, Z., and Albelda, S. (2012). Tumor-associated neutrophils: friend or foe? *Carcinogenesis* –.

Fridlender, Z.G., Sun, J., Kim, S., Kapoor, V., Cheng, G., Ling, L., Worthen, G.S., and Albelda, S.M. (2009). Polarization of tumor-associated neutrophil phenotype by TGF-beta: "N1" versus "N2" TAN. *Cancer Cell* 16, 183–194.

Fridlender, Z.G., Sun, J., Mishalian, I., Singhal, S., Cheng, G., Kapoor, V., Horng, W., Fridlender, G., Bayuh, R., Worthen, G.S., et al. (2012). Transcriptomic analysis comparing tumor-associated neutrophils with granulocytic myeloid-derived suppressor cells and normal neutrophils. *PLoS ONE* 7, e31524.

Friedkin, N.E. (2015). Theoretical Foundations for Centrality Measures. *American Journal of Sociology* 96, 1478–1504.

Funamizu, N., Hu, C., Lacy, C., Schetter, A., Zhang, G., He, P., Gaedcke, J., Ghadimi, M.B., Ried, T., Yfantis, H.G., et al. (2013). Macrophage migration inhibitory factor induces epithelial to mesenchymal transition, enhances tumor aggressiveness and predicts clinical outcome in resected pancreatic ductal adenocarcinoma. *Int. J. Cancer* 132, 785–794.

- Fusaroli, P., Spada, A., Mancino, M.G., and Caletti, G. (2010). Contrast harmonic echo-endoscopic ultrasound improves accuracy in diagnosis of solid pancreatic masses. *Clin. Gastroenterol. Hepatol.* 8, 629–34.e1–2.
- Gabrilovich, D.I., and Nagaraj, S. (2009). Myeloid-derived suppressor cells as regulators of the immune system. *Nature Reviews Immunology* 9, 162–174.
- Gabrilovich, D.I., Ostr, S., Ostrand-Rosenberg, S., -Rosenberg, and Bronte, V. (2012). Coordinated regulation of myeloid cells by tumours. *Nature Reviews. Immunology* 12, 253–268.
- Gajewski, T.F., Schreiber, H., and Fu, Y.-X. (2013). Innate and adaptive immune cells in the tumor microenvironment. *Nat. Immunol.* 14, 1014–1022.
- Garroway, C.J., Bowman, J., Carr, D., and Wilson, P.J. (2008). Applications of graph theory to landscape genetics. *Evol Appl* 1, 620–630.
- Gatti, R.A., and Good, R.A. (1971). Occurrence of malignancy in immunodeficiency diseases. A literature review. *Cancer* 28, 89–98.
- Gentles, A.J., Newman, A.M., Liu, C.L., Bratman, S.V., Feng, W., Kim, D., Nair, V.S., Xu, Y., Khuong, A., Hoang, C.D., et al. (2015). The prognostic landscape of genes and infiltrating immune cells across human cancers. *Nat. Med.* 21, 938–945.
- Gillen, S., Schuster, T., Meyer Zum Büschenfelde, C., Friess, H., and Kleeff, J. (2010). Preoperative/neoadjuvant therapy in pancreatic cancer: a systematic review and meta-analysis of response and resection percentages. *PLOS Medicine* 7, e1000267.
- Girardi, M., Oppenheim, D.E., Steele, C.R., Lewis, J.M., Glusac, E., Filler, R., Hobby, P., Sutton, B., Tigelaar, R.E., and Hayday, A.C. (2001). Regulation of cutaneous malignancy by gammadelta T cells. *Science* 294, 605–609.
- Godiska, R., Chantry, D., Raport, C.J., Schweickart, V.L., Trong, H.L., and Gray, P.W. (1997). Monocyte chemoattractant protein-4: tissue-specific expression and signaling through CC chemokine receptor-2. *J Leukoc Biol* 61, 353–360.
- Gollob, J.A., Sciambi, C.J., Huang, Z., and Dressman, H.K. (2005). Gene expression changes and signaling events associated with the direct antimelanoma effect of IFN-gamma. *Cancer Res.* 65, 8869–8877.
- Gong, T.-T., Hu, D.-M., and Zhu, Q. (2012). Contrast-enhanced EUS for differential diagnosis of pancreatic mass lesions: a meta-analysis. *Gastrointest. Endosc.* 76, 301–309.
- Goubier, A., Dubois, B., Gheit, H., Joubert, G., Villard-Truc, F., Asselin-Paturel, C., Trinchieri, G., and Kaiserlian, D. (2008). Plasmacytoid dendritic cells mediate oral tolerance. *Immunity* 29, 464–475.
- Griffith, J.W., Sokol, C.L., and Luster, A.D. (2014). Chemokines and Chemokine Receptors: Positioning Cells for Host Defense and Immunity. *Annual Review of Immunology* 32, 659–702.
- Gu-Trantien, C., Migliori, E., Buisseret, L., de Wind, A., Brohée, S., Garaud, S., Noël, G., Dang Chi, V.L., Lodewyckx, J.-N., Naveaux, C., et al. (2017). CXCL13-producing TFH cells link immune suppression and adaptive memory in human breast cancer. *JCI Insight* 2.

- Guillerey, C., Huntington, N.D., and Smyth, M.J. (2016). Targeting natural killer cells in cancer immunotherapy. *Nat. Immunol.* 17, 1025–1036.
- Guo, H., Liu, Z., Xu, B., Hu, H., Wei, Z., Liu, Q., Zhang, X., Ding, X., Wang, Y., Zhao, M., et al. (2013). Chemokine receptor CXCR2 is transactivated by p53 and induces p38-mediated cellular senescence in response to DNA damage. *Aging Cell* 12, 1110–1121.
- Hammond, M.E., Lapointe, G.R., Feucht, P.H., Hilt, S., Gallegos, C.A., Gordon, C.A., Giedlin, M.A., Mullenbach, G., and Tekamp-Olson, P. (1995). IL-8 induces neutrophil chemotaxis predominantly via type I IL-8 receptors. *J. Immunol.* 155, 1428–1433.
- Hanahan, D., and Weinberg, R. (2011). Hallmarks of Cancer: The Next Generation. *Cell* 144, 646–674.
- Hao, L., Zeng, X.-P., Xin, L., Wang, D., Pan, J., Bi, Y.-W., Ji, J.-T., Du, T.-T., Lin, J.-H., Zhang, D., et al. (2017). Incidence of and risk factors for pancreatic cancer in chronic pancreatitis: A cohort of 1656 patients. *Dig Liver Dis.*
- Hertzer, K.M., Donald, G.W., and Hines, O.J. (2013). CXCR2: a target for pancreatic cancer treatment? *Expert Opinion on Therapeutic Targets* 17, 667–680.
- Highfill, S.L., Cui, Y., Giles, A.J., Smith, J.P., Zhang, H., Morse, E., Kaplan, R.N., and Mackall, C.L. (2014). Disruption of CXCR2-Mediated MDSC Tumor Trafficking Enhances Anti-PD1 Efficacy. *Science Translational Medicine* 6, 237ra67–237ra67.
- Hingorani, S., Petricoin, E., Maitra, A., Rajapakse, V., and Wright, C.V.E. (2003). Preinvasive and invasive ductal pancreatic cancer and its early detection in the mouse. *Cancer Cell* –.
- Hingorani, S.R., Wang, L., Multani, A.S., Combs, C., Deramaudt, T.B., Hruban, R.H., Rustgi, A.K., Chang, S., and Tuveson, D.A. (2005). Trp53R172H and KrasG12D cooperate to promote chromosomal instability and widely metastatic pancreatic ductal adenocarcinoma in mice. *Cancer Cell* 7, 469–483.
- Hiraoka, A., Yano Ki, K., Kagami, N., Takeshige, K., Mio, H., Anazawa, H., and Sugimoto, S. (2001). Stem cell growth factor: in situ hybridization analysis on the gene expression, molecular characterization and in vitro proliferative activity of a recombinant preparation on primitive hematopoietic progenitor cells. *Hematol. J.* 2, 307–315.
- Hiraoka, N., Ino, Y., Yamazaki-Itoh, R., Kanai, Y., Kosuge, T., and Shimada, K. (2015). Intratumoral tertiary lymphoid organ is a favourable prognosticator in patients with pancreatic cancer. *Br. J. Cancer* 112, 1782–1790.
- Hirsch, E., Katanaev, V.L., Garlanda, C., Azzolino, O., Pirola, L., Silengo, L., Sozzani, S., Mantovani, A., Altruda, F., and Wymann, M.P. (2000). Central role for G protein-coupled phosphoinositide 3-kinase gamma in inflammation. *Science* 287, 1049–1053.
- Hoff, Von, D.D., Ervin, T., Arena, F.P., Chiorean, E.G., Infante, J., Moore, M., Seay, T., Tjulandin, S.A., Ma, W.W., Saleh, M.N., et al. (2013). Increased survival in pancreatic cancer with nab-paclitaxel plus gemcitabine. *N. Engl. J. Med.* 369, 1691–1703.
- Houghton, A.M., Rzymkiewicz, D.M., Ji, H., Gregory, A.D., Egea, E.E., Metz, H.E., Stolz, D.B., Land, S.R., Marconcini, L.A., Kliment, C.R., et al. (2010). Neutrophil elastase-mediated degradation of IRS-1 accelerates lung tumor growth. *Nat. Med.* 16, 219–223.

- Hruban, R.H., Adsay, N.V., Albores-Saavedra, J., Compton, C., Garrett, E.S., Goodman, S.N., Kern, S.E., Klimstra, D.S., Klöppel, G., Longnecker, D.S., et al. (2001). Pancreatic intraepithelial neoplasia: a new nomenclature and classification system for pancreatic duct lesions. *Am. J. Surg. Pathol.* 25, 579–586.
- Hruban, R.H., Canto, M.I., Goggins, M., Schulick, R., and Klein, A.P. (2010). Update on familial pancreatic cancer. *Adv Surg* 44, 293–311.
- Huang, B., Pan, P.-Y., Li, Q., Sato, A.I., Levy, D.E., Bromberg, J., Divino, C.M., and Chen, S.-H. (2006). Gr-1+CD115+ immature myeloid suppressor cells mediate the development of tumor-induced T regulatory cells and T-cell anergy in tumor-bearing host. *Cancer Res.* 66, 1123–1131.
- Hussain, F., Wang, J., Ahmed, R., Guest, S.K., Lam, E.W.F., Stamp, G., and El-Bahrawy, M. (2010). The expression of IL-8 and IL-8 receptors in pancreatic adenocarcinomas and pancreatic neuroendocrine tumours. *Cytokine* 49, 134–140.
- Ijichi, H., Chytil, A., Gorska, A.E., Aakre, M.E., Fujitani, Y., Fujitani, S., Wright, C.V.E., and Moses, H.L. (2006). Aggressive pancreatic ductal adenocarcinoma in mice caused by pancreas-specific blockade of transforming growth factor-beta signaling in cooperation with active Kras expression. *Genes & Development* 20, 3147–3160.
- Ilic, M., and Ilic, I. (2016). Epidemiology of pancreatic cancer. *World J. Gastroenterol.* 22, 9694–9705.
- Iodice, S., Gandini, S., Maisonneuve, P., and Lowenfels, A.B. (2008). Tobacco and the risk of pancreatic cancer: a review and meta-analysis. *Langenbecks Arch Surg* 393, 535–545.
- Iyer, A.S., Osmanbeyoglu, H.U., and Leslie, C.S. (2017). Computational methods to dissect gene regulatory networks in cancer. *Current Opinion in Systems Biology* 2, 115–122.
- Izeradjene, K., Combs, C., Best, M., Gopinathan, A., Wagner, A., Grady, W.M., Deng, C.-X., Hruban, R.H., Adsay, N.V., Tuveson, D.A., et al. (2007). KrasG12D and Smad4/Dpc4 Haploinsufficiency Cooperate to Induce Mucinous Cystic Neoplasms and Invasive Adenocarcinoma of the Pancreas. *Cancer Cell* 11, 229–243.
- Jacks, T., Remington, L., Williams, B.O., Schmitt, E.M., Halachmi, S., Bronson, R.T., and Weinberg, R.A. (1994). Tumor spectrum analysis in p53-mutant mice. *Curr. Biol.* 4, 1–7.
- Jaffee, E.M., Hruban, R.H., Canto, M., and Kern, S.E. (2002). Focus on pancreas cancer. *Cancer Cell* 2, 25–28.
- Jain, A.K. (2010). Data clustering: 50 years beyond K-means. *Pattern Recognition Letters* 31, 651–666.
- Jamieson, T., Clarke, M., Steele, C.W., Samuel, M.S., Neumann, J., Jung, A., Huels, D., Olson, M.F., Sudipto, das, Nibbs, R.J.B., et al. (2012). Inhibition of CXCR2 profoundly suppresses inflammation-driven and spontaneous tumorigenesis. *Journal of Clinical Investigation* 122, 3127–3144.
- Jia, X., Miao, Z., Li, W., Zhang, L., Feng, C., He, Y., Bi, X., Wang, L., Du, Y., Hou, M., et al. (2014). Cancer-risk module identification and module-based disease risk evaluation: a case study on lung cancer. *PLoS ONE* 9, e92395.

- Jiang, H., Hegde, S., Knolhoff, B.L., Zhu, Y., Herndon, J.M., Meyer, M.A., Nywening, T.M., Hawkins, W.G., Shapiro, I.M., Weaver, D.T., et al. (2016). Targeting focal adhesion kinase renders pancreatic cancers responsive to checkpoint immunotherapy. *Nat. Med.* 22, 851–860.
- Jones, S., Zhang, X., Parsons, D.W., Lin, J.C.-H., Leary, R.J., Angenendt, P., Mankoo, P., Carter, H., Kamiyama, H., Jimeno, A., et al. (2008). Core signaling pathways in human pancreatic cancers revealed by global genomic analyses. *Science* 321, 1801–1806.
- Kamisawa, T., Wood, L.D., Itoi, T., and Takaori, K. (2016). Pancreatic cancer. *Lancet* 388, 73–85.
- Kato, H., Wang, D., Daikoku, T., Sun, H., Dey, S., and DuBois, R. (2013). CXCR2-Expressing Myeloid-Derived Suppressor Cells Are Essential to Promote Colitis-Associated Tumorigenesis. *Cancer Cell* 24, 631–644.
- Keane, M.G., Horsfall, L., Rait, G., and Pereira, S.P. (2014). A case-control study comparing the incidence of early symptoms in pancreatic and biliary tract cancer. *BMJ Open* 4, e005720.
- Klein, A.P., Brune, K.A., Petersen, G.M., Goggins, M., Tersmette, A.C., Offerhaus, G.J.A., Griffin, C., Cameron, J.L., Yeo, C.J., Kern, S., et al. (2004). Prospective risk of pancreatic cancer in familial pancreatic cancer kindreds. *Cancer Res.* 64, 2634–2638.
- Klein, W.M., Hruban, R.H., Klein-Szanto, A.J.P., and Wilentz, R.E. (2002). Direct correlation between proliferative activity and dysplasia in pancreatic intraepithelial neoplasia (PanIN): additional evidence for a recently proposed model of progression. *Mod. Pathol.* 15, 441–447.
- Koebel, C.M., Vermi, W., Swann, J.B., Zerafa, N., Rodig, S.J., Old, L.J., Smyth, M.J., and Schreiber, R.D. (2007). Adaptive immunity maintains occult cancer in an equilibrium state. *Nature* 450, 903–907.
- Kozuka, S., Sassa, R., Taki, T., Masamoto, K., Nagasawa, S., Saga, S., Hasegawa, K., and Takeuchi, M. (1979). Relation of pancreatic duct hyperplasia to carcinoma. *Cancer* 43, 1418–1428.
- Kumari, S., Nie, J., Chen, H.-S., Ma, H., Stewart, R., Li, X., Lu, M.-Z., Taylor, W.M., and Wei, H. (2012). Evaluation of Gene Association Methods for Coexpression Network Construction and Biological Knowledge Discovery. *PLoS ONE* 7, e50411.
- Kunzmann, V., Ramanathan, R.K., Goldstein, D., Liu, H., Ferrara, S., Lu, B., Renschler, M.F., and Hoff, V.D. (2017). Tumor Reduction in Primary and Metastatic Pancreatic Cancer Lesions With nab-Paclitaxel and Gemcitabine. *Pancreas* 46, 203–208.
- Kusmartsev, S., and Gabrilovich, D.I. (2003). Inhibition of myeloid cell differentiation in cancer: the role of reactive oxygen species. *J Leukoc Biol* 74, 186–196.
- La Cruz, De, M.S.D., Young, A.P., and Ruffin, M.T. (2014). Diagnosis and management of pancreatic cancer. *Am Fam Physician* 89, 626–632.
- Laganà, A., Perumal, D., Melnekoff, D., Readhead, B., Kidd, B.A., Leshchenko, V., Kuo, P.-Y., Keats, J., DeRome, M., Yesil, J., et al. (2017). Integrative network analysis identifies novel drivers of pathogenesis and progression in newly diagnosed multiple myeloma. *Leukemia* 2014, 636514.
- Le, D.T., Wang-Gillam, A., Picozzi, V., Greten, T.F., Crocenzi, T., Springett, G., Morse, M., Zeh, H., Cohen, D., Fine, R.L., et al. (2015). Safety and survival with GVAX pancreas prime and

- Listeria Monocytogenes-expressing mesothelin (CRS-207) boost vaccines for metastatic pancreatic cancer. *J. Clin. Oncol.* 33, 1325–1333.
- Lee, K.E., Spata, M., Bayne, L.J., Buza, E.L., Durham, A.C., Allman, D., Vonderheide, R.H., and Simon, M.C. (2016). Hif1a Deletion Reveals Pro-Neoplastic Function of B Cells in Pancreatic Neoplasia. *Cancer Discov* 6, 256–269.
- Lesina, M., Wörmann, S.M., Morton, J., Diakopoulos, K.N., Korneeva, O., Wimmer, M., Einwächter, H., Sperveslage, J., Demir, I.E., Kehl, T., et al. (2016). RelA regulates CXCL1/CXCR2-dependent oncogene-induced senescence in murine Kras-driven pancreatic carcinogenesis. *J. Clin. Invest.* 126, 2919–2932.
- Li, A., King, J., Moro, A., Sugi, M.D., Dawson, D.W., Kaplan, J., Li, G., Lu, X., Strieter, R.M., Burdick, M., et al. (2011). Overexpression of CXCL5 is associated with poor survival in patients with pancreatic cancer. *Am. J. Pathol.* 178, 1340–1349.
- Li, Q., Pan, P.-Y., Gu, P., Xu, D., and Chen, S.-H. (2004). Role of immature myeloid Gr-1+ cells in the development of antitumor immunity. *Cancer Res.* 64, 1130–1139.
- Lim, J.E., Chien, M.W., and Earle, C.C. (2003). Prognostic factors following curative resection for pancreatic adenocarcinoma: a population-based, linked database analysis of 396 patients. *Ann. Surg.* 237, 74–85.
- Ling, J., Kang, Y., Zhao, R., Xia, Q., Lee, D.-F., Chang, Z., Li, J., Peng, B., Fleming, J.B., Wang, H., et al. (2012). KrasG12D-induced IKK2/β/NF-κB activation by IL-1α and p62 feedforward loops is required for development of pancreatic ductal adenocarcinoma. *Cancer Cell* 21, 105–120.
- Liu, F., Wu, H.Y., Wesselschmidt, R., Kornaga, T., and Link, D.C. (1996). Impaired production and increased apoptosis of neutrophils in granulocyte colony-stimulating factor receptor-deficient mice. *Immunity* 5, 491–501.
- Liu, L., Gritz, D., and Parent, C.A. (2014). PKC II acts downstream of chemoattractant receptors and mTORC2 to regulate cAMP production and myosin II activity in neutrophils. *Molecular Biology of the Cell* 25, 1446–1457.
- Lo, A., Wang, L.-C.S., Scholler, J., Monslow, J., Avery, D., Newick, K., O'Brien, S., Evans, R.A., Bajor, D.J., Clendenin, C., et al. (2015). Tumor-Promoting Desmoplasia Is Disrupted by Depleting FAP-Expressing Stromal Cells. *Cancer Res.* 75, 2800–2810.
- Loehrer, P.J., Feng, Y., Cardenes, H., Wagner, L., Brell, J.M., Cella, D., Flynn, P., Ramanathan, R.K., Crane, C.H., Alberts, S.R., et al. (2011). Gemcitabine alone versus gemcitabine plus radiotherapy in patients with locally advanced pancreatic cancer: an Eastern Cooperative Oncology Group trial. *J. Clin. Oncol.* 29, 4105–4112.
- London, C.A., Lodge, M.P., and Abbas, A.K. (2000). Functional responses and costimulator dependence of memory CD4+ T cells. *J. Immunol.* 164, 265–272.
- Lu, C., Redd, P.S., Lee, J.R., Savage, N., and Liu, K. (2016). The expression profiles and regulation of PD-L1 in tumor-induced myeloid-derived suppressor cells. *Oncoimmunology* 5, e1247135.
- Lutz, E.R., Wu, A.A., Bigelow, E., Sharma, R., Mo, G., Soares, K., Solt, S., Dorman, A., Wamwea, A., Yager, A., et al. (2014). Immunotherapy converts nonimmunogenic pancreatic

- tumors into immunogenic foci of immune regulation. *Cancer Immunol Res* 2, 616–631.
- Maccioni, F., Martinelli, M., Ansari, A.I., N., Kagarmanova, A., De Marco, V., Zippi, M., and Marini, M. (2010). Magnetic resonance cholangiography: past, present and future: a review. *Eur Rev Med Pharmacol Sci* 14, 721–725.
- Maddipati, R., and Stanger, B.Z. (2015). Pancreatic Cancer Metastases Harbor Evidence of Polyclonality. *Cancer Discov* 5, 1086–1097.
- Maeda, S., Kuboki, S., Nojima, H., Shimizu, H., Yoshitomi, H., Furukawa, K., Miyazaki, M., and Ohtsuka, M. (2017). Duffy antigen receptor for chemokines (DARC) expressing in cancer cells inhibits tumor progression by suppressing CXCR2 signaling in human pancreatic ductal adenocarcinoma. *Cytokine* 95, 12–21.
- Mahalingam, D., Patel, M.R., Sachdev, J.C., Hart, L.L., Halama, N., Ramanathan, R.K., Sarantopoulos, J., Liu, X., Yazji, S., Jäger, D., et al. (2016). Anti-oxidized macrophage migration inhibitory factor (oxMIF) antibody imalumab (BAX69) in advanced solid tumors: Final results of first-in-human phase 1 study. *Ann Oncol* 27.
- Mantovani, A., Sozzani, S., Locati, M., Allavena, P., and Sica, A. (2002). Macrophage polarization: tumor-associated macrophages as a paradigm for polarized M2 mononuclear phagocytes. *Trends Immunol.* 23, 549–555.
- Manz, M.G., and Boettcher, S. (2014). Emergency granulopoiesis. *14*, 302–314.
- Marbach, D., Costello, J.C., Küffner, R., Vega, N.M., Prill, R.J., Camacho, D.M., Allison, K.R., Aderhold, A., Allison, K.R., Bonneau, R., et al. (2012). Wisdom of crowds for robust gene network inference. *Nat. Methods* 9, 796–804.
- Marsden, P.V. (2002). Egocentric and sociocentric measures of network centrality. *Social Networks* 24, 407–422.
- Matloubian, M., Concepcion, R.J., and Ahmed, R. (1994). CD4+ T cells are required to sustain CD8+ cytotoxic T-cell responses during chronic viral infection. *J. Virol.* 68, 8056–8063.
- Matsushita, H., Vesely, M.D., Koboldt, D.C., Rickert, C.G., Uppaluri, R., Magrini, V.J., Arthur, C.D., White, J.M., Chen, Y.-S., Shea, L.K., et al. (2012). Cancer exome analysis reveals a T-cell-dependent mechanism of cancer immunoediting. *Nature* 482, 400–404.
- Matthaei, H., Schulick, R.D., Hruban, R.H., and Maitra, A. (2011). Cystic precursors to invasive pancreatic cancer. *Nat Rev Gastroenterol Hepatol* 8, 141–150.
- MD, P.B.E.L., and Lippitz, B.E. (2013). Cytokine patterns in patients with cancer: a systematic review. *The Lancet Oncology* 14, e218–e228.
- Mei, J., Liu, Y., Dai, N., Favara, M., Greene, T., Jeyaseelan, S., Poncz, M., Lee, J.S., and Worthen, G.S. (2010). CXCL5 regulates chemokine scavenging and pulmonary host defense to bacterial infection. *Immunity* 33, 106–117.
- Mei, J., Liu, Y., Dai, N., Hoffmann, C., Hudock, K.M., Zhang, P., Guttentag, S.H., Kolls, J.K., Oliver, P.M., Bushman, F.D., et al. (2012). Cxcr2 and Cxcl5 regulate the IL-17/G-CSF axis and neutrophil homeostasis in mice. *Journal of Clinical Investigation* 122, 974–986.

- Midha, S., Chawla, S., and Garg, P.K. (2016). Modifiable and non-modifiable risk factors for pancreatic cancer: A review. *Cancer Letters* 381, 269–277.
- Miller, J.A., Oldham, M.C., and Geschwind, D.H. (2008). A systems level analysis of transcriptional changes in Alzheimer's disease and normal aging. *J. Neurosci.* 28, 1410–1420.
- Mishalian, I., Bayuh, R., Levy, L., Zolotarov, L., Michaeli, J., and Fridlender, Z.G. (2013). Tumor-associated neutrophils (TAN) develop pro-tumorigenic properties during tumor progression. *Cancer Immunology, Immunotherapy* 62, 1745–1756.
- Moffitt, R.A., Marayati, R., Flate, E.L., Volmar, K.E., Loeza, S.G.H., Hoadley, K.A., Rashid, N.U., Williams, L.A., Eaton, S.C., Chung, A.H., et al. (2015). Virtual microdissection identifies distinct tumor- and stroma-specific subtypes of pancreatic ductal adenocarcinoma. *Nat. Genet.* 47, 1168–1178.
- Moore, M.J., Goldstein, D., Hamm, J., Figer, A., Hecht, J.R., Gallinger, S., Au, H.J., Murawa, P., Walde, D., Wolff, R.A., et al. (2007). Erlotinib plus gemcitabine compared with gemcitabine alone in patients with advanced pancreatic cancer: a phase III trial of the National Cancer Institute of Canada Clinical Trials Group. *J. Clin. Oncol.* 25, 1960–1966.
- Morandi, F., Horenstein, A.L., Chillemi, A., Quarona, V., Chiesa, S., Imperatori, A., Zanellato, S., Mortara, L., Gattorno, M., Pistoia, V., et al. (2015). CD56brightCD16- NK Cells Produce Adenosine through a CD38-Mediated Pathway and Act as Regulatory Cells Inhibiting Autologous CD4+ T Cell Proliferation. *J. Immunol.* 195, 965–972.
- Morel, Y., Truneh, A., Sweet, R.W., Olive, D., and Costello, R.T. (2001). The TNF superfamily members LIGHT and CD154 (CD40 ligand) costimulate induction of dendritic cell maturation and elicit specific CTL activity. *J. Immunol.* 167, 2479–2486.
- Mouriès, J., Moron, G., Schlecht, G., Escriou, N., Dadaglio, G., and Leclerc, C. (2008). Plasmacytoid dendritic cells efficiently cross-prime naive T cells in vivo after TLR activation. *Blood* 112, 3713–3722.
- Movahedi, K., Guiliams, M., van den Bossche, J., van den Bergh, R., Gysemans, C., Beschin, A., de Baetselier, P., and van Ginderachter, J.A. (2008). Identification of discrete tumor-induced myeloid-derived suppressor cell subpopulations with distinct T cell-suppressive activity. *Blood* 111, 4233–4244.
- Mukaka, M.M. (2012). Statistics corner: A guide to appropriate use of correlation coefficient in medical research. *Malawi Med J* 24, 69–71.
- Myron Kauffman, H., McBride, M.A., Cherikh, W.S., Spain, P.C., Marks, W.H., and Roza, A.M. (2002). Transplant tumor registry: donor related malignancies. *Transplantation* 74, 358–362.
- Nagaraj, S., Gupta, K., Pisarev, V., Kinarsky, L., Sherman, S., Kang, L., Herber, D.L., Schneck, J., and Gabilovich, D.I. (2007). Altered recognition of antigen is a mechanism of CD8+ T cell tolerance in cancer. *Nature Medicine* 13, 828–835.
- Nasser, M.W., Raghuwanshi, S.K., Malloy, K.M., Gangavarapu, P., Shim, J.-Y., Rajarathnam, K., and Richardson, R.M. (2007). CXCR1 and CXCR2 activation and regulation. Role of aspartate 199 of the second extracellular loop of CXCR2 in CXCL8-mediated rapid receptor internalization. *J. Biol. Chem.* 282, 6906–6915.

- Neesse, A., Frese, K.K., Bapiro, T.E., Nakagawa, T., Sternlicht, M.D., Seeley, T.W., Pilarsky, C., Jodrell, D.I., Spong, S.M., and Tuveson, D.A. (2013). CTGF antagonism with mAb FG-3019 enhances chemotherapy response without increasing drug delivery in murine ductal pancreas cancer. *Proc. Natl. Acad. Sci. U.S.A.* 110, 12325–12330.
- Newman, A.M., Liu, C.L., Green, M.R., Gentles, A.J., Feng, W., Xu, Y., Hoang, C.D., Diehn, M., and Alizadeh, A.A. (2015). Robust enumeration of cell subsets from tissue expression profiles. *Nat. Methods* 12, 453–457.
- Nielsen, N., Ødum, N., Ursø, B., Lanier, L.L., and Spee, P. (2012). Cytotoxicity of CD56(bright) NK cells towards autologous activated CD4+ T cells is mediated through NKG2D, LFA-1 and TRAIL and dampened via CD94/NKG2A. *PLoS ONE* 7, e31959.
- Novitskiy, S.V., Forrester, E., Pickup, M.W., Gorska, A.E., Chytil, A., Aakre, M., Polosukhina, D., Owens, P., Yusupova, D.R., Zhao, Z., et al. (2014). Attenuated transforming growth factor beta signaling promotes metastasis in a model of HER2 mammary carcinogenesis. *Breast Cancer Res.* 16, 425.
- Noy, R., and Pollard, J.W. (2014). Tumor-associated macrophages: from mechanisms to therapy. *Immunity* 41, 49–61.
- Nywening, T.M., Wang-Gillam, A., Sanford, D.E., Belt, B.A., Panni, R.Z., Cusworth, B.M., Toriola, A.T., Nieman, R.K., Worley, L.A., Yano, M., et al. (2016). Targeting tumour-associated macrophages with CCR2 inhibition in combination with FOLFIRINOX in patients with borderline resectable and locally advanced pancreatic cancer: a single-centre, open-label, dose-finding, non-randomised, phase 1b trial. *Lancet Oncol.* 17, 651–662.
- Oettle, H., Neuhaus, P., Hochhaus, A., Hartmann, J.T., Gellert, K., Ridwelski, K., Niedergethmann, M., Zülke, C., Fahlke, J., Arning, M.B., et al. (2013). Adjuvant chemotherapy with gemcitabine and long-term outcomes among patients with resected pancreatic cancer: the CONKO-001 randomized trial. *Jama* 310, 1473–1481.
- Okada, T., Ngo, V.N., Ekland, E.H., Förster, R., Lipp, M., Littman, D.R., and Cyster, J.G. (2002). Chemokine requirements for B cell entry to lymph nodes and Peyer's patches. *J. Exp. Med.* 196, 65–75.
- Oliphant, C.J., Barlow, J.L., and McKenzie, A.N.J. (2011). Insights into the initiation of type 2 immune responses. *Immunology* 134, 378–385.
- Olive, K.P., Jacobetz, M.A., Davidson, C.J., Gopinathan, A., McIntyre, D., Honess, D., Madhu, B., Goldgraben, M.A., Caldwell, M.E., Allard, D., et al. (2009). Inhibition of Hedgehog signaling enhances delivery of chemotherapy in a mouse model of pancreatic cancer. *Science* 324, 1457–1461.
- Padovan, E., Spagnoli, G.C., Ferrantini, M., and Heberer, M. (2002). IFN-alpha2a induces IP-10/CXCL10 and MIG/CXCL9 production in monocyte-derived dendritic cells and enhances their capacity to attract and stimulate CD8+ effector T cells. *J Leukoc Biol* 71, 669–676.
- Pagès, F., Galon, J., Dieu-Nosjean, M.-C., Tartour, E., Sautès-Fridman, C., and Fridman, W.-H. (2010). Immune infiltration in human tumors: a prognostic factor that should not be ignored. *Oncogene* 29, 1093–1102.
- Pandiyan, P., Zheng, L., Ishihara, S., Reed, J., and Lenardo, M.J. (2007). CD4+CD25+Foxp3+

regulatory T cells induce cytokine deprivation-mediated apoptosis of effector CD4⁺ T cells. *Nat. Immunol.* 8, 1353–1362.

Panopoulos, A.D., Zhang, L., Snow, J.W., Jones, D.M., Smith, A.M., Kasmi, E.I., K.C., Liu, F., Goldsmith, M.A., Link, D.C., Murray, P.J., et al. (2006). STAT3 governs distinct pathways in emergency granulopoiesis and mature neutrophils. *Blood* 108, 3682–3690.

Pardoll, D.M. (2012). The blockade of immune checkpoints in cancer immunotherapy. *Nature Reviews Cancer* 12, 252–264.

Parronchi, P., De Carli, M., Manetti, R., Simonelli, C., Sampognaro, S., Piccinni, M.P., Macchia, D., Maggi, E., Del Prete, G., and Romagnani, S. (1992). IL-4 and IFN (alpha and gamma) exert opposite regulatory effects on the development of cytolytic potential by Th1 or Th2 human T cell clones. *J. Immunol.* 149, 2977–2983.

Perra, N., and Fortunato, S. (2008). Spectral centrality measures in complex networks. *Phys Rev E Stat Nonlin Soft Matter Phys* 78, 036107.

Pinnacle, Saintigny, P., Massarelli, E., Lin, S., Ahn, Y.H., Chen, Y., Goswami, S., Erez, B., O'Reilly, M.S., Liu, D., et al. (2013). CXCR2 Expression in Tumor Cells Is a Poor Prognostic Factor and Promotes Invasion and Metastasis in Lung Adenocarcinoma. *Cancer Research* 73, 571–582.

Pitt, J.M., Vétizou, M., Daillère, R., Roberti, M.P., Yamazaki, T., Routy, B., Lepage, P., Boneca, I.G., Chamillard, M., Kroemer, G., et al. (2016). Resistance Mechanisms to Immune-Checkpoint Blockade in Cancer: Tumor-Intrinsic and -Extrinsic Factors. *Immunity* 44, 1255–1269.

Prima, V., Kaliberova, L.N., Kaliberov, S., Curiel, D.T., and Kusmartsev, S. (2017). COX2/mPGES1/PGE2 pathway regulates PD-L1 expression in tumor-associated macrophages and myeloid-derived suppressor cells. *Proc. Natl. Acad. Sci. U.S.A.* 114, 1117–1122.

Pylayeva-Gupta, Y., Grabocka, E., and Bar-Sagi, D. (2011). RAS oncogenes: weaving a tumorigenic web. *Nature Reviews. Cancer* 11, 761–774.

Pylayeva-Gupta, Y., Lee, K.E., Hajdu, C.H., Miller, G., and Bar-Sagi, D. (2012). Oncogenic Kras-induced GM-CSF production promotes the development of pancreatic neoplasia. *Cancer Cell* 21, 836–847.

Qiao, G., Qin, J., Kunda, N., Calata, J.F., Mahmud, D.L., Gann, P., Fu, Y.-X., Rosenberg, S.A., Prabhakar, B.S., and Maker, A.V. (2017). LIGHT Elevation Enhances Immune Eradication of Colon Cancer Metastases. *Cancer Res.* 77, 1880–1891.

Qin, Z., Schwartzkopff, J., Pradera, F., Kammertoens, T., Seliger, B., Pircher, H., and Blankenstein, T. (2003). A critical requirement of interferon gamma-mediated angiostasis for tumor rejection by CD8⁺ T cells. *Cancer Res.* 63, 4095–4100.

Qureshi, O.S., Zheng, Y., Nakamura, K., Attridge, K., Manzotti, C., Schmidt, E.M., Baker, J., Jeffery, L.E., Kaur, S., Briggs, Z., et al. (2011). Trans-endocytosis of CD80 and CD86: a molecular basis for the cell-extrinsic function of CTLA-4. *Science* 332, 600–603.

Rahib, L., Smith, B.D., Aizenberg, R., Rosenzweig, A.B., Fleshman, J.M., and Matrisian, L.M. (2014). Projecting cancer incidence and deaths to 2030: the unexpected burden of thyroid, liver, and pancreas cancers in the United States. *Cancer Res.* 74, 2913–2921.

- Ramachandran, V., Arumugam, T., Hwang, R.F., Greenson, J.K., Simeone, D.M., and Logsdon, C.D. (2007). Adrenomedullin is expressed in pancreatic cancer and stimulates cell proliferation and invasion in an autocrine manner via the adrenomedullin receptor, ADMR. *Cancer Res.* 67, 2666–2675.
- Reid, M.D., Basturk, O., Thirabanjasak, D., Hruban, R.H., Klimstra, D.S., Bagci, P., Altinel, D., and Adsay, V. (2011). Tumor-infiltrating neutrophils in pancreatic neoplasia. *Mod. Pathol.* 24, 1612–1619.
- Rennert, P.D., James, D., Mackay, F., Browning, J.L., and Hochman, P.S. (1998). Lymph Node Genesis Is Induced by Signaling through the Lymphotoxin β Receptor. *Immunity* 9, 71–79.
- Rhim, A., Mirek, E., Aiello, N., Maitra, A., Bailey, J., McAllister, F., Reichert, M., Beatty, G., Rustgi, A., Vonderheide, R., et al. (2012). EMT and Dissemination Precede Pancreatic Tumor Formation. *Cell* 148, 349–361.
- Robertson, M.J. (2002). Role of chemokines in the biology of natural killer cells. *J Leukoc Biol* 71, 173–183.
- Rodriguez, P.C., Quiceno, D.G., Zabaleta, J., Ortiz, B., Zea, A.H., Piazuelo, M.B., Delgado, A., Correa, P., Brayer, J., Sotomayor, E.M., et al. (2004). Arginase I production in the tumor microenvironment by mature myeloid cells inhibits T-cell receptor expression and antigen-specific T-cell responses. *Cancer Res.* 64, 5839–5849.
- Rooney, M.S., Shukla, S.A., Wu, C.J., Getz, G., and Hacohen, N. (2015). Molecular and genetic properties of tumors associated with local immune cytolytic activity. *Cell* 160, 48–61.
- Royal, R.E., Levy, C., Turner, K., Mathur, A., Hughes, M., Kammula, U.S., Sherry, R.M., Topalian, S.L., Yang, J.C., Lowy, I., et al. (2010). Phase 2 trial of single agent Ipilimumab (anti-CTLA-4) for locally advanced or metastatic pancreatic adenocarcinoma. *J. Immunother.* 33, 828–833.
- Rustgi, A.K. (2006). The molecular pathogenesis of pancreatic cancer: clarifying a complex circuitry. *Genes & Development* 20, 3049–3053.
- Sadik, C.D., Kim, N.D., and Luster, A.D. (2011). Neutrophils cascading their way to inflammation. *Trends in Immunology* 32, 452–460.
- Sagiv, J.Y., Michaeli, J., Assi, S., Mishalian, I., Kisos, H., Levy, L., Damti, P., Lumbroso, D., Polyansky, L., Sionov, R.V., et al. (2015). Phenotypic diversity and plasticity in circulating neutrophil subpopulations in cancer. *Cell Rep* 10, 562–573.
- Sauane, M., Gopalkrishnan, R.V., Sarkar, D., Su, Z.Z., Lebedeva, I.V., Dent, P., Pestka, S., and Fisher, P.B. (2003). MDA-7/IL-24: novel cancer growth suppressing and apoptosis inducing cytokine. *Cytokine Growth Factor Rev.* 14, 35–51.
- Sauer, B., and Henderson, N. (1988). Site-specific DNA recombination in mammalian cells by the Cre recombinase of bacteriophage P1. *Proc. Natl. Acad. Sci. U.S.A.* 85, 5166–5170.
- Scheffzek, K., Ahmadian, M.R., Kabsch, W., Wiesmüller, L., Lautwein, A., Schmitz, F., and Wittinghofer, A. (1997). The Ras-RasGAP complex: structural basis for GTPase activation and its loss in oncogenic Ras mutants. *Science* 277, 333–338.

- Scheidig, A.J., Burmester, C., and Goody, R.S. (1999). The pre-hydrolysis state of p21ras in complex with GTP: new insights into the role of water molecules in the GTP hydrolysis reaction of ras-like proteins. *Structure* 7, 1311–S1312.
- Schett, G., Elewaut, D., McInnes, I.B., Dayer, J.-M., and Neurath, M.F. (2013). How Cytokine Networks Fuel Inflammation: Toward a cytokine-based disease taxonomy. *Nat. Med.* 19, 822–824.
- Schiwon, M., Weisheit, C., Franken, L., Gutweiler, S., Dixit, A., Meyer-Schwesinger, C., Pohl, J.-M., Maurice, N., Thiebes, S., Lorenz, K., et al. (2014). Crosstalk between Sentinel and Helper Macrophages Permits Neutrophil Migration into Infected Uroepithelium. 1–13.
- Schoenberger, S.P., Toes, R.E., van der Voort, E.I., Offringa, R., and Melief, C.J. (1998). T-cell help for cytotoxic T lymphocytes is mediated by CD40-CD40L interactions. *Nature* 393, 480–483.
- Schroder, K., Hertzog, P.J., Ravasi, T., and Hume, D.A. (2004). Interferon-gamma: an overview of signals, mechanisms and functions. *J Leukoc Biol* 75, 163–189.
- Seifert, L., Werba, G., Tiwari, S., Giau Ly, N.N., Alothman, S., Alqunaibit, D., Avanzi, A., Barilla, R., Daley, D., Greco, S.H., et al. (2016). The necrosome promotes pancreatic oncogenesis via CXCL1 and Mincle-induced immune suppression. *Nature* 532, 245–249.
- Serrano, M., Lee, H., Chin, L., Cordon-Cardo, C., Beach, D., and DePinho, R.A. (1996). Role of the INK4a locus in tumor suppression and cell mortality. *Cell* 85, 27–37.
- Shankaran, V., Ikeda, H., Bruce, A.T., White, J.M., Swanson, P.E., Old, L.J., and Schreiber, R.D. (2001). IFN γ and lymphocytes prevent primary tumour development and shape tumour immunogenicity. *Nature* 410, 1107–1111.
- Shen, M., Hu, P., Donskov, F., Wang, G., Liu, Q., and Du, J. (2014). Tumor-associated neutrophils as a new prognostic factor in cancer: a systematic review and meta-analysis. *PLoS ONE* 9, e98259.
- Shen-Orr, S.S., and Gaujoux, R. (2013). Computational deconvolution: extracting cell type-specific information from heterogeneous samples. *Current Opinion in Immunology* 25, 571–578.
- Shiao, S.L., Ruffell, B., DeNardo D.G., Faddegon B.A., Park C.C., and Coussens L.M. (2015). TH2-Polarized CD4(+) T Cells and Macrophages Limit Efficacy of Radiotherapy. *Cancer Immunol. Res.* 5, 518-525.
- Shin, S.H., Kim, S.C., Song, K.B., Hwang, D.W., Lee, J.H., Lee, D., Lee, J.W., Jun, E., Park, K.-M., and Lee, Y.-J. (2015). A comparative study of laparoscopic vs. open distal pancreatectomy for left-sided ductal adenocarcinoma: a propensity score-matched analysis. *J. Am. Coll. Surg.* 220, 177–185.
- Shojaei, F., Singh, M., Thompson, J.D., and Ferrara, N. (2008). Role of Bv8 in neutrophil-dependent angiogenesis in a transgenic model of cancer progression. *Proc. Natl. Acad. Sci. U.S.a.* 105, 2640–2645.
- Shojaei, F., Wu, X., Zhong, C., Yu, L., Liang, X.-H., Yao, J., Blanchard, D., Bais, C., Peale, F.V., van Bruggen, N., et al. (2007). Bv8 regulates myeloid-cell-dependent tumour angiogenesis. *Nature* 450, 825–831.

- Siegel, R.L., Miller, K.D., and Jemal, A. (2017). Cancer Statistics, 2017. *CA Cancer J Clin* 67, 7–30.
- Singhal, S., Bhojnagarwala, P.S., O'Brien, S., Moon, E.K., Garfall, A.L., Rao, A.S., Quatromoni, J.G., Stephen, T.L., Litzky, L., Deshpande, C., et al. (2016). Origin and Role of a Subset of Tumor-Associated Neutrophils with Antigen-Presenting Cell Features in Early-Stage Human Lung Cancer. *Cancer Cell* 30, 120–135.
- Sinha, P., Clements, V.K., Bunt, S.K., Albelda, S.M., and Ostrand-Rosenberg, S. (2007). Cross-talk between myeloid-derived suppressor cells and macrophages subverts tumor immunity toward a type 2 response. *J. Immunol.* 179, 977–983.
- Sirard, C., la Pompa, de, J.L., Elia, A., Itie, A., Mirtsos, C., Cheung, A., Hahn, S., Wakeham, A., Schwartz, L., Kern, S.E., et al. (1998). The tumor suppressor gene *Smad4/Dpc4* is required for gastrulation and later for anterior development of the mouse embryo. *Genes & Development* 12, 107–119.
- Sivakumar, S., de Santiago, I., Chlon, L., and Markowitz, F. (2017). Master Regulators of Oncogenic KRAS Response in Pancreatic Cancer: An Integrative Network Biology Analysis. *PLOS Medicine* 14, e1002223.
- Smyth, M.J., Thia, K.Y., Street, S.E., Cretney, E., Trapani, J.A., Taniguchi, M., Kawano, T., Pelikan, S.B., Crowe, N.Y., and Godfrey, D.I. (2000). Differential tumor surveillance by natural killer (NK) and NKT cells. *J. Exp. Med.* 191, 661–668.
- Sohn, T.A., Yeo, C.J., Cameron, J.L., Koniaris, L., Kaushal, S., Abrams, R.A., Sauter, P.K., Coleman, J., Hruban, R.H., and Lillemoe, K.D. (2000). Resected adenocarcinoma of the pancreas-616 patients: results, outcomes, and prognostic indicators. *J. Gastrointest. Surg.* 4, 567–579.
- Sparmann, A., and Bar-Sagi, D. (2004). Ras-induced interleukin-8 expression plays a critical role in tumor growth and angiogenesis. *Cancer Cell* 6, 447–458.
- Spicer, J.D., McDonald, B., Cools-Lartigue, J.J., Chow, S.C., Giannias, B., Kubes, P., and Ferri, L.E. (2012). Neutrophils promote liver metastasis via Mac-1-mediated interactions with circulating tumor cells. *Cancer Res.* 72, 3919–3927.
- Spiegel, A., Brooks, M.W., Houshyar, S., Reinhardt, F., Ardolino, M., Fessler, E., Chen, M.B., Krall, J.A., DeCock, J., Zervantonakis, I.K., et al. (2016). Neutrophils Suppress Intraluminal NK Cell-Mediated Tumor Cell Clearance and Enhance Extravasation of Disseminated Carcinoma Cells. *Cancer Discov* 6, 630–649.
- Spitzer, M.H., Carmi, Y., Reticker-Flynn, N.E., Kwek, S.S., Madhiredy, D., Martins, M.M., Gherardini, P.F., Prestwood, T.R., Chabon, J., Bendall, S.C., et al. (2017). Systemic Immunity Is Required for Effective Cancer Immunotherapy. *Cell* 168, 487–502.e15.
- Stadtmann, A., and Zarbock, A. (2012). CXCR2: From Bench to Bedside. *Front Immunol* 3, 263.
- Steele, C.W., Karim, S.A., Leach, J.D.G., Bailey, P., Upstill-Goddard, R., Rishi, L., Foth, M., Bryson, S., McDaid, K., Wilson, Z., et al. (2016). CXCR2 Inhibition Profoundly Suppresses Metastases and Augments Immunotherapy in Pancreatic Ductal Adenocarcinoma. *Cancer Cell* 29, 832–845.

- Stoppacciaro, A., Melani, C., Parenza, M., Mastracchio, A., Bassi, C., Baroni, C., Parmiani, G., and Colombo, M.P. (1993). Regression of an established tumor genetically modified to release granulocyte colony-stimulating factor requires granulocyte-T cell cooperation and T cell-produced interferon gamma. *J. Exp. Med.* 178, 151–161.
- Strauss, L., Sangaletti, S., Consonni, F.M., Szebeni, G., Morlacchi, S., Totaro, M.G., Porta, C., Anselmo, A., Tartari, S., Doni, A., et al. (2015). RORC1 Regulates Tumor-Promoting “Emergency” Granulo-Monocytopenia. *Cancer Cell* 28, 253–269.
- Street, S.E., Cretney, E., and Smyth, M.J. (2001). Perforin and interferon-gamma activities independently control tumor initiation, growth, and metastasis. *Blood* 97, 192–197.
- Street, S.E.A., Hayakawa, Y., Zhan, Y., Lew, A.M., MacGregor, D., Jamieson, A.M., Diefenbach, A., Yagita, H., Godfrey, D.I., and Smyth, M.J. (2004). Innate immune surveillance of spontaneous B cell lymphomas by natural killer cells and gammadelta T cells. *J. Exp. Med.* 199, 879–884.
- Stromnes, I.M., Brockenbrough, J.S., Izeradjene, K., Carlson, M.A., Cuevas, C., Simmons, R.M., Greenberg, P.D., and Hingorani, S.R. (2014). Targeted depletion of an MDSC subset unmasks pancreatic ductal adenocarcinoma to adaptive immunity. *Gut* 63, 1769–1781.
- Stuart, J.M., Segal, E., Koller, D., and Kim, S.K. (2003). A gene-coexpression network for global discovery of conserved genetic modules. *Science* 302, 249–255.
- Subramanian, A., Tamayo, P., Mootha, V.K., Mukherjee, S., Ebert, B.L., Gillette, M.A., Paulovich, A., Pomeroy, S.L., Golub, T.R., Lander, E.S., et al. (2005). Gene set enrichment analysis: a knowledge-based approach for interpreting genome-wide expression profiles. *Proc. Natl. Acad. Sci. U.S.A.* 102, 15545–15550.
- Surve, C.R., To, J.Y., Malik, S., Kim, M., and Smrcka, A.V. (2016). Dynamic regulation of neutrophil polarity and migration by the heterotrimeric G protein subunits Gai-GTP and Gβγ. *Sci Signal* 9, ra22–ra22.
- Swiecki, M., and Colonna, M. (2015). The multifaceted biology of plasmacytoid dendritic cells. *Nature Reviews Immunology* 15, 471–485.
- Tak, T., Tesselaar, K., Pillay, J., Borghans, J.A.M., and Koenderman, L. (2013). What's your age again? Determination of human neutrophil half-lives revisited. *J Leukoc Biol* 94, 595–601.
- Takahashi, T., Tagami, T., Yamazaki, S., Uede, T., Shimizu, J., Sakaguchi, N., Mak, T.W., and Sakaguchi, S. (2000). Immunologic self-tolerance maintained by CD25(+)CD4(+) regulatory T cells constitutively expressing cytotoxic T lymphocyte-associated antigen 4. *J. Exp. Med.* 192, 303–310.
- Takeda, K., Hayakawa, Y., Smyth, M.J., Kayagaki, N., Yamaguchi, N., Kakuta, S., Iwakura, Y., Yagita, H., and Okumura, K. (2001). Involvement of tumor necrosis factor-related apoptosis-inducing ligand in surveillance of tumor metastasis by liver natural killer cells. *Nat. Med.* 7, 94–100.
- Tamada, K., Shimozaaki, K., Chapoval, A.I., Zhai, Y., Su, J., Chen, S.F., Hsieh, S.L., Nagata, S., Ni, J., and Chen, L. (2000). LIGHT, a TNF-like molecule, costimulates T cell proliferation and is required for dendritic cell-mediated allogeneic T cell response. *J. Immunol.* 164, 4105–4110.
- Tamada, K., Ni, J., Zhu, G., Fiscella, M., Teng, B., van Deursen, J.M.A., and Chen, L. (2002a).

Cutting edge: selective impairment of CD8⁺ T cell function in mice lacking the TNF superfamily member LIGHT. *J. Immunol.* 168, 4832–4835.

Tamada, K., Tamura, H., Flies, D., Fu, Y.-X., Celis, E., Pease, L.R., Blazar, B.R., and Chen, L. (2002b). Blockade of LIGHT/LTbeta and CD40 signaling induces allospecific T cell anergy, preventing graft-versus-host disease. *J. Clin. Invest.* 109, 549–557.

Tong, A.W., Nemunaitis, J., Su, D., Zhang, Y., Cunningham, C., Senzer, N., Netto, G., Rich, D., Mhashilkar, A., Parker, K., et al. (2005). Intratumoral injection of INGN 241, a nonreplicating adenovector expressing the melanoma-differentiation associated gene-7 (mda-7/IL24): biologic outcome in advanced cancer patients. *Mol. Ther.* 11, 160–172.

Ugucioni, M., Mackay, C.R., Ochensberger, B., Loetscher, P., Rhis, S., LaRosa, G.J., Rao, P., Ponath, P.D., Baggiolini, M., and Dahinden, C.A. (1997). High expression of the chemokine receptor CCR3 in human blood basophils. Role in activation by eotaxin, MCP-4, and other chemokines. *J. Clin. Invest.* 100, 1137–1143.

Umemoto, E., Otani, K., Ikeno, T., Verjan Garcia, N., Hayasaka, H., Bai, Z., Jang, M.H., Tanaka, T., Nagasawa, T., Ueda, K., et al. (2012). Constitutive plasmacytoid dendritic cell migration to the splenic white pulp is cooperatively regulated by CCR7- and CXCR4-mediated signaling. *J. Immunol.* 189, 191–199.

van Someren, E.P., Vaes, B.L.T., Steegenga, W.T., Sijbers, A.M., Dechering, K.J., and Reinders, M.J.T. (2006). Least absolute regression network analysis of the murine osteoblast differentiation network. *Bioinformatics* 22, 477–484.

Vivian, J., Rao, A.A., Nothaft, F.A., Ketchum, C., Armstrong, J., Novak, A., Pfeil, J., Narkizian, J., Deran, A.D., Musselman-Brown, A., et al. (2017). Toil enables reproducible, open source, big biomedical data analyses. *Nat. Biotechnol.* 35, 314–316.

Vonderheide, R.H., and Bayne, L.J. (2013). Inflammatory networks and immune surveillance of pancreatic carcinoma. *Current Opinion in Immunology* 25, 200–205.

Voskoglou-Nomikos, T., Pater, J.L., and Seymour, L. (2003). Clinical predictive value of the in vitro cell line, human xenograft, and mouse allograft preclinical cancer models. *Clin. Cancer Res.* 9, 4227–4239.

Waddell, N., Pajic, M., Patch, A.-M., Chang, D.K., Kassahn, K.S., Bailey, P., Johns, A.L., Miller, D., Nones, K., Quek, K., et al. (2015). Whole genomes redefine the mutational landscape of pancreatic cancer. *Nature* 518, 495–501.

Wall, L., Burke, F., Barton, C., Smyth, J., and Balkwill, F. (2003). IFN-gamma induces apoptosis in ovarian cancer cells in vivo and in vitro. *Clin. Cancer Res.* 9, 2487–2496.

Wang, G., Lu, X., Dey, P., Deng, P., Wu, C.C., Jiang, S., Fang, Z., Zhao, K., Konaparthi, R., Hua, S., et al. (2016). Targeting YAP-Dependent MDSC Infiltration Impairs Tumor Progression. *Cancer Discov* 6, 80–95.

Wang, J., Chen, G., Li, M., and Pan, Y. (2011). Integration of breast cancer gene signatures based on graph centrality. *BMC Syst Biol* 5, S10.

Wang, Q.L., Chen, X., Zhang, M.H., Shen, Q.H., and Qin, Z.M. (2015). Identification of hub genes and pathways associated with retinoblastoma based on co-expression network analysis. *Genetics*

and *Molecular Research* 14, 16151–16161.

Wang, W., Abbruzzese, J.L., Evans, D.B., Larry, L., Cleary, K.R., and Chiao, P.J. (1999). The nuclear factor-kappa B RelA transcription factor is constitutively activated in human pancreatic adenocarcinoma cells. *Clin. Cancer Res.* 5, 119–127.

Wang, X., Li, Y., Tian, H., Qi, J., Li, M., Fu, C., Wu, F., Wang, Y., Cheng, D., Zhao, W., et al. (2014). Macrophage inhibitory cytokine 1 (MIC-1/GDF15) as a novel diagnostic serum biomarker in pancreatic ductal adenocarcinoma. *BMC Cancer* 14, 578.

Wculek, S.K., and Malanchi, I. (2015). Neutrophils support lung colonization of metastasis-initiating breast cancer cells. *Nature* 528, 413–417.

Wee, S., Jagani, Z., Xiang, K.X., Loo, A., Dorsch, M., Yao, Y.-M., Sellers, W.R., Lengauer, C., and Stegmeier, F. (2009). PI3K pathway activation mediates resistance to MEK inhibitors in KRAS mutant cancers. *Cancer Res.* 69, 4286–4293.

West, N.R., McCuaig, S., Franchini, F., and Powrie, F. (2015). Emerging cytokine networks in colorectal cancer. *Nature Reviews Immunology* 15, 615–629.

Winograd, R., Byrne, K.T., Evans, R.A., Odorizzi, P.M., Meyer, A.R.L., Bajor, D.L., Clendenin, C., Stanger, B.Z., Furth, E.E., Wherry, E.J., et al. (2015). Induction of T-cell Immunity Overcomes Complete Resistance to PD-1 and CTLA-4 Blockade and Improves Survival in Pancreatic Carcinoma. *Cancer Immunol Res* 3, 399–411.

Witkiewicz, A.K., McMillan, E.A., Balaji, U., Baek, G., Lin, W.-C., Mansour, J., Mollaei, M., Wagner, K.-U., Koduru, P., Yopp, A., et al. (2015). Whole-exome sequencing of pancreatic cancer defines genetic diversity and therapeutic targets. *Nat Commun* 6, 6744.

Wolfe, C.J., Kohane, I.S., and Butte, A.J. (2005). Systematic survey reveals general applicability of “guilt-by-association” within gene coexpression networks. *BMC Bioinformatics* 6, 227.

Xu, X., Gera, N., Li, H., Yun, M., Zhang, L., Wang, Y., Wang, Q.J., and Jin, T. (2015). GPCR-mediated PLC β / γ /PKC β /PKD signaling pathway regulates the cofilin phosphatase slingshot 2 in neutrophil chemotaxis. *Molecular Biology of the Cell* 26, 874–886.

Yamamoto, T., Yagi, S., Kinoshita, H., Sakamoto, Y., Okada, K., Uryuhara, K., Morimoto, T., Kaihara, S., and Hosotani, R. (2015). Long-term survival after resection of pancreatic cancer: a single-center retrospective analysis. *World J. Gastroenterol.* 21, 262–268.

Yang, S., He, P., Wang, J., Schetter, A., Tang, W., Funamizu, N., Yanaga, K., Uwagawa, T., Satoskar, A.R., Gaedcke, J., et al. (2016a). A Novel MIF Signaling Pathway Drives the Malignant Character of Pancreatic Cancer by Targeting NR3C2. *Cancer Res.* 76, 3838–3850.

Yang, Y., Han, L., Yuan, Y., Li, J., Hei, N., and Liang, H. (2014). Gene co-expression network analysis reveals common system-level properties of prognostic genes across cancer types. *Nat Commun* 5, 3231.

Yang, Z., Algesheimer, R., and Tessone, C.J. (2016b). A Comparative Analysis of Community Detection Algorithms on Artificial Networks. *Sci Rep* 6, 30750.

Yoshihara, K., Shahmoradgoli, M., Martínez, E., Vegesna, R., Kim, H., Torres-Garcia, W., Treviño, V., Shen, H., Laird, P.W., Levine, D.A., et al. (2013). Inferring tumour purity and stromal

and immune cell admixture from expression data. *Nat Commun* 4, 2612.

Youn, J.-I., Collazo, M., Shalova, I.N., Biswas, S.K., and Gabrilovich, D.I. (2012). Characterization of the nature of granulocytic myeloid-derived suppressor cells in tumor-bearing mice. *Journal of Leukocyte Biology* 91, 167–181.

Youn, J.-I., Kumar, V., Collazo, M., Nefedova, Y., Condamine, T., Cheng, P., Villagra, A., Antonia, S., McCaffrey, J.C., Fishman, M., et al. (2013). Epigenetic silencing of retinoblastoma gene regulates pathologic differentiation of myeloid cells in cancer. *Nat. Immunol.* 14, 211–220.

Youn, J.-I., Nagaraj, S., Collazo, M., and Gabrilovich, D.I. (2008). Subsets of myeloid-derived suppressor cells in tumor-bearing mice. *J. Immunol.* 181, 5791–5802.

Yu, P., Lee, Y., Liu, W., Chin, R.K., Wang, J., Wang, Y., Schietinger, A., Philip, M., Schreiber, H., and Fu, Y.-X. (2004). Priming of naive T cells inside tumors leads to eradication of established tumors. *Nat. Immunol.* 5, 141–149.

Zea, A.H., Rodriguez, P.C., Atkins, M.B., Hernandez, C., Signoretti, S., Zabaleta, J., McDermott, D., Quiceno, D., Youmans, A., O'Neill, A., et al. (2005). Arginase-producing myeloid suppressor cells in renal cell carcinoma patients: a mechanism of tumor evasion. *Cancer Res.* 65, 3044–3048.

Zhang, B., and Horvath, S. (2005). A general framework for weighted gene co-expression network analysis. *Stat Appl Genet Mol Biol* 4, Article17.

Zhang, W., N, N., Nandakumar, N., akumar, Shi, Y., Manzano, M., Smith, A., Graham, G., Gupta, S., Vietsch, E.E., et al. (2014). Downstream of Mutant KRAS, the Transcription Regulator YAP Is Essential for Neoplastic Progression to Pancreatic Ductal Adenocarcinoma. *Science Signaling* 7, ra42–ra42.

Zhao, G.Q., Liaw, L., and Hogan, B.L. (1998). Bone morphogenetic protein 8A plays a role in the maintenance of spermatogenesis and the integrity of the epididymis. *Development* 125, 1103–1112.

Zhao, W., Langfelder, P., Fuller, T., Dong, J., Li, A., and Hovarth, S. (2010). Weighted gene coexpression network analysis: state of the art. *J Biopharm Stat* 20, 281–300.

Zhou, S.-L., Zhou, Z.-J., Hu, Z.-Q., Huang, X.-W., Wang, Z., Chen, E.-B., Fan, J., Cao, Y., Dai, Z., and Zhou, J. (2016). Tumor-Associated Neutrophils Recruit Macrophages and T-Regulatory Cells to Promote Progression of Hepatocellular Carcinoma and Resistance to Sorafenib. *Gastroenterology* 150, 1646–1658.e17.

Zhu, Y., Knolhoff, B.L., Meyer, M.A., Nywening, T.M., West, B.L., Luo, J., Wang-Gillam, A., Goedegebuure, S.P., Linehan, D.C., and DeNardo, D.G. (2014). CSF1/CSF1R blockade reprograms tumor-infiltrating macrophages and improves response to T-cell checkpoint immunotherapy in pancreatic cancer models. *Cancer Res.* 74, 5057–5069.

Zlotnik, A., and Yoshie, O. (2012). The Chemokine Superfamily Revisited. *Immunity* 36, 705–716.

Zou, W. (2005). Immunosuppressive networks in the tumour environment and their therapeutic relevance. *Nature Reviews Cancer* 5, 263–274.